Technical Report Documentation Page

1. Report No.	2. Government Accession No.	3. Recipient's Catalog No.
FHWA/TX-98/1175-2		

4. Title and Subtitle	5. Report Date
DEVELOPMENT OF DYNAMIC ANALYSIS TECHNIQUES FOR FALLING-WEIGHT DEFLECTOMETER DATA	November 1992; Resubmitted: July 1993, November 1994, July 1997
	6. Performing Organization Code
7. Author(s) Allen H. Magnuson and Robert L. Lytton	8. Performing Organization Report No. Research Report 1175-2
9. Performing Organization Name and Address Texas Transportation Institute The Texas A&M University System College Station, Texas 77843-3135	10. Work Unit No. (TRAIS)
	11. Contract or Grant No. Study No. 0-1175
12. Sponsoring Agency Name and Address Texas Department of Transportation Research and Technology Transfer Office P. O. Box 5080 Austin, Texas 78763-5080	13. Type of Report and Period Covered Interim: September 1987 - August 1992
	14. Sponsoring Agency Code

15. Supplementary Notes

Research performed in cooperation with the Texas Department of Transportation and the U.S. Department of Transportation, Federal Highway Administration.

Research Study Title: Development of Dynamic Analysis Techniques for Falling-Weight Deflectometer Data

16. Abstract

Results of computations of pavement layer properties are presented for 24 Texas asphaltic concrete (AC) pavement sections. Layer properties were computed using dynamically analyzed Falling-Weight Deflectometer (FWD) time history data. Asphaltic concrete (AC) surface layer creep compliance data, lower layer moduli and subgrade sublayer thicknesses were extracted from the FWD data using a computerized back-calculation process. The Pavement Dynamic Analysis Procedure (PDAP) developed for the project is described.

All 24 sections including two pavement sections with known near-surface bedrock were successfully analyzed, giving realistic values for the AC layer creep parameters, lower layer moduli, and lower subgrade layer thickness. A graphical comparison study of pavement deflection frequency response functions is presented. The agreement for the pavements showed what appears to be severe lateral modal vibration interference in the innermost sensors at frequencies between 30 and 80 Hz.

Back-calculated layer data was compared with laboratory data from pavement samples. Laboratory creep data of AC layer samples agreed well with back-calculated data. Resonant column data on base course and subgrade moduli was used by highway engineers for pavement performance evaluation and prediction.

17. Key Words	18. Distribution Statement
Pavements, Pavement Materials, Pavement Dynamic Analysis, Falling Weight Deflectometer, Asphalt Materials, Pavement Evaluation, Asphaltic Concrete Creep, Asphaltic Materials	No restrictions. This document is available to the public through NTIS: National Technical Information Service 5285 Port Royal Road Springfield, Virginia 22161

19. Security Classif.(of this report)	20. Security Classif.(of this page)	21. No. of Pages	22. Price
Unclassified	Unclassified	222	

Form DOT F 1700.7 (8-72) Reproduction of completed page authorized

DEVELOPMENT OF DYNAMIC ANALYSIS TECHNIQUES FOR FALLING-WEIGHT DEFLECTOMETER DATA

by

Dr. Allen H. Magnuson

and

Dr. Robert L. Lytton

Research Report 1175-2
Research Study Number 0-1175
Research Study Title: Development of Dynamic Analysis Techniques for Falling-Weight Deflectometer Data

Sponsored by the
Texas Department of Transportation
In Cooperation with
U.S. Department of Transportation
Federal Highway Administration

November 1992
Resubmitted: July 1993, November 1994, July 1997

TEXAS TRANSPORTATION INSTITUTE
The Texas A&M University System
College Station, Texas 77843-3135

IMPLEMENTATION STATEMENT

One of the major recommendations of the study is that the implementation of the FWD-based Pavement Dynamic Analysis Procedure (PDAP) be initiated as soon as practicable. The PDAP was developed for the Texas Department of Transportation (TxDOT) as a tool for pavement evaluation and performance prediction. The implementation process, because of the novelty and complexity of the analysis procedure, will initially require continuous interaction between the study investigators and the users (TxDOT). A detailed plan for implementation is given in Chapter VIII.

DISCLAIMER

The contents of this report reflect the views of the authors who are responsible for the opinions, findings, and conclusions presented herein. The Principal Investigator of the project was Dr. R. L. Lytton. The co-investigator, Dr. A. H. Magnuson, drafted the report. The results, opinions, interpretations, conclusions and recommendations of the investigators do not necessarily reflect the official views or policies of the Federal Highway Administration or the Texas Department of Transportation. This report does not constitute a standard, or specifications, or regulations. This report is not intended for construction, bidding or permit purposes.

The software and the User's Manual for the Pavement Dynamic Analysis Procedure (PDAP) described herein are Copyright (c) 1993 by R. L. Lytton and A. H. Magnuson, Texas Transportation Institute, The Texas A & M System. All rights reserved.

The authors reserve the right to, or assign to the Texas Transportation Institute the right to, claim any invention or discovery conceived or first actually reduced to practice in the course of or under this contract, including any art, method, process, machine, manufacture, design or composition of matter, or any new and useful improvement thereof which is or may be patentable under the patent law of the United States of America or any foreign country.

ACKNOWLEDGEMENTS

The project investigators wish to acknowledge the many contributions of Mr. Robert C. Briggs, Engineer of Pavement Management of the TxDOT Division D-8, Pavement Design, to the project. His steadfast support, suggestions, technical guidance, and encouragement during the development of the project are particularly appreciated.

Thanks to Dr. N. Stubbs of the Texas A&M Civil Engineering Department for expert assistance and guidance in systems identification techniques and in the development of the PAVE-SID back-calculation program. Thanks to Dr. J. Uzan of the Technion Institute for his computations using the JACOB-SID back-calculation program. Thanks to Dr. K. Stokoe of the Civil Engineering Department at the University of Texas, Austin, for conducting the resonant column tests on the subgrade samples, and for kindly providing the data. Thanks to Dr. Fuming Wang for assistance and guidance in using the FUSID back-calculation program.

Thanks to Dr. W. Yang for performing the Summer 1989 FWD field tests. Thanks to Mr. T. Scullion for providing the FWD test-site data. Thanks to Mr. F. Germann for acquiring the March 1988 TxDOT District 1 FWD test data. Thanks to Dr. G. K. Bakas for performing the AC creep compliance tests, for developing the resonant column test apparatus, and for performing the resonant column tests on the base course samples.

Thanks to Mr. A. K. Reddy for developing the FWD-FFT program and for preparing the FWD time history and frequency response function plots. Thanks to Messrs. M. Muralidar and A. K. Reddy for their assistance in the T&E and PAVE-SID back-calculations. Thanks to Mr. V. Torpunuri for developing the PAVE-SID program and for assisting in the computations.

TABLE OF CONTENTS

LIST OF FIGURES

Figure **Page**

LIST OF TABLES

Page

ABBREVIATIONS

AC -	Asphaltic Concrete
ESALS -	Equivalent Single Axle Loadings
FWD-FFT -	Falling-Weight Deflectometer Fourier Transform (Program for computing FFTs and frequency response functions of FWD data.)
FEM -	Finite Element Method
FFT -	Fast Fourier Transform
FRF -	(Pavement Deflection) Frequency Response Function
FUSID -	Current Pavement System Identification Computer Program (for Back-calculation of pavement layer properties from FWD data.)
FWD -	Falling-Weight Deflectometer
H-S-H -	Hard-Soft-Hard Pavement
H/S -	Hard-Over-Soft Pavement
JACOB-SID-	Time-Domain Pavement System Identification Computer Program (for Back-calculation of pavement layer properties from FWD data.)
PAVE-SID -	Original Pavement System Identification Computer Program (for Back-calculation of pavement layer properties from FWD data.)
PDAP -	Pavement Dynamic Analysis Procedure
SCALPOT -	Scalar Potential (Program for computing dynamic pavement surface deflections using scalar potentials and given pavement layer properties.)
S/H -	Soft-Over-Hard Pavement (Unusual)
SI -	Structural Index
SID -	Computerized Systems IDentification Back-Calculation Procedure
T&E -	Trial-and-Error (Back-calculation Procedure)
TTI -	Texas Transportation Institute, Texas A & M University
TxDOT -	Texas Department of Transportation

METRIC (SI*) CONVERSION FACTORS

APPROXIMATE CONVERSIONS TO SI UNITS

Symbol	When You Know	Multiply By	To Find	Symbol
		LENGTH		
in	inches	2.54	centimeters	cm
ft	feet	0.3048	meters	m
yd	yards	0.914	meters	m
mi	miles	1.61	kilometers	km
		AREA		
in^2	square inches	6.452	centimeters squared	cm^2
ft^2	square feet	0.0929	meters squared	m^2
yd^2	square yards	0.836	meters squared	m^2
mi^2	square miles	2.59	kilometers squared	km^2
ac	acres	0.395	hectares	ha
		MASS (weight)		
oz	ounces	28.35	grams	g
lb	pounds	0.454	kilograms	kg
T	short tons (2000 lb)	0.907	megagrams	Mg
		VOLUME		
fl oz	fluid ounces	29.57	milliliters	mL
gal	gallons	3.785	liters	L
ft^3	cubic feet	0.0328	meters cubed	m^3
yd^3	cubic yards	0.765	meters cubed	m^3
Note: Volumes greater than 1000 L shall be shown in m^3.				
		TEMPERATURE (exact)		
°F	Fahrenheit temperature	5/9 (after subtracting 32)	Celsius temperature	°C

APPROXIMATE CONVERSIONS TO SI UNITS

Symbol	When You Know	Multiply By	To Find	Symbol
		LENGTH		
mm	millimeters	0.039	inches	in
m	meters	3.28	feet	ft
yd	meters	1.09	yards	yd
km	kilometers	0.621	miles	mi
		AREA		
mm^2	millimeters squared	0.0016	square inches	in^2
m^2	meters squared	10.764	square feet	ft^2
yd^2	kilometers squared	0.39	square miles	mi^2
ha	hectares (10,000 m^2)	2.53	acres	ac
		MASS (weight)		
g	grams	0.0353	ounces	oz
kg	kilograms	2.205	pounds	lb
Mg	megagrams (1000 kg)	1.103	short tons	T
		VOLUME		
mL	milliliters	0.034	fluid ounces	fl oz
L	liters	0.264	gallons	gal
m^3	meters cubed	35.315	cubic feet	ft^3
m^3	meters cubed	1.308	cubic yards	yd^3
		TEMPERATURE (exact)		
°C	Celsius temperature	9/5 (then add 32)	Fahrenheit temperature	°F

These factors conform to the requirement of FHWA Order 5190.1A

*SI is the symbol for the International System of Measurements

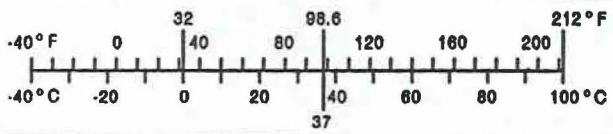

SUMMARY

All pavement engineers know that asphalt pavements are viscoelastic and this basic fact governs how they respond to traffic loads and weather stresses. It also controls how rapidly or slowly these pavements develop distress such as fatigue cracking, rutting, and thermal cracking. A wish that all pavement engineers have had for many years, and even decades, is to be able to test these pavements *in the field* and to determine from these measurements the viscoelastic properties of the layers of an asphalt pavement that are so important in determining the performance and service life of that pavement.

The dynamic analysis procedure that was developed partly in study 1175 and is described in the report that is summarized here fulfills many of the wishes of these pavement engineers. Dynamic analysis uses data from the Falling Weight Deflectometer (FWD) to determine most of the desired properties and thicknesses of pavement layers. The data that are used are the full time history of the load impulse applied to the pavement by the FWD drop weight and of the surface deflections measured by the geophones. The analytical process of converting these field data into material properties and thicknesses of each pavement layer is termed "back-calculation." The FWD impulse loading closely simulates axle loads due to vehicles traveling at highway speeds.

Study Objectives:

- To develop a pavement dynamic analysis procedure based on FWD time history data.

- To demonstrate that the dynamic analysis procedure can be used to extract realistic values for key pavement layer properties. To verify quantitatively the values of back-calculated layer properties by comparison with laboratory data from pavement samples.

Advantages of FWD Testing

- The impulsive dropweight force on the pavement closely simulates traffic loads at highway speeds.
- FWD testing is economical and fast, and provides a large amount of data.
- Many state and federal highway agencies already have FWD units.
- FWD data is acquired nondestructively.
- AC creep compliance data can be computed from FWD data and dynamic analysis.
- Pavement cracking and rutting can be predicted from the creep compliance.
- Pavement layer materials are undisturbed.
- Computed pavement data reflects the actual three-dimensional state of stress in the pavement layers as they respond to the FWD surface force impulse.

Creep, Cracking, and Rutting

Asphalt layer creep properties can be extracted by the back-calculation process using dynamic analysis of FWD field data. This creep data is of utmost importance in predicting rutting, fatigue cracking, thermal cracking, and reflection cracking, all of which are major types of pavement distress. At present, dynamic back-calculation is the only procedure that can obtain this vital information using nondestructively-acquired field data.

One of the most important single items of information about the structural condition of a pavement is how long will it last until it needs major repair or rehabilitation? The connection between AC creep data, cracking, and rutting and pavement remaining life was

established. The log-log slope (m) (of the AC creep compliance curve) is a key element for predicting pavement cracking and rutting.

Site Selection

As a test of the analysis method that was developed, the full FWD time history data were collected on 24 Texas sites and analyzed. The pavement characteristics in this study included sites with overlays, near-surface bedrock, cement-stabilized base courses, asphalt-stabilized base courses, lime-stabilized subbases, and clay, sand, gravel, rock and/or silt subgrades. Also included are two sites in which the driller's log data showed near-surface bedrock.

Pavement Dynamic Analysis Procedure (PDAP)

A description of the TTI FWD Pavement Dynamic Analysis back-calculation Procedure (PDAP) is given. The procedure consists of three computer programs: FWD-FFT, SCALPOT, and FUSID or PAVE-SID. FWD-FFT computes the frequency response functions from FWD data, SCALPOT computes pavement deflections given layer properties, and the SID program(s) perform the back-calculation.

Pavement Frequency Response Functions

The computation of and use of pavement frequency response functions for pavement dynamic analysis are described. The pavement frequency response functions are computed from the FWD time history data. The pavement frequency response functions characterize the dynamic response of the pavement. They represent the steady-state time-harmonic vertical surface deflections per unit force. There is one frequency response function for each deflection sensor. Each frequency response function has a frequency-dependent magnitude and phase angle.

Three types of pavement configuration were identified from the FWD frequency response functions:

- Hard-over-soft (H/S),
- Hard-soft-hard (H-S-H), and
- Soft/hard (S/H).

Twelve of the 24 sections are classified as H-S-H, 11 sections as H/S, and one section as S/H. An interpretation of the FWD responses as surface waves is also given. This shows how the lower frequency energy penetrates deeper into the pavement, giving information on the deeper layers. The high frequency response, with shorter wavelengths, gives information on the near-surface layers.

Vertical Mode Effect

For the H-S-H sections, the FWD magnitude frequency response functions for the outer sensors have a peak indicating a vertical modal effect caused by the presence of a stiff lower subgrade layer. In order to fit the computed outer sensor magnitude data, it is necessary to split up the subgrade into a finite thickness upper sublayer and a semi-infinite stiffer lower sublayer. This is necessary even in sections where drilling log data does not indicate bedrock or any other reasons for a stiff lower sublayer. Thickness of the upper subgrade is back-calculated by trial-and-error. After taking into account the sublayering, the computed results replicates the FWD data magnitude peaks for the H-S-H sites.

Transverse Vibration Modes

An apparent lateral vibration mode causes interference in the inner sensor magnitude plots computed using the FWD data. For seven of the 24 sites, the inner sensor interference is severe in the 30-80 Hz frequency range. The lateral modal effect is shown to be related to pavement stiffness, with the effect increasing as stiffness decreases. The sites are also separated into thick, medium and thin, based on AC layer thickness, which is (for a fixed

temperature) related to stiffness. The thin pavements had the worst transverse mode effects. Since the computer model cannot take into account azimuthal asymmetries such as lateral modes or pavement edge effects, the lateral mode features could not be replicated in the computed responses. For the thin pavements, the back-calculation curve-fitting is performed satisfactorily by averaging over the questionable data features.

Temperature Effects

FWD testing is done at one site twice, once with a cool temperature and another with a warm temperature. By back-calculating AC creep properties at both temperatures, a temperature susceptibility constant is computed using a temperature correction procedure described in the report. The result is found to give a value in agreement with published data. This shows that one can correct for temperature directly, using FWD data at two or more temperatures. Using dynamic analysis, it is not necessary to introduce empirical temperature correction factors for the AC modulus.

Comparison Plots

Comparison plots of pavement frequency response functions are presented for all the sites. Frequency response functions computed using FWD data are plotted along with predicted values using the SCALPOT pavement deflection program and back-calculated layer data. The graphical comparison study results show good agreement between the predicted and the FWD field data for magnitudes and phase angles for all seven sensor locations. The computed results replicate the FWD data magnitude peaks for sites with hard bottoms, i.e. hard-soft-hard sections (vertical mode effect).

Lateral modal vibrations, possibly caused by pavement edge effects, are present in the FWD data for the thin sections. The lateral mode is not simulated in the computer model which assumes axisymmetry about the vertical axis located at the dropweight centerline.

Back-Calculation

Back-calculated pavement layer properties for each section are presented. The back-calculated variables that are produced by the computer program are:

- AC Layer,
  - Creep Compliance Parameters (D_0, D_1, m),
  - Effective Modulus,
- Base Course Moduli,
- Subgrade Moduli,
  - Upper Subgrade,
  - Lower Subgrade, and
- Thickness of Upper Subgrade Layer.

AC effective moduli are found to decrease with temperature, and values fall within the expected ranges as measured in the laboratory. The AC layer log-log slope (m) values fall in the expected range, as compared to values obtained in laboratory creep tests. The base, subbase, and subgrade moduli also were shown to fall within their expected ranges. For some of the thinnest sections, the AC layer and unbound base course were combined into one layer. The combined layer was found to behave as a viscoelastic layer, but with a higher log-log slope (m) than the thicker AC layers.

Two methods of back-calculation were used in this study: a user trial-and-error process and an automated Systems Identification (SID) process that systematically converges final values of the variables while satisfying a least-squares criterion. The SID procedure generally produced better values than the trial-and-error process.

Laboratory/Back-Calculation Comparison

A quantitative comparison study of back-calculated layer properties and laboratory data from samples was conducted. AC constant stress creep data and resonant column data on the base course and subgrade materials were acquired from tests on core and bulk

samples. Good quantitative agreement was found between back-calculated data and laboratory data for AC layer creep parameters, base course moduli, and subgrade moduli: agreement was typically within +/- 30 percent.

Conclusions

- The FWD-based pavement dynamic analysis procedure is now available for trial use by the Texas Department of Transportation as a tool for pavement evaluation and performance prediction studies.

- The positive results of the FWD/Lab comparison studies indicate that the dynamic analysis procedure is accurate enough to compute the key pavement properties related to pavement performance and life. The efficacy of the dynamic analysis procedure as a tool for pavement performance, evaluation, and design studies was established.

- The layered viscoelastic model used by the SCALPOT program is adequate for representing the pavement dynamic responses.

- The accuracy of the back-calculation procedure (error was typically less than ±30 percent) was comparable to the uncertainties and variability in the laboratory results.

- The SID back-calculation procedure was shown to be able to produce realistic values of key pavement layer properties, consistently, for a wide range of pavement types and thicknesses.

- The FWD dynamic analysis procedure described here can be used to determine pavement characteristics such a layer thickness and material properties, and pavement width.

- The PDAP can compute, for sections with hard-soft-hard layering, the upper subgrade sublayer thickness and/or depth to bedrock.

- The PDAP can be used to analyze very thin pavements by combining the AC seal coat layer and the base course granular layer into one layer.

- The PDAP can be used to compute AC surface layer creep compliance parameters for thick and medium-thick layers.

- The PDAP can be used to compute base course, subbase, and subgrade sublayer moduli.

- The PDAP can be used to compute the AC layer temperature susceptibility from FWD test data taken at two or more temperatures.

- The PDAP can be used to compute AC creep compliance data for any temperature (i.e. perform temperature corrections) using the time-temperature shift method and the temperature susceptibility data.

All of these data are directly applicable to the prediction asphalt pavement distress and future performance.

Recommendations

One of the major recommendations of the study is that TxDOT begin the implementation process for the FWD-based Pavement Dynamic Analysis Procedure (PDAP) as soon as practicable.

Implementation

- The implementation process should include an intensive three day short course on pavement dynamic analysis, accompanied by hands-on experience on a desktop microcomputer or other computer intended for use with pavement analysis.

- TxDOT should develop a manual for FWD Test Procedures for Pavement Dynamic Analysis.

- One of the first steps in the implementation process is for TxDOT to require that, in all FWD data acquisition, time history data is to be recorded, even if the data is only needed (initially) for static analysis. The time history data can be used (eventually) for computing baseline data on pavement condition.

CHAPTER I
INTRODUCTION

The advantages of using nondestructive testing devices for pavement evaluation and performance prediction are well understood. Falling-weight deflectometer (FWD) systems are in widespread use for nondestructive pavement testing and evaluation.

However, up to the present, only a small fraction of the data that can be collected by the FWD is used for pavement evaluation. Usually only the peak loads and peak deflections of each of the geophone sensors are used in the static analysis of the pavement. The static analysis assumes that the FWD peak deflection data represents a static deflection basin.

Much more data or information about the pavement responses can be acquired and written to disk as an option for the FWD units. This information exists in the form of digitized time histories of the dropweight force and surface deflection pulses.

This report presents the results of an in-depth study of the use of the full time history data in a dynamic analysis of pavements. This type of analysis provides much additional useful, and even essential, information on the current pavement condition and its remaining life.

FALLING-WEIGHT DEFLECTOMETERS

The FWD is used to measure pavement properties in-place (i.e., in-situ) on in-service highways. FWD units use a time-impulse pavement surface force generated by dropweights. Using geophones, pavement surface deflections are measured at various distances from the dropweight. A diagram of a FWD unit is given in Figure 1.

ADVANTAGES OF DYNAMIC ANALYSIS

There are a number of major advantages to using FWD time history measurements and dynamic analysis.

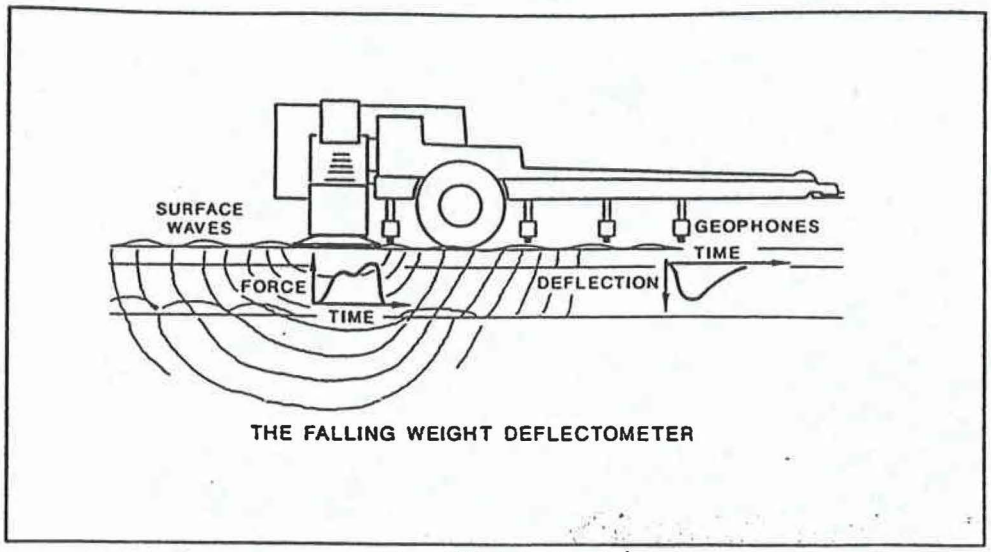

Figure 1. Falling-Weight Deflectometer Apparatus

- The cost of collecting and reducing the data, and producing the later properties of thickness and viscoelastic material properties is less expensive than acquiring the same data by any other means.

- FWD data acquisition and data analysis is fast and automated.

- FWD testing is nondestructive.

- FWD force impulse approximates the axle load traveling at highway speeds.

- Many agencies already have the FWD apparatus.

- Back-calculated pavement layer properties are based on the undisturbed state of the materials.

- Back-calculated data reflects the actual instantaneous, three-dimensional state of stress of the layer materials as they respond to the dropweight force.

FWD dynamic analysis presents an excellent opportunity to evaluate and predict pavement performance for many more sites than could be analyzed by any other method because of funding constraints. FWD dynamic analysis is much more economical than laboratory testing of pavement samples with subsequent analysis. For the same cost, an order of magnitude more sites can be analyzed using FWD time history data.

CURRENT PRACTICE

At present, pavement layer moduli can be extracted from the FWD data using peak values of the time history responses. Static analysis methods are used to model the pavement response in the back-calculation process (Uzan, Lytton and Germann, 1988). The peaks of the FWD deflections are assumed to form a static deflection basin that is optimally curve-fit to a computed basin by using a layered elastic model for the pavement and by varying the pavement layer moduli.

FWD-type force impulse pavement testing devices can be used to economically and nondestructively compute pavement layer properties (Lytton, Roberts and Stoffels, 1986). These devices or FWDs are an improvement over earlier steady-state oscillator devices such as the Dynaflect. They can obtain information on the full frequency spectrum of interest in one drop test, so that data acquisition is much faster and cheaper. TxDOT has twelve 8000-Series Dynatest Falling-Weight Deflectometer units which have been used primarily to acquire data for static analysis.

FWD DATA

Figure 2 shows a typical set of FWD time history plots for force and displacements. The FWD pulses are measured for a 60 millisecond (msec) time interval. The force plot is shown inverted. The seven deflection pulses are shown also, with deflection decreasing as distance from the dropweight increases. For this study the deflections were measured at distances of 0, 1, 2, 3, 4, 5, and 6 ft. from the dropweight center. Appendix A shows FWD time history plots for dropweight force and the displacement sensors for the 24 sites analyzed here.

FFTs of FWD Data

A dynamic analysis was performed on the time history (pulse) data using Fast Fourier Transforms (FFTs). Pavement frequency response functions were subsequently computed from the FFT data. The frequency response functions represent steady-state oscillatory magnitudes

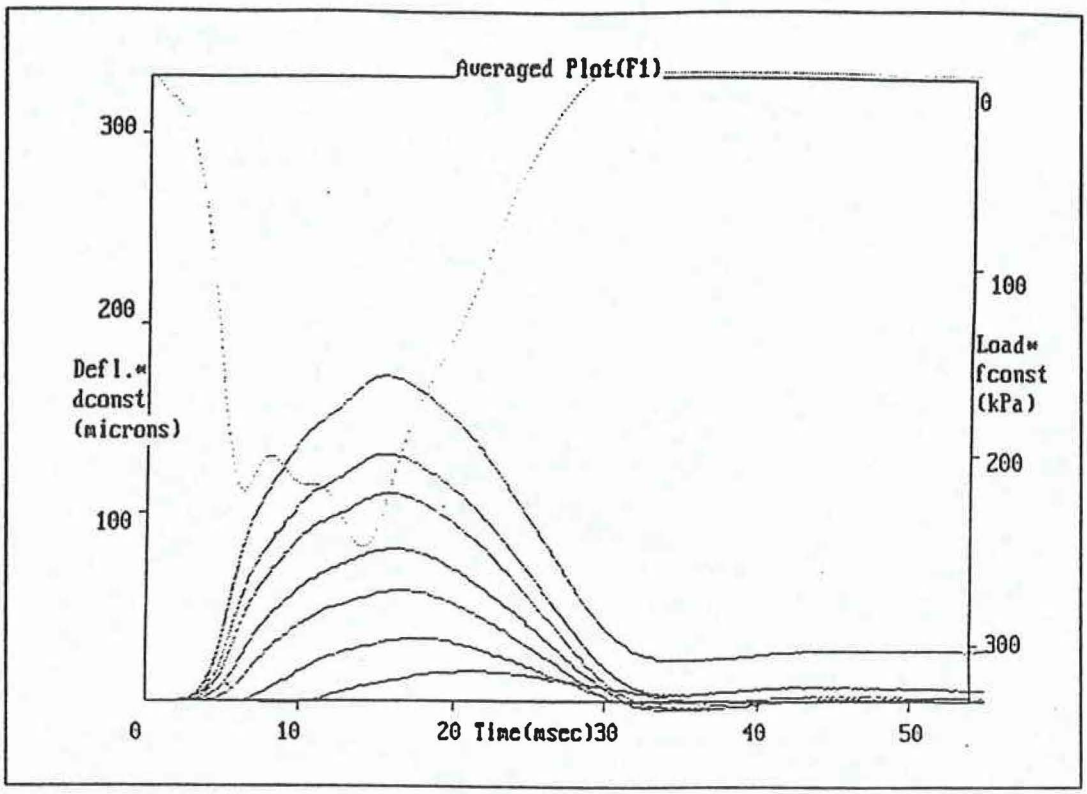

Figure 2. Typical Falling-Weight Deflectometer Time History Data Plots

and phase angles of pavement deflections per unit force as a function of frequency. The frequency response functions characterize, in effect, the dynamic response of the pavement.

Pavement layer properties were extracted using the pavement dynamic analysis procedure (PDAP) described in Chapter III. The PDAP uses a "forward" solution to the time-harmonic layered viscoelastic halfspace problem and an iterative inversion or systems identification (SID) program.

The results of this study support Lytton's recommendation of using Falling-Weight Deflectometer (FWD) data for pavement dynamic analysis. In the early 1970's, Lytton recognized that asphaltic concrete (AC) creep compliance data could be used to predict pavement failure from cracking and rutting. He has developed analytical relationships between AC creep properties and pavement cracking and rutting (Lytton 1989, 1990). Lytton also recognized the potential value of using force impulse testing devices (FWDs) together with pavement dynamic analysis to study asphaltic concrete (AC) creep compliance, pavement cracking, pavement rutting, and pavement remaining life.

PAVEMENT FAILURE MODES

The major modes of pavement failure are rutting and cracking, both of which can be predicted using mechanistic approaches (Magnuson, 1993). Rutting or permanent deformation were characterized in Kenis's (1978) VESYS pavement performance computer program using the "mu-alpha" parameters. The "mu-alpha" expressions characterize the viscoelastic permanent strain under cyclic (repeated) loading. Kenis's "alpha" (α) is related to the log-log slope (m) as follows.

$$\alpha = 1 - m$$

Paris' (1963) law is used to predict fatigue cracking. Paris' fatigue cracking analysis was generalized to treat viscoelastic materials by Schapery (1981). For AC pavements, both cracking and rutting are strongly dependent on the log-log slope (m) of the AC creep compliance curve.

Both the "mus" and "alphas" for permanent deformation and the cracking parameters are directly related algebraically to the AC layer creep parameters, especially the slope (m) of the creep curve, plotted on log-log axes (Lytton, 1990). By using nondestructive FWD testing to measure AC creep compliance and mechanistic descriptions of pavement cracking and rutting, it is now possible to use these data to economically predict the performance (life) of these sections, as well as to measure other layer properties. The cost of obtaining these data using non-destructive FWD testing is much lower than obtaining the same data from laboratory testing of cores, making this way of obtaining pavement material properties a very attractive alternative. This has been the major motivation for the development of the TTI FWD dynamic analysis procedure.

STUDY BACKGROUND AND RELATED WORK

Two earlier related studies were performed at TTI on the same Texas sites used in this dynamic analysis.

- NCHRP Project 10-27: "Determination of Asphaltic Concrete Pavement Structural Properties by Nondestructive Testing", Project Final Report (Lytton, Germann, and Chou, 1990)

- Project 1123 "Nondestructive Test Procedures for Analyzing the Structural Condition of Pavements."

Both of these studies used static analysis of FWD data to compute pavement layer properties. The sites were in four TxDOT Districts having four climate types:

- District 1, Paris, Texas (Wet freeze)

- District 8, Abilene, Texas (Dry freeze)

- District 11, Lufkin, Texas (Wet no freeze)

- District 21, Brownsville, Texas (Dry no freeze)

Earlier studies took drilling log data and samples at these sites. Laboratory test data was obtained from the samples (Lytton, Germann, and Chou, 1990).

The TxDOT-sponsored dynamic analysis study was part of the FHWA Cooperative Program. The dynamic analysis study was initiated at TTI in FY 1988. The TTI/TxDOT Study was based on 24 Texas highway sections from four Texas highway districts, representing a wide range of pavement types and climates. Figure 3 shows the locations of the sites. Time history FWD data on the 24 sites was acquired and recorded in the Summer of 1989. Under this study, a dynamic analysis method was developed and used on these sections. See (Magnuson, Lytton, and Briggs, 1991) for some preliminary results.

In addition to the earlier Texas studies, two FWD-based dynamic back-calculation studies on SHRP sites have been conducted recently at TTI. These are:

- SHRP A-005 Project

- SHRP/IDEA Project 25

In the SHRP A-005 study, a pavement dynamic analysis was performed in the time domain using a back-calculation computer program developed by J. Uzan (Lytton, 1992).

In the SHRP/ IDEA study, 12 SHRP sites were analyzed. There were three sites from each of the four SHRP Regions. The sites were chosen to give a wide variation in pavement thickness, age and subgrade type. The 12 sites in the SHRP/IDEA project were selected from SHRP A-005 GPS sites so that the back-calculated moduli etc. could be compared to AC laboratory data from the SHRP A-005 project. The final report (Magnuson, 1993) gives study results. All twelve sites, including sites with near-surface bedrock, were successfully analyzed. A quantitative comparison study using A-005 lab data and SHRP/IDEA back-calculated values was performed, giving values for the back-calculated moduli, etc. within about ±30 percent of the laboratory data.

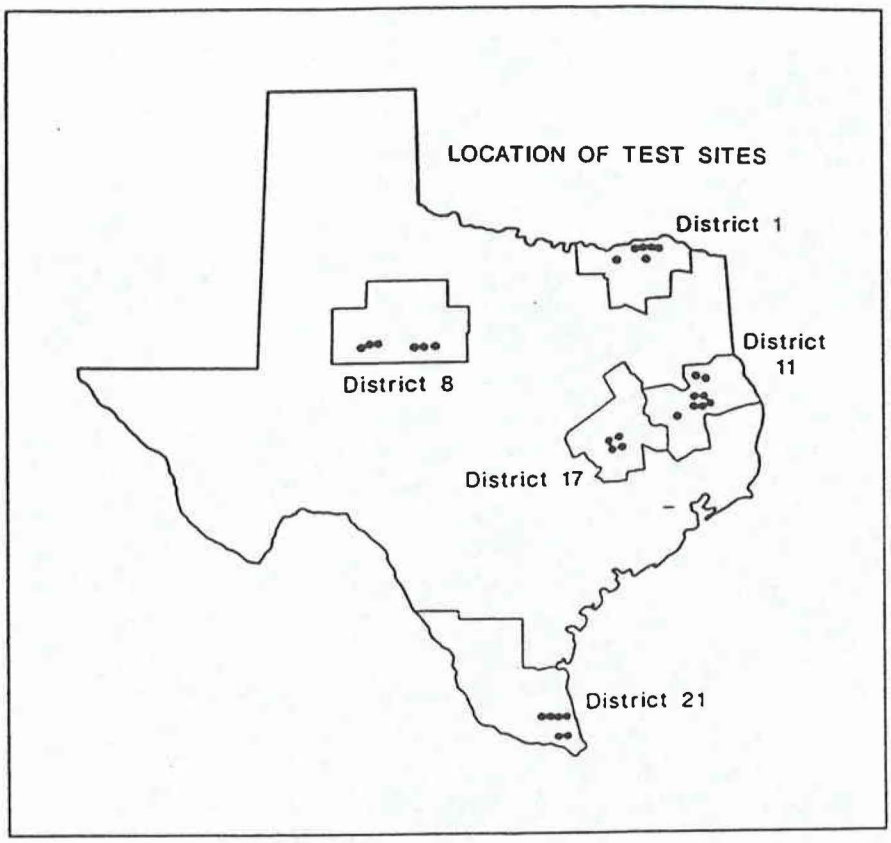

Figure 3. Map of Texas Showing Location of Sites Analyzed

SITE SELECTION

The 24 sites from the four TxDOT Districts used in the earlier studies and for the present study are identified as follows:

TABLE OF DISTRICTS

District	Dist. Hdqtrs.	No. of Sites
1	Paris	4
8	Abilene	6
11	Tyler	8
21	Pharr	6

These sites cover a wide range of AC surface course thicknesses, base course materials, climatic conditions, and subgrade soil types.

PAVEMENT SECTION CHARACTERISTICS

Table 1 shows the pavement section characteristics, which were taken from site drilling log data and lab data summary sheets from the two earlier related studies. The log data and lab test results are given in Lytton, et al. 1990. In Table 1, Columns 1 through 4 show the district number, site number, site designation, and highway designation (including milepost in some cases), respectively. Columns 5, 6, and 7 show the average surface temperature at the time of the FWD test, AC layer thickness, and reference pavement deflections. The reference displacements were taken as the displacements directly under the center of the load plate where the radius (r) equals zero (r = 0). Zero frequency displacements per unit force were taken from the pavement frequency response functions. These data give a good measure of the pavement stiffness at the time and temperature of the FWD test. Additional site data on the lower layers is given in Tables 3, 4, 5, and 6 in Chapter IV.

Table 1

Site Characteristics

District	Site	Site Desig-nation	Highway	FWD Avg Surface Temperature (deg F)	AC Thk (in)	Ref.Displ. @r = 0, f=0 (mils/10kip)
1	1	D01S1	FM 79	89	1.75	30
1	2	D01S3	SH 82	86.3	13.0	9
1	4	D01S4	FM 195	98	3.5	51
1	5	D01S5	SH 19&24	100	9.0	23
8	1	D08S1	FM 1983	108	1.0	45
8	2	D08S2	471	118	3.0	43
8	3	D08S3	I-20 mp 216	86	5.0	12
8	4	D08S4	I-20 mp 293	87	10.0	8
8	5	D08S5	I-20 mp 273.6	101	8.0	17
8	6	D08S6	FM 1235	97	1.0	41
11	1	D11S1	US 59 & Loop 224: mp 13.7	107	8.5	27
11	2	D11S2	US 59 & Loop 224: mp 19.5	102	8.0	26
11	3	D11S3	US 59 & Loop 224: mp 23.2	113	2.0	27
11	4	D11S4	FM 2864	101	1.0	57
11	5	D11S5	SH 7	88.5	1.0	38
11	6	D11S6	FM 2259 mp 3.5	115	2.0	35
11	7	D11S7	US 59 Southbound (across from D11S2)	88	-	8
11	8	D11S8	FM 355	106	1.5	35
21	1	D21S1	186 or 497	101.8	1.2	57
21	2	D21S2	FM 491	107	1.2	80
21	3	D21S3	US 77	90.9	2.2	16
21	4	D21S4	FM 1425 mp 5	116	4.0	55
21	5	D21S5	FM 1425 mp 3	116	6.0	37
21	6	D21S6	FM 88	115	3.0	76

FWD FIELD TESTS

FWD tests were performed for these sites in the summer of 1989. At each site, drops were made at five load levels corresponding to five different drop heights. Only the level 1 (lowest) load data (approx. 6000 lbs.) was used in the back-calculation because this minimized a frequency response function interference effect that will be discussed later. The FWD time history plots for Load 3 (about 12,000 lbs.) are given in Appendix A, Figures 61 to 84. These plots show the displacements without the pulse tail correction.

The tail correction was used to eliminate the discontinuity in the pulse data at the end of the FWD's 60 msec sampling interval. The pulses usually do not decay out completely after 60 msec. (See Magnuson, 1988a.)

The shapes of the pulse tail responses provide additional information on the pavement section. Characteristic truncated tail shapes can be classified as one of the following:

- Flat, shelf-like,
- Single overshoot,
- Decaying oscillation, and
- No (significant) tail.

Table 2 lists the sites and the type of pulse tail. Note that the flat, shelf tail occurs frequently for the r = 0 sensor. The flat shelf-like tail may be a measurement of pavement permanent deformation resulting from the dropweight load. This data may yield additional useful information on rutting, which is caused by accumulated permanent deformations from repeated design axle loadings. The oscillatory tails may indicate a (damped) natural frequency or vibration mode associated with vertical depth-dependence. A detailed technical analysis of the pulse tail data is beyond the scope of the present report, but should be performed as it may yield useful information on modal behavior and rutting.

Table 2

Tail Shapes for Pavement Deflection Time Histories

Site	Tail Shape			
	Small, None	Flat Shelf	Single Overshoot	Truncated Oscillation
D01S1	*	-	-	-
D01S3	*	-	-	-
D01S4	*(r>0)	*(r=0)	-	-
D01S5	*(r>0)	*(r=0)	-	-
D08S1	-	-	*	-
D08S2	-	*(Small)	-	-
D08S3	*	-	-	*
D08S4	-	-	-	*
D08S5	*(r>0)	*(r=0)	-	-
D08S6	-	*(r=0)	*(r>0)	-
D11S1	*(r>0)	*(r>0)	-	-
D11S2	-	-	*	-
D11S3	*	-	-	-
D11S4	*(r>0)	-	*(r=0,1)	-
D11S5	-	-	*(Strong)	-
D11S6	-	-	*	-
D11S7	-	-	-	*
D11S8	-	-	*	-
D21S1	*	-	-	-
D21S2	-	-	*	-
D21S3	-	*(r=0,1)	*(r>1)	-
D21S4	-	*(r>0)	*(r=0)	-
D21S5	*(r>0)	*(r=0)	-	-
D21S6	-	-	*	-

ADVANTAGES OF THE FWD-BASED DYNAMIC ANALYSIS

There are a number of advantages to FWD-based dynamic analysis over the usual laboratory testing of samples, as discussed above. One major advantage of FWD tests vs. lab tests is that one does not have to make assumptions about the stresses and physical properties of the pavement section at the time of the tests. This is because:

- Layer materials are undisturbed, and

- Data reflects the actual three-dimensional state of stress of the materials as they respond to the dropweight force.

In comparing the back-calculated subgrade moduli with laboratory data from samples, one must realize that the laboratory results reflect data from a (more or less) disturbed sample, while the FWD measurements are for the in-situ undisturbed state. Coring and boring samples taken into the lab will experience disturbances in sampling, handling, and storage. The microstructure of clay subgrade samples may be disturbed, moisture levels may vary, and assumed levels of confining stresses will also differ from in-situ values. Since the FWD dynamic analysis procedure measures in-situ properties, it is not necessary to assume values for confining stresses, temperature effects, and moisture content.

In addition, the pavement deformations reflect the actual three-dimensional state of stress in the vicinity of the dropweight. This is particularly important for unbound soil-type materials as they exhibit nonlinear stress-strain effects due to static and dynamic loads. The back-calculated layer properties represent "effective" linearized values that take into account the time-dependent nonlinear spatial stress field load-dependence in the vicinity of the dropweight.

Importance of the Log-Log Slope of the AC Creep Curve

The importance of the AC layer's log-log slope (m) of the creep curve has been discussed above. Recent results on research into AC low temperature cracking indicate similar relationships to creep parameters. Quoting from Roque, et al. (1992):

> *"The slope (m) of the linear portion of the log creep compliance-log time curve determined from the indirect tensile creep test, is one property that almost certainly will be found to be strongly related to the low temperature cracking performance of asphalt mixtures ... Figure 19 shows how one might establish a relationship between m and the amount of thermal cracking for a particular set of climatic conditions, pavement thickness, subgrade type, etc. The levels of cracking after 10 years were determined from the predictions ... and plotted in figure 19 as a function of the m values measured for each material."*

Roque's Figure 19, a plot of thermal cracking per 1000 ft. at ten years vs. log-log slope, is shown as Figure 4 here. This plot shows how sensitive cracking is to the log-log slope (m). These results indicate that the log-log slope (m) obtained from dynamic back-calculation may be measurable to an acceptable level of accuracy at moderate temperatures as well.

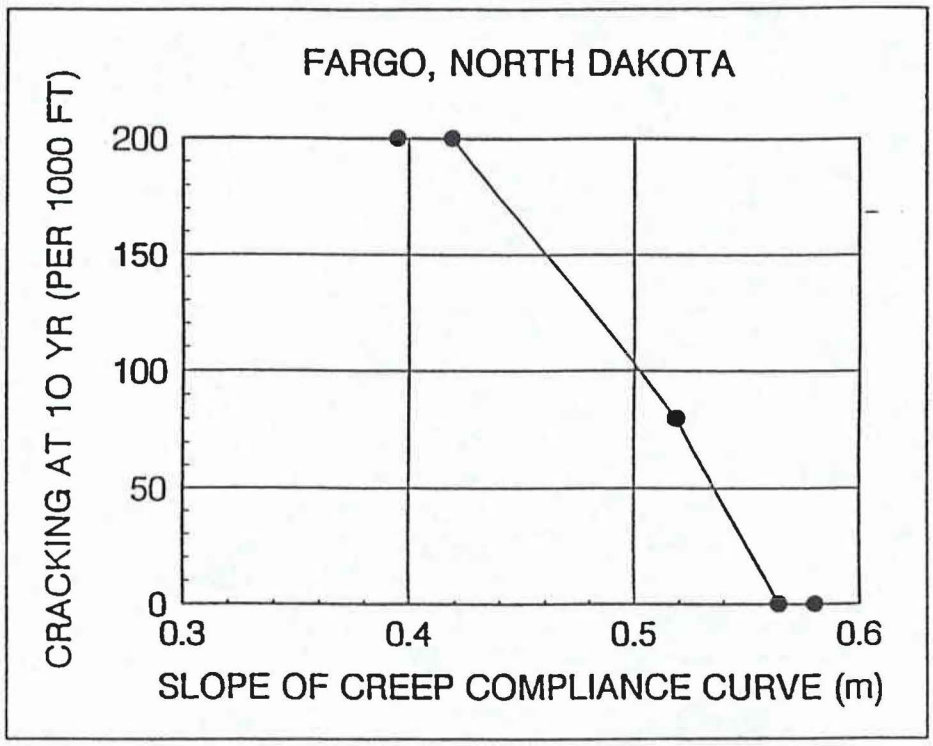

Figure 4. Cracking vs. Slope of Creep Compliance Curve (m)
(Roquet, 1992)

STUDY OBJECTIVES

- To develop and apply pavement dynamic analysis procedures using FWD time history data.

- To demonstrate that dynamic analysis can be used to extract realistic values for pavement layer properties.

- To verify the values of back-calculated layer properties by comparison with laboratory data from pavement samples.

- To show how the back-calculated pavement properties can be used in subsequent pavement design, evaluation, and performance prediction studies.

CHAPTER II

PAVEMENT FREQUENCY RESPONSE FUNCTIONS

The basic principles of frequency-domain analysis can be understood by a study of the dynamic response of the familiar spring-mass-damper system. Figure 5-a shows the system diagram.

SPRING-MASS-DAMPER SYSTEM ANALOGY

Figure 5-b shows normalized magnitudes as they vary with damping. The underdamped lumped-mass system has a well-defined natural frequency (ω_n). The damping ratio is defined as:

$$c/c_c < 1$$

where

c = Damping Ratio

c_c = Critical Damping Ratio.

The system's frequency response function magnitude shows magnification near its natural frequency (ω_n). The damping has a strong effect on the magnification in the vicinity of the natural frequency. Magnification increases as damping decreases.

VIBRATION MODES IN BEAMS AND PLATES

Distributed systems like beams and plates have distinct modes of vibration. Figures 6-a and 6-b show the transverse modes of vibration for a free beam. Each vibration mode has its own frequency. A given point on the beam or plate will oscillate vertically like the spring-mass-damper system. A stiff AC pavement layer can act as a vibrating plate resting on an elastic or viscoelastic foundation (i.e., the base course and subgrade). The pavement may have several modes of vibration transversely and/or longitudinally.

PAVEMENT VIBRATION MODES

Pavements can also have vertical modes of vibration caused by alternating hard-soft-hard (H-S-H) layering. The layering is due to the depth dependence of the subgrade sublayer moduli. Indications of pavement modal behavior are evident in the pavement's frequency response functions as will be shown later in the report. Figure 6-c shows vertical mode vibration formation by repeated reflection of compressional and/ or shear waves. The peaks in the magnitude curve indicate vertical modal behavior whereby wave energy is partially trapped in the softer subgrade layer as shown in Figure 6-c. Vertical modal behavior can be thought of as multiple reflections off the harder upper and lower layers. The repeated reflections cause constructive interference in the radial wave propagation, resulting in the modal behavior. At a given frequency, the modal behavior cannot "set up" until the radial distance (r) exceeds some minimum value; thus, it is more likely to appear in the outer sensor deflections.

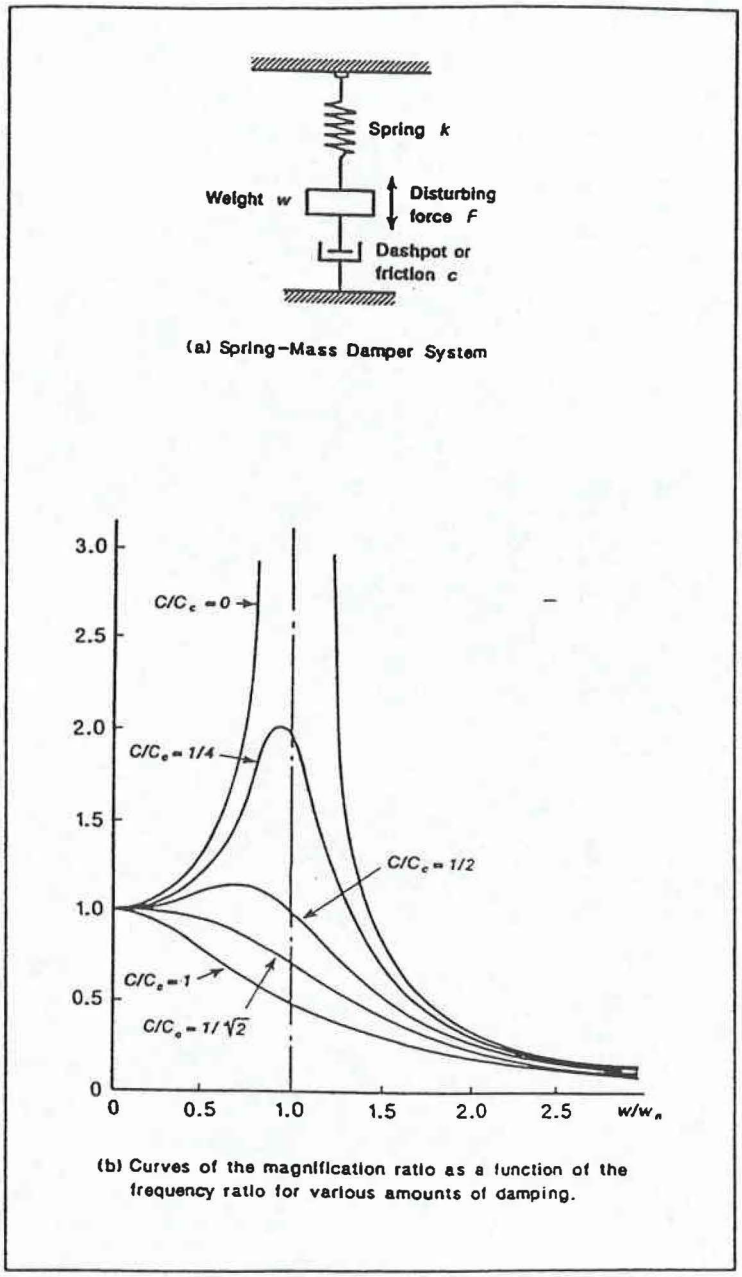

Figure 5. Spring-Mass-Damper System (Wylie, 1960)

Frequency-domain procedures are used here because useful insight can be gained into the modal response characteristics of the pavement, facilitating interpretation of response data. Frequency domain analysis gives information on the pavement's vertical and lateral modal behavior.

The subgrade sublayering is determined from vertical modal information, giving useful information on the pavement configuration, as illustrated in Figure 6-C. FWD frequency analysis also gives more data to work with in the back-calculation process: one has magnitude and phase angle data for all seven sensors, giving 14 curves for each test condition.

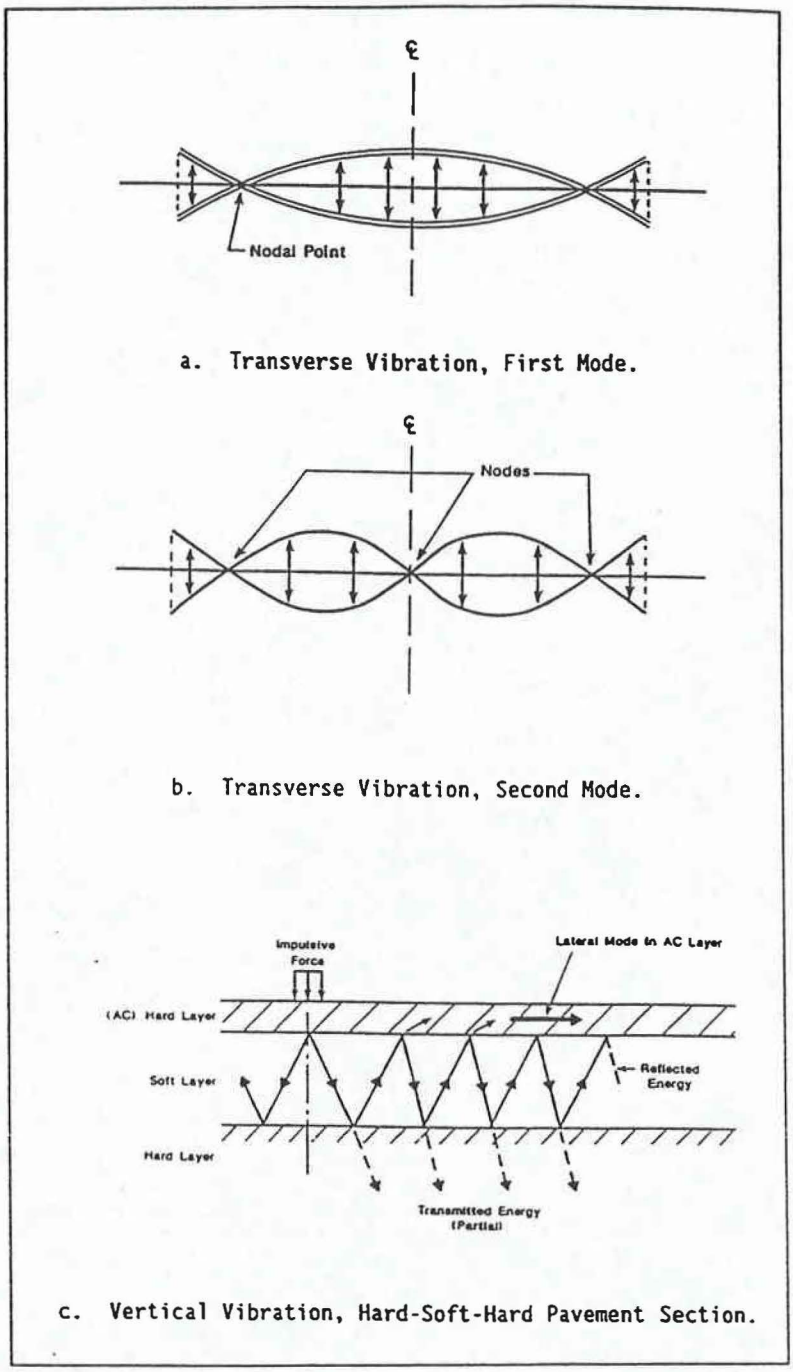

Figure 6. Modal Responses of the Asphaltic Concrete Layer

PAVEMENT FREQUENCY RESPONSE FUNCTIONS

Pavement frequency response functions characterize the linear dynamic pavement deflection response to surface forces. For FWD studies, the particular dynamic responses of interest are the vertical surface deflections resulting from the vertical surface force. They are

expressed as magnitude and phase angle plots vs. frequency, representing the steady-state time-harmonic response of the pavement to a sinusoidal surface force of constant amplitude. They are computed by dividing the Fast Fourier Transforms (FFTs) of the displacements by the FFTs of the dropweight force (Magnuson, 1988a).

Effect of Pavement Configuration

Typical pavement deflection frequency response functions computed from FWD time history data are shown in Figures 7 and 8 for a Hard-Over-Soft (H/S) section and a Hard-Soft-Hard (H-S-H) section, respectively. Figure 7-a shows magnitude response and Figure 7-b shows phase angle response for Site D01S3. The magnitude responses in Figure 7-a show for the H/S pavement a monotonic decrease in displacement with frequency for a fixed radial distance (r) from the dropweight center. The plots show seven radii (r), corresponding to the seven sensors at r = 0, 1, 2, 3, 4, 5, 6, and 7 ft. The decrease in deflection magnitude with frequency (i.e. attenuation) is caused by inertial (mass) effects in accordance with Newton's Second Law. The magnitudes decrease with radial distance (r) for a fixed frequency because of surface wave spreading of the form

$$\sqrt{1/r},$$

where r is the distance from the dropweight center. The phase angle curves in Figure 7-b start at the origin and increase monotonically with frequency, forming a fan-like pattern from the origin because the phase angles increase with distance (r) as well.

Figure 8-a shows the magnitude response and Figure 8-b shows the phase angle response for an H-S-H pavement (Site D08S4) having near-surface bedrock. These plots appear markedly different from the H/S pavement responses in Figure 7. The magnitude plots for the outer sensors (r = 4, 5, and 6 ft.) exhibit a marked peak at about 30 Hz instead of the monotonic decrease seen in the H/S section. The phase angle curves show a phase reversal, and the curves appear to fan-out at a frequency of about 15-20 Hz, having a jog or break at this frequency.

The FWD frequency response function data at the mid-to-lower frequencies can sense or respond to layers to a depth of about 10 to 15 ft. A more complicated layer structure than the four-layered one in Figure 9 may be needed if the substrata varies within this depth range.

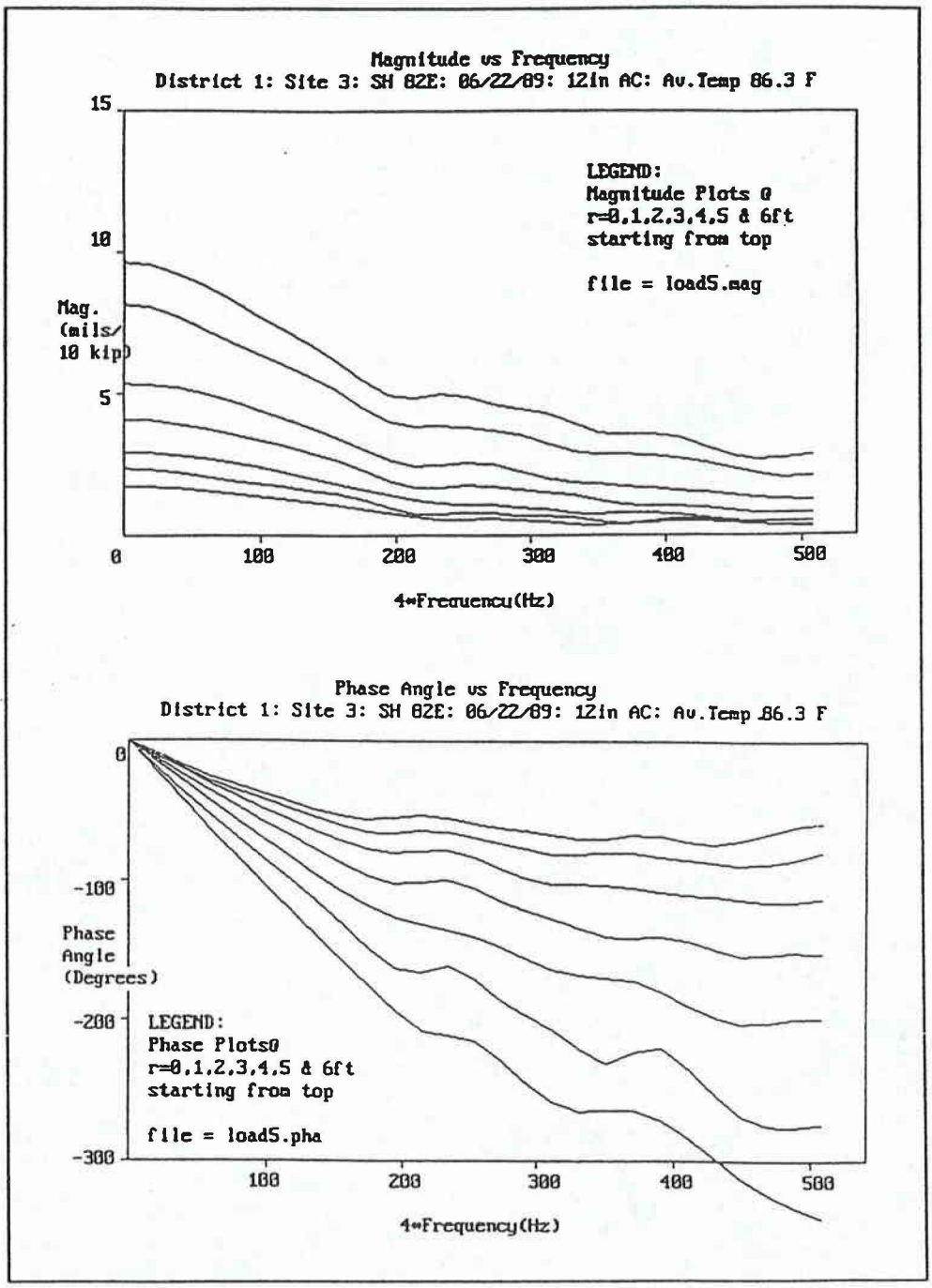

Figure 7. Pavement Frequency Response Functions for a Hard-Over-Soft (H/S) Section

Subgrade sublayering can occur naturally for sedimentary soils. Usually the subgrade stiffness will increase with increasing depth. This results in the hard-soft-hard (H-S-H) section.

Computed responses are based on an idealized pavement layer configuration as shown in Figures 9 and 10 for an H/S section and an H-S-H section, respectively. For an H/S section, the modulus decreases with depth for all layers, as shown in Figure 9. The usual layer structure for an H/S section is listed as follows.

- AC Surface Course (Hard)
- Base Course (Hard)
- Subbase, If Any (Soft)
- Subgrade (Soft)

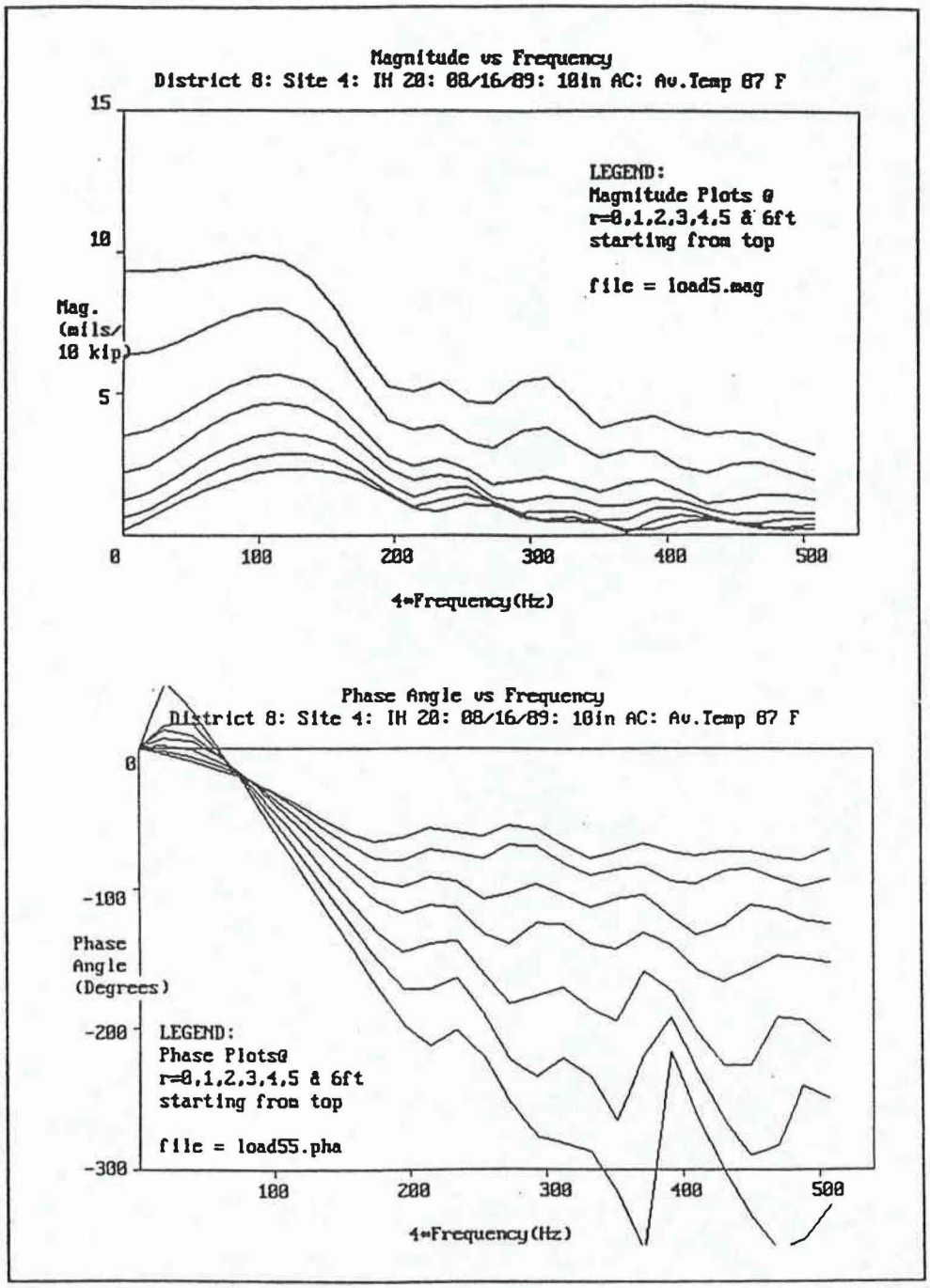

Figure 8. Pavement Frequency Response Functions for a Hard-Soft-Hard (H-S-H) Section

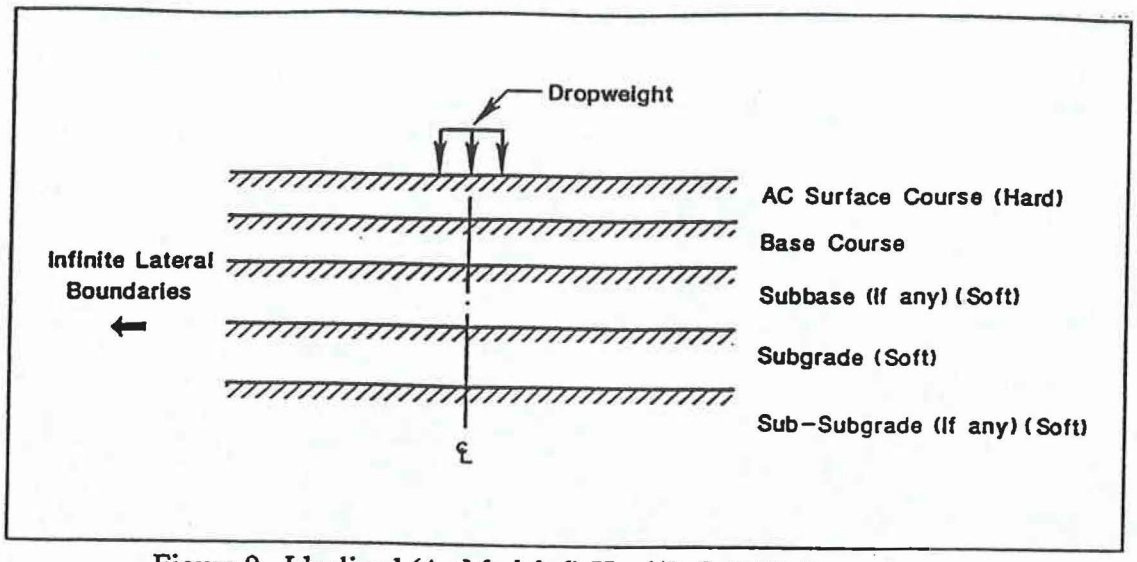

Figure 9. Idealized (As Modeled) Hard/Soft (H/S) Pavement

Figure 10 shows an idealized five-layer configuration for an H-S-H pavement having a harder lower subgrade layer. The majority of pavements exhibit (to some extent) H-S-H-behavior in the FWD frequency response functions. That is, the AC, base, and subbase (hard) layers lie above the (soft) upper subgrade layer which in turn has one or more harder subgrade sublayers. The lower sublayer may be (but is not necessarily) near-surface bedrock. The usual layer structure for the H-S-H section is listed as follows.

- AC Surface Course (Hard)
- Base Course (Hard)
- Subbase, If Any (Soft)
- Upper Subgrade (Soft)
- Lower Subgrade (Hard)

The frequency response functions computed using FWD data have numerous irregular features such as cusps, nulls, and peaks. This is because the real pavement configuration is more complicated than the idealized ones shown in Figures 9 and 10. Some physical and geometrical "irregularities" of a real pavement are shown in Figure 11. Pavement edge effects may be present or the subgrade may have sublayers, which may or may not be flat and level with a smooth interface. Any of these irregularities can give rise to frequency response function anomalies, i.e., fine features not seen in the responses for the idealized layered configurations in Figures 9 and 10.

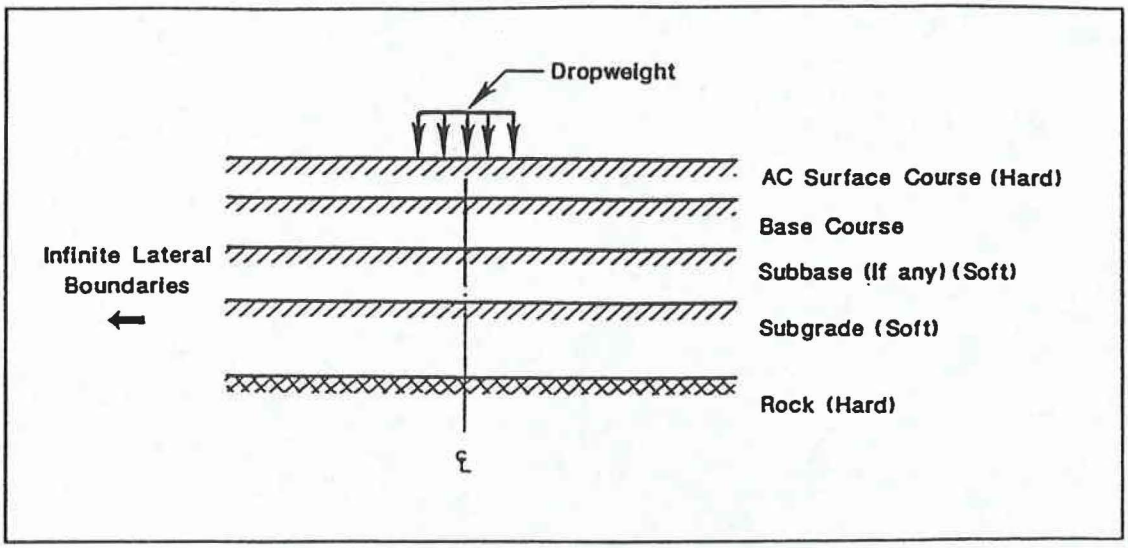

Figure 10. Idealized (As Modeled) Hard-Soft-Hard (H-S-H) Pavement

Frequency Ranges

The pavement section frequency response functions have four main frequency ranges, each with its own physical characteristics and significance as described below:

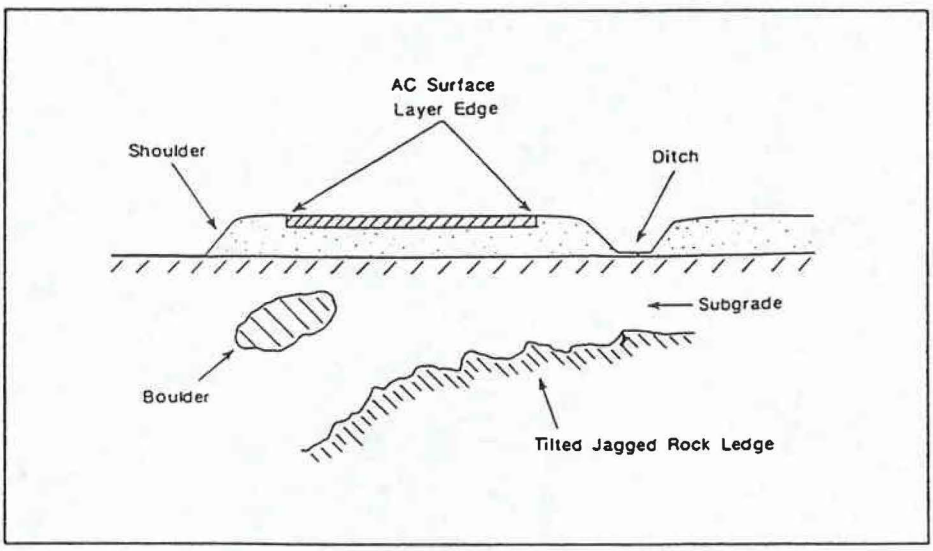

Figure 11. Pavement Section Irregularities not Accounted for in the Multi-Layered Pavement Model

- <u>0-9 Hz</u>: **Very Low Frequency Range**

Computed responses from the SCALPOT program (described in the next Chapter) are unrealistic here because of limitations of the 3-parameter creep model used for the AC layer. The three-parameter model is invalid for very low frequencies, where it is too compliant and the displacements are overpredicted. (See Appendix B for a discussion of AC creep compliance.)

- 10-35 Hz: **Low Frequency Range**

Upper subgrade, lower subgrade, and bedrock layer moduli tend to dominate responses in this range because of long wavelengths and deep penetration of the surface wave into the bottom.

- 35-75 Hz: **Middle Frequency Range**

The hard-soft-hard pavement magnitude peak usually occurs in this region. Data for some sites is dominated in this frequency range by a dip followed by a peak for magnitude data or a peak for the phase angle. These features were analyzed in detail in Magnuson (1992). These features are tentatively attributed to lateral modal vibrations caused by the finite width of the pavement, as described earlier.

- 75-120 Hz: **High Frequency Range**

The AC section layer and base course tend to dominate responses in this range because the wavelengths are shorter with shallower penetration into the bottom. This frequency range is usually the most important in back-calculation. It is the range most sensitive to the AC surface layer creep properties that are related to pavement life.

Responses as Surface Waves

The frequency response functions represent, in effect, surface waves or Rayleigh waves that propagate as ring waves on the pavement surface, not unlike ripples in a pond resulting from a dropped stone (Lamb, 1904). The transient surface waves resulting from the FWD dropweight force impulse are shown in Figures 12-a and 12-b. A three-dimensional view is in Figure 12-a and a cross-section of a surface wave is shown in Figure 12-b.

Two steady-state time-harmonic waves propagating in the x-direction are shown in cross-section in Figures 13-a and 13-b. The longer, low frequency surface wave in Figure 13-b penetrates to deeper depths, while the short high frequency wave in Figure 13-a has a shallower surface penetration. This means that the high frequency data is more sensitive to the AC surface layer and, to a lesser extent, the base course. The low frequency waves are dominated by the deep sub-subgrade and, to a lesser extent, the subgrade layer.

Summary of Pavement Frequency-Domain Analysis

Pavement Frequency-Domain Analysis is used to characterize, i.e., completely describe, the pavement's linear dynamic response. It is useful for insight into modal effects. Vertical and transverse modal effects are present in the FWD frequency data. The modal analysis data can be used to determine the overall pavement type, i.e. whether it is Hard-Soft-Hard (H-S-H), Hard/Soft (H/S), or Soft/Hard (S/H). Vertical modal data in the frequency response functions can also be used to subdivide the subgrade layer to determine the depth to bedrock, or depth to the lower (hard) subgrade sublayer.

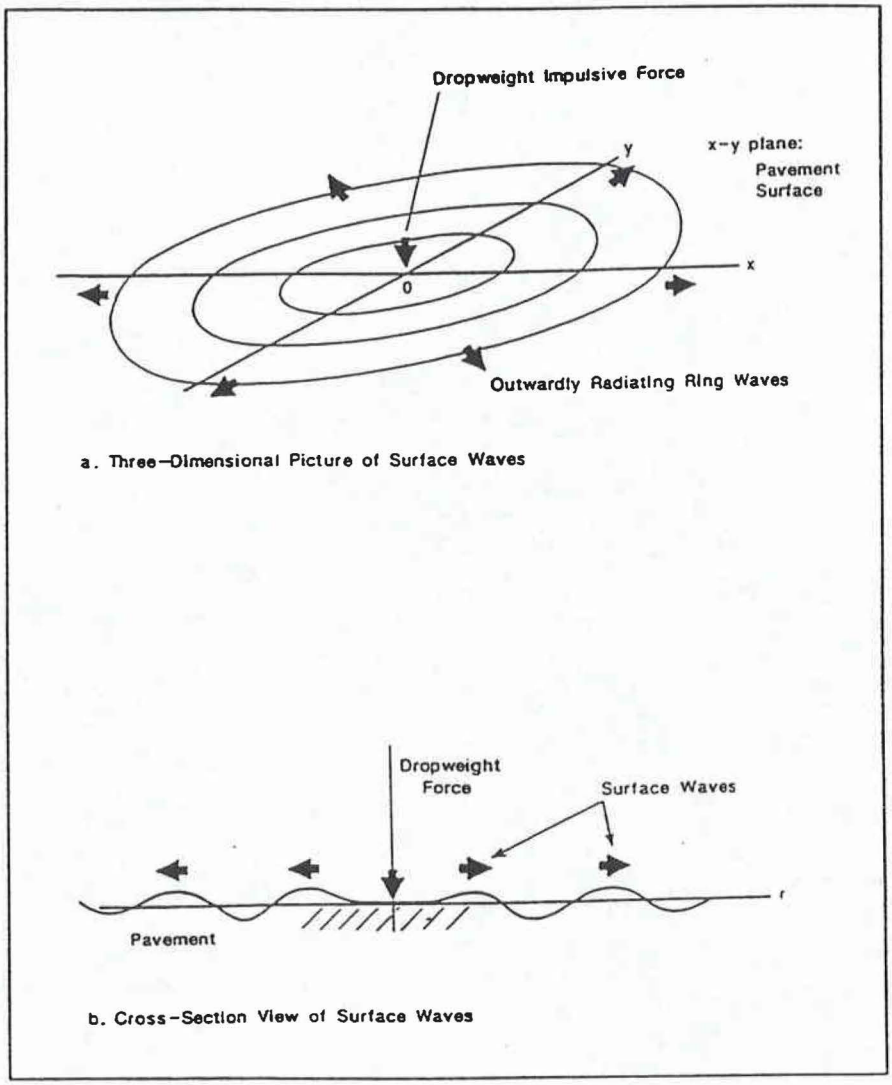

Figure 12. Surface Waves on Pavement
a.) Three-Dimensional View of Surface Waves
b.) Cross-Section of Surface Wave

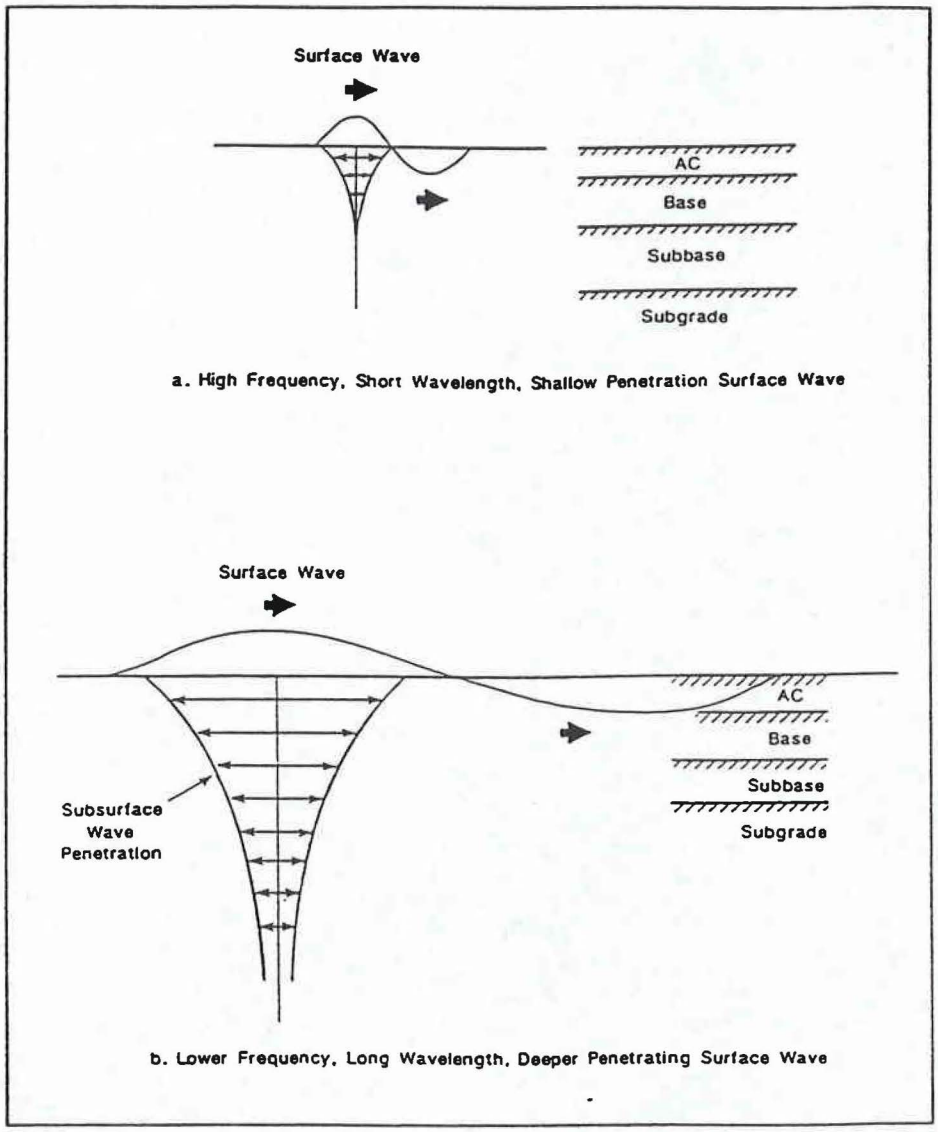

Figure 13. Surface Wave Penetration into the Pavement Subsurface:
a.) High Frequency, Short Wavelength Surface Wave
b.) Lower Frequency, Long Wavelength Surface Wave

CHAPTER III
PAVEMENT DYNAMIC ANALYSIS PROCEDURE

The TTI/TxDOT FWD pavement dynamic analysis procedure consists of (in effect) three computer programs: FWD-FFT, SCALPOT and PAVE-SID. These computer programs are described briefly below.

FWD-FFT Program

The FWD-FFT program performs the frequency analysis of the FWD time history data (Magnuson, 1988a). A preprocessor program computes the pulse "tail correction," performs a spatial statistical analysis (averaging the pulse data over the ten stations at each site), and plots the results. The main program computes the pavement frequency response functions using a fast Fourier transform (FFT) algorithm, performing a complex division of the seven displacement FFTs by the force FFT.

SCALPOT Program

The SCALPOT program computes pavement deflection frequency response functions given pavement layer properties. In SCALPOT each layer can be characterized as a damped "elastic" solid or as a viscoelastic material using a three-parameter creep compliance function as described in Appendix B. The SCALPOT program is described in Magnuson, 1988b, and Magnuson, Lytton and Briggs, 1991. The multi-layering algebra for the viscoelastic halfspace is given in Magnuson, 1975.

PAVE-SID Program

The PAVE-SID program performs an iterative computerized back-calculation procedure to extract pavement layer properties. The PAVE-SID program development is described in

Torpunuri, 1990. The SID program uses the frequency response functions generated by FWD-FFT and sensitivity matrix data generated by SCALPOT.

PDAP: Pavement Dynamic Analysis Procedure

The above three programs and how they interact in the iterative back-calculation process is described in Appendix C, a users manual for the TTI pavement dynamic analysis procedure.

EXTRACTION OF PAVEMENT LAYER PROPERTIES

The problem is this: one cannot directly measure pavement layer properties when given deflection data. The SCALPOT program is a solution to the forward problem as indicated in Figure 14. The forward problem can be stated as follows:

"Given the pavement layer properties, compute the surface displacements."

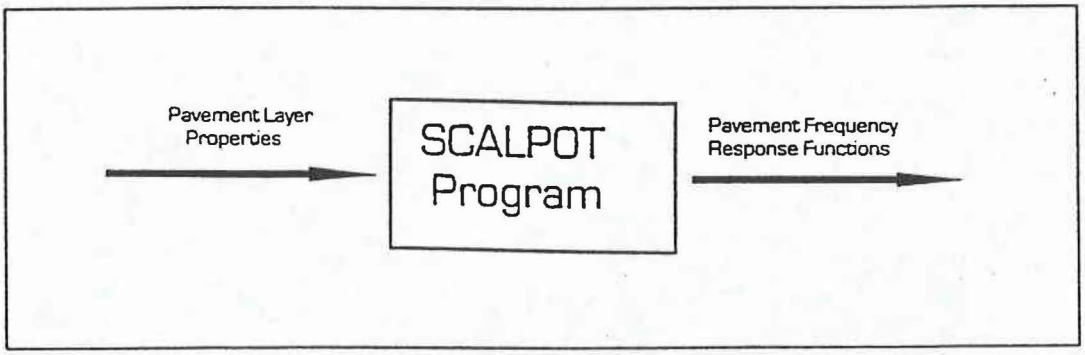

Figure 14. Solution to the Forward Problem for Pavement Dynamics

This is the usual way engineering boundary-value problems are formulated and solved. Unfortunately, this is the reverse of what is usually needed.

What is needed is a direct solution to the pavement layer property problem, or the solution to the inverse problem as indicated in Figure 15. The inverse problem is stated as:

"Given pavement deflection data, compute pavement layer properties."

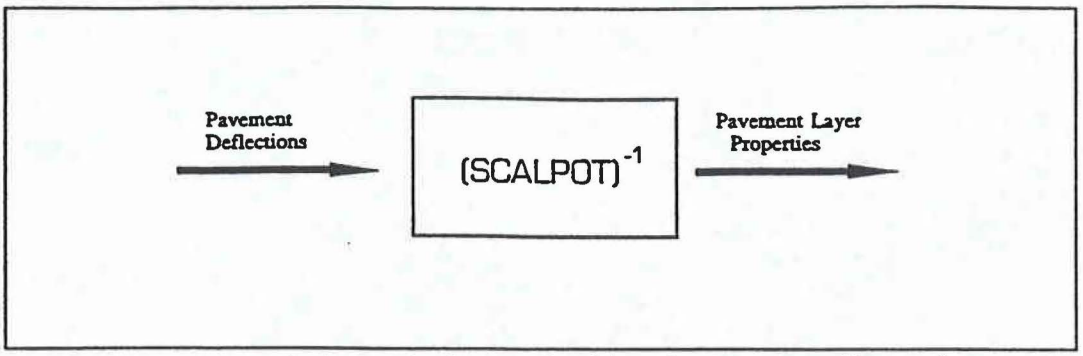

Figure 15. Solution to the Inverse Problem for Pavement Dynamics

Mathematical solutions to inverse problems are more difficult to obtain than forward solutions. Solutions for the inverse problem for three-dimensional wave problems have not been developed; therefore, indirect iterative back-calculation procedures must be used.

Inversion Procedure

The simplest inversion process is to use trial and error: i.e., assume or estimate values for the input parameters and compute the responses using a solution to the forward problem (e.g. the SCALPOT program). The computed responses are then compared to the FWD or field data. The initial input variables in the forward problem are then modified using physical "rules" to improve agreement with the field data and the response is then re-computed. This process is repeated until satisfactory agreement with the field data is achieved. The trial-and-error phase was used in this study to obtain initial estimates of the layer properties for use in the SID computations. The pavement section configuration (i.e. subgrade sublayering) is also established in the trial-and-error process.

The computerized (SID) inversion or back-calculation process for FWD dynamic analysis is shown schematically in Figure 16. This process uses all three computer programs: FWD-FFT, SCALPOT, and PAVE-SID. The FWD-FFT program computes pavement frequency response functions for comparison with computed values. The PAVE-SID program is used to compute updated incremental values for the back-calculated pavement layer properties. For input data, the PAVE-SID program uses the pavement sensitivity (gradient) matrix, which is generated by repeated runs of SCALPOT after successively incrementing the input parameters of interest.

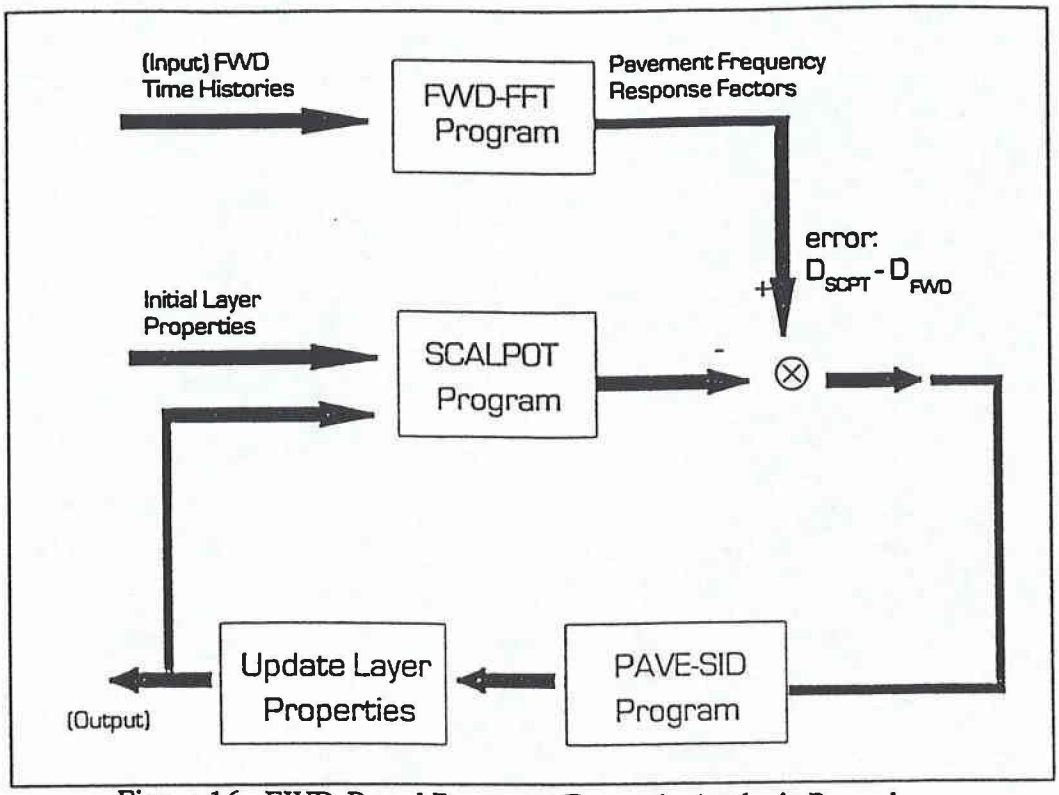

Figure 16. FWD-Based Pavement Dynamic Analysis Procedure Block Diagram

AC MATERIAL CREEP COMPLIANCE

Creep compliance data is customarily acquired in the laboratory from unconfined constant stress compressional creep tests of AC core samples. As mentioned above, the log-log slope (m) of the AC creep curve is the key element in predicting pavement remaining life. A typical AC material creep curve and its log-log slope are shown in Figure 17. The creep curve has a characteristic sigmoidal shape, where the response has three parts or regions.

- The small time elastic response, or glassy response (due to glassy phase of the asphaltic binder).

- The intermediate sloping region caused by delayed elastic (i.e. viscoelastic) response and/or irreversible viscoelastic response. The maximum slope (m) of the curve (on a log-log plot) is indicated in the Figure.

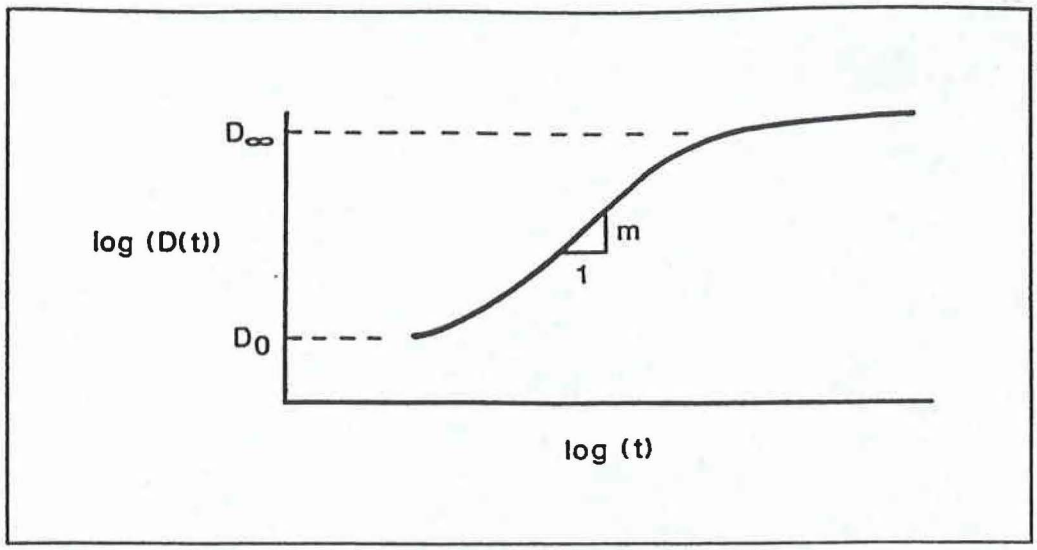

Figure 17. AC Creep Compliance Function Plotted on a Log-Log Scale

- The large time limiting response, corresponding to the setting of the AC mixture. Here the material is less stiff than the glassy phase.

Effective Modulus

For comparative purposes, an effective modulus for the AC material can be computed from the back-calculated creep data. This is useful to compare with resilient modulus data. The effective modulus is defined in Appendix B using the nominal 20 msec loading time of the FWD pulse. The effective modulus is roughly equivalent to the resilient modulus, although its value is somewhat higher because the resilient modulus (usually) uses a loading time of 100 msec. Additional information (equations, etc.) on two, three, and four-parameter creep compliance functions is also given in Appendix B.

BACK-CALCULATION FOR LAYER PROPERTIES

There are two stages to the FWD dynamic back-calculation process.

- **Trial-and-Error Procedure**
- **The Systems Identification (SID) Computerized Procedure**

The Trial & Error Back-Calculation Procedure

This process is used to obtain the initial pavement configuration, particularly with respect to subdivision of the subgrade and the possible presence of near-surface bedrock. It is also used to obtain a first approximation to the pavement layer properties to be back-calculated. The process is graphical and is based on data overlay plots. The SCALPOT generated predicted frequency response functions are repeatedly plotted over the FWD-FFT-generated FWD frequency response functions while varying the properties being back-calculated. The final trial-and-error overlay plots for all 24 sections are given in Appendices D, E, and F.

In the T&E back-calculation process the pavement layer moduli and unknown layer thicknesses are systematically modified to improve agreement between computed responses and FWD field data. From the above observations on pavement frequency response functions, the following "rules" for T&E back-calculation can be listed.

Useful Observations for Trial & Error Back-Calculation

- An increase in the modulus of any layer results in a decrease in the pavement deflection's magnitude and phase angle.

- The responses at lower frequencies (approx. 5 to 35 Hz) are dominated by the stiffnesses (moduli) of the deeper layers (i.e. for H-S-H sections, the lower subgrade and to a lesser extent, the upper subgrade).

- The responses at higher frequencies (75-120 Hz) are more sensitive to AC surface layer stiffness (or creep parameters) and, to a lesser extent, the base course modulus.

- The shape of the magnitude curve in the 35 to 75 Hz range is governed by the moduli of the intermediate layers (i.e. the subbase, if any, and the top subgrade sublayer). An interference effect tentatively attributed to lateral mode vibration may appear in this frequency range.

- Excessive separation between the computed r = 0 and r = 1 ft. magnitude plots usually indicates that the base course modulus is too low relative to the AC modulus.

- The AC layer log-log slope (m) governs the overall slope of the r =0 magnitude curve (with respect to frequency). Steeper FWD magnitude slopes indicate higher m values.

- Magnitude plots of FWD data for H-S-H pavements have a peak for the outer sensors in the 20-60 Hz range, as shown in Figure 8-a. The magnitude of the computed peak and its location on the frequency axis can be adjusted by varying the upper subgrade modulus and the upper subgrade layer thickness, respectively. The peak frequency of the magnitude plots for the outer sensors increases as the thickness of the upper subgrade layer decreases, as illustrated in Figure 18. The height of the peak can be varied by varying the contrast or differences in moduli between the hard upper layers, the soft upper subgrade, and the hard lower subgrade layer. An increase in contrast gives an increase in the peak. This effect is shown in Figure 19.

There is a limit as to how good the agreement between predicted and FWD data can be achieved with T&E back-calculation. At some point one can improve agreement for one feature of the curves only at the expense of other features, so no overall improvement is achieved. For the sites analyzed here, the T&E procedure took approximately 3 to 10 SCALPOT runs per site.

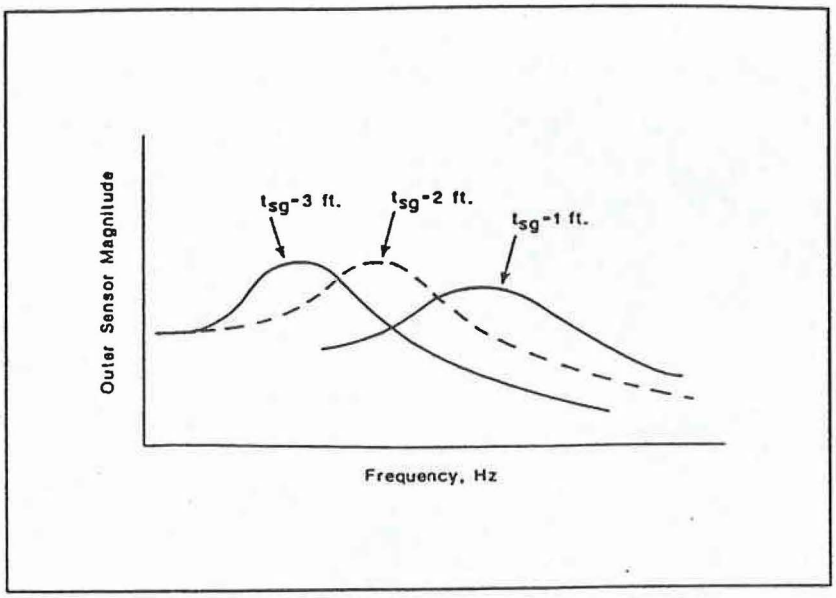

Figure 18. Effect of Upper Subgrade Thickness on Magnitude of Outer Sensor Frequency Response Functions

Any significant improvement over these T&E results can only be done with a computerized procedure: i.e., a SID program.

One can also use static back-calculation (using, e.g., Modulus II Program, in Uzan et al., 1988) to obtain initial estimates of layer moduli for the SID back-calculation stage. At some point in the future, when more experience has been gained, the trial-and-error back-calculation procedure can be automated using expert systems techniques.

The Systems Identification (SID) Back-Calculation Procedure

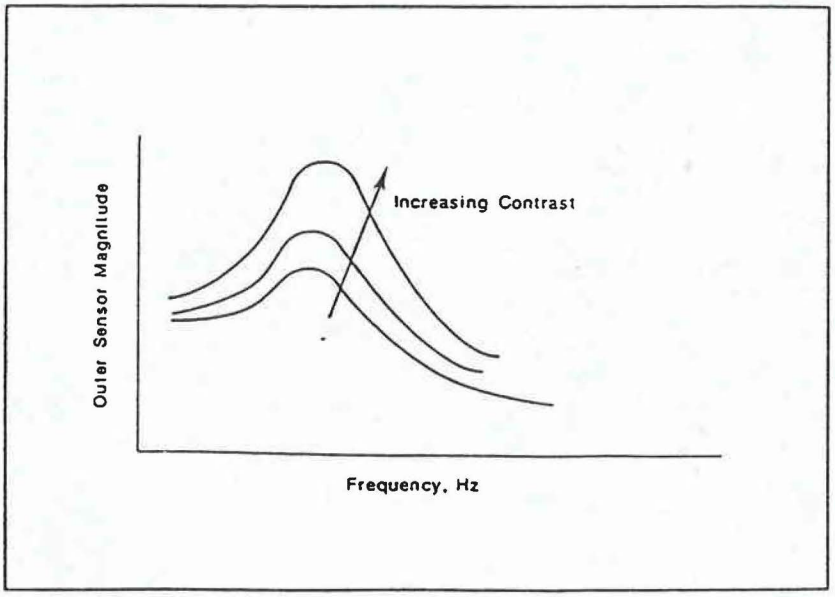

Figure 19. Effect of Modulus Contrast on the Magnitude of the Outer Sensor Frequency Response Functions.

Figure 16 shows the SID back-calculation procedure in block diagram form. SID back-calculations on the 24 Texas sites using PAVE-SID were performed in Summer, 1992. However, a joint SHRP A-005/ TxDOT 1175 computer program comparison/validation study was conducted in Fall, 1992. As a result of the study, some algebraic errors were found to be coded into the SCALPOT program. These were corrected in January 1993. Consequently, the earlier PAVE-SID back-calculation results were invalid, and the SID computations were rerun for only three sites, using two different programs.

Three SID procedures have been developed at TTI. They are listed as follows.

- PAVE-SID (V. Torpunuri, 1990)
- JACOB-SID: Dr. J. Uzan's program (Lytton, 1992)
- FUSID: Dr. F. Wang's procedure (Wang & Lytton, 1993; see Appendix C)

To expedite the computations, the SID procedures developed by J. Uzan and F. Wang were used. The JACOB-SID program was also used to analyze 24 sections for the SHRP A-005 Project (Lytton, 1992). The FUSID procedure was developed to back-calculate laboratory data for the SHRP A-005 Project (Wang and Lytton, 1993). The FUSID procedure was adapted for use on FWD dynamic analysis in January 1993. (See Appendix C: Users' Manual for Pavement

Dynamic Analysis Procedure (PDAP)). The FUSID procedure is much more convenient to run than the original PAVE-SID procedure.

The JACOB-SID program used a DEC workstation computer and the UNIX operating system. The JACOB-SID program was used on one Project 1175 site.

Both the PAVE-SID and FUSID procedures are performed on IBM/PC/AT compatible desktop computers using the DOS operating system. The trial-and-error pavement layer back-calculation results described above are intended for use as the first approximation (i.e., seed values) in the iterative SID back-calculation procedure. Because of time limitations, the full SID procedure was done on only three sections: D01S3, D08S3, and D08S1. For the rest of the sections, only the trial-and-error results are presented here.

The SCALPOT Input Data Set

The SCALPOT program computations require a set of physical data for each of the pavement layers. Thicknesses of the AC surface layer, base course, and subbase were taken from Projects 1123 and RF7026 drillers logs (Lytton et al., 1990). Weight density data was taken from Project 1123 laboratory data sheets. Poisson ratios were assumed. If necessary, for H-S-H sections subgrade sublayer thicknesses were T&E back-calculated. Damping ratios for the "elastic" lower layers were assumed. Values for the moduli and creep compliance constants were back-calculated using initial estimates to start the iterative back-calculation process.

CHAPTER IV

PAVEMENT LAYER BACK-CALCULATION RESULTS

To facilitate interpretation of the results, the 24 sections were separated into three groups based on AC layer thickness: thick, medium, and thin. There were seven thick sections, five medium, and twelve thin. Averaged values of section properties for the three groups are shown in Table 3.

Table 3

Averaged Pavement Data Based on AC Layer Thickness

Rel. AC Thk	No. of Sections	AC Layer thk (ft)	Max Defl mils/10kip	Surface Temp (F)
Thick	8*	0.69	14	89
Medium	5	0.48	37	106
Thin	12	0.14	53	105

* Site D01S5 was tested at two temperatures.

Note from Table 3 that the thick sections happened to have significantly lower (16-17 deg F) average temperatures than the medium and thin sections. The lower temperatures were probably the cause of the much lower average maximum deflections for the thick sections.

Back-Calculation Results

For all sites, the following pavement layer properties were back-calculated using the procedure described in Chapter III.

- **AC Layer Creep Compliance Parameters** (D_0, D_1, and m, as defined in Appendix B.)
- **Base Course Modulus**
- **Subbase (If Any) Modulus**
- **Upper Subgrade Modulus**
- **Lower Subgrade Modulus**

PAVEMENT LAYER PROPERTIES

Values of the back-calculated pavement layer properties for each section are presented in Tables 4, 5, and 6 for the thick, medium, and thin pavements, respectively. Additional layer data is also given to aid in the interpretation of the results. The data in each Table appears as follows.

- Column 1: Site, date of final back-calculation, and comment on agreement of FWD frequency response function data
- Column 2: Layer thicknesses in ft.
- Column 3: Back-calculated layer moduli in psi.
- Column 4: Back-calculated log-log slope (m) of the creep curve (for viscoelastic layer only)
- Column 5: Descriptions of layer materials and FWD test temperatures

DISCUSSION OF RESULTS

Temperature Dependence of AC Moduli

The effect of temperature on the effective modulus of the AC layers for the thick and medium sections is shown graphically in Figure 20. While there is some scatter, the linear least-squares fit shows a marked decrease of modulus with temperature, as would be expected. The scatter is due to mix variation, pavement
age differences, and measurement error. Average values and maxima and minima are given below:

Thick Pavement AC Effective Moduli

Average = 516,000 psi
Maximum = 1,000,000 psi
Minimum = 85,000 psi

Temperatures

Average = 89.4° F
Minimum = 86° F
Maximum =102° F

Medium-Thick Section AC Moduli

Average = 96,000 psi
Maximum = 260,000 psi
Minimum = 30,000 psi

Temperatures

Average = 105.6° F
Minimum = 91° F
Maximum = 116° F

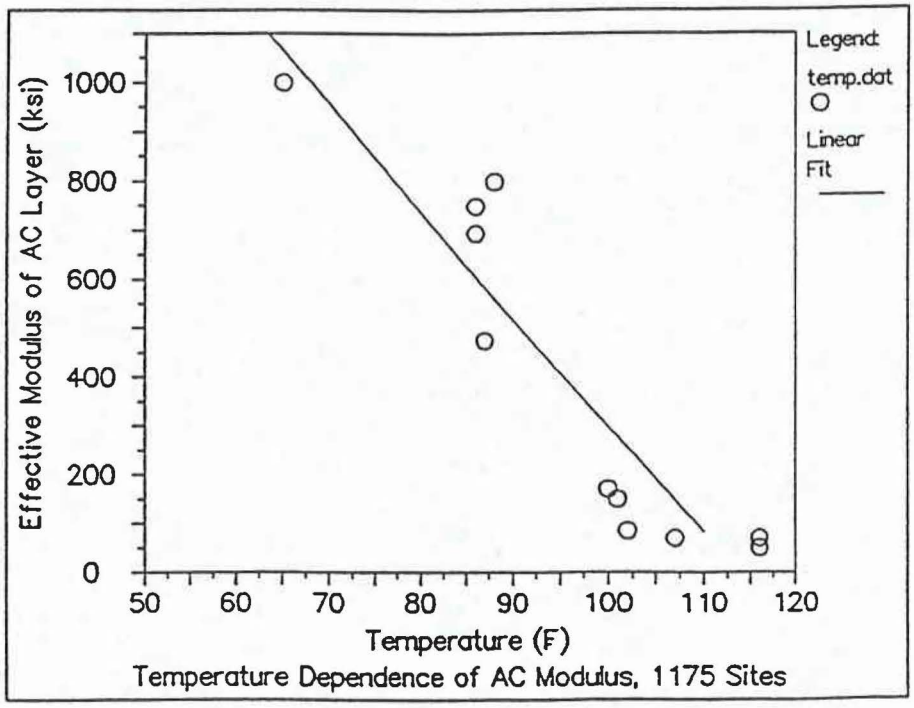

Figure 20. Effect of Temperature on AC Layer Effective Modulus

Table 4
Thick Pavements: Back-Calculated Pavement Layer Properties

Site Number	Layer Thickness (ft)	Layer Modulus (psi)	m V-E exp	Layer Description
1. D01S3	1.0	695,200	0.25	HMAC: avg surf temp 86.3 F
(6/30/92)				at TCs: 85 F at TC1
excell	1.83	15,000	-	Base: sandy
	1.67	18,100	-	SG1: clay
	inf	23,000	-	SG2: clay
2. D01S5				
a. warm	0.75	171,400	0.25	HMAC: at TCs: avg surf temp 100 F
(6/17/92)				Surf: 104 F, 94 F at TC1
good	0.58	29,860	-	Base: sandstone
	0.83	15,970	-	SB: treated (lime)
	inf	16,000	-	SG: clay, SSG: sandy to 14 ft.
b. cool	0.75	1,000,000	0.25	HMAC: TC surf temp 65 F, TC1(9") 62 F
(7/08/92)	0.58	29,860	-	Base: sandstone
excell	0.83	15,970	-	SB: treated (lime)
	inf	21,000	-	SG: clay, SSG: sandy to 14 ft.
3. D08S3:	0.42	750,000	0.35	HMAC: avg surf temp 86 F
(7/08/92)	1.5	50,000	-	Base: limestone
excell	4.32	30,000	-	Subgrade: sand
	inf	30,000	-	SG2: rock at 6.5 ft
4. D08S4	0.833	476,000	0.25	HMAC: avg surf temp 87 F
(6/30/92)	0.917	83,330	-	Base + Subbase: crushed limestone
excell	1.0	15,000	-	SG: clay
	3.0	20,830	-	SG: clay, SSG: sandy clay
	inf	41,670	-	SSG2: rock at 8.5 ft.
5. D08S5	0.67	150,000	0.35	avg surf temp 101 f: 101 F at TC1
(7/07/92)	1.08	41,670	-	Base: red limestone
good	6.0	22,000	-	SG: clay
	inf	25,000	-	sandy: water at 12.5 ft
6. D11S2	0.65	85,000	0.35	AC (4 sublayers): avg surf temp 102 F
(7/08/92)	1.15	41,700	-	Base: iron ore gravel
gd/excel	inf	13,900	-	SG: sand to 15 ft
7. D11S7	0.458	800,000	0.25	1.5" surf trt + 4" asph base:
(7/08/92)				avg surf temp 87.7 F
excell	0.792	400,000	-	Base 2: 10.5" 6-7 % cement-trt. Sand
	10.0	22,000	-	SG: sand ?
	inf	38,000	-	SSG: sand ?

Table 5

Medium Thickness Pavements:
Back-Calculated Pavement Layer Properties

Site Number	Layer Thickness (ft)	Layer Modulus (psi)	M V-E Exp	Layer Description
1. D01S4 (6/30/92)	0.292	30,000	0.50	HMAC: avg surf temp 98° F at TCs: Surf: 96 F
good	0.5	30,000	0.50	B: Oklahoma rock base (combined AC+Base)
	3.0	14,000	-	SG: sandy clay
	inf	16,000	-	SSG: clay to 11 ft.
2. D11S1 (7/13/92)	0.74	70,000	0.50	3" AC + 4.2" asph trt sand + 1.7" AC avg surf temp 107 F
excell	0.66	10,000	0.50	SB: sand
	2.0	30,000	-	sandy clay with gravel
	inf	35,000	-	silty clay with groundwater to 13.4 ft.
3. D21S3 (7/06/92)	0.187	260,000	0.25	HMAC: avg surf temp 90.9 at TCs: Surf: 93 F (air). 97 F at TC1
good	0.353	260,000	0.25	Base 1: asphalt treated (Combined AC+Base 1)
	0.50	40,000	-	Base 2: lime treated flex
	1.26	30,560	-	Subbase: lime treated
	inf	25,000	-	SG: sand
4. D21S4 (7/06/92)	0.333	50,000	0.25	HMAC: avg surf temp 116 F: at TCs: 100 F at TC1
good	0.42	50,000	-	Base: lime treated calacie (flex)
	4.50	8,000	-	SG1: clay
	inf	10,420	-	SG2: clay: groundwater at 11 ft.
5. D21S5 (7/13/92)	0.5	70,000	0.35	HMAC avg surf temp 116 F @TCs:108 F at TC1:(2" overlay+2"asph)
excell	0.5	40,000	0.35	Base: calacie flex
	4.0	13,890		SG1: dark sandy clay
	3.5	8,330		SG2: dark sandy clay
	inf	15,000		SG3: dk sandy clay: groundwater @8.5 ft.

Table 6

Thin Pavements:
Back-Calculated Pavement Layer Properties

Site Number	Layer Thickness (ft)	Layer Modulus (psi)	m V-E exp	Layer Description
1. D01S1	0.146	1,000,00	0.50	HMAC: avg surf Temp: 89° F
(6/29/92)	0.4375	100,000	0.50	Base: crushed limestone
excell	8.0	13,890	-	SG1: sand
	inf	15,000	-	SG2: silty sand to 14 ft.
2. D08S1	0.75	25,000	0.35	HMAC: avg surf temp 108° F
(8/04/92)				Base: limestone (combined AC+base)
excell	4.00	12,900	-	SG: sand
adj. SID	inf	20,560	-	SSG: white sandy w/ limestone to 12 ft.
3. D08S2	0.25	20,000	0.5	HMAC: avg surf temp 118° F
(7/13/92)	0.42	15,000	0.5	Base: pit run
good	6.0	24,000	-	SG: sand
	inf	26,000	-	SSG2: sandy clay w/ water to 10 ft.
4. D08S6	0.08	40,000	0.50	HMAC: 1" seal coat: avg surf temp 97° F
(6/23/92)	0.75	40,000	0.50	Base: limestone(combined AC+Base layer)
excell	2.0	10,000		SG1: clay
	inf	20,000		SG2: clay w/ water to 10.75 ft.
5. D11S3	0.17	50,000	0.50	HMAC: avg surf temp 113° F
(7/06/92)	0.58	60,000	0.50	Base: crushed limestone
good	0.48	27,780		SB: iron ore gravel
	8.0	22,000		SG: sand (6 ft thk)
	inf	22,920		SSG: sandy clay to 11 ft.
6. D11S4	0.10	15,000	0.50	1" seal coat: avg surf temp 101° F
(7/08/92)	0.775	15,000	0.50	Base: 9.5" iron ore gravel
ok				(combined AC+Base)
	1.0	18,000		SG: sandy clay w. silt
	2.0	25,000		SG: sandy clay w. silt
	5.0	33,000		SG: sandy clay w. silt
	inf	40,000		SSG: sandy clay w. gravel to 13.8 ft.
7. D11S5	0.10	40,000	0.50	AC (1" surf trt):avg surf temp 88.5° F
(7/07/92)	0.80	40,000	0.50	Base: 10" iron ore gravel
good				(combined AC and base)
	2.0	20,000		SG: silty sand
	8.0	12,000		SG: silty sand
	inf	10,500		SSG: ditto (hole caves in at 12 ft).

Table 6, Continued

Site Number	Layer Thickness (ft)	Layer Modulus (psi)	m V-E exp	Layer Description
8. D11S6	0.166	27,100	0.50	AC (2" surf trt):avg surf temp 114.8° F
(7/06/92)	0.666	27,100	0.50	Base: 8" 4 % cement-trt iron ore
good				(combined AC+Base)
	2.0	20,000		SG1: 2" untrt iron ore + ? SG
	6.0	25,000		SG2: ?
	inf	80,000		SSG: ?
9. D11S8	0.125	40,000	0.60	AC(1.5" surf trt):avg surf temp 105.6° F
(7/08/92)	0.666	40,000	0.60	Base: 8" 6-7 % cemxt-trt. sand
good				(combined AC+Base)
	4.0	15,000		SG: sand ?
	inf	50,000		SSG: sand ?
10. D21S1	0.46	35,000	0.35	comb: 0.1 ft AC+.36 ft calacie flex
(7/16/92)				Base: avg surf temp 101.8 F
good				at TCs: Surf: 105 F, 100 F at TC1
	0.37	10,000	0.35	Subbase: lime trt salvage
	9.00	10,000		SG1: sand
	inf	12,000		SG2: sand: groundwater at 10 ft.
11. D21S2	0.75	15,000	0.25	AC: avg surf temp 107 F
(6/16/92)				at TCs: Surf: 105 F, 122 F at TC1
good				Comb:AC+Base:1" surf trt+calacie flex
	0.33	17,360		SG1: clay
	5.00	6,940		SG2: clay
	inf	9,000		SG3: clay: groundwater at 11 ft.
12. D21S6	0.25	15,000	.50	HMAC: avg surf temp 115 F
(7/08/92)				@TCs: 119 F at TC1, 101 F at TC2
good	0.583	10,750	0.50	Base: calacie
	3.5	10,000		SG: sandy clay
	inf	17,000		SSG: sandy clay (more clay)
				(no gw to 12 ft.)

Log-Log Slope (m) Values

In the T&E back-calculation the log-log slope (m) was initially assumed as m = 0.25 as this is an average value. The VE/Elastic ratio (α) was fixed as 30 throughout, based on recent laboratory results from SHRP A-005 data. The high value of α signifies that the AC viscoelastic

response is predominantly viscous. Ranges of back-calculated m for the three groups are shown below.

Log-Log Slope (m)

Layer	m range
Thick:	0.25-0.35
Medium:	0.25-0.50
Thin:*	0.25-0.60

* Combined AC Seal Coat and Base Course Layer

Base Course and Subgrade Moduli

Unbound Base Course Moduli

Average (all sections) = 39,200 psi
Maximum = 100,000 psi
Minimum = 11,000 psi

Upper Subgrade (SG1) Moduli

Average = 17,500 psi
Maximum = 30,000 psi
Minimum = 8,000 psi

Lower Subgrade (SG2) Moduli (for (H-S-H) sections only)

Average = 27,000 psi
Maximum = 80,000 psi
Minimum = 10,000 psi

The base course and upper subgrade modulus values fell within the expected typical ranges for the respective pavement layers. The lower subgrade modulus values are considerably higher than the upper subgrade values. The higher moduli indicate a stiff subgrade sublayer. Causes of the stiffer layer are discussed in Chapter V. A quantitative comparison of moduli using laboratory data taken from samples is given in Chapter VI.

Upper Subgrade Thickness

Upper subgrade thickness was computed by T&E back-calculation for H-S-H sections where the subgrade was subdivided. Figure 21 shows how the thickness of the upper subgrade

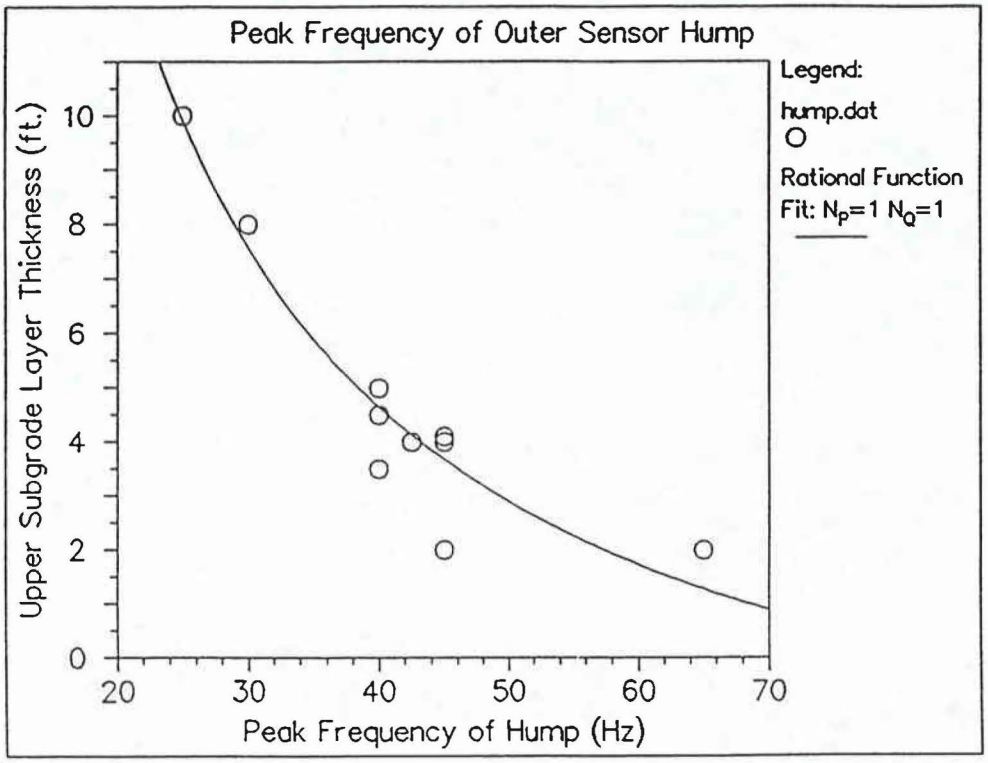

Figure 21. Effect of Outer Sensor Magnitude Peak Frequency on Upper Subgrade Layer Thickness

layer varies with the outer sensor magnitude peak frequencies. In this plot, the sites with the most pronounced H-S-H configurations were used. One sees from the least-squares fit that the layer thickness decreases as the peak frequency increases. This is what one would expect, as the high frequencies correspond to shorter times; therefore, a wave passing down through the soft upper sublayer and reflecting off the stiffer layer will take more time to arrive at the surface as the thickness of the soft layer increases. This was shown in Figure 6-c. The thicker layer will have the lower peak frequency.

There is some scatter in Figure 21 because for some sites there was more than one soft layer in-between the hard surface layers and the hard lower subgrade layer. The rational

function fit in Figure 21 can be used to estimate upper subgrade thickness directly from FWD pavement frequency response function magnitude plots.

Figure 21 can be used in static back-calculation studies if the time history data is recorded. Then the FWD-FFT program can be used to compute the FWD frequency response functions. This would give a more accurate layering representation for the sites, which will result in more accurate statically back-calculated moduli. This may be a good way to initiate implementation for pavement dynamic analysis.

TREATMENT OF THE AC LAYER SECTIONS

There were nine sections where the AC layer was a surface seal coat two inches or less in thickness. It was felt that for these sections the AC binder had negligible effect on the stiffness of the combined AC-base course layer. This seems reasonable, especially when the average temperature of these sections was over 100° F. Therefore, the AC seal coat and granular base course layers were combined and treated as one in the back-calculation process. The sections with combined AC and base course were as follows.

- D01S4
- D08S1
- D08S6
- D11S4
- D11S5
- D11S6
- D11S8
- D21S1
- D21S2

In the back-calculation it was necessary to treat the combined surface layer as a viscoelastic material instead of as a damped elastic solid. This was necessary to obtain good agreement with the r = 0 magnitude data in the frequency response functions. (This will be discussed in Chapter V.) The viscoelastic behavior of the combined layer course was not expected because six of the sites had an unbound base course. The log-log slopes (m) of the creep curves of the combined layers averaged

$$m = 0.5,$$

about twice that of the sections having thicker AC layers. The m value is probably due to Coulomb or dry friction rather than viscous friction.

A Canadian study (Holubec and Wilson, 1970) of unbound aggregate base course permanent deformation during cyclic loading measured the permanent deformation as a function of number of load cycles. The results indicated that the base course acted as an irreversible viscoelastic material. Irreversible viscoelastic behavior is associated with rutting. Kenis (1978), in his VESYS program, used his "mus and alphas" to measure irreversible viscoelastic behavior in all the pavement layers. These results imply that unbound soil materials also have reversible viscoelastic behavior. This is consistent with the m values found in this study. The back-calculated m is probably mostly due to reversible viscoelasticity.

The values of effective moduli of the combined layers were consistent with those of the unbound base courses of the stiffer sections, averaging about 30,000 psi. Data on each of the combined sections and averages are given in Table 7 below. Column 1 gives the site, and column two gives the average surface temperature at the time of the FWD test. Column three shows the thickness of the combined (AC plus base course) layer, while column four gives the back-calculated effective modulus (E_{eff}), as defined in Appendix B. Column five gives the back-calculated log-log slope (m), and finally, column six is a description of the base course material. Average values of temperature, thickness, modulus, and m were computed for the nine sites. The results are given at the bottom of Table 7.

Table 7

Properties of Combined AC and Base Course Layer

Site	Temp (F)	Tot.Thk (ft)	Eeff (psi)	m (slope)	Base Material
D01S4	98	0.79	30,000	0.5	Okla. rock
D08S1	108	0.75	25,000	0.35	Limestone
D08S6	97	0.83	40,000	0.5	Limestone
D11S4	101	0.88	15,000	0.5	Iron ore gravel
D11S5	89	0.90	40,000	0.5	Iron ore gravel
D11S6	115	0.83	27,000	0.5	4 % cement-trt. iron ore
D11S8	106	0.79	40,000	0.6	6-7 % cement-trt. sand
D21S1	102	0.46	30,000	0.5	Calacie flex
D21S2	107	0.75	15,000	0.25	Calacie flex
Averages (All Sites):	103	0.78	29,100	0.47	----

SECTIONS WITH APPARENT NEAR-SURFACE BEDROCK

For the two sites (D08S3 and D08S4) with bedrock noted in the drillers log, the subgrade was subdivided into upper and lower sublayers with the lowest layer representing the bedrock. The lower (bedrock) sublayer moduli would be expected to show a substantial increase over the upper subgrade moduli. This was the case for the D08S4 site, but the D08S3 site showed no sign of a hard lower subgrade layer.

Back-calculated sub-subgrade modulus values at four other sites show high values indicative of bedrock or some other cause of a stiff layer. These sublayering results are shown in Table 8 below.

Table 8

Subgrade Sublayering Results

Site	Drillers Log Data	Depth to Bedrock (ft.)	Lower SG Modulus (psi)	Upper SG Modulus (psi)	Modulus Ratio (Lower/Upper)
D08S4	rock @ 8.5 ft	5.7	42,000	15,000	2.8
D08S3	rock @ 6.5 ft	-	30,000	30,000	1.0*
D11S7	sand s.g.	11.4	22,000	10,000	2.2
D21S5	clay: g.w.@ 8.5 ft	8.5	15,000	8,300	1.8
D11S6	(no samples)	8.9	80,000	20,000	4.0
D11S8	(no samples)	4.8	50,000	15,000	3.33

* Not subdivided.

The first two columns in Table 8 show the site number and the drillers log data for the subgrade and/or bedrock. The third column shows the back-calculated depth to the lower subgrade sublayer (or bedrock) in ft. The fourth column shows the lower subgrade sublayer modulus in psi. To show the contrast in subgrade moduli with depth, the upper subgrade sublayer modulus is given in column five. The lower/upper modulus ratios are given in the last column. The maximum ratio was 4. Note that for site D08S4, where the driller noted bedrock, the back-calculated depth to bedrock is close to, but does not agree exactly with, the log data. For this site the apparent discrepancy in bedrock depths may be due to the following factors.

- The FWD data may have been taken at a different station with different depth to bedrock than the log data.

- The driller's sensing of bedrock may not be the same as the FWD dynamic surface wave bedrock.

The driller senses bedrock when the drill bit no longer rapidly advances into the soil, i.e., when the material shear strength suddenly increases. The FWD's dynamic wave response to bedrock is based on material stiffness (i.e., moduli, or more properly shear and compressional wave speeds) rather than failure in shear. The layer transitions for shear strength and stiffness may not occur at exactly the same depth.

For Site D08S3, no indication of bedrock was found in the FWD data, in spite of the driller's log note indicating bedrock. The test sites were 100 ft. long, so the bedrock could have varied in depth over the length of the test site, or the driller may have struck an isolated rock in the sand subgrade. This site is analyzed in more detail in Chapter VII.

For sites D11S6, D11S7, and D11S8 no drilling data was available, so no definite explanation for the stiffer subgrades can be made. For site D21S5, groundwater was struck in the clay subgrade at 8.5 ft., close to the (drillers observed) depth to bedrock in Table 8. The saturated subgrade (as indicated by the presence of groundwater) will have a higher compressional wave speed, or a stiffer response, and a higher modulus value than the overlying material.

TEMPERATURE EFFECTS ON AC LAYER: SITE D01S5

FWD tests were run in March,1988, and June 1989, for site D01S5. Surface temperatures were (from Table 1) 64 and 100 deg. F, respectively, giving a temperature difference of 36 deg. F. The FWD back-calculation procedure was used on the FWD data at both temperatures. The back-calculation results for both temperatures are shown in Table 9 below.

Table 9

Site D01S5 Temperature Effect Results

Variable	64 deg F Result	100 deg F Result
AC Layer E_{eff}(ksi)	1000	150
AC Layer V-E Slope (m)	0.25	0.25
Base Course Modulus (ksi)	30	30
Subbase Modulus (ksi)	16	16
Subgrade Modulus (ksi)	21	16

Note the big change in effective modulus of the AC layer due to the 36 deg. F temperature change. The AC modulus was higher by a factor of 6.7 for the lower temperature. The moduli for the base course and subbase remained the same, but the modulus for the clay subgrade at the cooler temperature was higher by a factor of 31 percent. This moderate change in clay subgrade modulus may reflect a change in the clay's (unsaturated) moisture content more than a temperature change per se. Since the site at 64° F had the higher modulus, its moisture content was probably lower. Subgrade moisture was not measured at the time of the FWD tests, so this cannot be confirmed.

Time-Temperature Shift

The viscoelastic data for the AC layer can be corrected for temperature using the time-temperature shift relations given in Appendix B (Fitzgerald and Lai, 1970). The creep compliance curve for any temperature can be shifted horizontally to represent the creep compliance at another temperature. The time-temperature shift can be computed if the temperature susceptibility (ß) is known. The susceptibility is a physical property of the AC mixture characterizing the change in modulus with temperature. The susceptibility was computed for the AC layer using the back-calculated data for both temperatures and the shift relations given in Appendix B. The computed value for the susceptibility was:

$$ß = 0.094.$$

This value of ß falls in the mid-range of values found in the literature (Fitzgerald and Lai, 1970; Sharma and Kim, 1975; and Sherwood and Kenis, 1972), and so it appears to be realistic. This indicates that the temperature susceptibility of an asphalt mix in the field can be computed from nondestructively acquired FWD data. This also means that the AC layer viscoelastic (creep) properties at a given site can be computed for any temperature using back-calculated susceptibilities obtained from FWD tests done at two or more temperatures. There is no need to use externally generated temperature correction factors.

SID BACK-CALCULATION RESULTS

Because of time limitations, the full back-calculation was performed on only three sites. The results of the SID back-calculation are given in Chapter VI.

Back-Calculation Summary

The back-calculated variables are listed below.

- AC Layer:
  - Creep Parameters (D_0, D_1, m)
  - Effective Modulus
- Base Course Moduli
- Subgrade Moduli:
  - Upper Subgrade
  - Lower Subgrade (for H-S-H sections)
- Thickness of Upper Subgrade Layer (for H-S-H sections)

The values for all the back-calculated variables were reasonable, or in the right range, based on published and unpublished data. The temperature susceptibility of an asphalt mix in the field was computed from nondestructively acquired FWD data at two temperatures.

A method for analyzing thin sections was also developed. The thin pavement analysis method consists of combining the seal coat layer with the base course layer, and treating the combined layer as a viscoelastic material. The results were consistent with published data on unbound granular material.

CHAPTER V
GRAPHICAL COMPARISON STUDY RESULTS

The graphical comparison study is based on pavement deflection frequency response function plots given in Appendices D, E, and F for thick, medium, and thin pavements, respectively. Comparison plots of magnitude vs. frequency and phase angle vs. frequency are shown for all sensor locations (r = 0, 1.0, 2.0, 3.0, 4.0, 5.0, and 6.0 ft.). In each figure two separate data sets are plotted:

- Pavement frequency response functions computed from FWD field data using the FWD-FFT program (this data is plotted as solid lines) and

- Computed frequency response data (from the SCALPOT program) using back-calculated layer moduli, AC creep data and subgrade sublayer thicknesses (this data is plotted with symbols).

In Appendices D, E, and F, for each site the graphical comparison between FWD field data and SCALPOT computed responses is shown in four plots given in this order:

- Magnitudes vs. Frequency for the Inner Sensors
  (r = 0, 1.0, 2.0, and 3.0 ft.),

- Phase Angles vs. Frequency for the Inner Sensors
  (r = 0, 1.0, 2.0, and 3.0 ft.),

- Magnitudes vs. Frequency for the Outer Sensors
  (r = 4.0, 5.0, and 6.0 ft.), and

- Phase Angles vs. Frequency for the Outer Sensors
  (r = 4.0, 5.0, and 6.0 ft.).

INTERPRETATION OF THE PLOTS

In evaluating the comparison plots two things must be kept in mind.

- For each site there are fourteen curves to be fit: seven magnitude vs. frequency and seven phase angle vs. frequency plots. All 14 curves must be fit with the same pavement layer dataset. Only 6 or 7 layer properties (moduli, creep data, and thicknesses) are varied in the fitting process. One cannot expect as good agreement as when fitting to just one curve on an x-y plot using perhaps 3 or 4 parameters in a least-squares polynomial or spline fit.

- The computer results in general do not follow the fine features seen in the FWD data. There are numerous dips, peaks, and cusped features in the magnitude and phase angle plots at various frequencies. The computed results can only take into account vertical layered (depth) changes in material properties. Other features may be caused by geometrical or physical irregularities not accounted for in the uniform layered model used by the SCALPOT program. Some of these unaccounted-for features were shown in Figure 11. Perhaps the most important ones are azimuthal asymmetries such as pavement edges.

Hard-Soft-Hard (H-S-H) Sections

The effect of a hard bottom on the pavement frequency response functions can be modeled by the SCALPOT program because it is a vertical layering effect as shown in Figure 10. For hard-soft-hard (H-S-H) sections, the magnitude responses for the outer sensors (usually the r = 4, 5, and 6 ft. sensors) have a peak lying between 20-60 Hz. This was seen in Figure 8 for site D08S4, where the peak was about 30 Hz for all three outer sensors.

Inspection of the back-calculated subdivided subgrade moduli in Tables 4, 5, and 6 shows that 12 of the 24 sections are to some extent H-S-H even in the absence of bedrock detected by the driller. (Recall that the lower subgrade has a larger modulus than the upper subgrade.) The presence of the stiffer lower layer is also indicated in the peaks of the magnitude curve that in turn indicate vertical modal behavior as shown in Figure 6-c.

As was mentioned in Chapter IV, in order to analyze the H-S-H sections, it was necessary to split up the subgrade into two sublayers: a finite thickness upper layer and a stiffer semi-infinite halfspace in order to fit the computed low frequency, outer sensor magnitude data to duplicate the peak. This was necessary even in sections where drilling log data does not indicate bedrock or any other cause for a hard sublayer.

In the absence of bedrock, the subgrade layer moduli may still increase with depth for any one of or a combination of the following reasons, depending on the geotechnical or geological conditions at the site.

- **Clay Consolidation** With time clay particles or platelets polarize, i.e., they align themselves electrically. The clay undergoes a series of transformations electro-mechanically and chemically, turning in stages to marl, shale, and, in the presence of heat, to slate. Generally, the deeper sediment layers are older, so the lower layers will tend to be stiffer. Clay subgrades may then have sublayering at relatively shallow depths. The sublayers may be marl or shale and/or clay at any intermediate stage of consolidation.

- **Clay Suction** Unsaturated clays experience suction, or a pressure below ambient or atmospheric, due to surface tension. This causes cohesive forces in the material, which contribute to (increase) the material stiffness and rigidity. The cohesion and moduli increase as the moisture content decreases. Lower layers or sublayers with lower moisture content should have higher moduli.

- **Ground Water** (i.e. saturated unbound soil) In the presence of known ground water, the subgrade should be divided into two layers: the above-ground-water layer (partially saturated) and the saturated layer. The lower layer will have a higher compressional wave speed because the air voids are filled with water. This will result in a higher compressional wave speed and an increase in both Young's modulus and Poisson ratio.

- **Confining Stresses** The confining stresses of the subgrade soil for unbound materials like sand and gravel will increase with depth. The confining stresses increase with depth because of the weight of the overlying layers (overburden), similar to the increase in hydrostatic pressure with depth for liquids. In soil the confining stresses are usually separated into vertical and horizontal components. These components can be estimated using empirical relationships. The increase in confining stresses with depth results in an increase in the subgrade modulus with depth.

One or more of these effects (as well as undetected bedrock) may be present in a given pavement section.

Hard/Soft (H/S) Sections

Eleven of the 24 sites had H/S sections. These did not show peaks in the outer sensor magnitude frequency response function data.

Soft/Hard (S/H) Section

Only one site had a S/H section: Site D11S4, a thin AC layer section having a sandy clay subgrade. The upper layers are seen to be less stiff than the lower layers from the moduli given in Table 6 and Figure 148, where the outer sensor magnitudes are seen to increase with frequency. This may be a result of excessive near-surface moisture over a dryer clay subgrade.

LATERAL MODAL EFFECT

In the frequency range of about 30-80 Hz, four out of the 24 sites have severe peaking and partial nulls in the FWD magnitude data and a peaking feature in the phase angle data. These features are shown in Figures 22 and 23. The features are most pronounced for the innermost (r = 0, r = 1 ft.) sensors, with the r = 0 sensor invariably being the worst. These features are tentatively attributed to lateral or transverse vibratory responses or standing waves (i.e., modal effects) caused by the pavement's finite width. Recall that the idealized laterally

infinite layer structure shown in Figures 9 and 10 cannot take into account pavement lateral asymmetries or edge effects. The sites with severe lateral modal effects are listed below.

- D11S5
- D11S8
- D21S1
- D21S6

For sites with severe lateral mode effects, the FWD data in the middle frequency range (approx. 30-80 Hz) must be disregarded for the inner (r = 0 and 1 ft.) sensors. In this region the computed data is fit to an imaginary mean line, in effect "averaging out" the modal features in the curves with respect to frequency. The averaging process is illustrated in Figures 22 and 23 for the magnitude dip-peak feature and the phase angle peaking feature, respectively. The averaging can be justified because the lateral modal effect should not appreciably affect the overall energy level of the deflections. It merely rearranges the signal's frequency content.

CLASSIFICATION OF SITES

To aid in the interpretation of the comparison plots, the 24 sections were separated into three groups based on AC layer thickness. This was done because of similarities in the features of the curves for each thickness grouping. The groups are listed as follows:

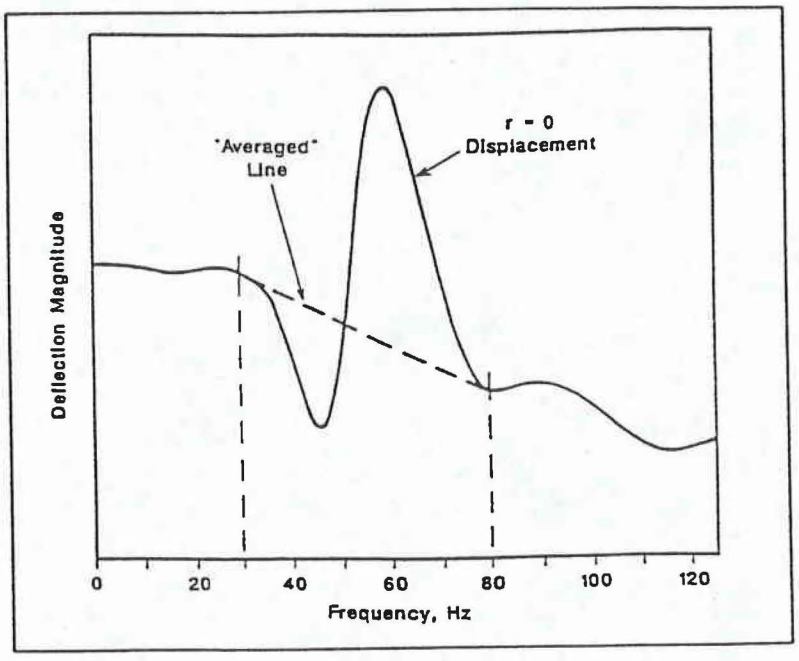

Figure 22. Phase Angle Plot for (r=0) Deflection, Showing Averaging Process

- Thick sections (7 Sites, Plots in Appendix D),
- Medium-thick sections (5 Sites, Plots in Appendix E), and
- Thin sections (12 Sites, Plots in Appendix F).

Thick Sections

The thick sites are listed as follows along with the figure numbers for the pavement frequency response functions.

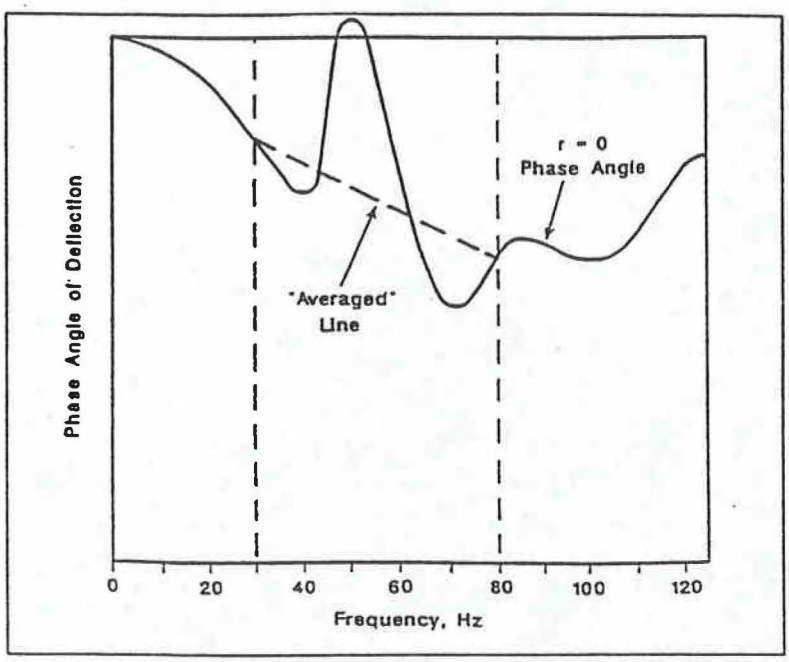

Figure 23. Magnitude Plot for (r=0) Deflection, Showing Averaging Process

Thick Sections

Site		Figure Nos.
D01S3		31 to 38
D01S5	warm	86 to 89
"	cool	90 to 93
D08S3		39 to 46
D08S4		94 to 97
D08S5		98 to 101
D11S2		102 to 105
D11S7		106 to 109

As might be expected, the stiffest sites have the thickest AC layers and cooler temperatures, as can be seen in the layer data in Table 4. These sites have small or weak lateral mode effects. The exception is site D01S5 with the warm temperature (100° F). The FWD data for Site D01S5 (warm) in Figure 24 shows a moderate-sized lateral modal feature at 30-80 Hz. The computed response in Figure 24 does not show the lateral modal effect because the computer model does not take layer asymmetries (such as pavement edges) into account. The lateral modal feature is more subdued in the D01S5 cool temperature (64° F) magnitude plot in Figure 25. This indicates that the effect increases as the pavement stiffness decreases. In this case the stiffness increase is due solely to the temperature decrease.

Site D11S7 exhibits in Figure 26 strong H-S-H behavior with a peak in the magnitude plots at about 20 Hz. This feature was also well replicated by the computer predictions because the vertical modal behavior can be modeled in the SCALPOT program by a vertical variation in subgrade sublayer moduli.

Medium-Thick Sections

These are listed as follows along with the corresponding figure numbers for the frequency response functions.

Medium-Thick Sections

Site	Figure Nos.
D01S4	110 to 113
D11S1	114 to 117
D21S3	118 to 121
D21S4	122 to 125
D21S5	126 to 129

The medium-thick sites have small to medium lateral mode interference. Site D21S4 in Figure 27 exhibits moderate H-S-H behavior with a peak in the outer sensor magnitudes at 40-45 Hz. Again the computed peak replicates (approximately) the FWD peak as it is a vertical modal effect.

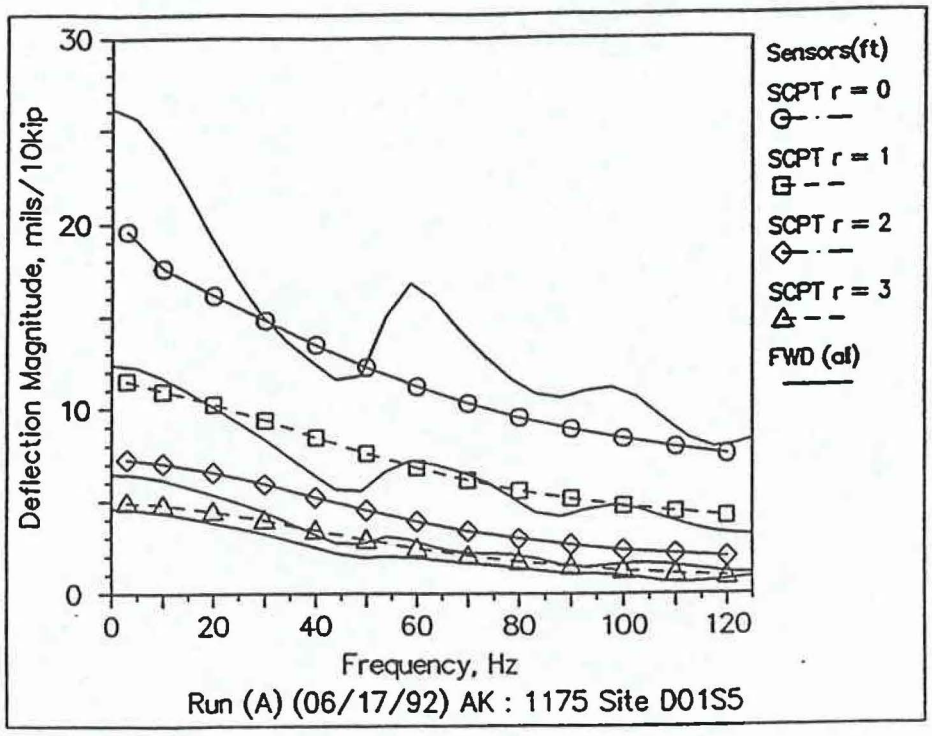

Figure 24. Site D01S5 (100° F); Inner Sensor Magnitude Frequency Response Functions

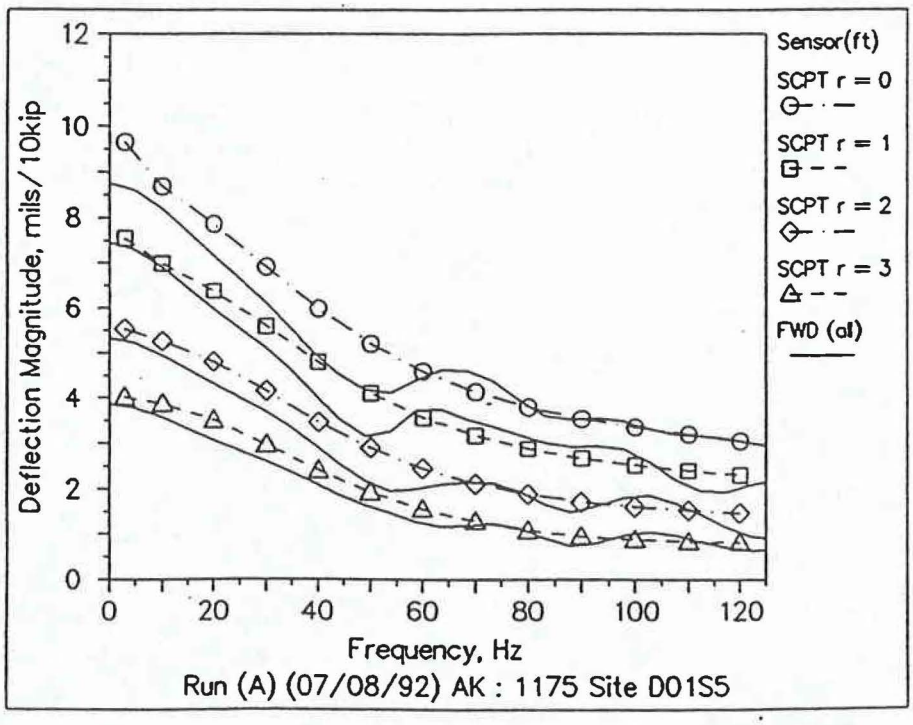

Figure 25. Site D01S5 (64° F); Inner Sensor Magnitude Frequency Response Functions

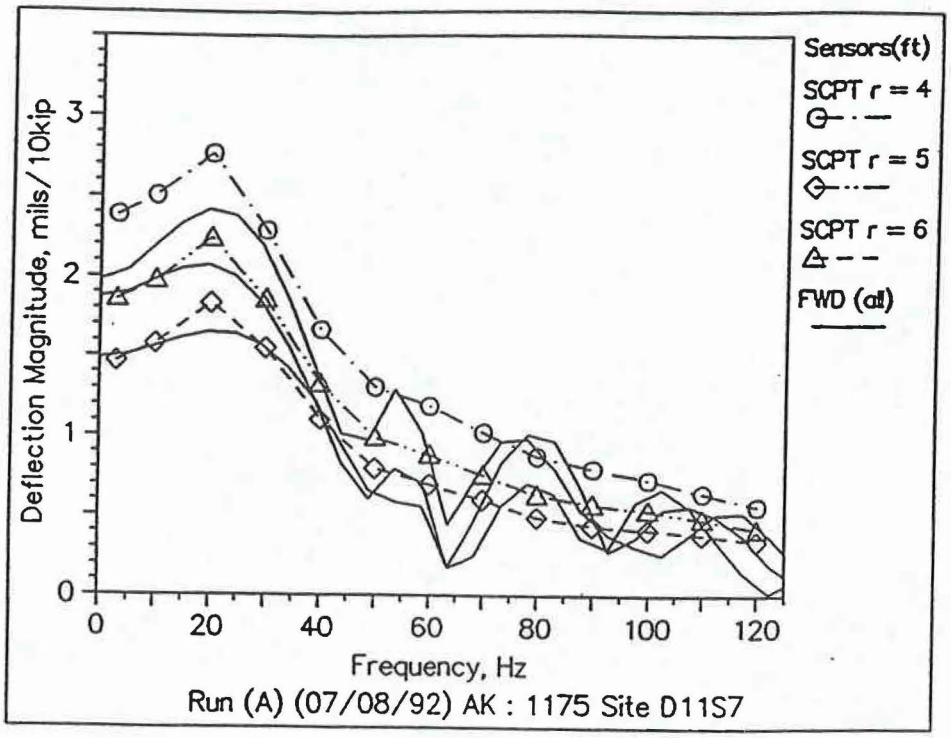

Figure 26. Site D11S7 Outer Sensor Magnitude Frequency Response Functions, Showing Peaking Due to H-S-H Layering

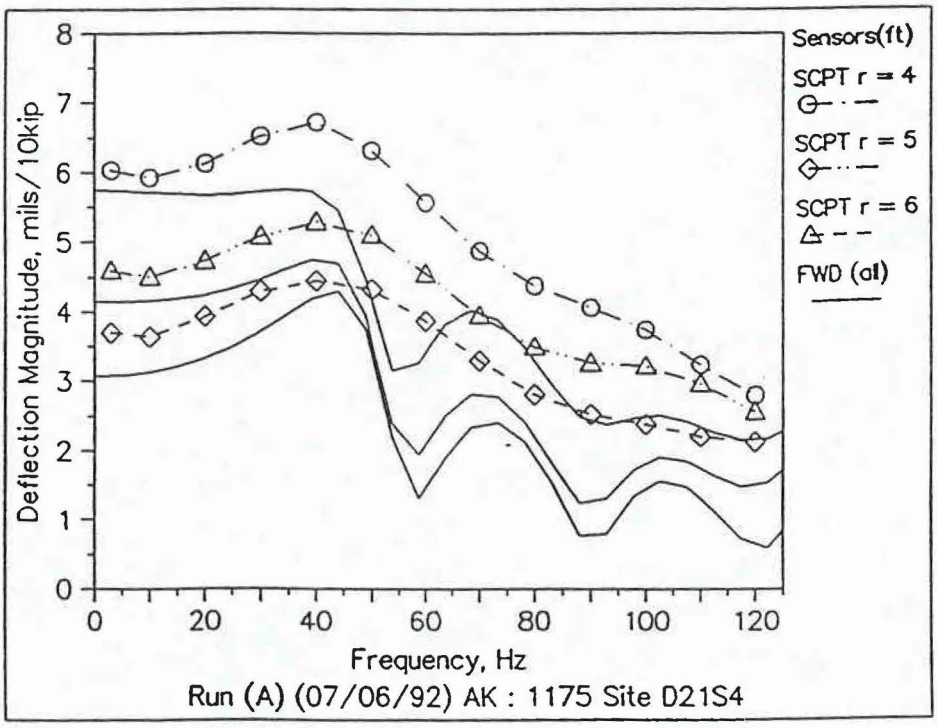

Figure 27. Site D21S4 Outer Sensor Magnitude Frequency Response Functions, Showing Peak Due to H-S-H- Layering

Thin Sections

The thin sections are listed below along with the corresponding Figure numbers for the comparison plots. Comments on interference severity and section type are also given in the table below.

Thin Sections

Site	Figure Numbers	Interference Severity	Section Type
D01S1	130 to 133	S-M	H/S
D08S1	47 to 54	Large	H-S-H
D08S2	134 to 137	Large	H/S
D08S6	138 to 141	S-M	H-S-H
D11S3	142 to 145	Large	H/S
D11S4	146 to 149	Large	S/H
D11S5	150 to 153	Very large	H/S
D11S6	154 to 157	Med-Large	H-S-H
D11S8	158 to 161	Large	H-S-H
D21S1	162 to 165	Large	H-S-H (weak)
D21S2	166 to 169	Medium	H-S-H (weak)
D21S6	170 to 173	Large	H-S-H

The thinnest AC layer sites have medium to large lateral mode vibration effects. Figures 28, 29, and 30 show the lateral modal effect. Figure 28 shows a large magnitude interference in the Site D08S1 (r = 0) deflection plot.

The worst modal interference occurred for Site D11S5. Figures 29 and 30 show the plots for magnitude and phase angle, respectively. The transverse interference is the most pronounced for the (r = 0) deflection. The lateral modal feature's dip-to-peak distance in Figure 29 is about 30 mils, which is almost as large as the maximum deflection at zero frequency. The phase angles for all the sensors in Figure 30 are grossly affected by the effect. A phase angle second harmonic or higher order mode is apparent at 90-95 Hz. For the sites analyzed there did not appear to be any connection between interference severity and subgrade sublayering, or pavement section type: i.e., H/S vs. H-S-H.

Severity of the Lateral Modal Effect

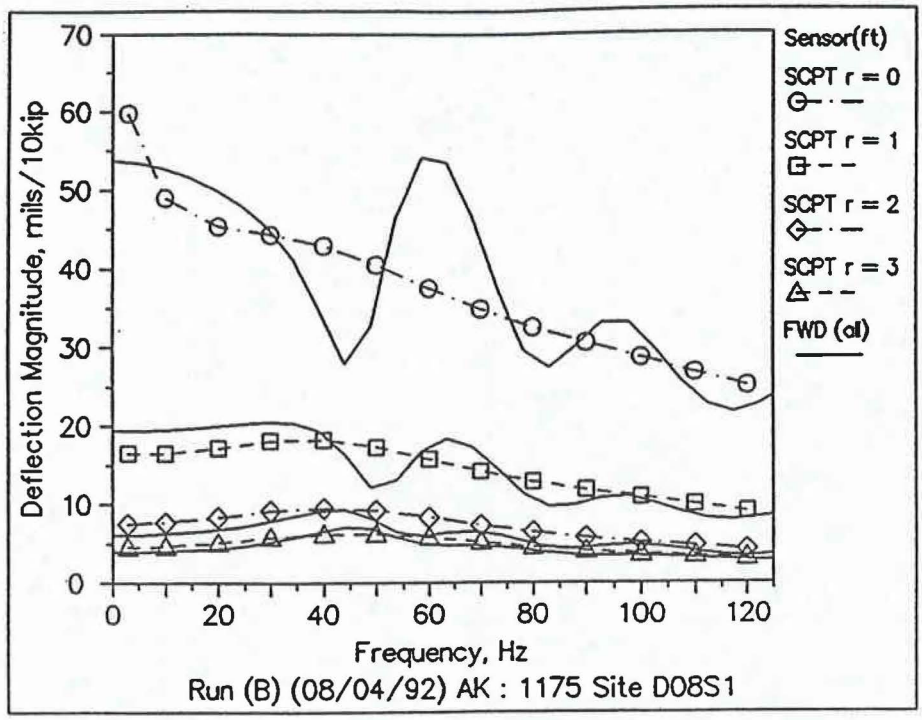

Figure 28. Site D08S1: Magnitude Frequency Response Function for Inner Sensors, Showing Large Transverse Modal Features

The modal effect severity is directly related to pavement AC layer stiffness as affected by AC layer thickness and temperature. Table 10 has been prepared to illustrate this. For each thickness grouping, the maximum deflections, AC layer thicknesses and surface temperatures were averaged. These averages together with relative modal severity appear in Table 10.

Table 10

Averaged Site Characteristics

Rel AC Thickness	Max. Defl. @ r = 0 (mil/10kip)	Severity of Modal Vibration	AC Layer Thickness avg (ft)	AC Layer Surface Temp. avg (deg F)
Thick	14	Small	0.69	89
Medium	37	Small-Medium	0.48	106
Thin	53	Large-Medium	0.14	105

It is apparent from Table 10 that the severity of the lateral modal effect increases as the pavement stiffness decreases. The stiffness is indicated by the value of maximum deflection in column 2. Stiffness increases with AC layer thickness and decreases with temperature. The pavements with the thinnest AC layers have the most severe interference. The thick pavements happened to have low surface temperatures on the average. The thickest pavements show the weakest interference vibration severity. Why this is so is not known at this time.

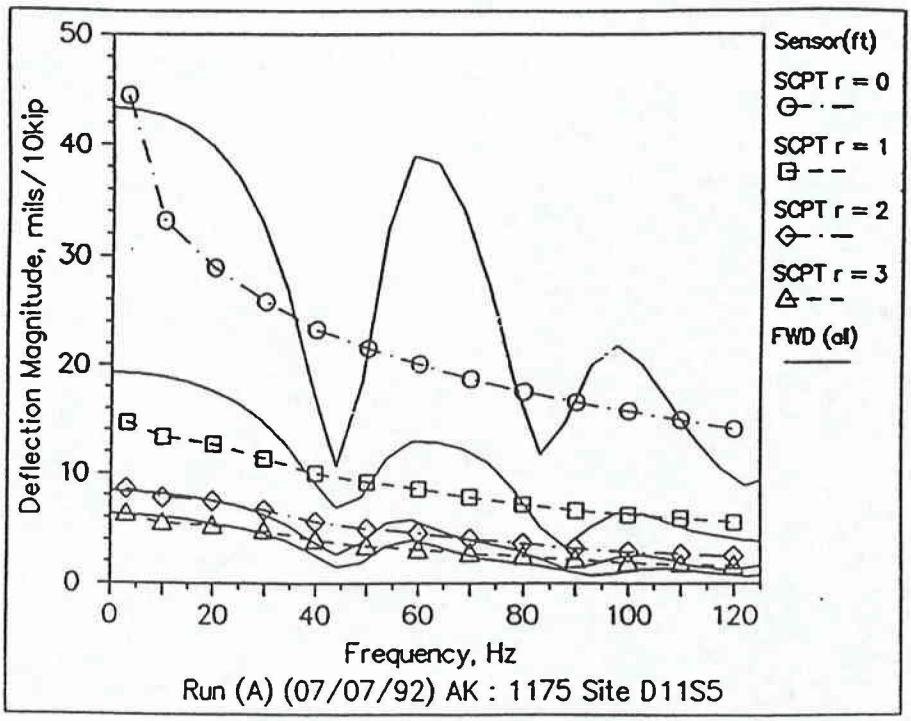

Figure 29. Site D11S5: Magnitude Frequency Response Function for Inner Sensors, Showing Large Transverse Modal Features

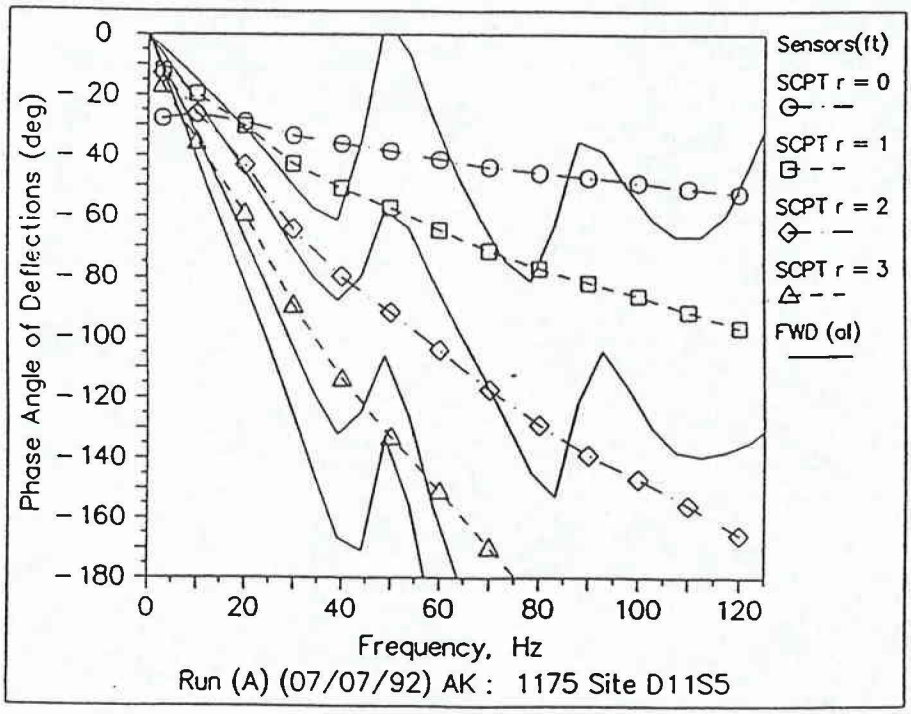

Figure 30. Site D11S5: Phase Angle Frequency Response Functions for Inner Sensors, Showing Large Transverse Modal Features

Summary of Graphical Comparison

The graphical comparison study was based on pavement frequency response functions. Computed frequency response functions compared well with ones computed from FWD data. Sites were grouped that had similar frequency response function shapes. Two types of groupings were found: pavement thickness groupings based on (r = 0) sensor behavior and pavement stiffness, and groupings based on subgrade sublayering configuration.

The pavement stiffness groupings were designated as: Thick, Medium-Thick, and Thin. The sites also exhibited three section configurations based on subgrade sublayering. These configurations exhibited similar behavior of the outer sensor magnitudes. The configurations were: Hard/Soft, Hard-Soft-Hard, and Soft/Hard. Eleven sites had H/S layering. Twelve of the sites had the H-S-H configuration with a divided subgrade with the lower layer stiffer than the upper. Only one site had Soft/Hard layering.

Two types of modal effects were apparent in the frequency response function shapes. The two major modal effects are described as follows.

- **Vertical Mode**: Associated with (H-S-H) pavements. See Figure 6-c. Effect modeled satisfactorily with vertical sublayering.

- **Transverse Mode(s)**: (See Figures 6-a and 6-b.) These cannot be modeled with a simple layered representation, as they arise from axial asymmetries such as pavement edge effects. A work-around procedure was developed that gives good back-calculation results.

Computed results for thick pavements showed the best agreement with FWD frequency response functions, and the medium-thickness sites were next. Thin sections tended to have severe anomalous behavior attributed to the transverse modal behavior.

Most very thin AC pavements were satisfactorily treated by combining the AC seal coat and the base course into one layer and treating the combined layer as a viscoelastic layer.

The overall conclusion was that the layered viscoelastic model used by the SCALPOT program was adequate for representing the pavement dynamic responses.

CHAPTER VI

SID BACK-CALCULATION RESULTS AND REWORK

Time limitations prevented a full SID analysis of all 24 sections. Therefore only three sites were given the full SID back-calculation treatment. Two thick sites (Sites D01S3 and D08S3) and one thin pavement site (Site D08S1) were chosen for the SID analysis. Results for two SID programs: FUSID and JACOB-SID are presented. For reasons discussed in Chapter IV, the original SID program (PAVE-SID) was replaced by the FUSID program in January 1993.

Two sets of frequency response functions for each site are presented in figures as indicated in Table 11. Table 11 also indicates the SID programs used.

Table 11

SID Back-Calculated Sites

Site	Figure Nos.	AC Thk.	SID Program
D01S3	31-38	Thick	FUSID
D08S3	39-46	Thick	FUSID
D08S1	47-54	Thin	JACOB-SID

There are eight plots on four pages for each of the three sites. The four pages show the pavement frequency response functions in the following order.

- Inner Sensor Magnitude (Figs. 31, 32)
- Outer Sensor Magnitude (Figs. 33, 34)
- Inner Sensor Phase Angle (Figs. 35, 36)
- Outer Sensor Phase Angle (Figs. 37, 38)

Comparison of SID Results to T&E Results

The SID plots for Sites D01S3 and D08S3 are compared to the T&E back-calculation results in Figures 31-38 and 39-46, respectively. These are presented to show the improvement in agreement from the T&E to the SID back-calculated results.

For Sites D01S3 and D08S3, each page has two plots: the top plot shows the T&E back-calculation results, and the bottom plot shows the FUSID back-calculation results. The T&E results and the SID results used FWD data at different loadings and from different stations at the same site. The back-calculated layer data (moduli, etc.) for these sites are compared in Table 12.

Site D01S3 Comparison

Figures 31-38 show the comparison of T&E back-calculated (top plot) results to SID (bottom plot) results. One sees an overall improvement in the SID B-C predictions *versus* the corresponding T&E responses for all sensors and all frequencies. The overall ($r = 0$) magnitude plot in Figure 31 is low. This indicates that the effective AC modulus is too high. The SID result in Figure 32 is much better. The T&E phase angles in Figure 37 were consistently underpredicted. The SID results in Figure 38 agree much more closely.

Table 12 below compares values for back-calculated SID and T&E layer data. One sees that the T&E m of 0.25 was underpredicted relative to the SID value of 0.62. The underpredicted T&E phase angles are a result of the low m value. From Table 12 one also sees that for D01S3 the AC effective modulus for the T&E result is much higher than the SID value. This is consistent with the Figure 31 observations given above. The Table also shows that the T&E base course modulus was underpredicted. However, Table 12 does show that the D01S3 SID and T&E moduli for both subgrade sublayers were quite close.

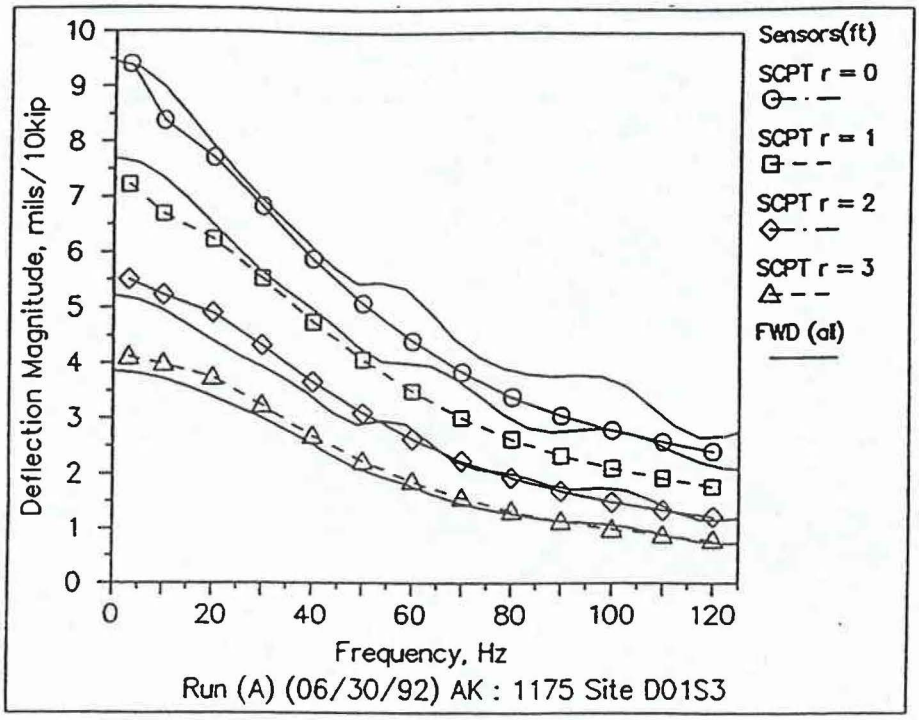

Figure 31. Section D01S3: T&E Fit for Magnitude Plot for Inner Displacements (r=0, 1.0, 2.0, and 3.0 ft.)

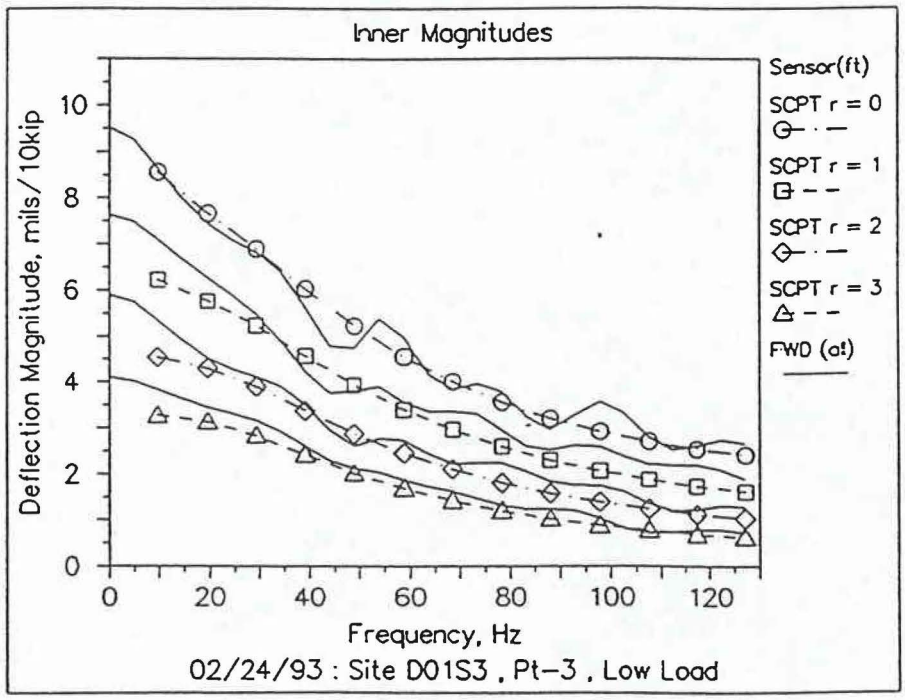

Figure 32. Section D01S3: FUSID Fit for Magnitude Plot for Inner Displacements (r=0, 1.0, 2.0, and 3.0 ft.)

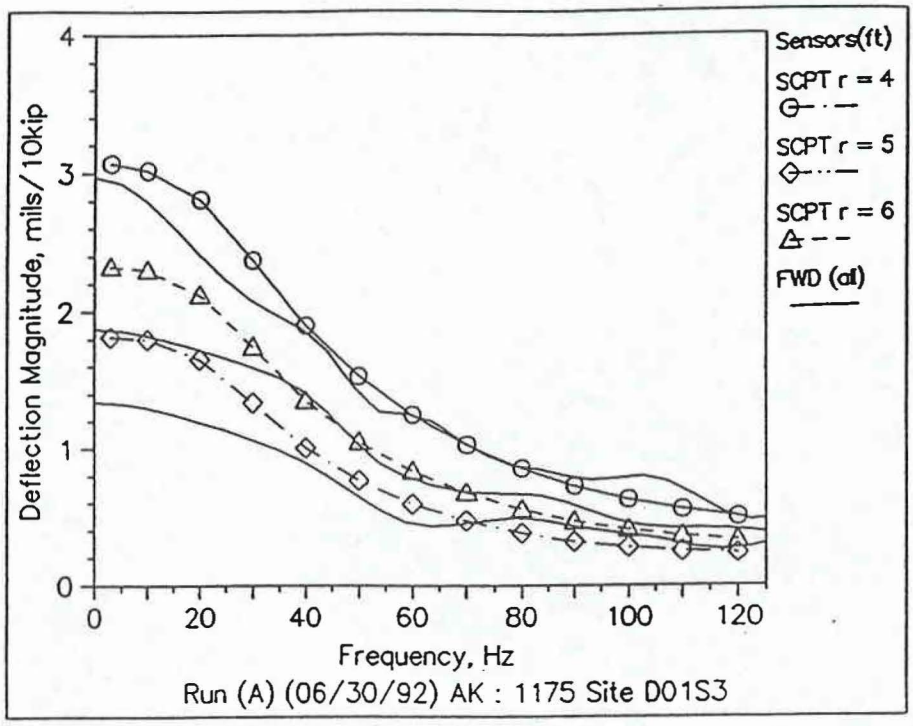

Figure 33. Section D01S3: T&E Fit for Magnitude Plot for Outer Displacements (r=4, 5.0, and 6.0 ft.)

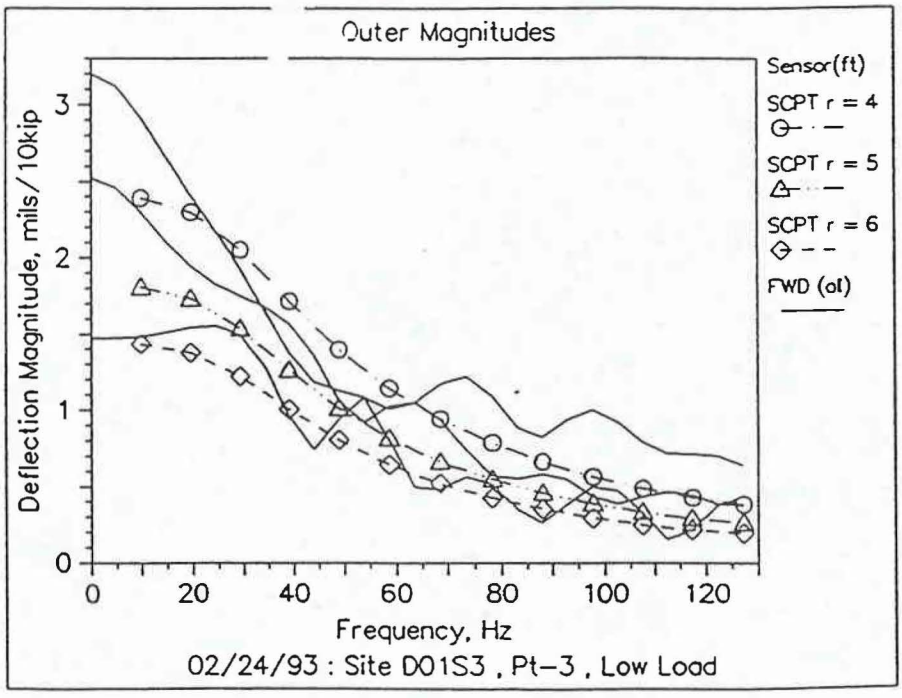

Figure 34. Section D01S3: FUSID Fit for Magnitude Plot for Outer Displacements (r=4, 5.0, and 6.0 ft.)

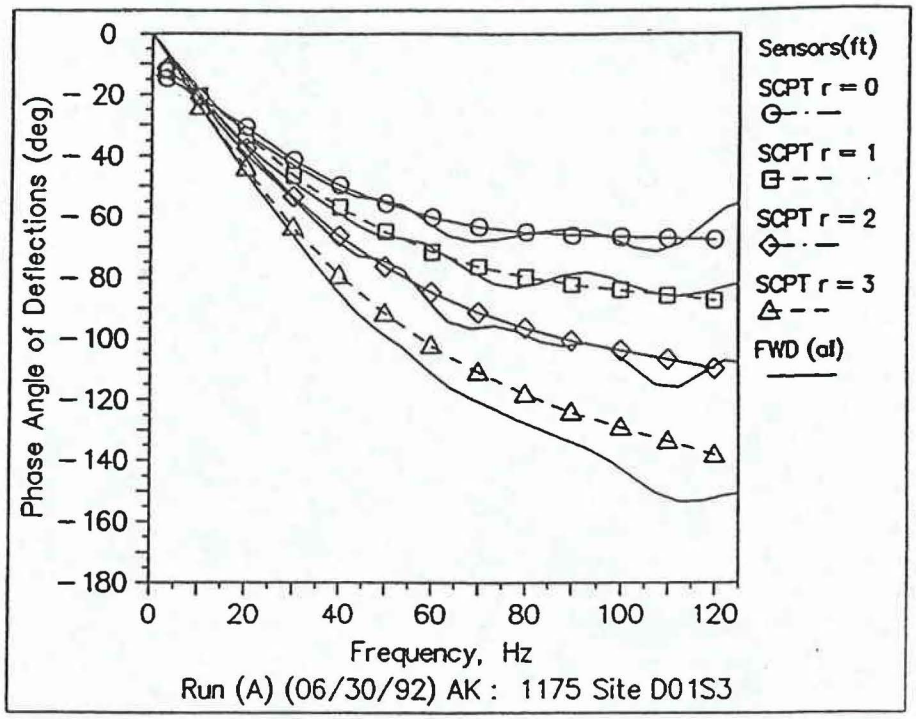

Figure 35. Section D01S3: T&E Fit for Phase Angle Plot for Inner Displacements (r=0, 1.0, 2.0, and 3.0 ft.)

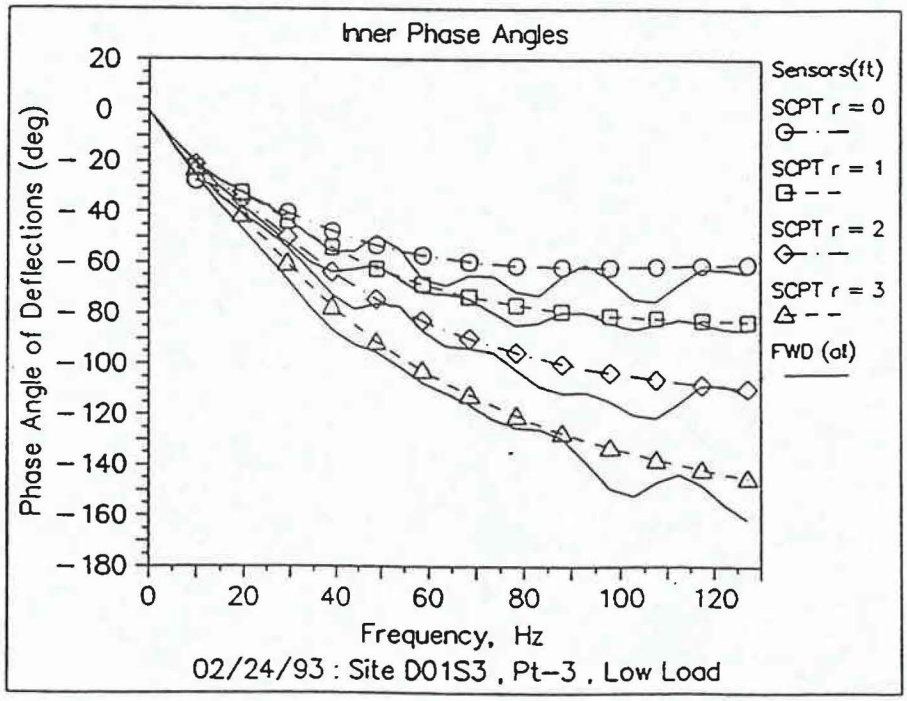

Figure 36. Section D01S3: FUSID Fit for Phase Angle Plot for Inner Displacements (r=0, 1.0, 2.0, and 3.0 ft.)

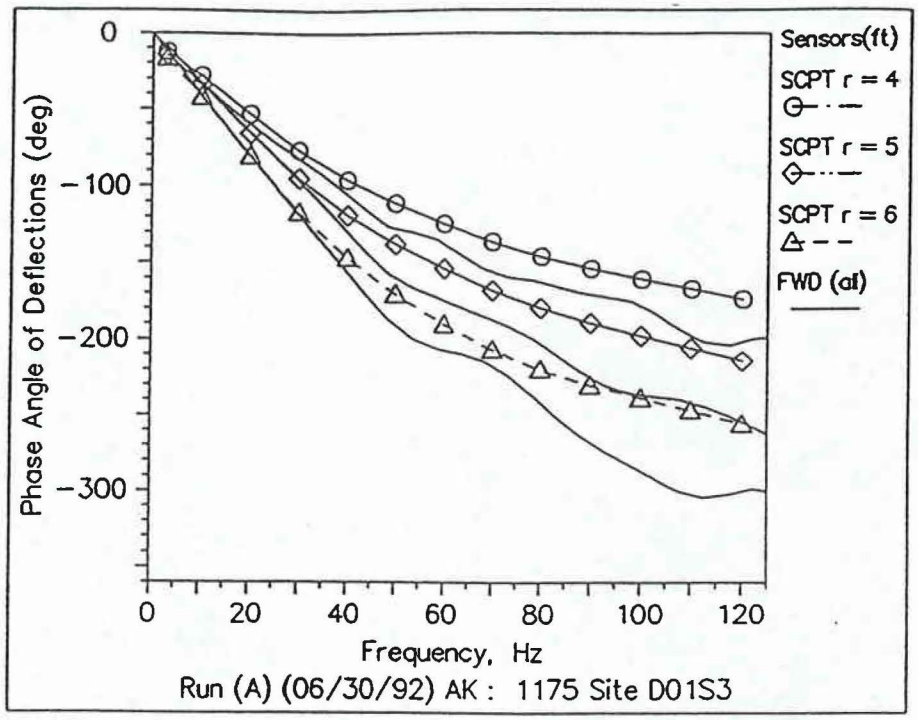

Figure 37. Section D01S3: T&E Fit for Phase Angle Plot for Outer Displacements (r=4.0, 5.0, and 6.0 ft.)

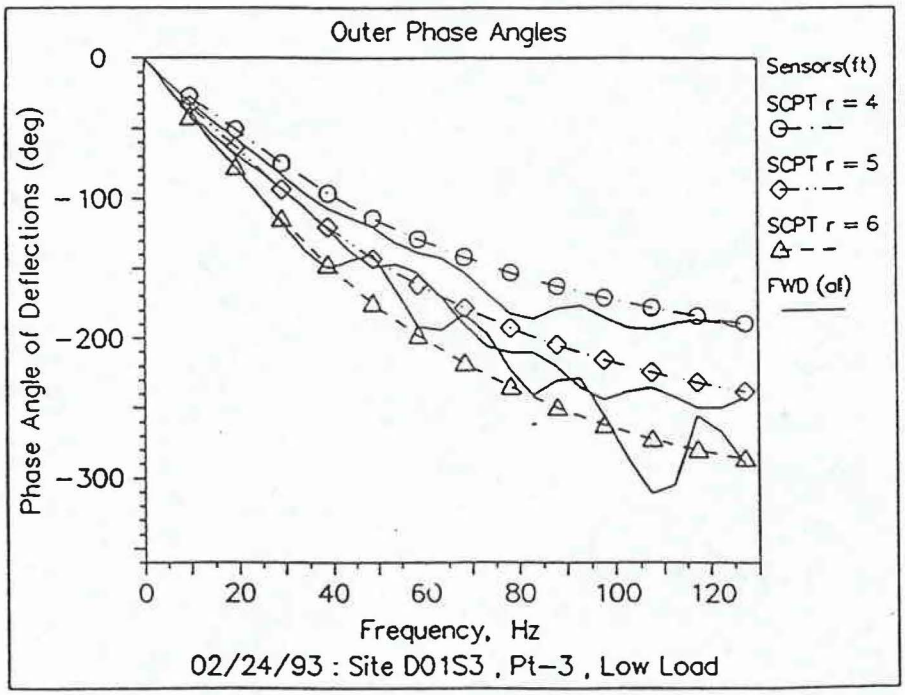

Figure 38. Section D01S3: FUSID Fit for Phase Angle Plot for Outer Displacements (r=4.0, 5.0, and 6.0 ft.)

Table 12

SID/T&E Back-Calculation Comparison

Sites D01S3 and D08S3

(FUSID B-C)

Site =>	D01S3		D08S3	
	SID B-C	T&E B-C	SID B-C	T&E B-C
AC Layer				
Eeff (psi)	446,000	695,200	616,500	750,000
Log-log slope (m)	0.62	0.25	0.72	0.35
VE/El Ratio (α)	33.6	20.0	104.2	20.0
Base course				
Mod. (psi)	24,700	15,000	45,700	50,000
Subgrade 1				
Mod. (psi)	20,500	18,100	22,400	30,000
Thk (ft)	1.667	1.667	10.0	Not Subdiv
Subgrade 2				
Mod. (psi)	26,100	23,000	45,600	30,000

Site D08S3 Comparison

In Figures 40, 42, 44, and 46 for Site D08S3 one sees good agreement of computed (using FUSID B-C data) *versus* FWD data. Moderate transverse modal features, centered at about 60 Hz are apparent in the inner sensor FWD data. The computed responses do not exhibit the lateral modal effect because (as discussed in Chapter III) it is not modeled.

The Figure 44 outer magnitude FWD and computed responses show a peak at 20-25 Hz, indicating an H-S-H pavement configuration. The corresponding FWD data in Figure 42 shows a shoulder instead of a peak. This indicates a marginal H/S configuration. Recall that the T&E results and the SID results used FWD data at different loadings and from different stations at the same site. The different results for the same site give an indication of the variability of the subgrade over the hundred-foot-long test section.

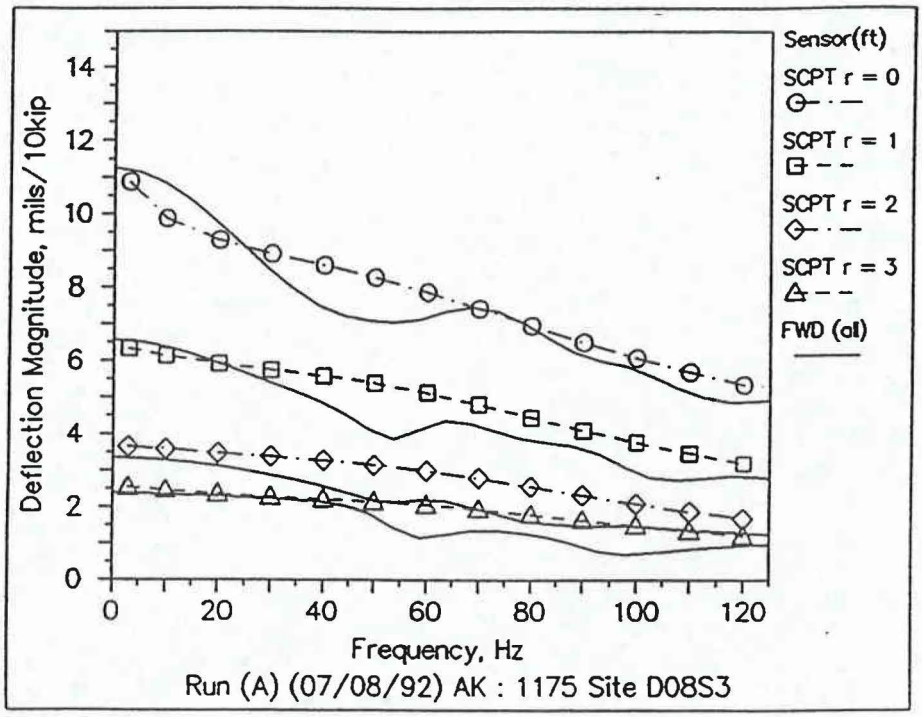

Figure 39. Section D08S3: T&E Fit for Inner Displacement Magnitudes (r=0, 1.0, 2.0, and 3.0 ft.)

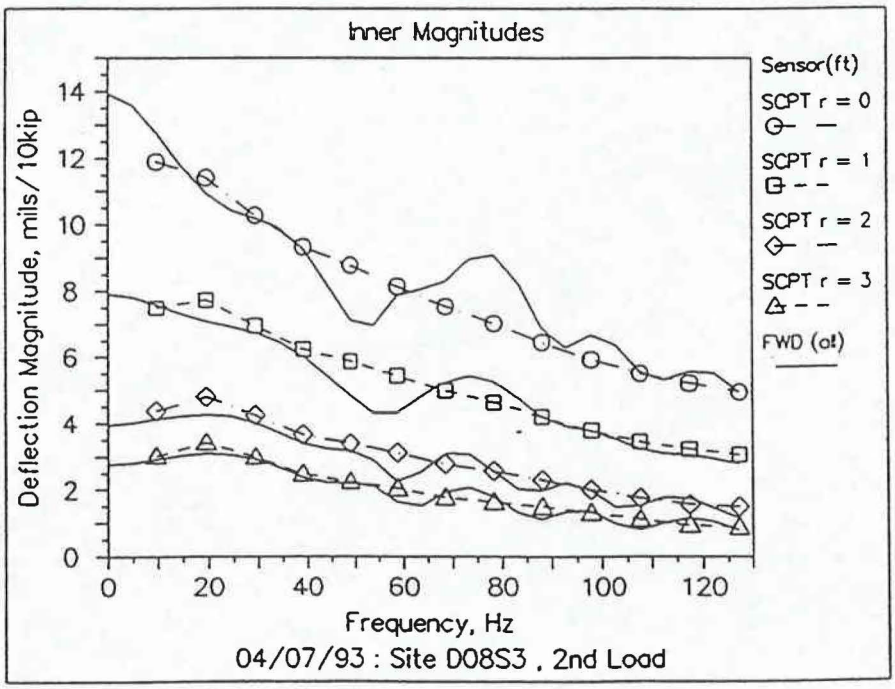

Figure 40. Section D08S3: FUSID Fit for Inner Displacement Magnitudes (r=0, 1.0, 2.0, and 3.0 ft.)

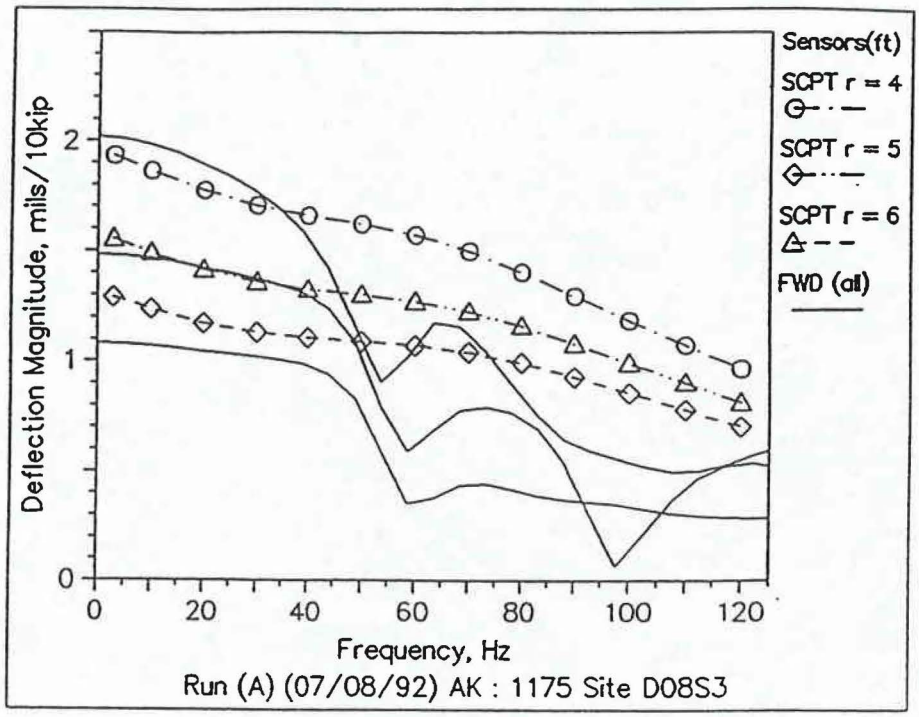

Figure 41. Section D08S3: T&E Fit for Outer Displacement Magnitudes (r=4.0, 5.0, and 6.0 ft.)

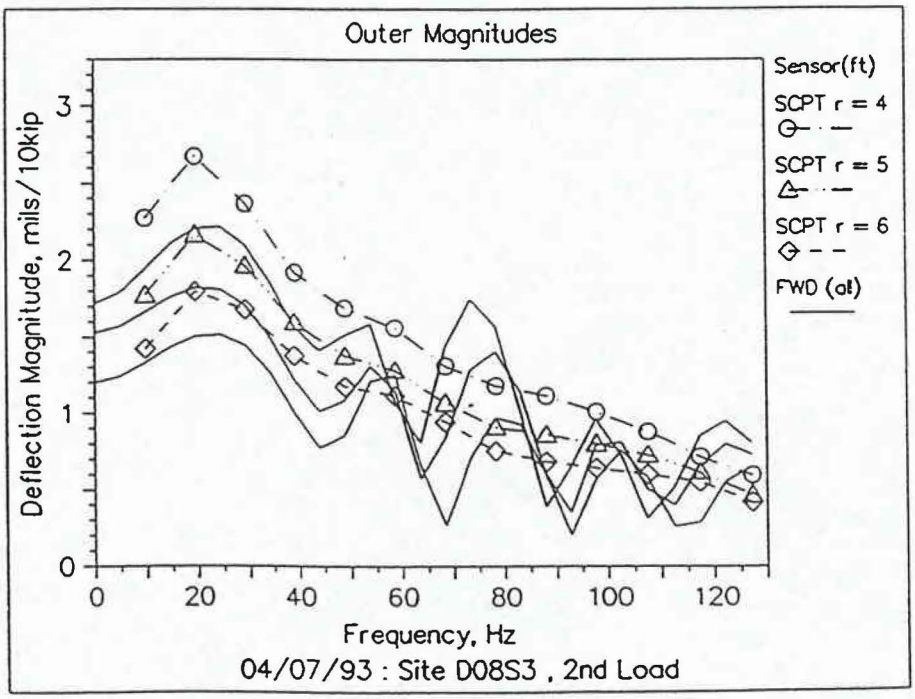

Figure 42. Section D08S3: FUSID Fit for Outer Displacement Magnitudes (r=4.0, 5.0, and 6.0 ft.)

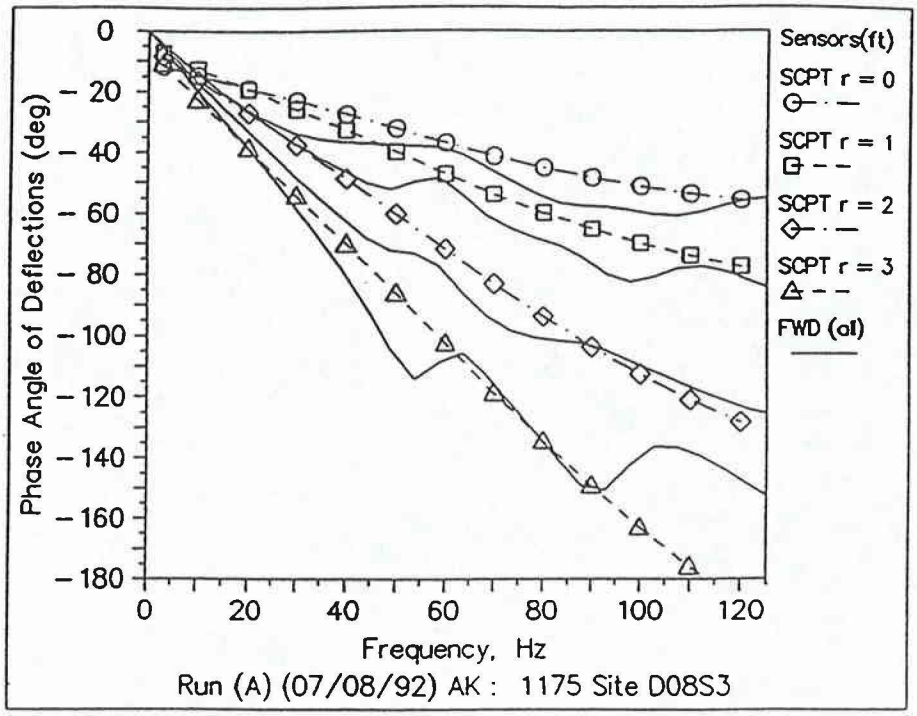

Figure 43. Section D08S3: T&E Fit for Inner Displacement Phase Angles (r=0, 1.0, 2.0, and 3.0 ft.)

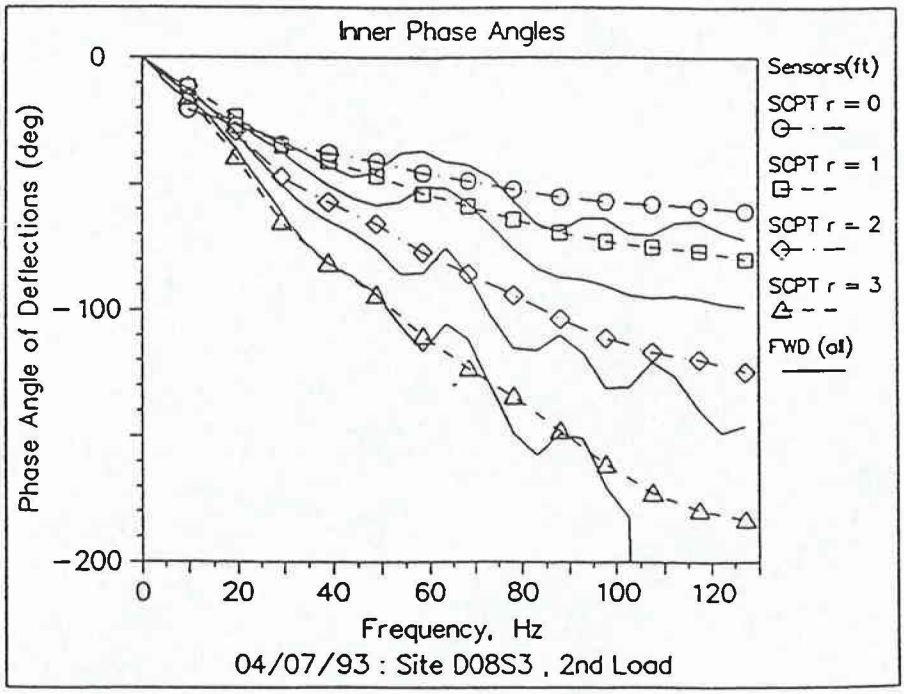

Figure 44. Section D08S3: FUSID Fit for Inner Displacement Phase Angles (r=0, 1.0, 2.0, and 3.0 ft.)

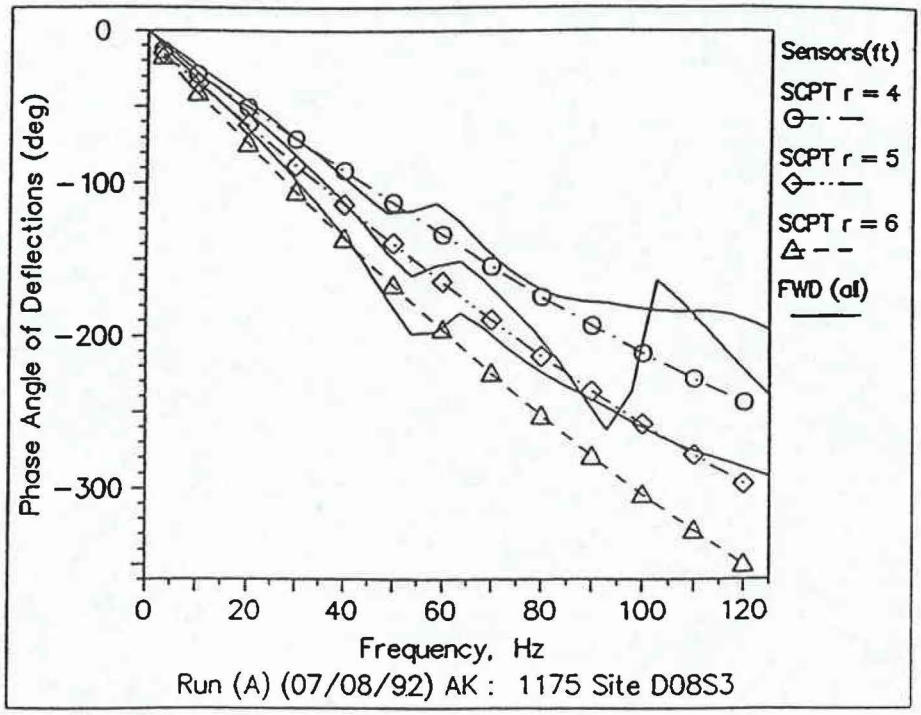

Figure 45. Section D08S3: T&E Fit for Outer Displacement Phase Angles (r=4.0, 5.0, and 6.0 ft.)

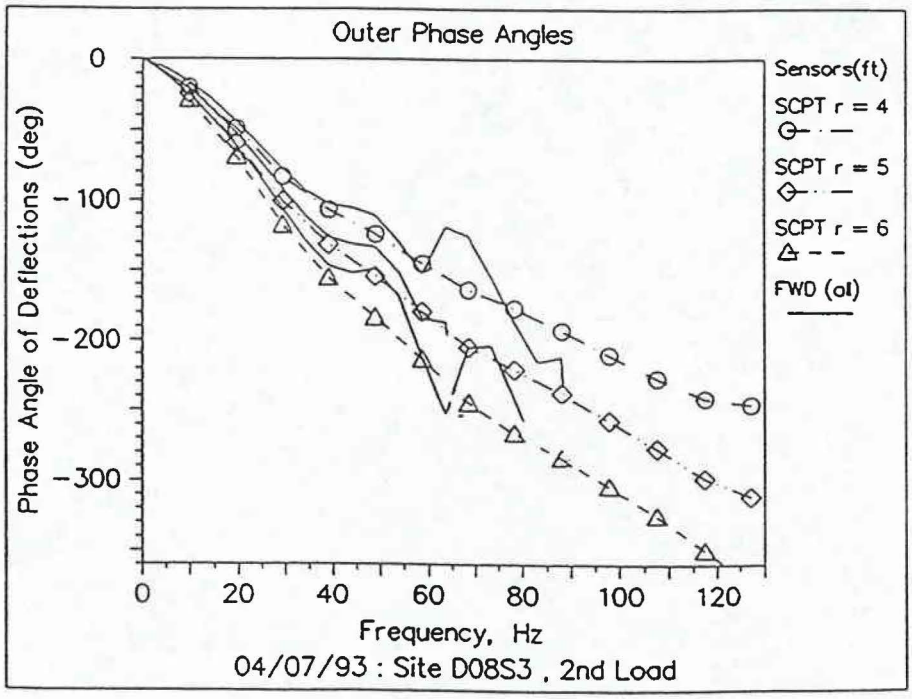

Figure 46. Section D08S3: FUSID Fit for Outer Displacement Phase Angles (r=4.0, 5.0, and 6.0 ft.)

Also note the much better overall agreement of the SID data over the T&E data, which is of course to be expected. The T&E data in Figure 39 shows the (r = 0) curve to be too flat, as the m is too low. The SID results in Figure 40 show much better agreement for all the sensors. In Figure 43 the outer sensor T&E magnitude data is over-predicted at the high frequencies. The SID fit in Figure 44 shows much better agreement.

Site D08S1 (Thin Pavement) Rework

For Site D08S1, frequency response function plots were prepared for comparison of uncorrected SID back-calculation results and re-worked or adjusted SID results. The re-worked SID results are shown in the top plots, and the (uncorrected) SID result is shown on the bottom plot.

For site D08S1, the JACOB-SID back-calculated results in Figures 47-54 showed generally good agreement except for the r = 0 displacement magnitude and phase angle data. Site D08S1 has a strong lateral modal effect, as can be seen in Figures 47, 48, 51, and 52. The modal effect is strongest for the r = 0 and r = 1 ft. sensor magnitude and phase data. The computed SID curves cannot duplicate the modal effect, so the responses were visually averaged over the affected frequency range, as discussed in Chapter III, and as shown in Figures 22 and 23.

In Figure 48 the SID-computed (r = 0) magnitude is seen to be underpredicted for the higher frequencies and overpredicted for the low frequencies relative to the FWD data. As the frequency approaches zero, the computed magnitude goes to infinity. The overall slope of the predicted magnitude curve is too steep, indicating a too-high m value. In Figure 52 the SID-computed (r = 0) phase angle is seen to be seriously overpredicted at the higher frequencies, also indicating a too-high m value. This discrepancy for the (r = 0) SID m data is serious because the r = 0 sensor data is the most sensitive to the AC layer properties, which in turn are the most important for pavement life prediction.

The D08S1 site is a thin pavement and has a severe lateral modal effect in the FWD data, as seen in Figures 47, 48, 51, and 52. The fitting of the curves for this site for the rework assume an averaging over the modal features as was illustrated in Figures 22 and 23.

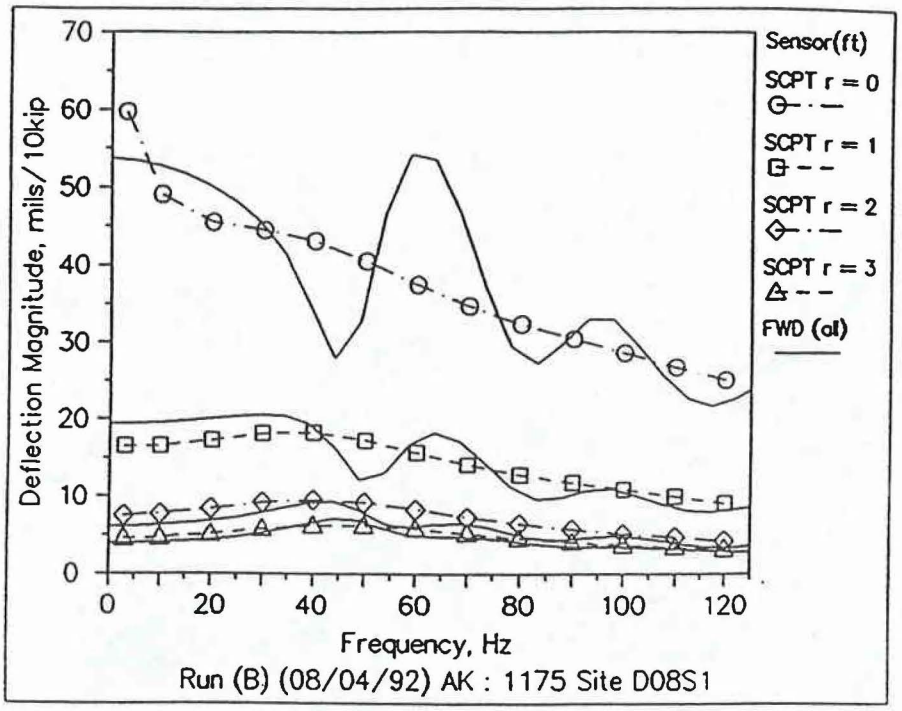

Figure 47. Section D08S1: SID Fit for Magnitude Plot for Inner Displacements (r=0, 1.0, 2.0, and 3.0 ft.)

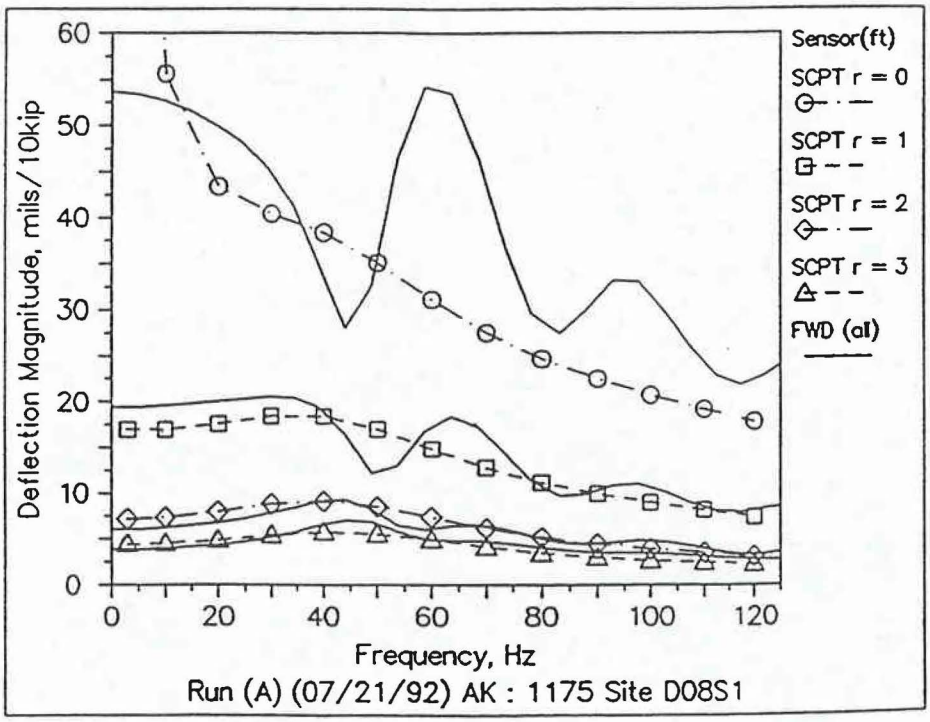

Figure 48. Section D08S1: SID Fit for Magnitude Plot for Inner Displacements (r=0, 1.0, 2.0, and 3.0ft.)

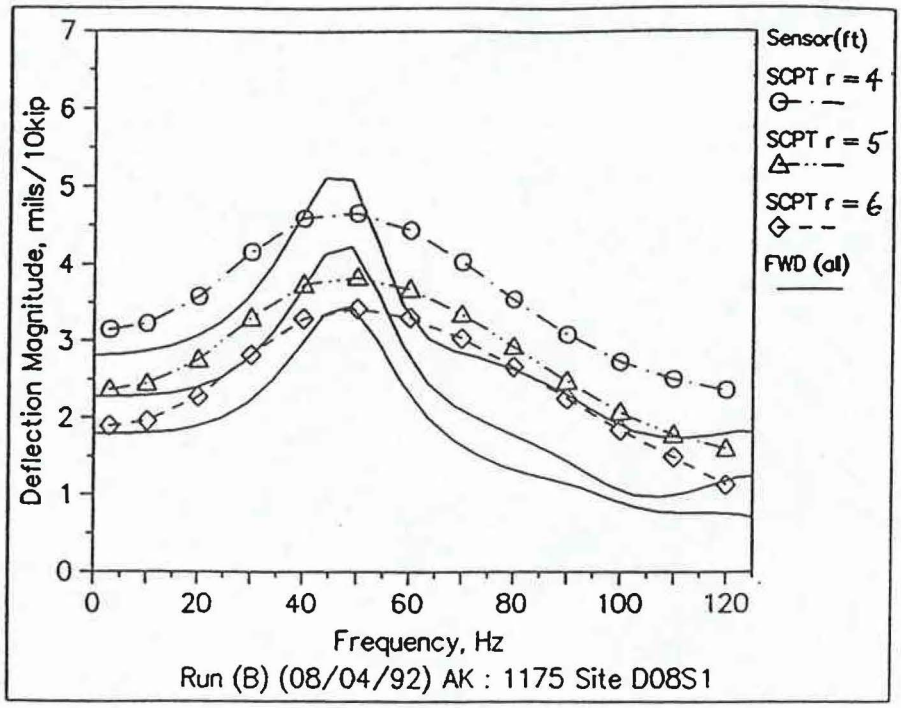

Figure 49. Section D08S1: Adjusted SID Fit for Magnitude Plot for Outer Displacements (r=4.0, 5.0, and 6.0 ft.)

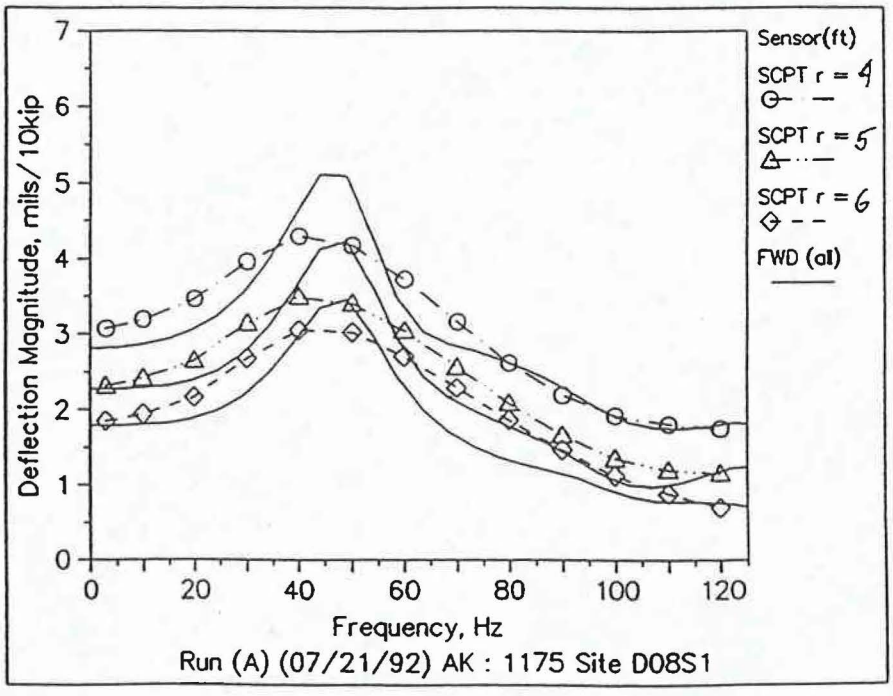

Figure 50. Section D08S1: SID Fit for Magnitude Plot for Outer Displacements (r=4.0, 5.0, and 6.0 ft.)

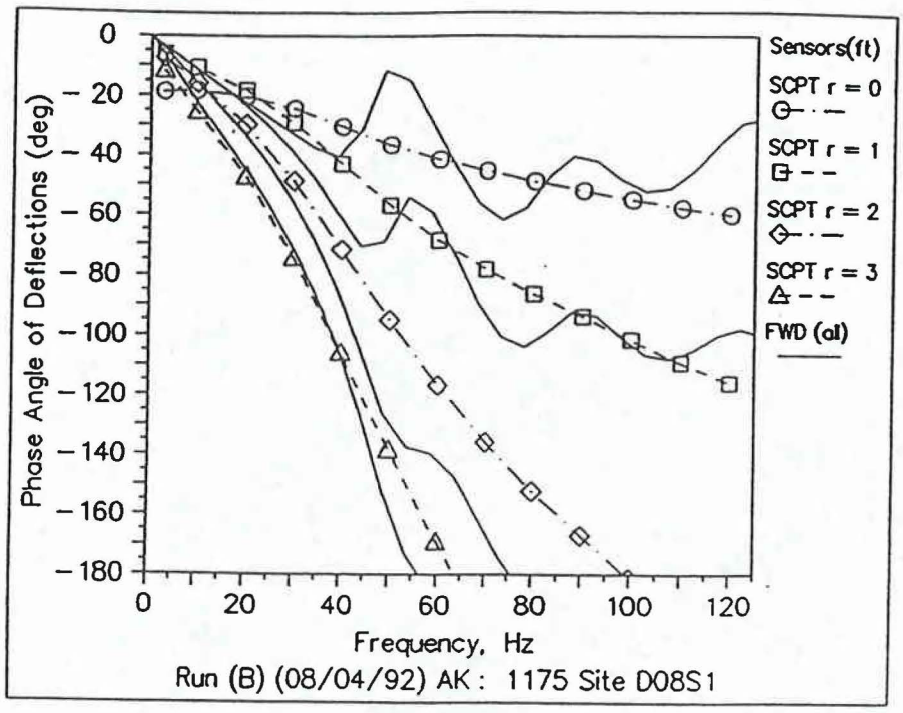

Figure 51. Section D08S1: Adjusted SID Fit for Phase Angle Plot for Inner Displacements (r=0, 1.0, 2.0, and 3.0 ft.)

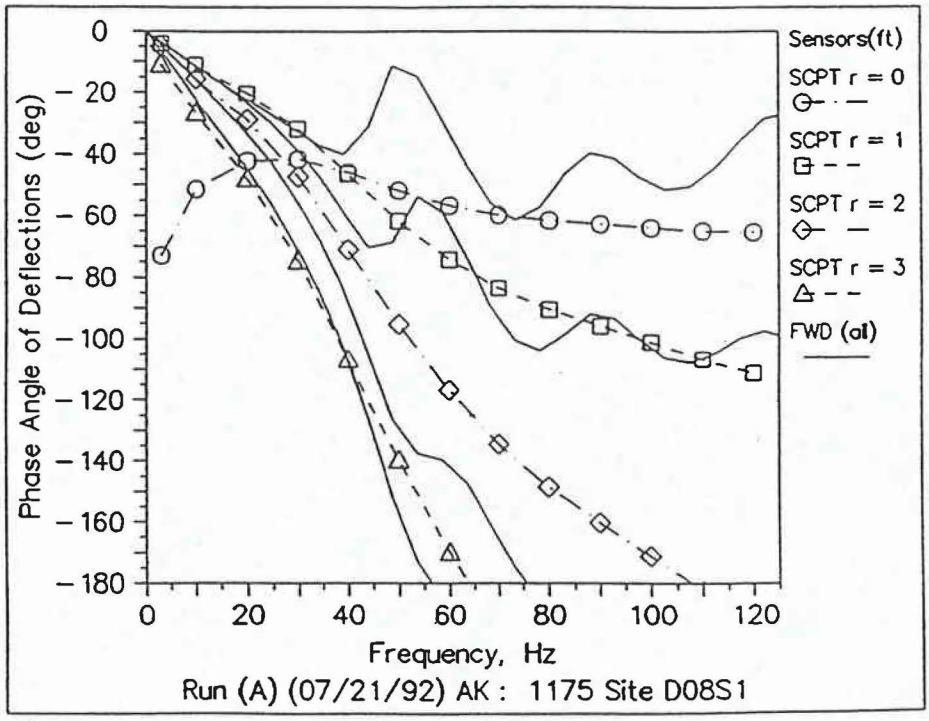

Figure 52. Section D08S1: SID Fit for Phase Angle Plot for Inner Displacements (r=0, 1.0, 2.0, and 3.0 ft.)

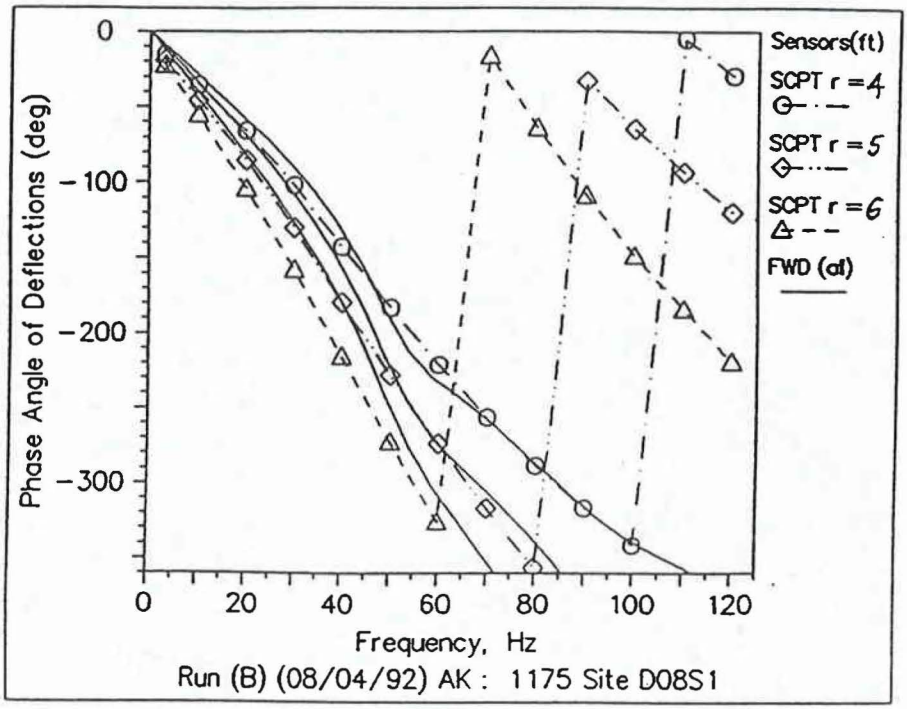

Figure 53. Section D08S1: Adjusted SID Fit for Phase Angle Plot for Outer Displacements (r=4.0, 5.0, and 6.0 ft.)

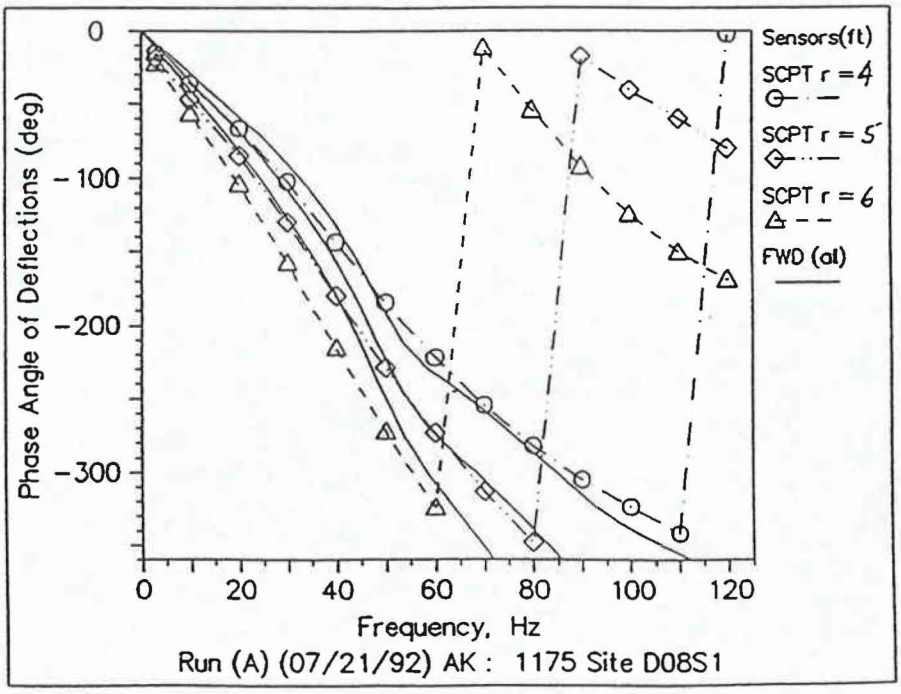

Figure 54. Section D08S1: SID Fit for Phase Angle Plot for Outer Displacements (r=4.0, 5.0, and 6.0 ft.)

Table 13 shows the D08S1 back-calculated AC layer data. One sees from Table 13 that the SID back-calculated log-log slope (m) is 1.0, which is unrealistically high. Because of this discrepancy, the SID results for Site D08S1 were reworked by trial-and-error (T&E) back-calculation. More realistic values for the AC layer creep parameters and base course moduli were introduced into the D08S1 SCALPOT input data set on a trial-and-error basis to achieve better agreement of the (r = 0) sensor data. This took three SCALPOT runs, after which much better overall (i.e., all sensors, all frequencies) agreement with the frequency response data was achieved. The reworked comparison plots are seen as the top plots in Figures 47, 49, 51, and 53, for inner magnitude, inner phase angle, outer magnitude, and outer phase angle, respectively. After adjustment, much better graphical agreement of (r = 0) magnitude is seen in Figure 47 *versus* the raw SID result in Figure 48. A similar improvement in (r = 0) phase angle is seen in Figure 51 *versus* Figure 52.

For Site D08S1, it was not necessary in the rework to modify the SID back-calculated moduli for the subbase and subgrade layers. The raw SID back-calculation results and T&E reworked SID results are given in Table 13.

Table 13

Site D08S1 Back-Calculation Comparison-
AC Layer Only

Surface Temperature: 108° F

	Raw SID B-C Result	Adjusted SID B-C Result
E_{EFF}(psi)	19,400	25,000
Log-log slope (m)	1.0	0.35
VE/E Ratio α	399	30.0

Causes of the SID Discrepancies

The probable major causes of the Site D08S1 SID discrepancies requiring rework or adjustments of the SID results are show below.

- Unrealistic low frequency behavior of AC Creep Representation
- Least-Squares Fitting

The unrealistic low frequency behavior of the AC layer (three-parameter) viscoelastic representation in the SCALPOT program is discussed in Appendix B. This problem can be readily corrected in the future as part of the further development or refinement of the dynamic analysis procedure.

The other possible cause of the discrepancies is the mathematical fitting of the curves in the SID procedure. The SID procedure minimizes the mean-square error. Minimization of the mean-square error may distort the curve shapes so they do not resemble the FWD-based data. For example, the SID tends to flatten the H-S-H section vertical mode outer sensor magnitude peak. The mean-square error minimization may be thrown off by the vertical mode peak feature in the H-S-H site data and by the lateral modal vibration effect.

The layered viscoelastic model cannot represent the lateral modal phenomenon, which was strong for this site. The "Recommendations" section gives proposed fixes for achieving better correlation.

Summary of SID Study

Three sites were analyzed in detail. The SID plots for Sites D01S3 and D08S3 were compared to the T&E back-calculation results. These results were presented to show the improvement in agreement from the T&E to the SID results.

- **Site D01S3** (Thick)

One sees an overall improvement in the SID B-C predictions *versus* the corresponding T&E responses for all sensors and all frequencies.

One sees an overall improvement in the SID B-C predictions *versus* the corresponding T&E responses for all sensors and all frequencies.

- **Site D08S3** (Thick)

One sees good overall agreement of computed SID data *versus* FWD data. Moderate transverse modal features are apparent in the FWD data. The computed responses do not exhibit this modal effect because it is not modeled in the SCALPOT program.

- **Site D08S1** (Thin) Rework

A comparison of uncorrected SID back-calculation results and re-worked or adjusted SID results was presented. The D08S1 site is a thin pavement and has a severe lateral modal effect in the FWD data.

CHAPTER VII
COMPARISON BETWEEN LABORATORY AND BACK-CALCULATED DATA

Coring and trench samples were taken at all but three of the sites in the earlier studies. No samples were taken for Sites D11S6, D11S7, or D11S8, all of which were new sites having cement-stabilized base courses.

LABORATORY TEST PROGRAM

A special laboratory testing program for the dynamic analysis project was performed using samples taken in the Project 1123 study. Three test series were run.

- Constant Stress Unconfined Creep Tests on the AC Core Samples
- Longitudinal and Torsional Resonant Column Tests on Reconstructed Base Course Core Samples
- Torsional Resonant Column Tests on Undisturbed Subgrade Core Samples

Five AC core samples from four sites were tested in unconfined compressive creep. Five bulk samples of granular base course material for four sites were reconstituted and were tested using a resonant column testing device developed by G. Bakas at TTI. This device can do both resonant column torsion and resonant column longitudinal tests. Nine undisturbed subgrade samples from seven sites were tested at U. T., Austin, using a torsional resonant column test apparatus.

AC Layer Creep Test Results

Five AC samples were tested in unconfined compressive creep at a temperature of 100 deg. F. The samples were from the sites with the thickest AC layers: D01S3, D08S3, D08S4 (two samples), and D08S5. The creep data plotted on a log-log scale was fit to a straight line.

The straight line corresponded to the two-parameter power-law creep compliance model as described in Appendix B. The model is presented here for convenience:

$$D(t) = A\, t^m$$

where

D(t) = The creep compliance,

A = The creep at t=1 sec.,

t = The time from start of loading, and

m = Log-log slope.

The two parameter relation was used to obtain creep compliance coefficient data (A and m) from the creep curves. The results are summarized in Table 14.

Table 14

AC Creep Compliance Data

Unconfined Compressive Constant Stress Creep Tests
T = 100° F

Site	Stress (psi)	Milli-Strain at t=1 sec	$A = \varepsilon/\sigma_0$ t=1 sec (1/psi)	Log-log Slope (m)	E_{EFF} (ksi)
D01S3	30.52	0.45	14.7e-6	0.38	388
D08S3	30.52	0.40	13.1e-6	0.30	305
D08S4					
upper	15.05	0.60	39.9e-6	0.51	258
lower	30.52	1.8	58.9e-6	0.48	157
D08S5	15.26	0.24	15.7e-6	0.36	339

AC Layer Lab Comparison

A comparison study of AC layer creep properties was conducted. The laboratory creep parameters in Table 14 were used to compute effective modulus and shifted creep curves. The back-calculated creep parameters were also used to compute effective modulus and creep curves. Comparison results are shown in Figures 55 to 58. The AC material comparisons are indicated by figure number in Table 15.

Table 15

AC Layer Comparison Plots

Figure	Layer Data
55	AC surface layer effective modulus
56	Log-log slopes of creep curve
57	Creep compliance curve D(t), Site D01S3
58	Creep compliance curve D(t), Site D08S3

Effective Modulus Results

Effective moduli as defined in Equation B-6 in Appendix B were computed from the back-calculated creep parameters, and the results are presented in Tables 4, 5, and 6. The back-

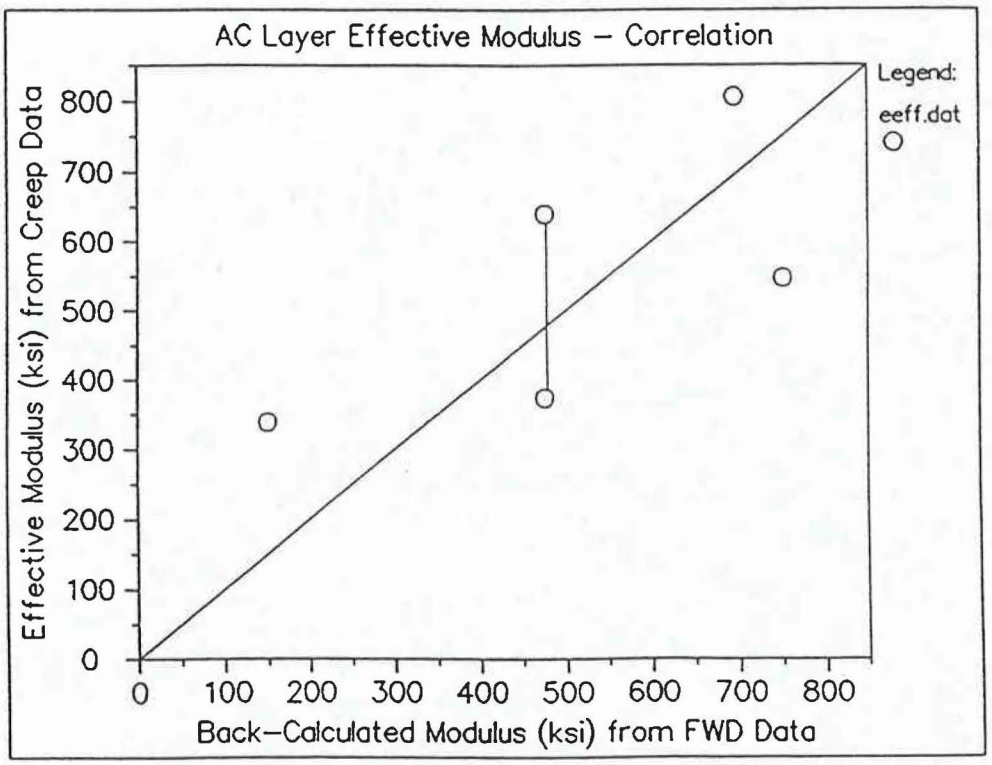

Figure 55. AC Modulus Computed From Creep Data vs. Back-Calculated Effective Modulus

calculated moduli were compared to effective moduli that were computed from the lab creep curves using the data in Table 14. The laboratory creep curves were corrected for temperature so

the lab data corresponded to the surface temperature at the time of the FWD tests. This was done using the time-temperature shift relation given in Equation B-9 of Appendix B. The time-temperature shift was computed from the temperature susceptibility (ß) as defined in Equation B-10. The temperature susceptibility was (in effect) back-calculated by shifting the lab data creep curve so that it matched the creep curve computed from the back-calculated creep parameters. The temperature corrected effective moduli from the lab data were then computed from the temperature corrected compliances using Equation B-6. The resulting comparison is shown in Figure 55 where lab values are plotted against back-calculated values. In Figure 55 one sees some scatter, but back-calculated data and laboratory data agree overall.

Log-Log Slope (m) Comparison

Back-calculated values of the creep log-log slope (m) were compared to lab creep data. Results are shown in Figure 56. Agreement is fair-to-good, showing the back-calculated values to be somewhat underpredicted, on the average. It was assumed, for the log-log slope (m) comparison, that the m was independent of temperature, so no temperature correction was necessary.

Creep Compliance Curve Comparison

Laboratory creep compliance curves are shown in Figures 57 and 58 for sites D01S3 and D08S1, respectively. As discussed in the effective modulus comparison above, the laboratory creep curves (at 100 deg. F) were shifted so that they coincided with the creep curves generated from the back-calculated creep parameters at the FWD field test temperatures. This was done by computing the time-temperature shift factors (a_T) as defined in Equations B-10 of Appendix B. The back-calculated temperature susceptibilities (ß) extracted from the temperature shift data were:

ß = 0.122 for D01S3 and

ß = 0.0714 for D08S1.

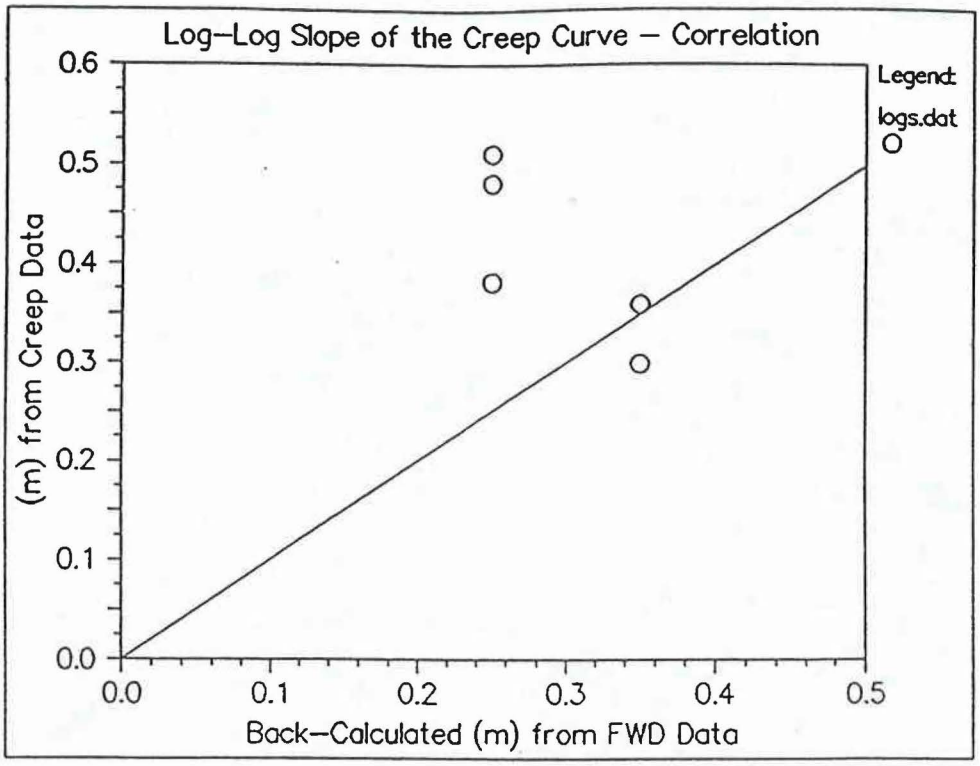

Figure 56. Log-Log Slope (m) from Creep Data vs.
(m) Back-Calculated from FWD Data

These back-calculated values fall within the expected range (0.05 to 0.12) as given in published sources (Fitzgerald and Lai, 1970 and Sharma and Kim, 1975). This is another indication of the validity of the back-calculated AC creep data. Recall that in Chapter IV the temperature susceptibility was computed from back-calculated creep data at two temperatures for Site D01S5. The computed susceptibility for this case was $\beta = 0.094$ for Site D01S5.

The creep curve for Site D01S3 (Figure 57) has an inflection point at about 100 sec., where the curve shifted upward and then continued parallel to the t<100 sec. data. The lab data indicates a more complex response than the two-parameter model. The creep data in Figure 58 for D08S3 agreed much better with the two-parameter model.

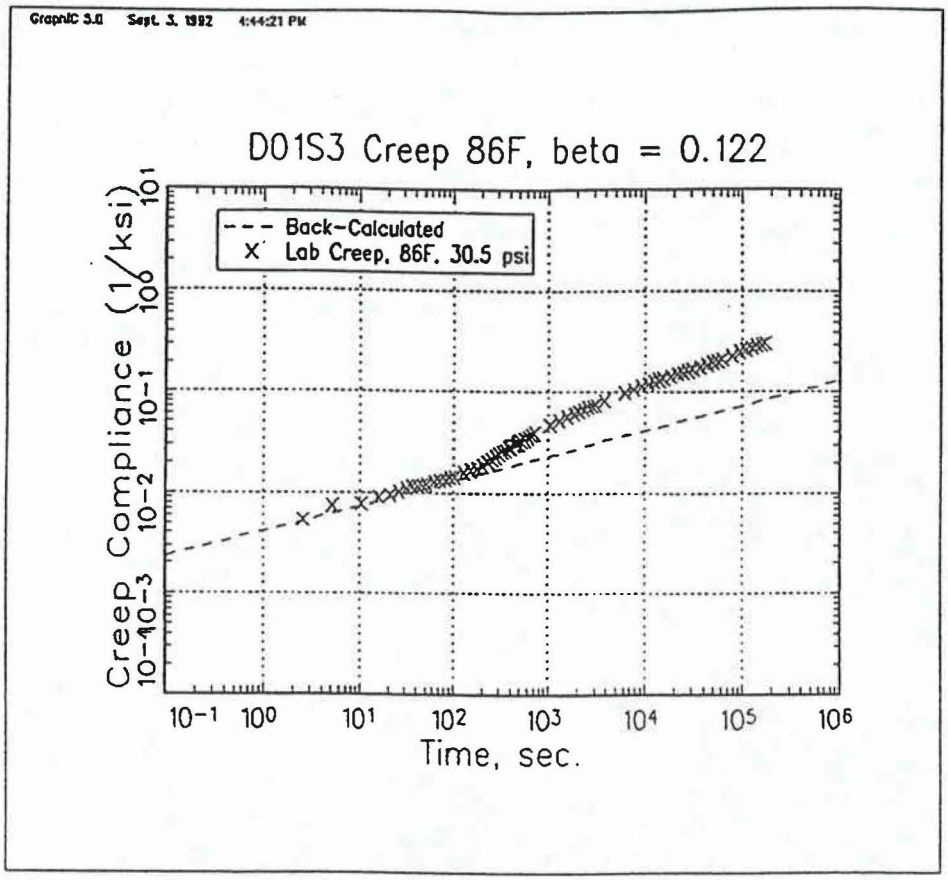

Figure 57. Site D01S3: AC Creep Compliance Function:
Back-Calculated vs. Laboratory Creep Test Data

Resonant column tests for base course samples with confining pressures were run for both torsional and longitudinal vibrations. Results are shown in tabular form in Table 16 and in graphical form in Figure 59. For the torsional resonant column data, the Young's modulus was computed from the measured shear modulus using an assumed Poisson ratio of 0.35. The diagonal line in Figure 59 is the perfect agreement line. There is considerable scatter with fair average agreement except for one point. Inspection of Table 16 shows that the site with poor agreement is D01S1, where the back-calculated value is about twice that of the laboratory value. In Table 16, there is some variation between the moduli obtained in the resonant column shear tests and the resonant column longitudinal vibration tests.

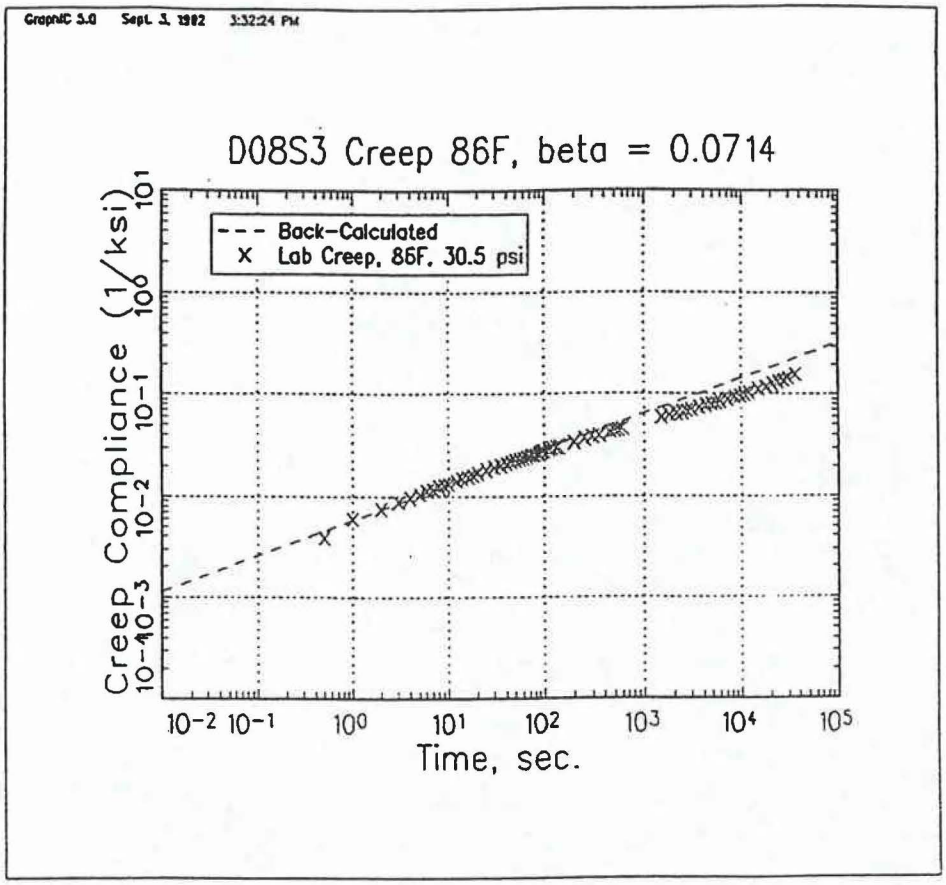

Figure 58. Site D08S3: AC Creep Compliance Function: Back-Calculated vs. Laboratory Creep Test Data

Table 16

Base Course Modulus Comparison with Resonant Column Data
(Ref: G. Bakas's Tests at TTI, 1990)

Site	E (ksi) from Long'l	E (ksi) From Torsion	E (ksi) Back-Calc
D01S1	52	47	100
D01S4	33	52	30
D08S3	56	55	50
D11S3	46	57	60
D21S4	61	50	50

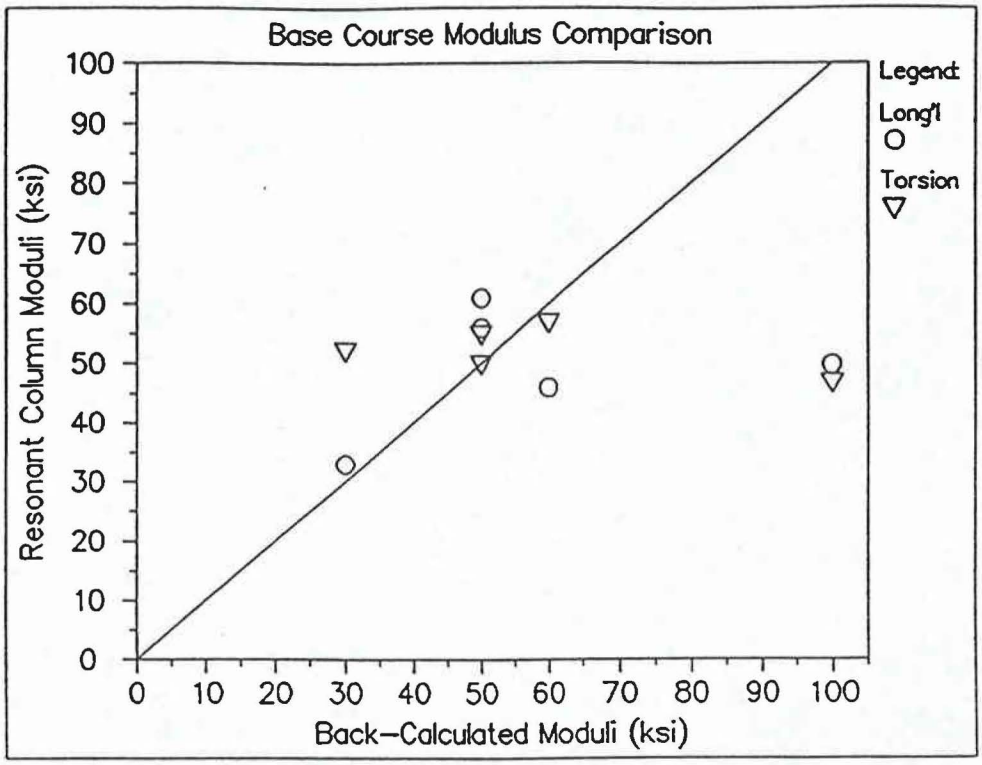

Figure 59. Base Course Modulus Comparison: Resonant Column Test Results vs. FWD Back-Calculated Values (From G. Bakas's, 1990 Data)

Table 17

Subgrade Modulus Comparison with Torsional Resonant Column Data
(From U.T. @ Austin Texas, 1992)

Site	Sample No.	Conf.Press. (psi)	G (psi)	E* (psi)	E (B.C.) (psi)
D01S1	9 Bott	3.2	5,556	15,000	13,900
D01S1	10 Top	2.4	3,056	8,250	"
D08S4	9 Top	12.0	10,069	27,200	20,800
D08S6	7 Top	12.0	6,944	18,750	20,000
D11S1	8 Top	12.0	15,972	43,100	35,000
D21S2	11 Top	6.1	3,611	9,750	9,000
D21S4	11 Top	3.2	4,306	11,630	10,400
D21S5	11 Bott	6.0	4,653	12,600	15,000
D21S5	9 Bott	5.9	9,722	26,250	"

* Poisson Ratio of 0.35 Was Assumed

RESONANT COLUMN TESTS FOR SUBGRADE SAMPLES

Resonant column tests for subgrade samples with various confining pressures were run in a torsional vibration device at U. T. at Austin in 1990. Results are shown in Table 17

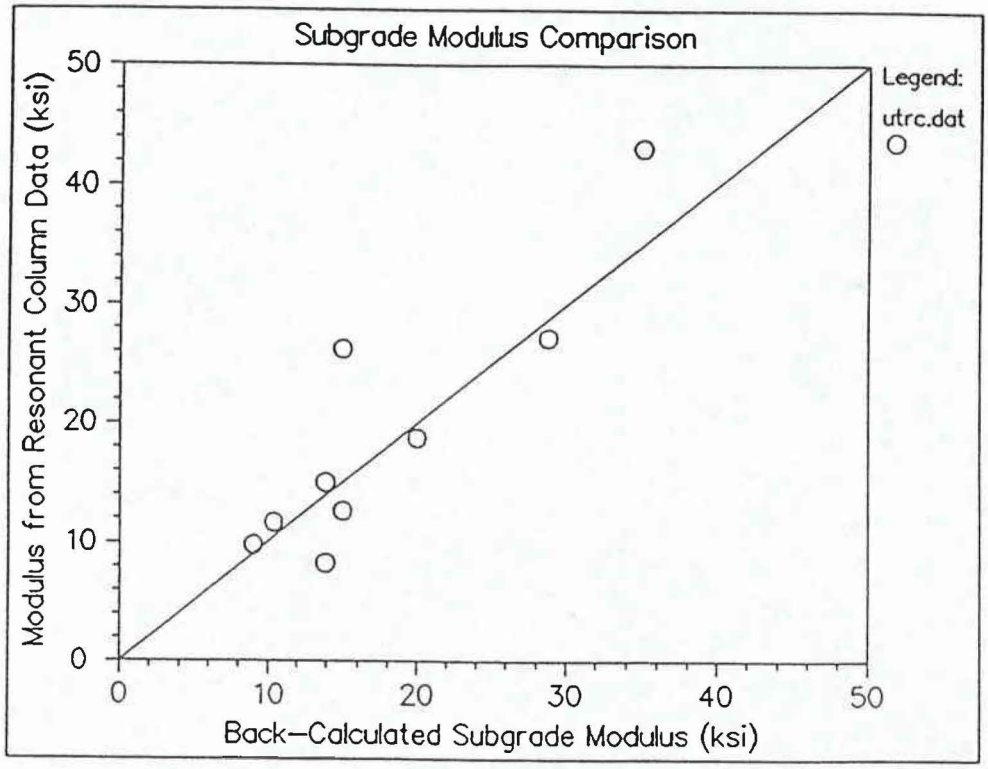

Figure 60. Subgrade Modulus Comparison: Resonant Column Test Results vs. FWD Back-Calculated Values (From K. Stoke's, 1992 Data)

and in Figure 60. The site, sample number, confining pressure, shear modulus (G), Lab Young's modulus (E), and back-calculated Young's modulus are listed in the columns of Table 17. (Note: There were unknown moisture and temperature differences between the Lab and FWD Data.)

Additional lab data was taken at higher confining pressures, but this data is not shown as the pressures were considered to be higher than in-situ values. For the torsional resonant column data, the Young's modulus was computed from the measured shear modulus using an assumed Poisson ratio of 0.35. The back-calculated subgrade modulus used in the comparison is for the subgrade layer closest in depth to the sample's depth. This was usually the sub-subgrade layer. The graphical results in Figure 60 show some scatter, but overall agreement is good.

Summary of the FWD/Lab Comparison Study

Good quantitative agreement was found between back-calculated data and laboratory data: typically within ±30 percent. This applies to the following:

- AC Layer Effective Modulus,
- AC Layer Log-Log Slope (m),
- AC Creep Compliance Curve,
- Base Course Modulus, and
- Subgrade Modulus (Upper Sublayer).

CHAPTER VIII
SUMMARY, CONCLUSIONS, AND RECOMMENDATIONS

SUMMARY

The advantages of using the FWD for nondestructive testing of highways for dynamic analysis were presented. FWD dynamic analysis provides a fast and economical method of obtaining in-situ data on pavement layer properties, including AC creep compliance data. The layer properties were extracted from the FWD time history data.

Creep, Cracking, and Rutting

The connection between AC creep data and cracking and rutting of pavements was discussed. The importance of the log-log slope (m) of the AC creep compliance curve in predicting pavement cracking and rutting was emphasized.

Site Selection

Site selection considerations and pavement section characteristics are presented for the 24 sites chosen. Included were two sites in which the driller's log data showed near-surface bedrock. A brief description of the TTI/TxDOT FWD dynamic analysis back-calculation procedure was given.

Frequency Response Functions

The computation of and use of pavement frequency response functions for pavement dynamic analysis was described. The pavement frequency response functions represent the steady-state time-harmonic vertical surface deflections per unit force. There is one frequency response function for each deflection sensor. Each frequency response function has a frequency dependent magnitude and phase angle.

The frequency response functions were used to back-calculate the thickness of the upper subgrade layer for sections with a H-S-H configuration. Frequency response function magnitude curve shapes were shown to indicate hard/soft (H/S) and hard-soft-hard (H-S-H) pavement types. An interpretation of the FWD responses as surface waves was also given, showing how the lower frequency energy penetrates deeper into the pavement, while high frequency components with shorter wavelengths give information on near-surface layers.

For most sections the FWD magnitude frequency response functions for the outer sensors have a peak indicating a stiffer lower layer. In order to "fit" the computed low frequency data, it was necessary to split up the subgrade into a finite thickness upper sublayer and a semi-infinite stiffer lower sublayer. This was necessary even in sections where drilling log data does not indicate bedrock or other reasons for a stiff sublayer. In addition to bedrock, clay consolidation, ground water, and confining stresses due to the overburden can cause a hard bottom. Three basic types of pavement configuration were found:

- H-S-H: Hard-soft-hard,
- H/S: Hard over soft, and
- S/H: Soft over hard.

Twelve of the 24 sections were classified as H-S-H, 11 sections were classified as H/S and one section was classified as S/H. The sites were separated into three groups based on AC layer thickness: thick, medium, and thin. Average values were given for each group. Measured (i.e. back-calculated) pavement layer properties for each section were presented. AC effective modulus was found to decrease with temperature, and values fell within the expected range. The AC layer log-log slope (m) values fell in the expected range, as compared to values obtained in laboratory creep tests. The base, subbase, and subgrade moduli also fell within their expected ranges. Results of a formal comparison study are described below.

Temperature Effects

FWD testing was done at one site (D01S5) twice, once with a cool temperature and another with a warm temperature. By back-calculating AC creep properties at both

temperatures, a temperature susceptibility constant was computed using a temperature correction procedure, and the result was found to give a realistic value.

SID Back-Calculation

Adjustment of the SID back-calculation procedure was necessary. This indicates the need to refine the closure criteria in the automated SID procedure and/or the viscoelastic model of the AC layer. For some of the thinnest sections, the AC layer and unbound base course were combined into one layer. The combined layer behaved as a viscoelastic layer but with a higher (m) log-log slope than the thicker AC layers.

Transverse Vibration Modes

An apparent lateral vibration mode caused interference in the inner sensor magnitude plots computed using the FWD data. The interference occurred in the 30-80 Hz range for the inner sensors for seven of the 24 sites. The back-calculation curve-fitting on these sites was done satisfactorily by averaging over the questionable data features. The lateral modal effect was related to pavement stiffness, with the effect increasing as stiffness decreases.

Comparison Plots

Comparison plots of pavement frequency response functions were presented for all the sites. Frequency response functions computed using FWD data were plotted along with predicted values using the SCALPOT pavement deflection program and back-calculated layer data. The graphical comparison study results showed generally good agreement between the predicted and the FWD field data for magnitudes and phase angles for all seven sensor locations. The computed results replicated the FWD data magnitude peaks for sites with hard bottoms, i.e. hard-soft-hard sections (vertical mode effect). Possible causes of discrepancies in detailed features between computed and field FWD data were discussed. Limitations of the computer model (primarily the idealized layering configuration) account for some of the discrepancies. Lateral modal vibrations or pavement edge effects may be present that are not simulated.

Laboratory/Back-Calculation Comparison

A comparison study of back-calculated layer properties and laboratory data generated from pavement samples was conducted. Good agreement was found for AC layer creep parameters, base course moduli, and subgrade moduli.

CONCLUSIONS

The overall conclusion was that the layered viscoelastic model used by the SCALPOT program was adequate for representing the pavement dynamic responses. The study of 24 Texas AC pavements included sites with overlays, near-surface bedrock, cement-stabilized base courses, asphalt-stabilized base courses, lime-stabilized subbases, and clay, sand, gravel, rock and/or silt subgrades. A comparison study of back-calculated AC, base course, and subgrade data with laboratory data indicated that the accuracy of the back-calculation procedure was consistent with the variability of the laboratory results.

The SID back-calculation procedure was able to produce consistently realistic values of key pavement layer properties for a wide range of pavement types and thicknesses. Overall results are positive indicating the efficacy of the FWD dynamic analysis procedure for use as a tool in future pavement performance, evaluation, and design studies.

Based on the results of the study, the FWD dynamic analysis procedure described here can perform several functions.

- Compute AC surface layer creep compliance parameters for thick and medium-thick layers using the three-parameter, power-law model. This includes the log-log slope parameter (m) that governs pavement remaining life associated with both cracking and rutting.

- Analyze very thin pavements by combining the AC seal coat layer and the base course granular layer into one layer. Creep compliance parameters can be computed for the combined AC-base course layer.

- Perform cyclic or repeated loading studies simulating vehicle axle loadings at highway speeds (e.g., ESALS). AC layer effective moduli can be computed for different load cycle durations for the AC layers using the creep compliance data. Permanent deformations can also be predicted from the compliance data.

- Compute base course, subbase, and subgrade sublayer moduli.

- Compute upper subgrade sublayer (if any) thickness and/or depth to bedrock.

- Compute the AC layer temperature susceptibility from FWD test data taken at two or more temperatures at least 20 to 30 degrees apart.

- Compute AC creep compliance data for any temperature (i.e., perform a temperature correction) using the time-temperature shift method and the susceptibility data.

- Determine pavement configuration or type. Three basic pavement types were found:

    1. Hard- over- soft: (H/S),
    2. Hard-soft-hard: (H-S-H), and
    3. Soft- over- hard: (S/H).

RECOMMENDATIONS

The major recommendation of the study is for TxDOT to begin the implementation process as soon as practicable. The FWD-based pavement dynamic analysis procedure is now available for initial trial use by the Texas Department of Transportation as a tool for pavement evaluation and performance prediction studies.

Implementation

The implementation process, because of the novelty and complexity of the analysis procedure, will require continuous interaction between the study investigators and the TxDOT users. The users will need time and experience to become experts in pavement dynamic analysis. In addition the users will most likely want to make certain improvements and modifications in the procedures to suit their specific requirements.

The pavement dynamic analysis procedure uses several methods of analysis and approaches that may be new to most highway engineers. Because of this, the implementation process should include an intensive three-day short course on pavement dynamic analysis, accompanied by hands-on experience with a desktop microcomputer.

FWD Data Acquisition for Dynamic Analysis

We recommend the following as first steps in the implementation process.

- TxDOT require that Time History data be recorded in addition to pulse peak values during FWD testing, even if the data is only needed initially for static analysis. This time history data on all tested sites can be used eventually for computing pavement dynamic baseline data. FWD testing for pavement performance and life prediction (based on dynamic analysis) should be done each six months.

- TxDOT develop a Testing Procedure Manual for FWD-Based Dynamic Analysis. TxDOT should define test section configuration, marking drop point locations so that drops are done at the same locations at each site.

Pavement Evaluation Recommendations

The TTI FWD dynamic analysis procedure in its present form can be used to compute layer properties of interest in pavement evaluation and pavement performance prediction. These properties are listed as follows.

- **AC Surface Course Resilient Modulus** (computed from creep parameters)

- **Subgrade Sublayer Thickness** (computed in the T&E process)

- **AC Surface Layer Damping:** In the form of the AC layer's creep compliance curve's log-log slope (m). This gives information on cracking and rutting.

- **AC Surface Layer Creep Compliance Computation:** This gives additional information on cracking and rutting.

- **Temperature Susceptibility:** This can be computed from time-temperature shift data. The data can be obtained from FWD tests at two or more temperatures. This data is used to perform temperature corrections in the AC material.

- **Base Course and Subgrade Moduli:** The back-calculated values compared well with laboratory data taken from samples.

- **AC Layer Permanent Deformation and Fatigue Determination:** Pavement rutting is directly related to permanent deformation. Fatigue is related to pavement cracking due to repeated loading. Both of these are related to the creep compliance data.

- **Pavement Structural Index (SI) for Fatigue and Rutting:** An SI for fatigue and an SI for rutting have been developed for cracking and rutting. The SI computation uses pavement layer properties back-calculated from dynamic analysis of FWD data.

Types of Pavements Where FWD Dynamic Analysis Can be Used

The above-mentioned pavement layer properties can be computed for these pavement types.

- **Thick pavements** - With 5" or more of AC and with cool temperatures, no problems are encountered in back-calculation.

- **Medium-thick pavements** - A correction procedure gives good back-calculation results in spite of (apparent) lateral mode interference effects in the frequency data.

- **Thin pavements** - These pavements (AC layer with 1" to 2" of asphaltic seal coat and granular base) can be analyzed by combining the seal coat and granular base course into one layer.

Further Development of the Procedure

To address these technical issues and to implement computer program improvements discussed in the text, the following plan of action is recommended.

- **Perform Validation Study of FWD Time History Pulses:** Perform a validation study of FWD time history pulses (for the full sampling period) using SHRP's FWD calibration system at the TAMU Riverside Campus. Take deflection measurements simultaneously with FWD sensors in the SHRP calibration device. See Appendix G, validation study of FWD displacement sensors.

- **Perform Pulse Tail Analysis:** Determine if permanent deformation is related to the flat (r = 0) pulse tails (See Table 2). Compute dynamic internal stresses in the AC layer using upgraded SCALPOT-type program. Use stress analysis results to compute the stresses, strains and displacements in the AC material and in the lower layer materials to estimate the permanent deformation in each layer. Compare with FWD pulse tail data.

- **Perform FWD-FFT Program Improvements:** Implement an improved FWD time pulse tail correction procedure that more accurately reflects pavement physical processes. Alternatively apply digital signal processing (DSP) windows filtering procedures to condition FWD pulse data.

- **Develop FWD Time-Domain Back-Calculation Analysis:** Perform inverse FFT on frequency domain results (as presented here) to compute displacement pulses and compare the result to FWD time history data. If necessary (based on the comparison), develop an alternative method for determining pavement layer properties using time-domain pulse data directly.

- **Perform SCALPOT Program Improvements and Additions:** Code up (linear) internal stress computational ability in SCALPOT. Use nonlinear finite element analysis to treat stress dependence of both modulus and Poisson ratio in the AC and granular layers. Code up improved low frequency creep compliance function for the AC layer. An improved AC layer viscoelastic representation valid at low frequencies can be implemented using a four-parameter model described in Appendix B. Develop code to compute temperature susceptibility.

- **Improve SID Program:** Code up error or "goodness of fit" computations.

- **Perform Pavement Edge Effect Study:** Perform dynamic finite element method (FEM) analysis of a pavement section with finite width of AC and base course layers. Use FEM analysis to simulate FWD load on surface and compute pavement surface deflections

at various points transversely and longitudinally on the roadway. If appropriate, develop pavement edge correction factors for the SCALPOT program based on results of this study.

- **Development of Pavement Performance Prediction Procedures:** For prediction of rutting, cracking, and serviceability loss, estimate the remaining life of the pavement.

- **Development of a User-Friendly Interface:** Make modifications for:
  - Output to screen display, hard copy from printer and/or to file,
  - Selecting options on running programs, and on data input and output variables.

REFERENCES

Fitzgerald, J. E. and J. S. Lai, (1970), "Initial Evaluation of the Effect of Synthetic Rubber Additives on the Thermorheological Properties of Asphalt Mixtures," Highway Research Record 313, pp. 18-31.

Holubec, I. and K. H. Wilson, (1970), "A Cyclic Creep Study of Pavement Materials," D.H.O. Report No. RR163, Ontario Joint Highway Research Programme, June.

Kenis, W. J. (1978), "Predictive Design Procedures, VESYS Users' Manual - An Interim Design Method for Flexible Pavement Using the VESYS Structural Subsystem," Report FHWA-RE-77-154.

Lai, J. S. and D. Anderson, (1973), "Irrecoverable and Recoverable Nonlinear Viscoelastic Properties of Asphalt Concrete," Highway Research Record No. 468, National Research Council, National Academy of Sciences.

Lamb, H., (1904), "On the Propagation of Tremors Over the Surface of an Elastic Soil," Philosophical Transactions of the Royal Society, Vol. 203, pp. 1-42.

Lytton, R. L., (1992), "Performance Models and Validation of Test Results," SHRP Quarterly Report, A-005 Project, Quarter 2 of 4, of Year 3, Texas Transportation Institute, Texas A&M University, July 15.

Lytton, R. L., (1990), "Materials Property Relationships for Modeling the Behavior of Asphalt-Aggregate Mixtures in Pavements," Memorandum, SHRP A-005 Project, Texas Transportation Institute, Materials, Pavements and Construction, Texas A&M University, June 7.

REFERENCES (Continued)

Lytton, R. L., F. Germann, and Y. J. Chou, (1990), "Determination of Asphalt Concrete Pavement Structural Properties by Nondestructive Testing; Phase II Final Report Appendices," Prepared for NCHRP, TRB, NRC, Texas A&M Research Foundation Project RF7026, Texas Transportation Institute, The Texas A&M University System, February.

Lytton, R. L., (1989), "Back-calculation of Pavement Layer Properties," Nondestructive Testing of Pavements and Back-calculation of Moduli, ASTM STP 1026, ASTM, 1916 Race St., Philadelphia, Pa. 19103.

Lytton, R. L., F. L. Roberts, and S. M. Stoffels, (1986), "Determination of Asphaltic Concrete Pavement Structural Properties by Nondestructive Testing," Final Report, Phase 1, NCHRP Project 10-27, Texas Transportation Institute, Texas A&M University, July.

Magnuson, Allen H., (1993), "Calculation of Pavement Layer Properties Using Dynamic Analysis of Falling-Weight Deflectometer Data," Final Report (Draft), SHRP/IDEA Project No. SHRP-88-ID026, Texas Transportation Institute, Division II, Materials, Pavements, and Construction, Texas A&M University, June 9.

Magnuson, Allen H., (1992), "The Use of FWD Time History Data for Pavement Dynamic Analysis," Texas Transportation Institute, Division II, Report ID-TM 1A (Draft), SHRP/IDEA Project Number SHRP-88-ID025, Texas A&M University, May 15.

Magnuson, A. H., R. L. Lytton, and R. Briggs, (1991), "Comparison of Computer Predictions and Field Data for Dynamic Analysis of Falling-Weight Deflectometer Data," *Transportation Research Record 1293, Back-calculation of Pavement Moduli*, Transportation Research Board, National Research Council, Washington, D. C. 1991, pp. 61-71.

REFERENCES (Continued)

Magnuson, Allen H., (1988a), "Dynamic Analysis of Falling-Weight Deflectometer Data," Report No. FHWA/TX-88/1175-1, Texas Transportation Institute, Texas A&M System, College Station, Texas 77843-3135, November.

Magnuson, Allen H., (1988b), "Computer Analysis of Falling-Weight Deflectometer Data, Part I: Vertical Displacement Computations on the Surface of a Uniform Halfspace Due to an Oscillating Surface Pressure Distribution," Report No. FHWA/TX-88/1215-1F, Texas Transportation Institute, Texas A&M System, College Station, Texas 77843-3135, November.

Magnuson, A. H. (1975), "The Acoustic Response in a Liquid Layer Overlaying a Multi-layered Viscoelastic Half-Space," *Journal of Sound and Vibration*, Vol. 43, No. 4, pp. 659-669.

Paris, P. and F. Ergodan (1963), "A Critical Analysis of Crack Propagation Laws," Trans. ASME Jnl. of Basic Negro., Vol. 85, Ser. D, #4, pp. 528-534, December.

Roque, R., D. R. Hiltunen, and S. M. Stoffels, (1992), "Results of the A-003A/A-005 Cooperative Testing Program for Low Temperature Cracking," Report from the Pennsylvania Transportation Institute, The Pennsylvania State University, March 10.

Schapery, R. A. (1981), "Nonlinear Fracture Analysis of Viscoelastic Composite Materials Based on a Generalized J Integral Theory," *Proc. Japan - U. S. Conference on Composite Materials*, Tokyo, Japan.

Sharma, M. G. and K. S. Kim, (1975), "Nonlinear Viscoelastic Properties of Bituminous Concretes," *Journal of Testing and Evaluation*, Vol. 3, No. 3., pp. 182-190, May.

Sherwood, James A. and William J. Kenis, (1972), "Sulphlex Pavement Performance Evaluations from Laboratory Tests," Transportation Research Record No. 852.

Torpunuri, V. S., (1990), "A Methodology to Identify Material Properties in Layered Viscoelastic Halfspaces," M.S. Thesis, Civil Engineering, Texas A&M University, College Station, Texas 77843, May.

Uzan, J., R. L. Lytton, and F. P. Germann, (1988), "General Procedure for Back-calculation of Moduli," *First Symposium on Nondestructive Testing of Pavements and Back-calculation of Moduli*, ASTM, Baltimore, Maryland.

Wang, F. and R. L. Lytton (1993), "Back-Calculation of FWD Data," Presented at the Annual Meeting of the Transportation Research Board, Washington, D. C., January.

Wylie, C. R. (1960), *Advanced Engineering Mathematics, Second Edition*, McGraw-Hill, New York.

APPENDIX A
FALLING-WEIGHT DEFLECTOMETER
TIME HISTORY PLOTS

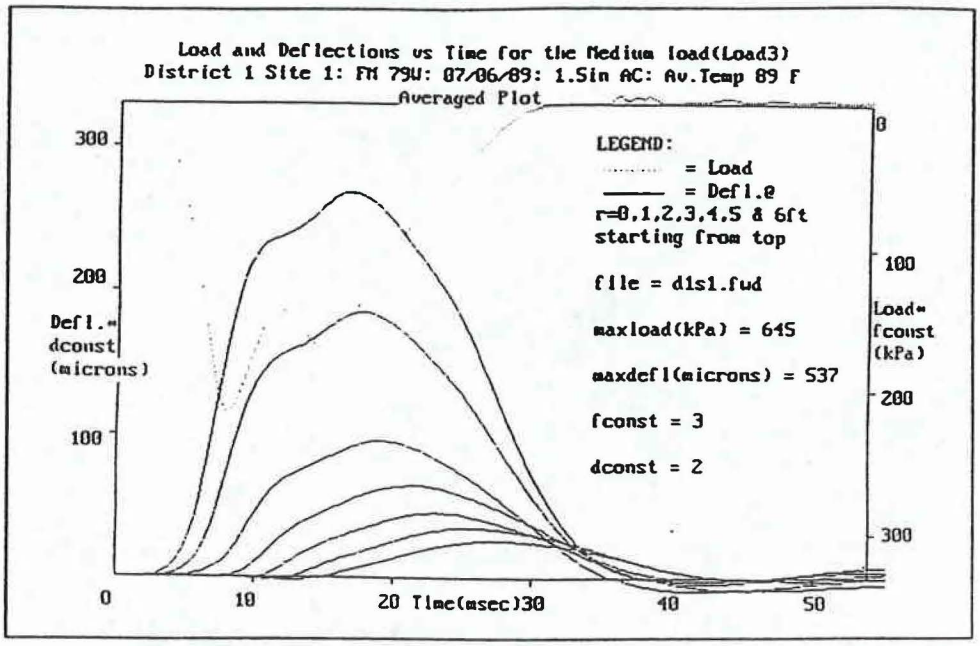

Figure 61. Section D01S1: FWD Time History Plots for FWD Force and Displacement Sensors (r=0, 1, 2, 3, 4, 5, and 6 ft.)

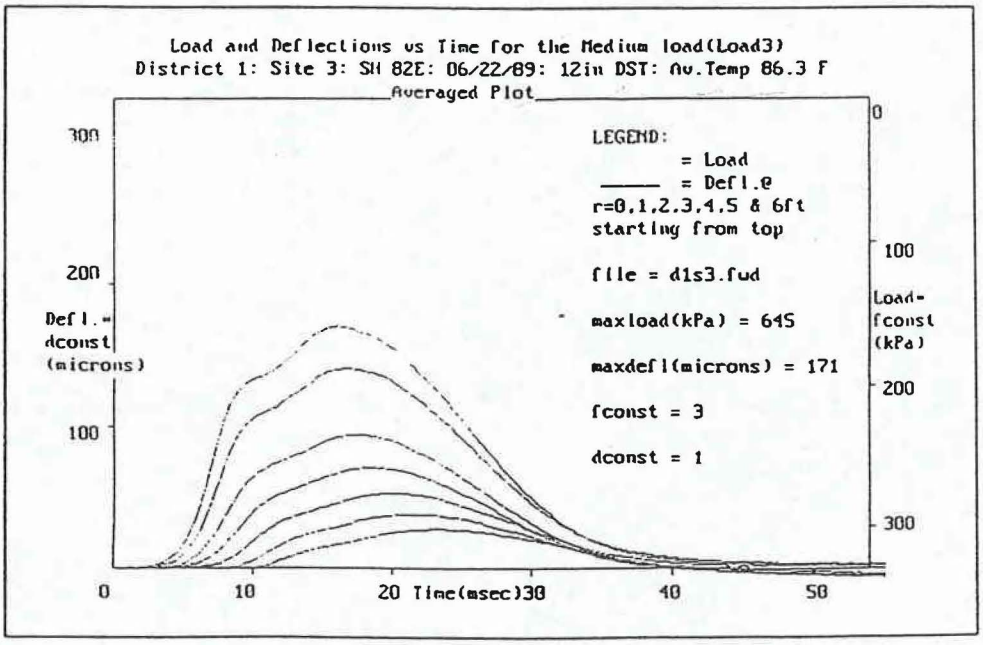

Figure 62. Section D01S3: FWD Time History Plots for FWD Force and Displacement Sensors (r=0, 1, 2, 3, 4, 5, and 6 ft.)

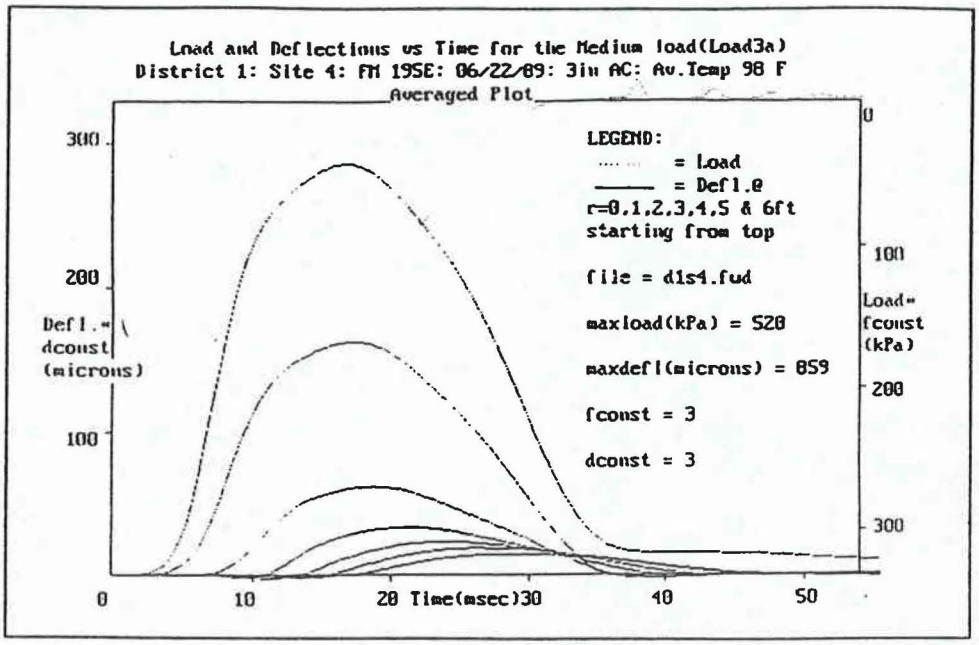

Figure 63. Section D01S4: FWD Time History Plots for FWD Force and Displacement Sensors (r=0, 1, 2, 3, 4, 5, and 6 ft.)

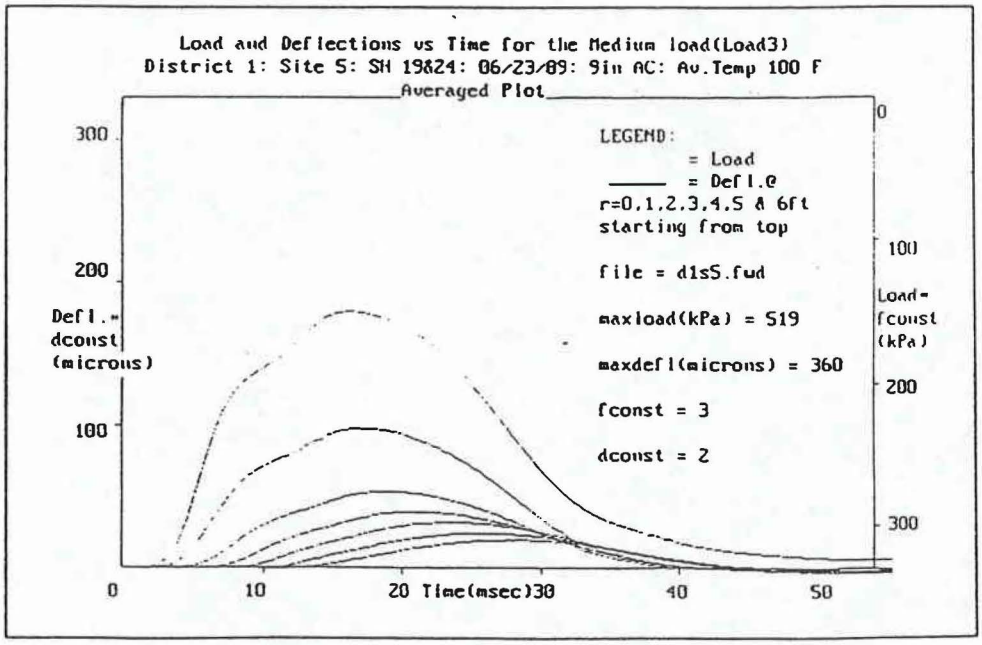

Figure 64. Section D01S5: FWD Time History Plots for FWD Force and Displacement Sensors (r=0, 1, 2, 3, 4, 5, and 6 ft.)

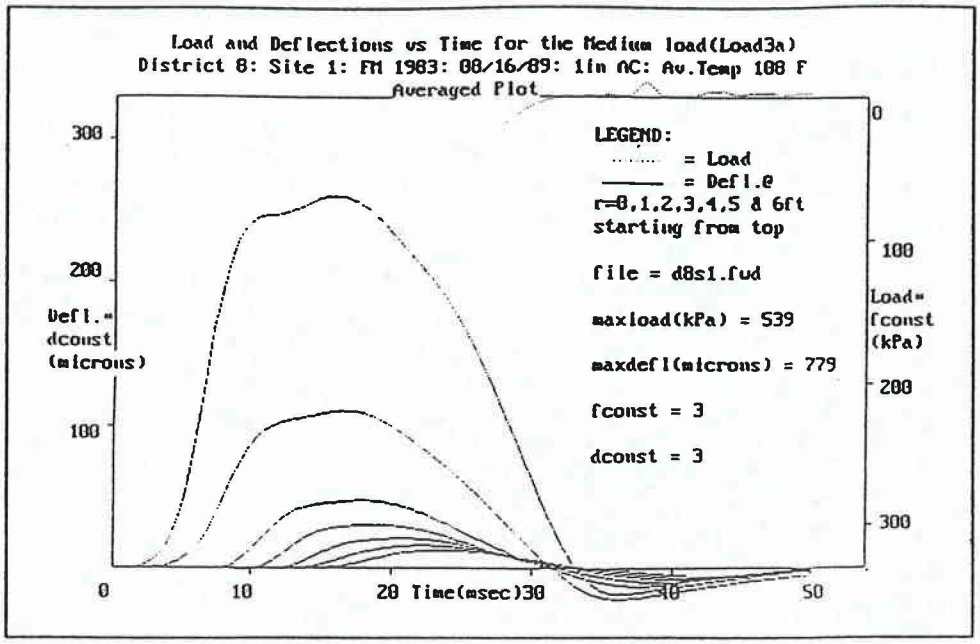

Figure 65. Section D08S1: FWD Time History Plots for FWD Force and Displacement Sensors (r=0, 1, 2, 3, 4, 5, and 6 ft.)

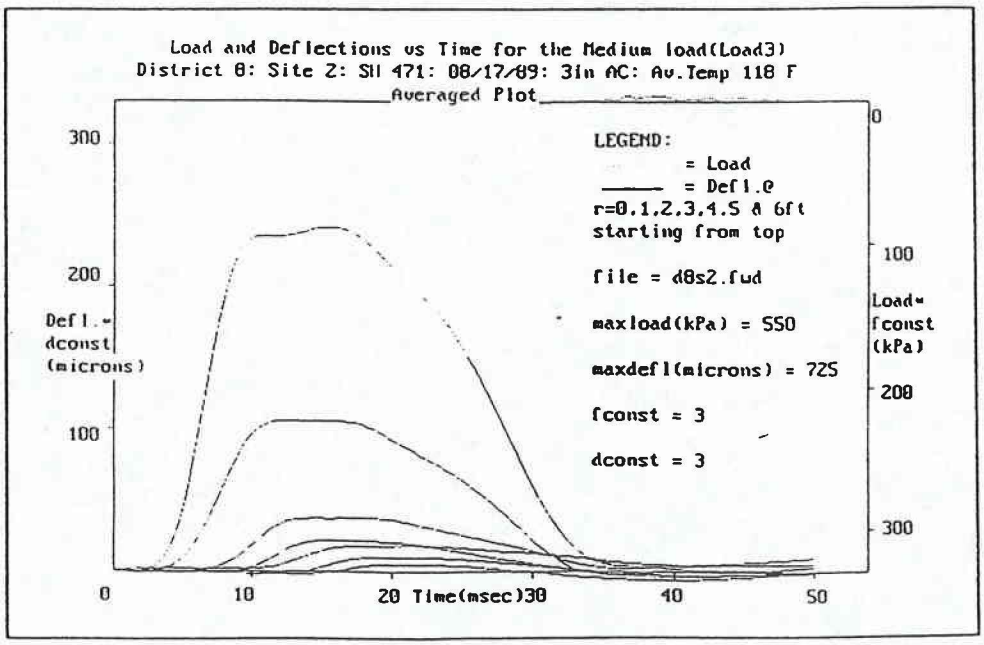

Figure 66. Section D08S2: FWD Time History Plots for FWD Force and Displacement Sensors (r=0, 1, 2, 3, 4, 5, and 6 ft.)

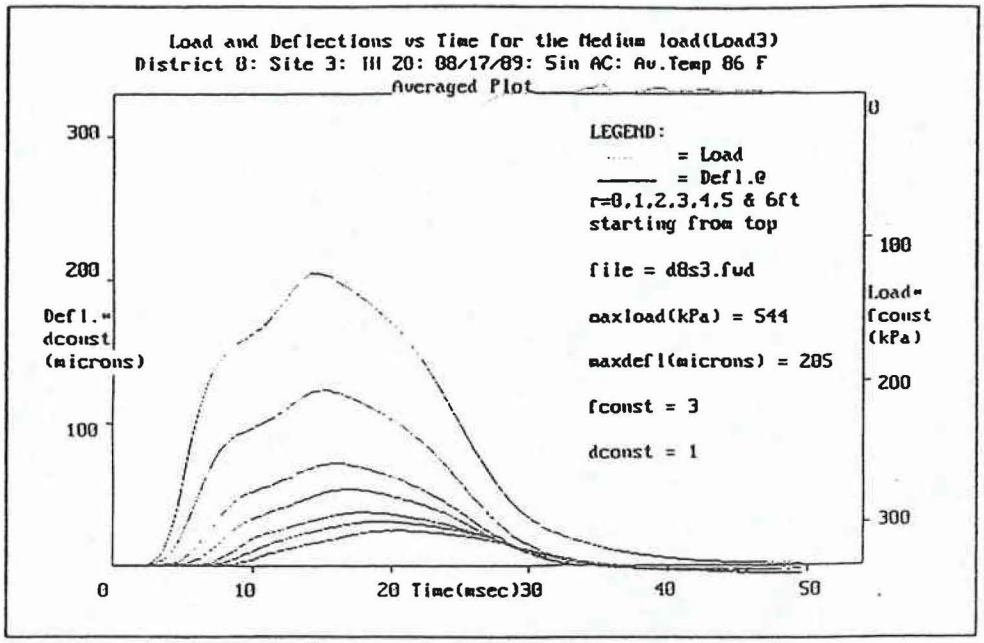

Figure 67. Section D08S3: FWD Time History Plots for FWD Force And Displacement Sensors (r=0,1,2,3,4,5, and 6 ft.)

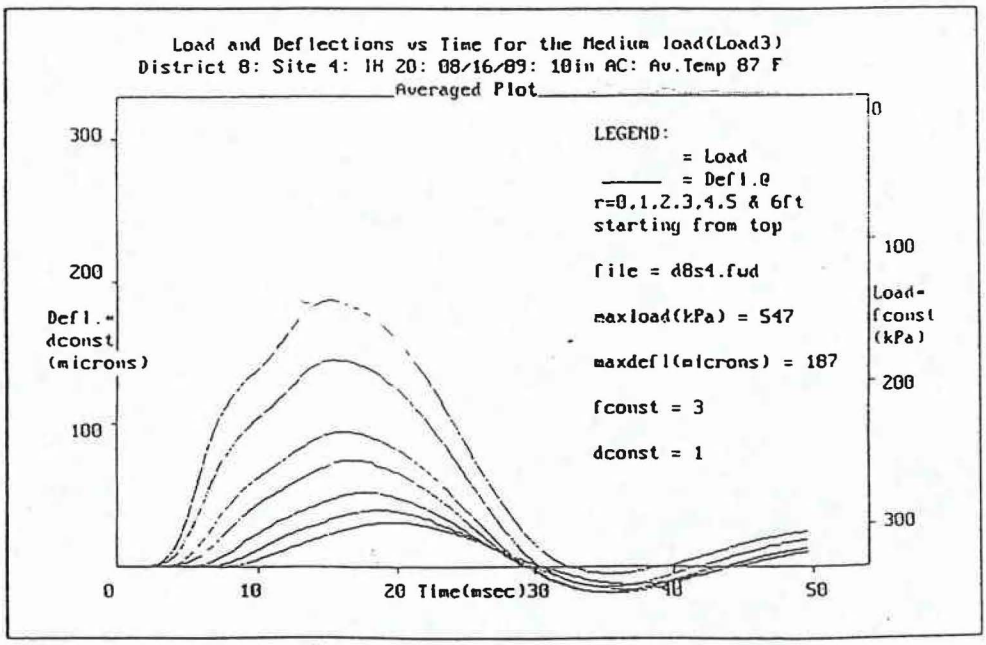

Figure 68. Section D018S4: FWD Time History Plots for FWD Force And Displacement Sensors (r=0,1,2,3,4,5, and 6 ft.)

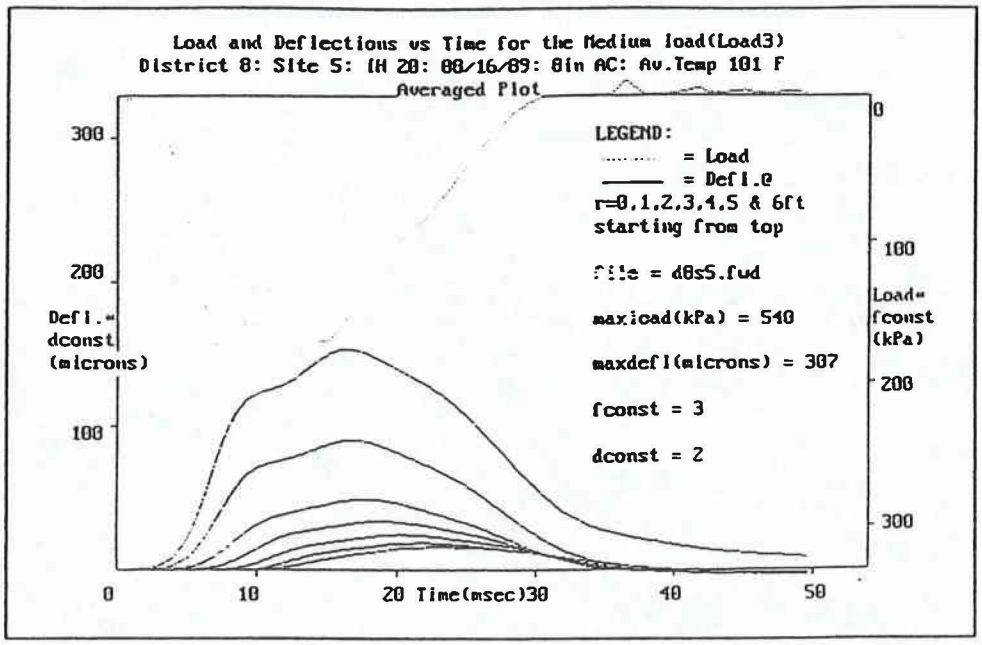

Figure 69. Section D08S5: FWD Time History Plots for FWD Force And Displacement Sensors (r=0,1,2,3,4,5, and 6 ft.)

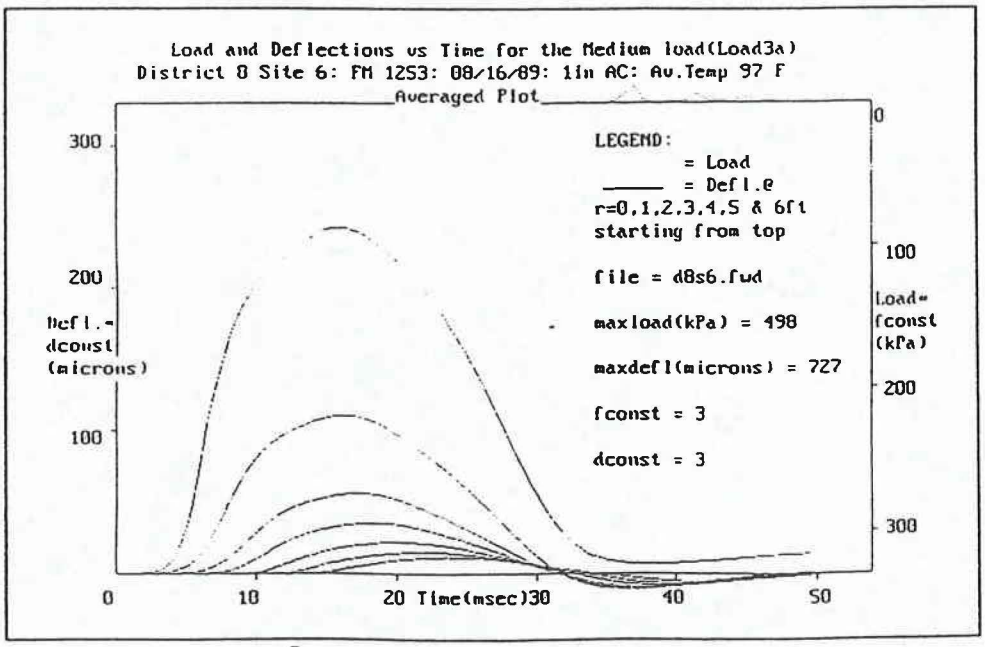

Figure 70. Section D08S6: FWD Time History Plots for FWD Force And Displacement Sensors (r=0,1,2,3,4,5, and 6 ft.)

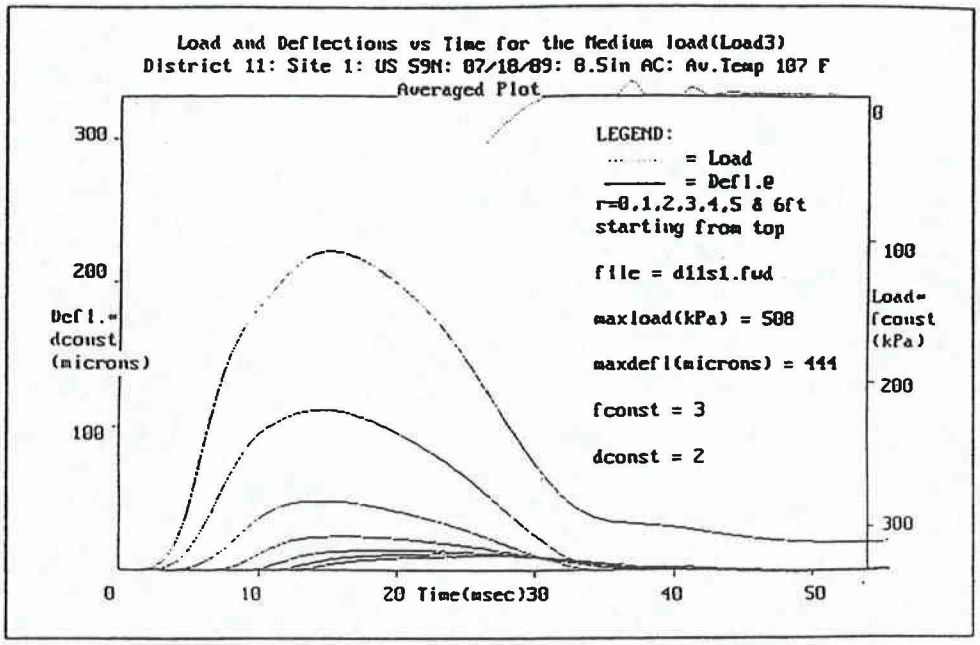

Figure 71. Section D11S1: FWD Time History Plots for FWD Force and Displacement Sensors (r=0, 1, 2, 3, 4, 5, and 6 ft.)

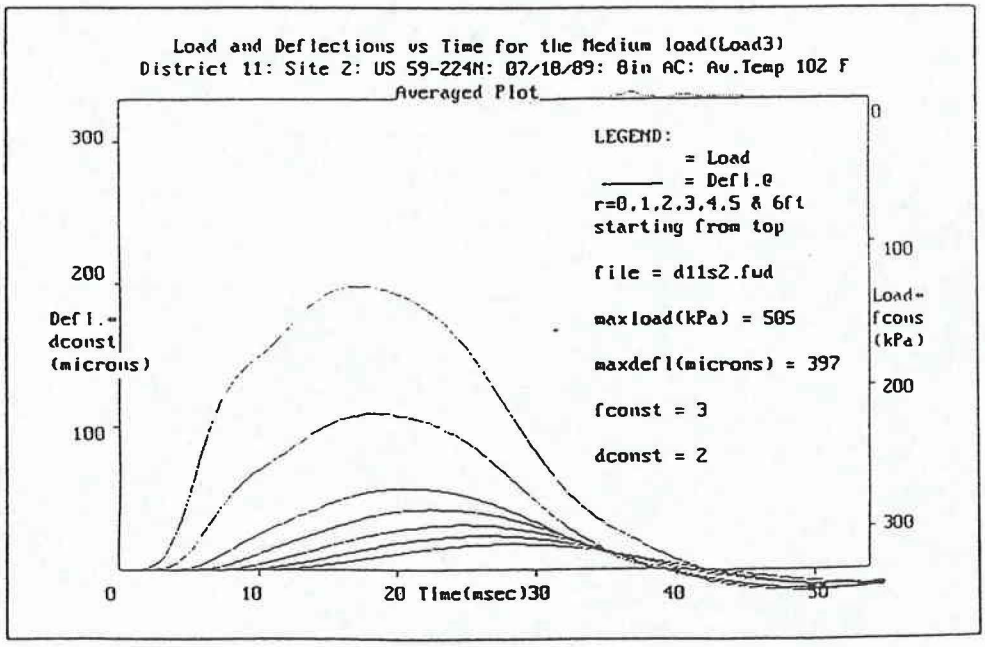

Figure 72. Section D11S2: FWD Time History Plots for FWD Force and Displacement Sensors (r=0, 1, 2, 3, 4, 5, and 6 ft.)

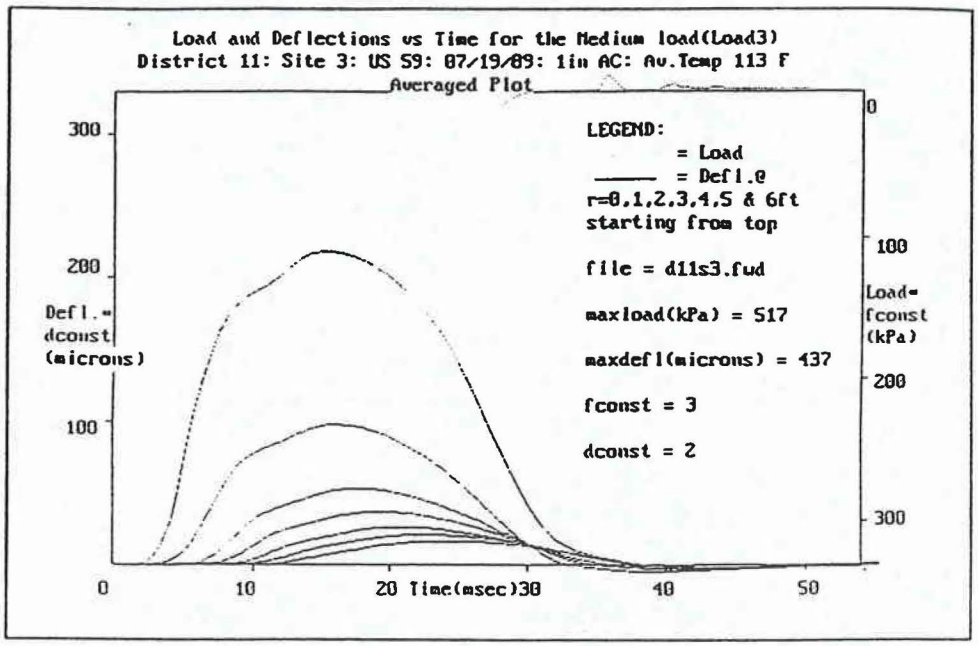

Figure 73. Section D11S3: FWD Time History Plots for FWD Force and Displacement Sensors (r=0, 1, 2, 3, 4, 5, and 6 ft.)

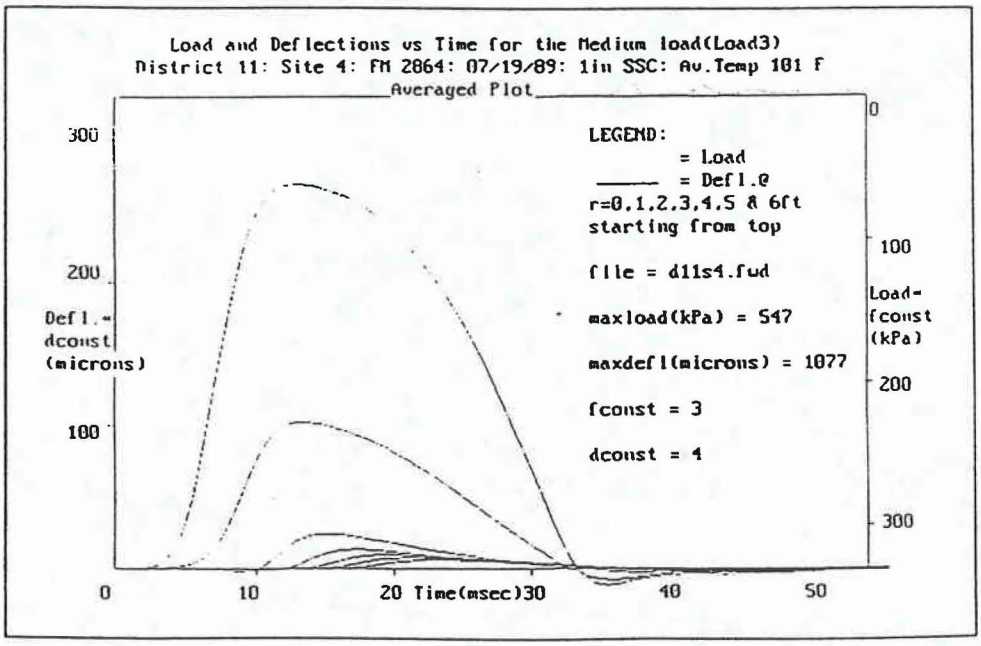

Figure 74. Section D11S4: FWD Time History Plots for FWD Force and Displacement Sensors (r=0, 1, 2, 3, 4, 5, and 6 ft.)

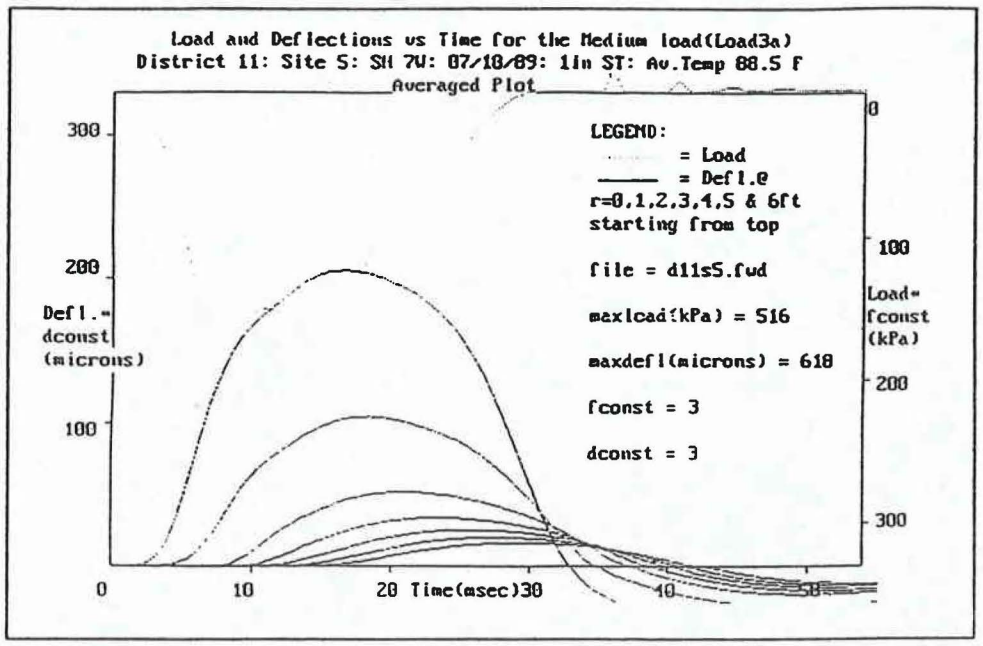

Figure 75. Section D11S5: FWD Time History Plots for FWD Force and Displacement Sensors (r=0, 1, 2, 3, 4, 5, and 6 ft.)

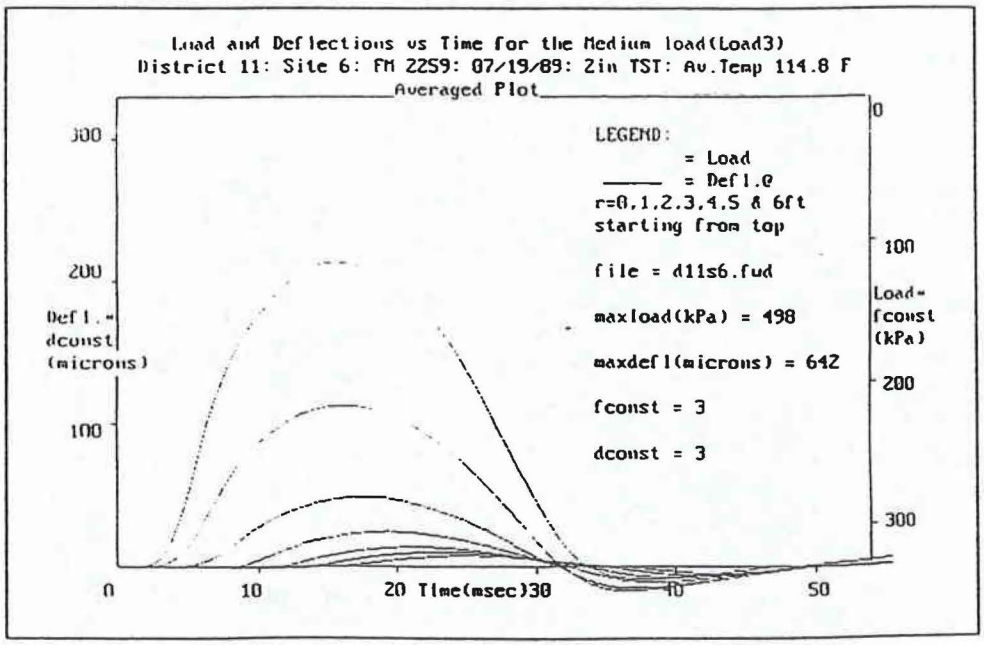

Figure 76. Section D11S6: FWD Time History Plots for FWD Force and Displacement Sensors (r=0, 1, 2, 3, 4, 5, and 6 ft.)

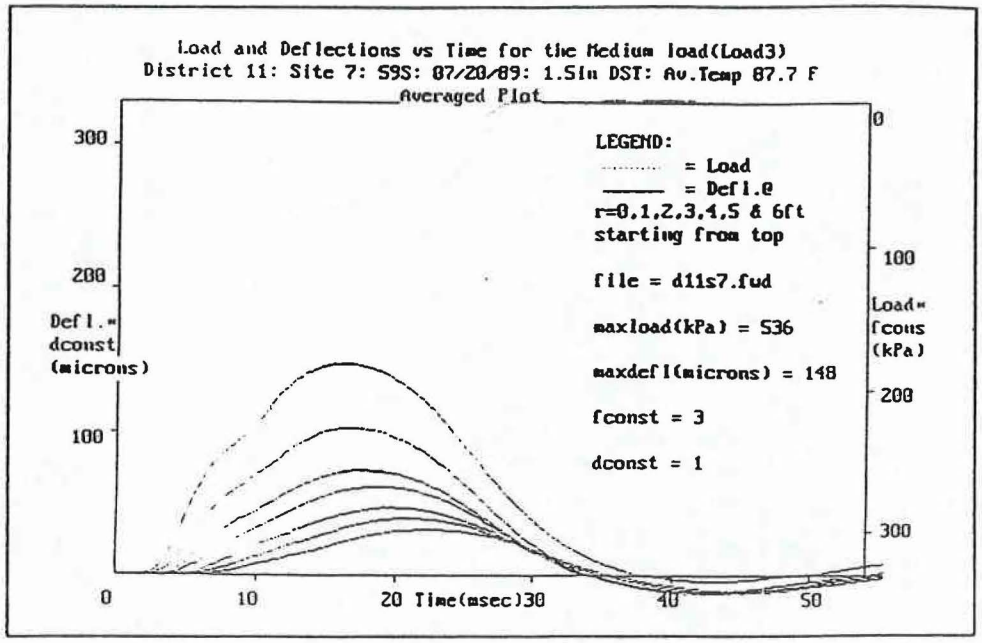

Figure 77. Section D11S7: FWD Time History Plots for FWD Force and Displacement Sensors (r=0, 1, 2, 3, 4, 5, and 6 ft.)

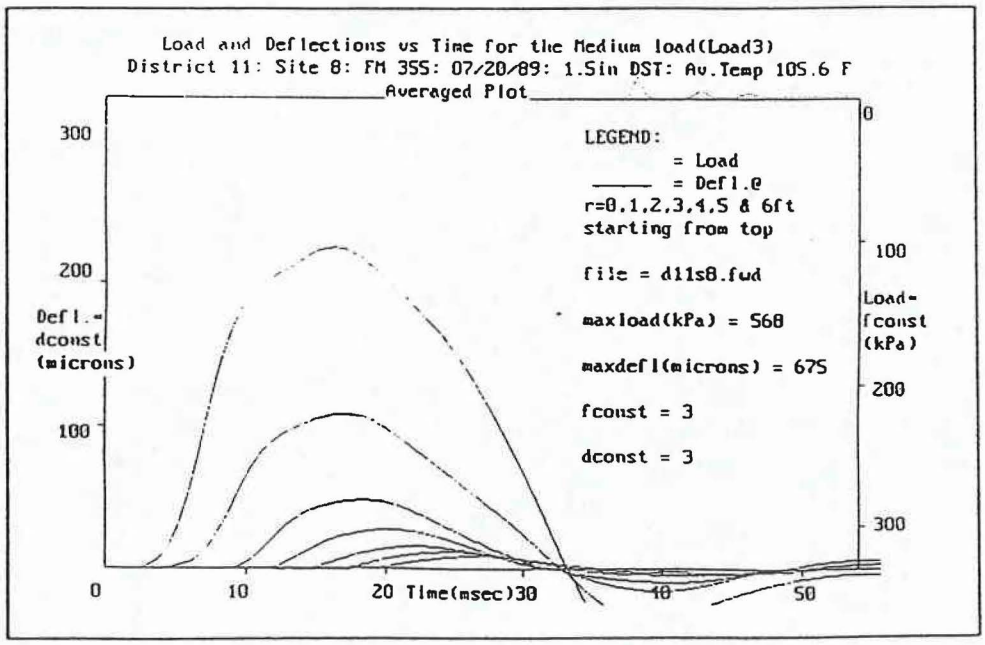

Figure 78. Section D11S8: FWD Time History Plots for FWD Force and Displacement Sensors (r=0, 1, 2, 3, 4, 5, and 6 ft.)

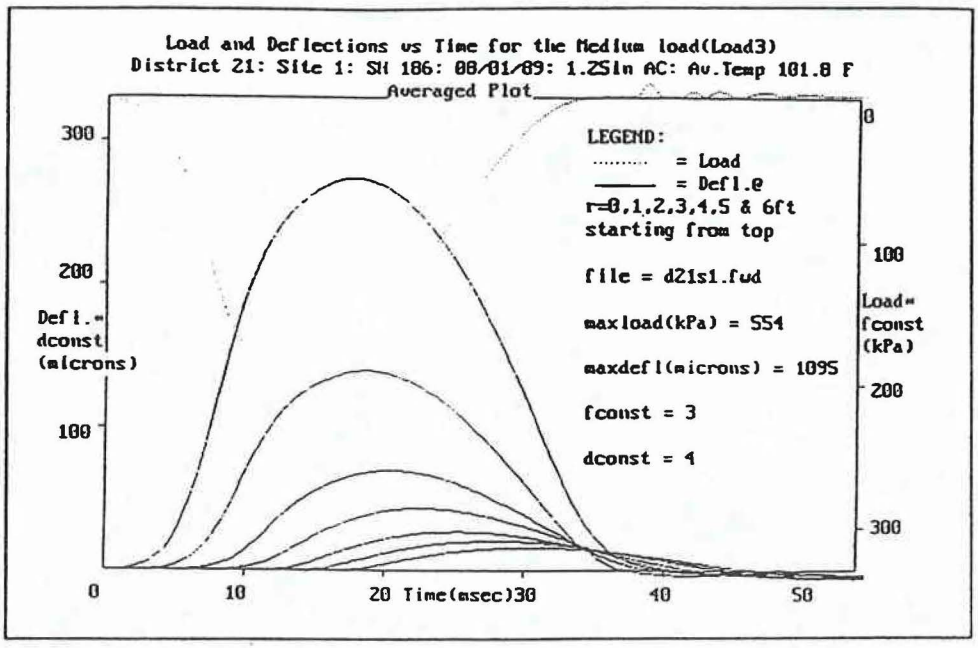

Figure 79. Section D21S1: FWD Time History Plots for FWD Force and Displacement Sensors (r=0, 1, 2, 3, 4, 5, and 6 ft.)

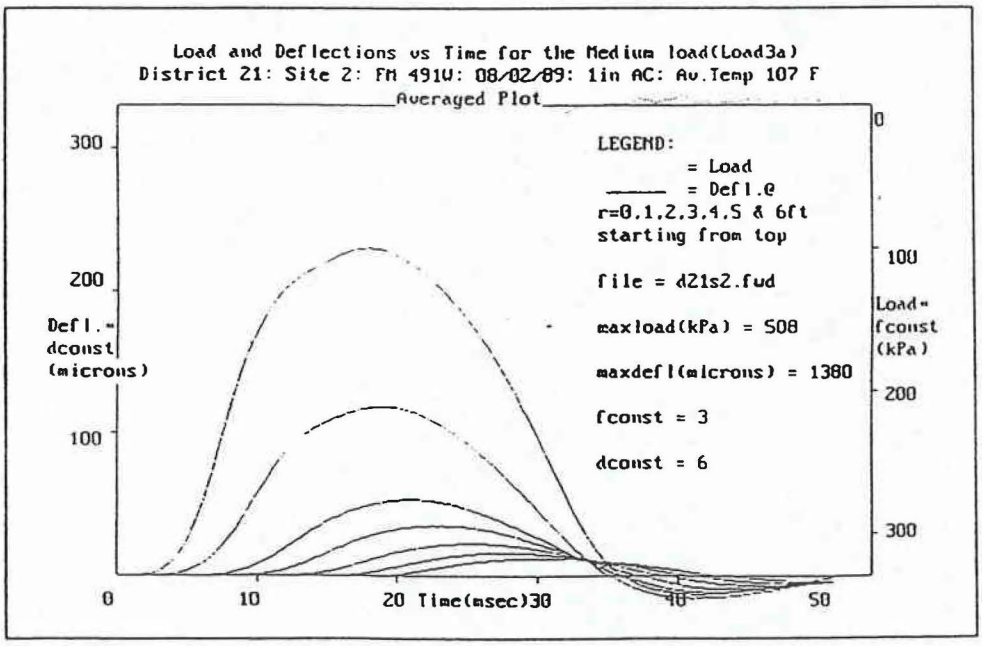

Figure 80. Section D21S2: FWD Time History Plots for FWD Force and Displacement Sensors (r=0, 1, 2, 3, 4, 5, and 6 ft.)

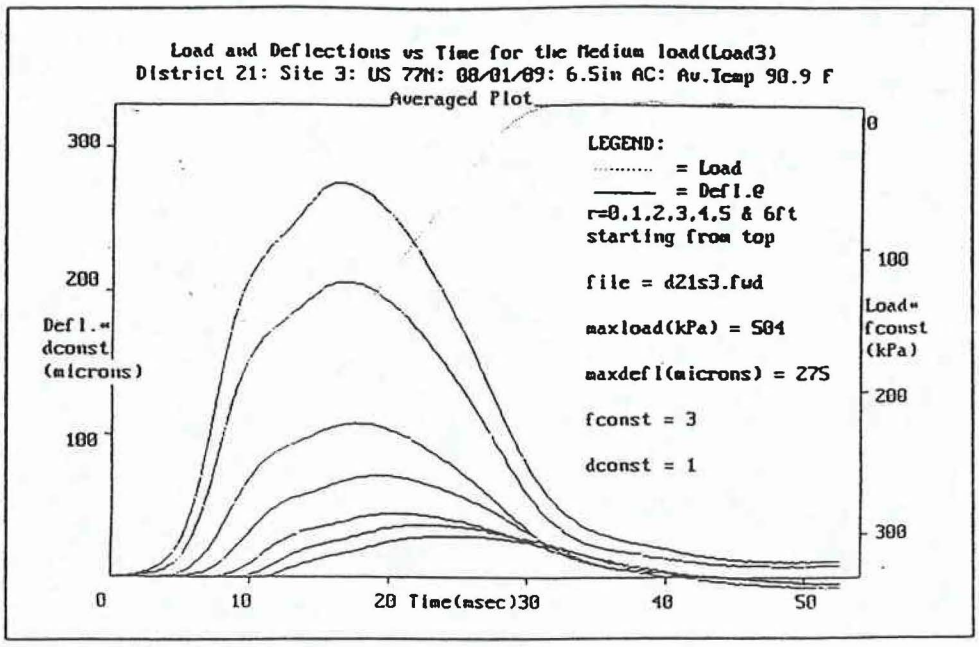

Figure 81. Section D21S3: FWD Time History Plots for FWD Force and Displacement Sensors (r=0, 1, 2, 3, 4, 5, and 6 ft.)

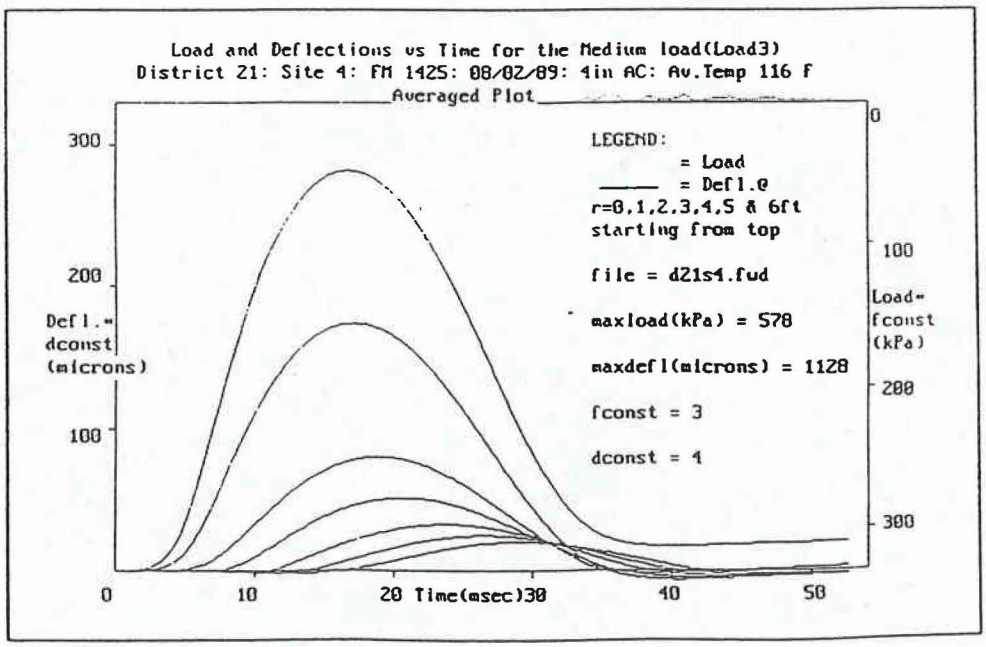

Figure 82. Section D21S4: FWD Time History Plots for FWD Force and Displacement Sensors (r=0, 1, 2, 3, 4, 5, and 6 ft.)

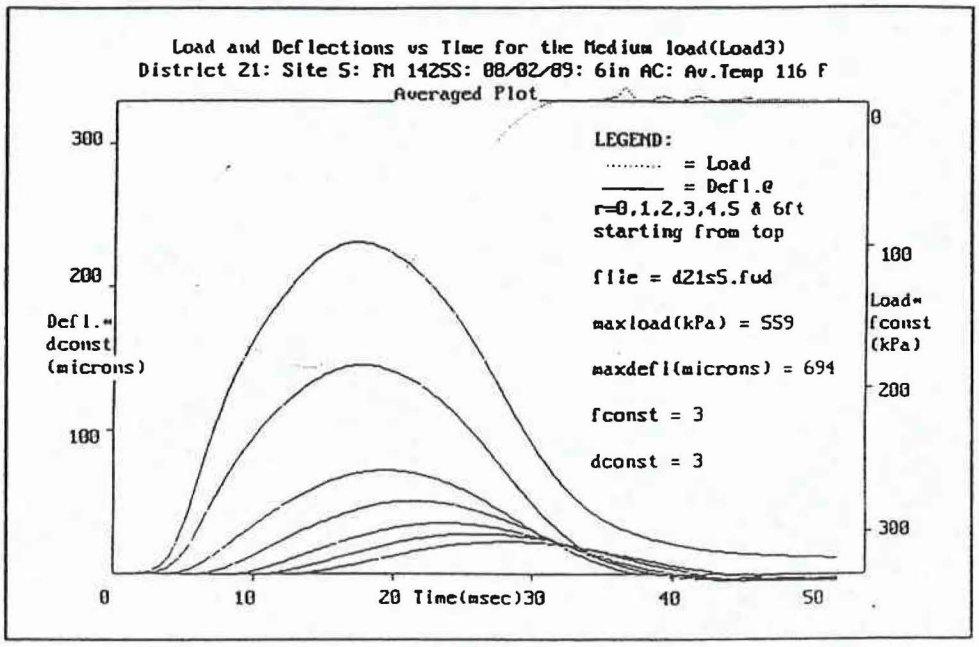

Figure 83. Section D21S5: FWD Time History Plots for FWD Force and Displacement Sensors (r=0, 1, 2, 3, 4, 5, and 6 ft.)

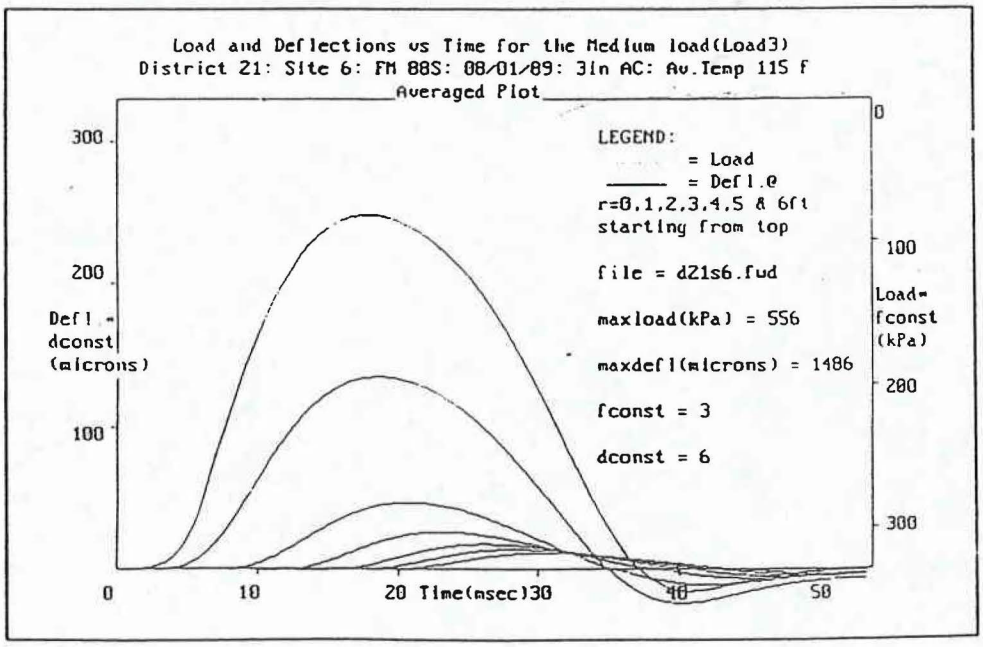

Figure 84. Section D21S6: FWD Time History Plots for FWD Force and Displacement Sensors (r=0, 1, 2, 3, 4, 5, and 6 ft.)

APPENDIX B

CREEP COMPLIANCE FUNCTIONS FOR ASPHALTIC CONCRETE MATERIALS

CREEP COMPLIANCE FUNCTIONS FOR ASPHALTIC CONCRETE MATERIALS

Asphaltic concrete material is a matrix of solid aggregate particles with an asphaltic binder. The adhesion or bonding between the asphaltic binder and the aggregate particles results in viscoelastic behavior of the AC mixture. A viscoelastic material has mechanical properties that are part solid and part liquid. The AC material deformations have three components: elastic response, delayed elastic response, and permanent or visco-plastic deformation. The AC layer and pavement section as a whole are subjected to internal stresses from compaction and external stresses from traffic loading on the surface.

Some of an asphaltic concrete material's mechanical properties may be characterized by its creep compliance function. Creep compliance data for moderate temperatures (approx. 40 to 100 deg. F) is customarily obtained from uniaxial unconfined constant stress compressional creep tests. These tests give creep curves as plots of strain vs. time for a suddenly applied constant stress (i.e., a step function loading). The relation between the creep compliance function and strain due to creep is given as

$$D(t) = \varepsilon(t)/\sigma_0, \quad \text{(B-1)}$$

where $D(t)$ = Creep compliance function,

$\varepsilon(t)$ = Longitudinal strain, and

σ_0 = Constant longitudinal stress.

AC highway materials are usually characterized mechanically using creep compliance functions based on a power-law in time. Commonly used expressions are presented below. The simplest model, two-parameter power-law creep can be written:

$$D(t) = A\, t^m, \quad \text{(B-2)}$$

where $D(t)$ is the creep compliance (units: 1/psi),

m is the log-log slope (exponent), and

A is the time t=1 sec. creep constant.

The parameter m is a material property characterizing the nonlinear time dependence of the creep. (Note that m = 1 corresponds to linear Newtonian viscosity as in a viscous fluid.) This relation (Equation B-2) when plotted on a log-log scale produces a straight line with a slope of m. The limiting behavior of this model is unrealistic for large times because the strain increases indefinitely like a liquid.

Three-Parameter Model

The following three-parameter model gives more realistic values for small times:

$$D(t) = D_0 + D_1 t^m, \quad \text{(B-3)}$$

where

D_0 = $1/E_0$ (Elastic response term due to solid matrix),

D_1 = Creep compliance constant (for nonlinear viscous term), and

m = exponent for nonlinear time dependence.

The relation in Equation B-3 is shown graphically in Figure 85-a. The TTI SCALPOT dynamic analysis program currently uses this (B-2) three-parameter model. Note that this model also has infinite response for large times.

For convenience, one may introduce the viscous/elastic compliance ratio ($\alpha = D_1/D_0$) into Equation B-3:

$$D(t) = D_0 (1 + \alpha t), \quad \text{(B-4)}.$$

Note the limiting behavior of Equation B-4.

$$D(0) = D_0$$

$$D(\infty) = \infty$$

The compliance at infinite time is infinite, which is physically unrealistic. Because of the final-value theorem in transform theory, the extremely long times correspond to extremely low frequencies. Therefore, errors in neglecting the large-time representation are concentrated at the very low frequencies. Responses at frequencies below about 3-10 Hz. should be disregarded when the three-parameter model is used. The three-parameter model is satisfactory for frequencies above about 10 Hz. A more realistic four-parameter compliance function is given below.

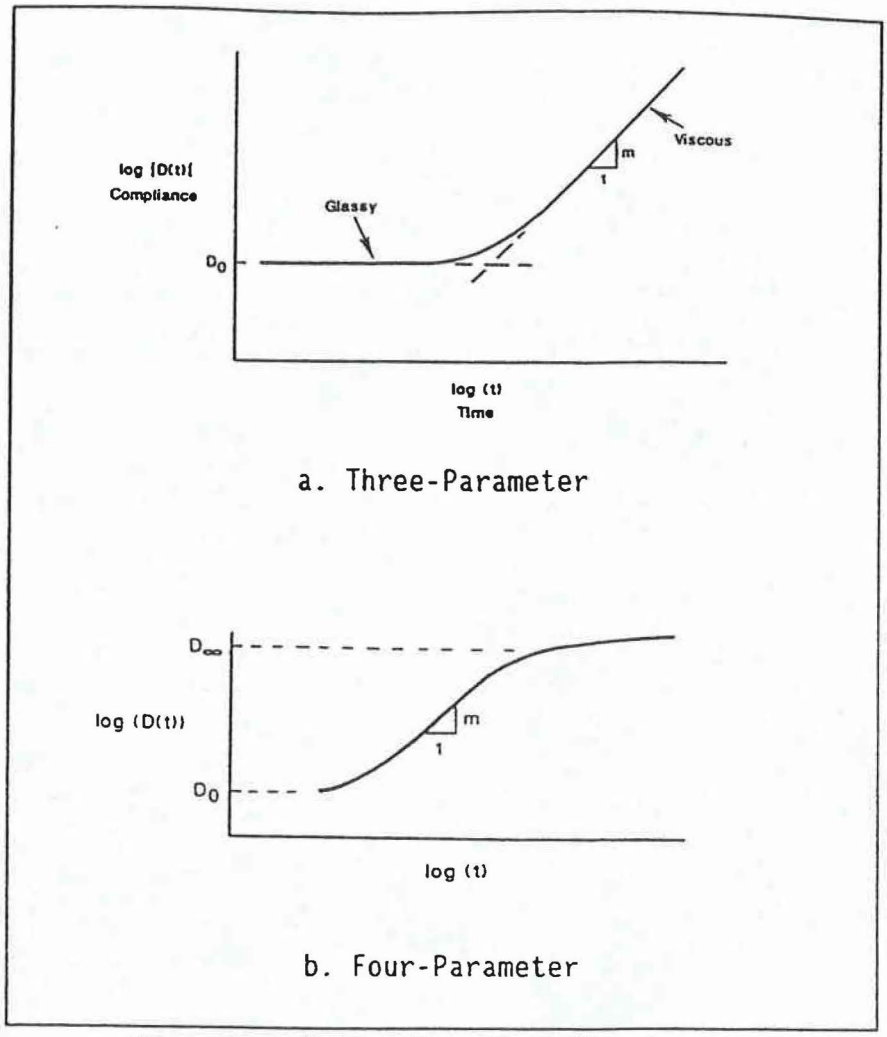

Figure 85. AC Creep Compliance Functions
a.) Three-Parameter
b.) Four-Parameter

Effective Modulus for the Three-Parameter Model

For comparative purposes, an effective modulus may be computed from the viscoelastic parameters in Equation B-4. The effective modulus is based on the nominal FWD load pulse time of 20 msec. The pulse peak occurs at 10 msec.

The 10 msec peak time is then defined as a characteristic time representative of the FWD load pulse. One then applies this time to Equation A-4 to compute an effective compliance (D_{EFF}) and its reciprocal, the effective modulus (E_{EFF}) as follows.

$$D_{EFF} = D_0 (1 + \alpha (0.01)^m) \quad \text{(B-5)}$$

Since moduli are reciprocals of compliances, we may define an effective modulus (with respect to the FWD force pulse) as

$$E_{eff} = 1 / D_{eff}, \text{ and}$$

$$E_{eff} = E_0 / (1 + \alpha t), \quad \text{(B-6)}$$

where $E_0 = 1 / D_0$.

This relation (B-6) was used to compute the effective moduli for the AC layers given in Tables 4, 5, and 6.

The Four-Parameter Model

The following four-parameter model gives realistic values for both small and large times:

$$D(t) = (D_0 + D_1 a t^m) / (1 + a t^m), \quad \text{(B-7)}$$

where $D(t)$ = creep compliance (units: 1/psi),

D_0 = elastic response term (t=0 response),

D_1 = viscous creep compliance constant (infinite time response),

m = exponent for nonlinear time dependence, and

a = constant.

Note from Equation B-7 that

$$D(0) = D_0 \text{ and}$$
$$D(l) = D_1.$$

The relation in Equation B-6 is shown graphically in Figure 84-b. This form, while most realistic physically, is difficult to implement in a frequency-domain program such as SCALPOT because a closed-form Fourier transform for the equation does not exist. However, the denominator in Equation B-6 can be expanded in a power series for small time as follows:

$$(1 + a\,t^m)^{-1} = 1 - a\,t^m + (a\,t^m)^2 - (a\,t^m)^3 + \ldots \quad \text{(B-8)}$$

After substituting expression (B-8) into equation (B-5) the compliance function can be readily transformed term by term using enough terms to achieve the required low frequency range. As discussed in the text, the four-parameter representation using this expansion will give more realistic low frequency response in the SCALPOT program and should improve back-calculation results for the AC creep compliance parameters.

The Time-Temperature Shift

The viscoelastic data for the AC layer can be corrected for temperature using the time-temperature shift relation (Fitzgerald and Lai, 1970). The creep compliance data for any temperature can be shifted horizontally (on the time axis) to represent the creep compliance at a different temperature. Physically this means that the creep at a cooler temperature and a larger time period is the same as creep at a warmer temperature and a smaller time. A creep master curve for a given mixture at some reference temperature (e.g. 70 deg. F) can be constructed from creep curves at a number of different temperatures. This is desirable as creep curves can be constructed for smaller times than the physical test apparatus can achieve. The time-temperature shift relation is given as

$$D(t,T_0) = D(t/a_T, T), \quad \text{(B-9)}$$

where D = Creep compliance,

t = Time,

T_0 = Reference temperature,

a_T = Time shift factor, and

T = Temperature.

Various expressions can be used for the time shift factor a_T. The simplest one and the one used in this study is

$$\log a_T = \beta(T-T_0), \quad \text{(B-10)}$$

where β is the temperature susceptibility. The susceptibility (β) is a physical property of the AC mixture and can be thought of as the sensitivity of the AC layer stiffness to temperature. (It is desirable for the susceptibility to be as small as possible.) The range of values for temperature susceptibility for AC mixtures based on published data (Fitzgerald and Lai, 1970; Sharma and Kim, 1972; and Sherwood and Kenis, 1968) is as follows.

$$0.05 \leq \beta \leq 0.12$$

The AC layer viscoelastic (creep) properties at a given site can be computed for any temperature using a back-calculated susceptibility obtained from FWD tests done at two or more widely varying temperatures. (Say, a variation of 20-30 deg. F or more.)

APPENDIX C

Users' Manual For Pavement Dynamic Analysis Procedure (PDAP) For Falling-Weight Deflectometer Data

Appendix C has been rewritten as a separate document.

APPENDIX D: THICK PAVEMENTS COMPARISON PLOTS - FREQUENCY RESPONSE FUNCTIONS FOR FWD PAVEMENT SURFACE DEFLECTIONS

Sites

D01S3 (See Figures 31-38)

D01S5

D08S3 (See Figures 39-46)

D08S4

D08S5

D11S2

D11S7

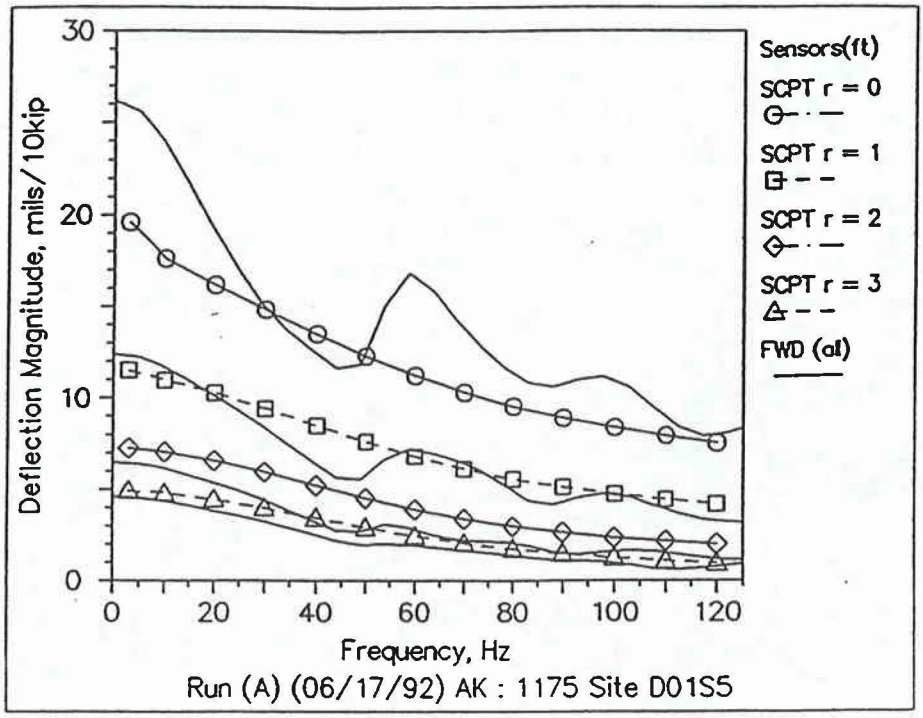

Figure 86. Section D01S5 (100°F) Magnitude Plot for Inner Displacements (r=0, 1.0, 2.0, and 3.0 ft.)

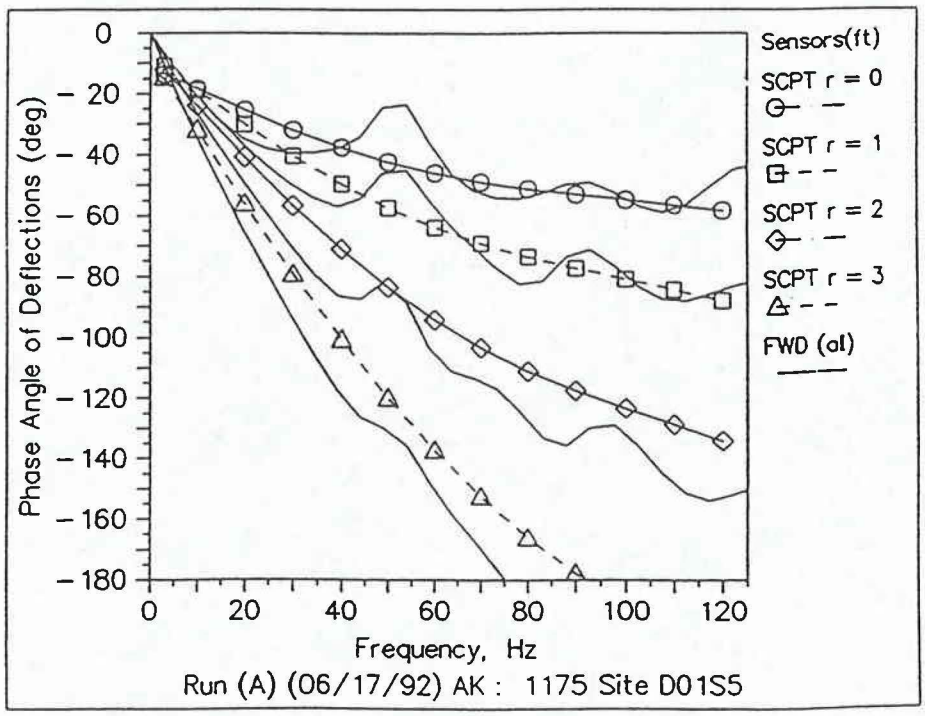

Figure 87. Section D01S5 (100°F) Phase Angle Plot for Inner Displacements (r=0, 1.0, 2.0, and 3.0 ft.)

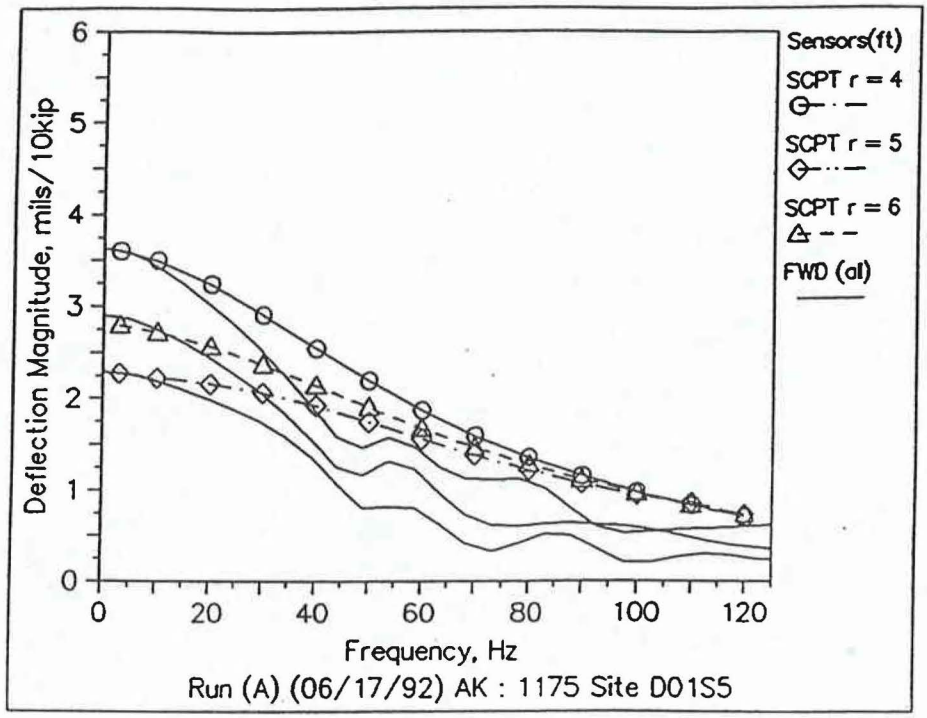

Figure 88. Section D01S5 (100°F) Magnitude Plot for Outer Displacements (r=4.0, 5.0, and 6.0 ft.)

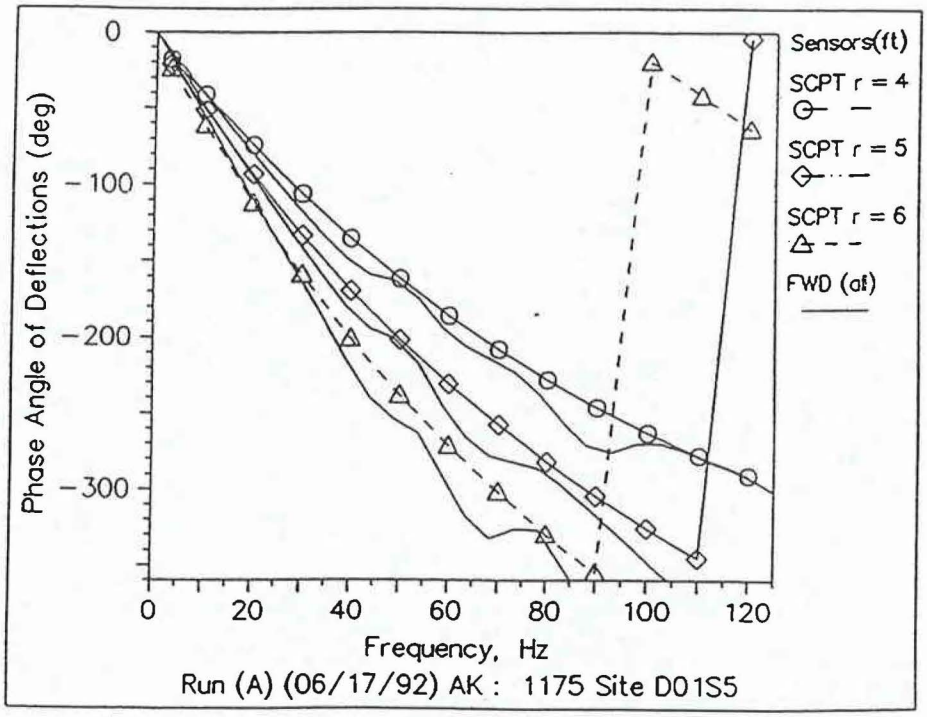

Figure 89. Section D01S5 (100°F) Phase Angle Plot for Outer Displacements (r=4.0, 5.0, and 6.0 ft.)

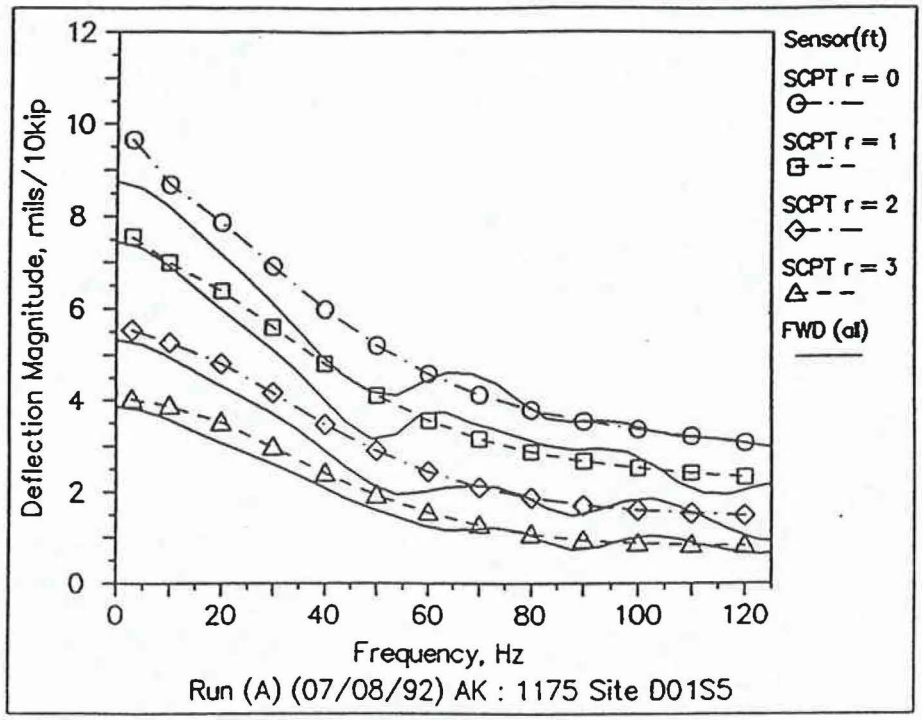

Figure 90. Section D01S5 (65°F) Magnitude Plot for Inner Displacements (r=0, 1.0, 2.0, and 3.0 ft.)

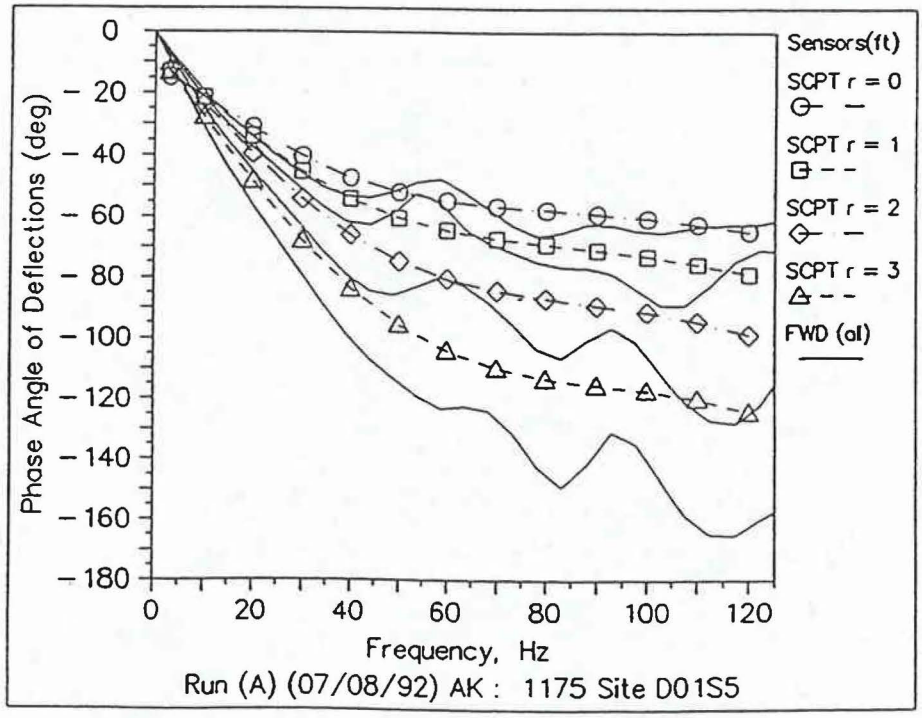

Figure 91. Section D01S5 (65°F) Phase Angle Plot for Inner Displacements (r=0, 1.0, 2.0, and 3.0 ft.)

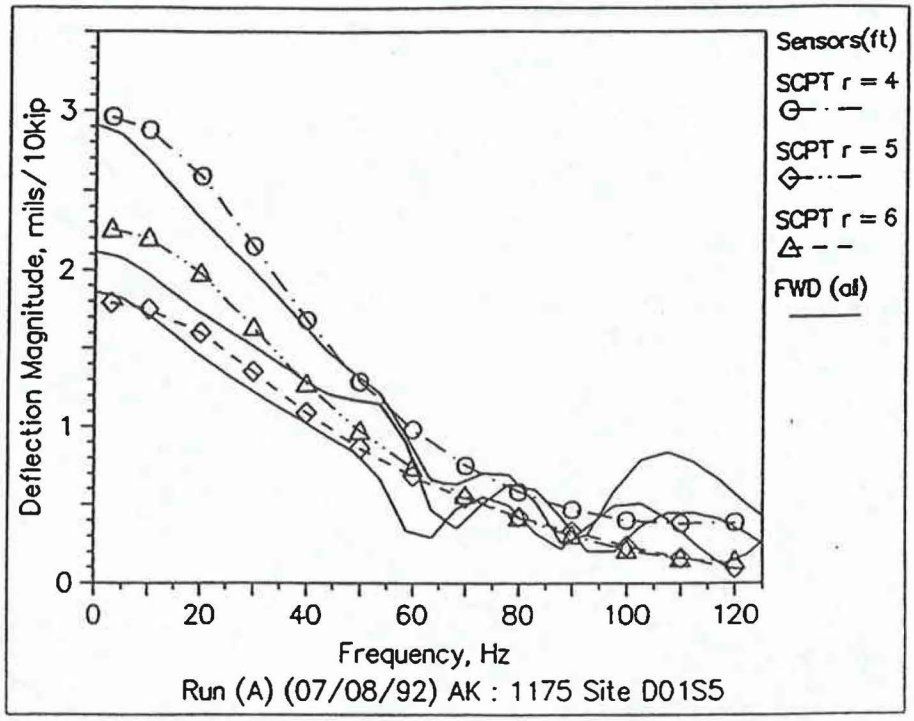

Figure 92. Section D01S5 (65°F) Magnitude Plot for Outer Displacements (r=4.0, 5.0, and 6.0 ft.)

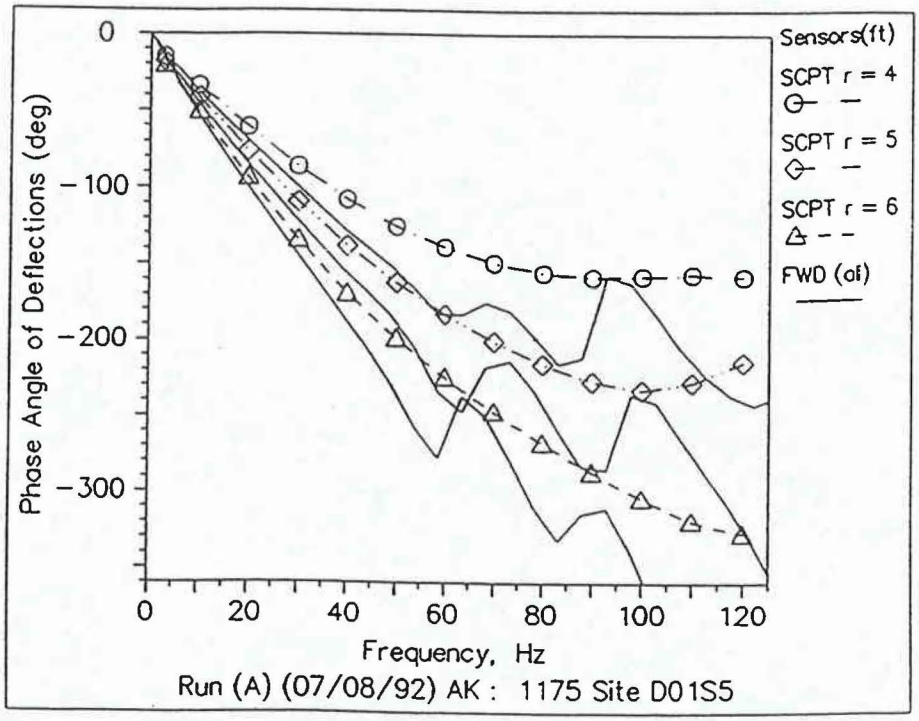

Figure 93. Section D01S5 (65°F) Phase Angle Plot for Outer Displacements (r=4.0, 5.0, and 6.0 ft.)

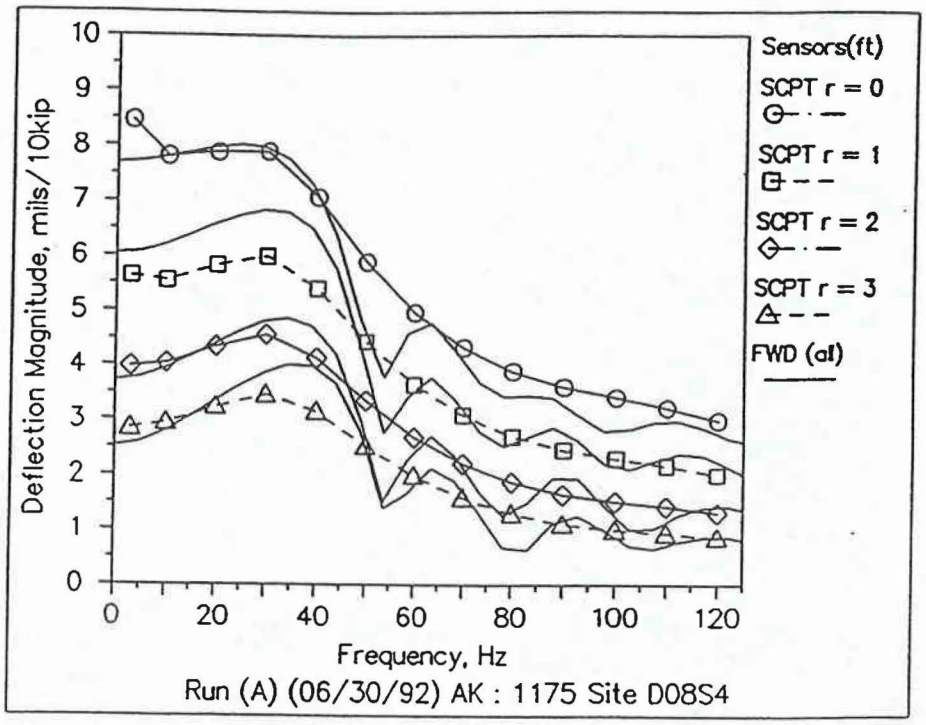

Figure 94. Section D08S4: Magnitude Plot for Inner Displacements (r=0, 1.0, 2.0, and 3.0 ft.)

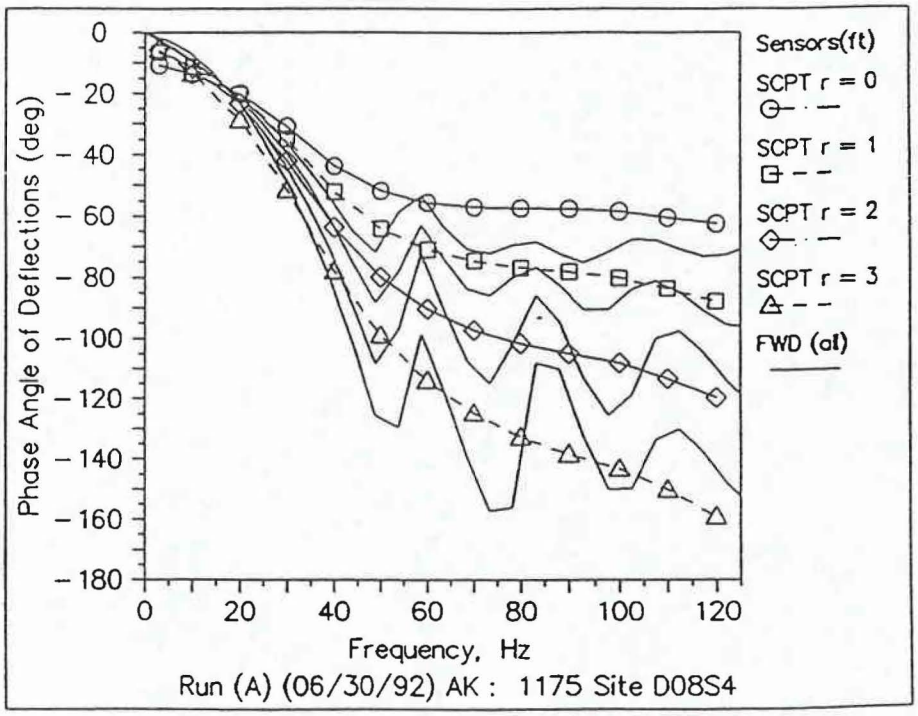

Figure 95. Section D08S4: Phase Angle Plot for Inner Displacements (r=0, 1.0, 2.0, and 3.0 ft.)

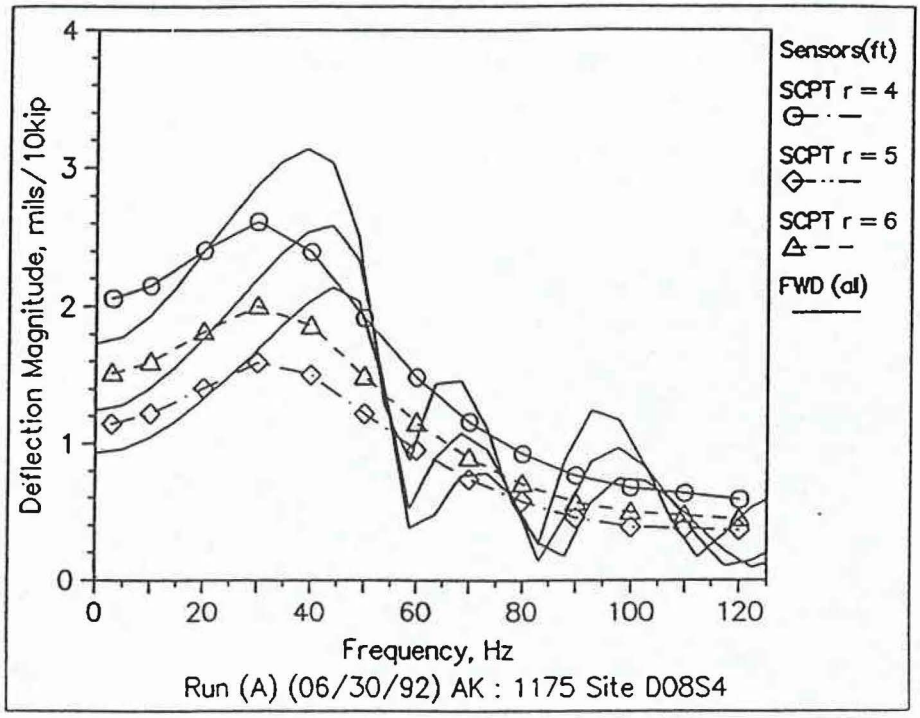

Figure 96. Section D08S4: Magnitude Plot for Outer Displacements (r=4.0, 5.0, and 6.0 ft.)

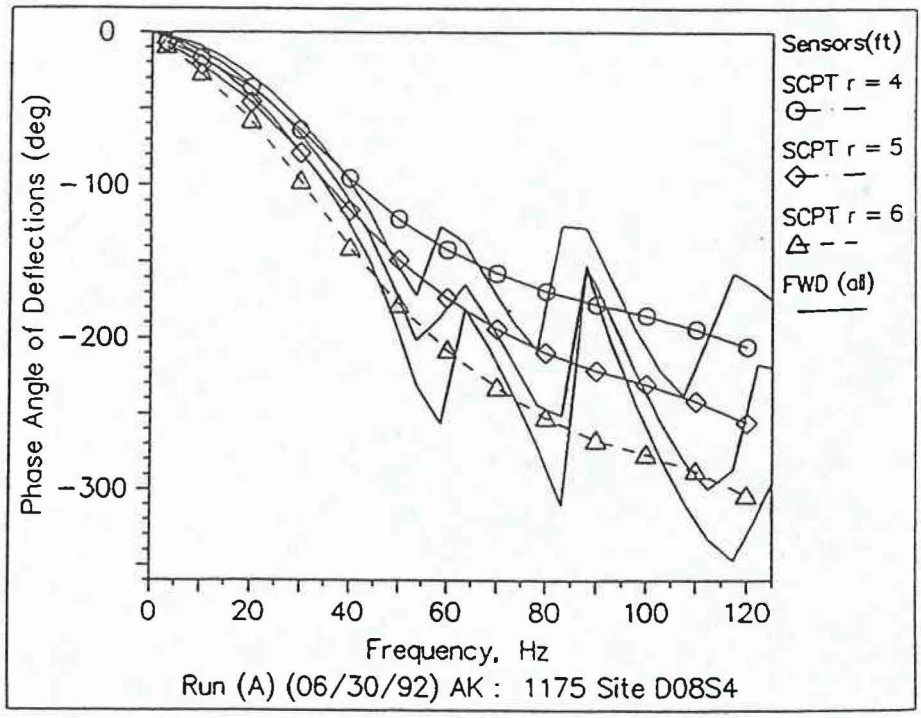

Figure 97. Section D08S4: Phase Angle Plot for Outer Displacements (r=4.0, 5.0, and 6.0 ft.)

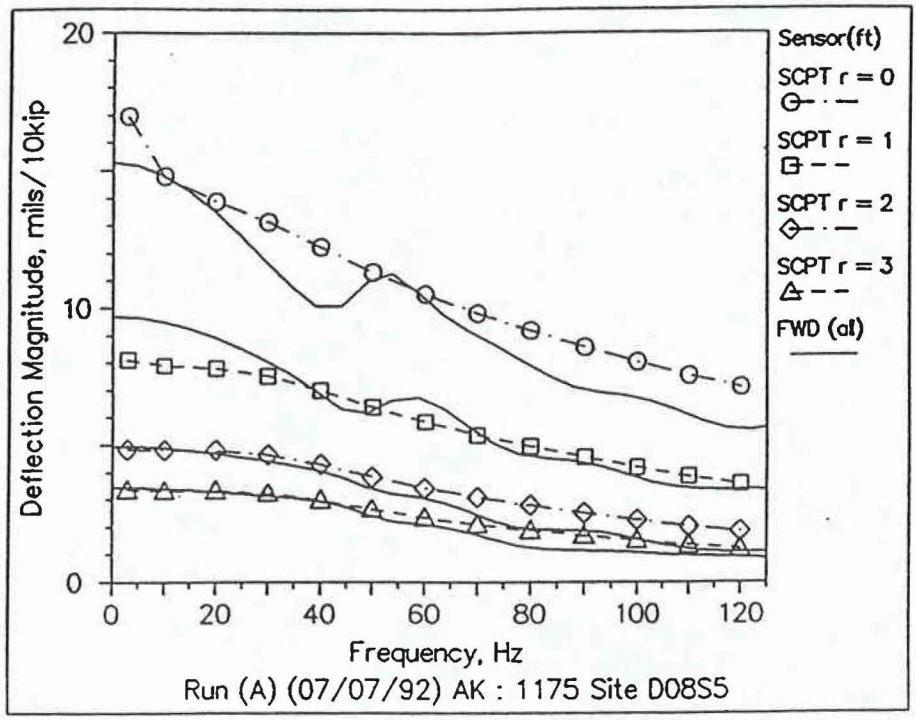

Figure 98. Section D08S5: Magnitude Plot for Inner Displacements (r=0, 1.0, 2.0, and 3.0 ft.)

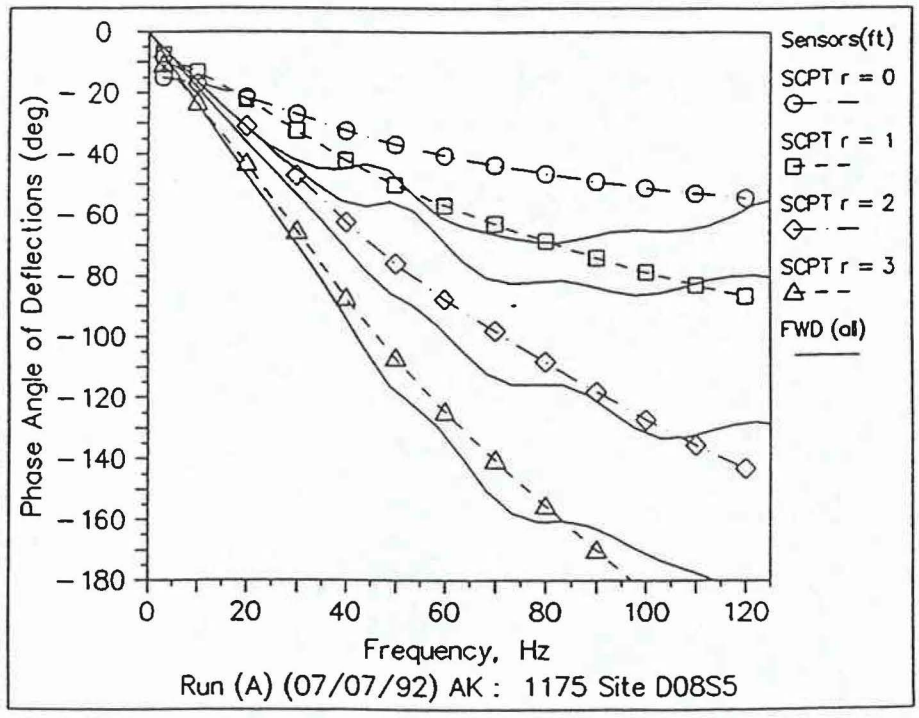

Figure 99. Section D08S5: Phase Angle Plot for Inner Displacements (r=0, 1.0, 2.0, and 3.0 ft.)

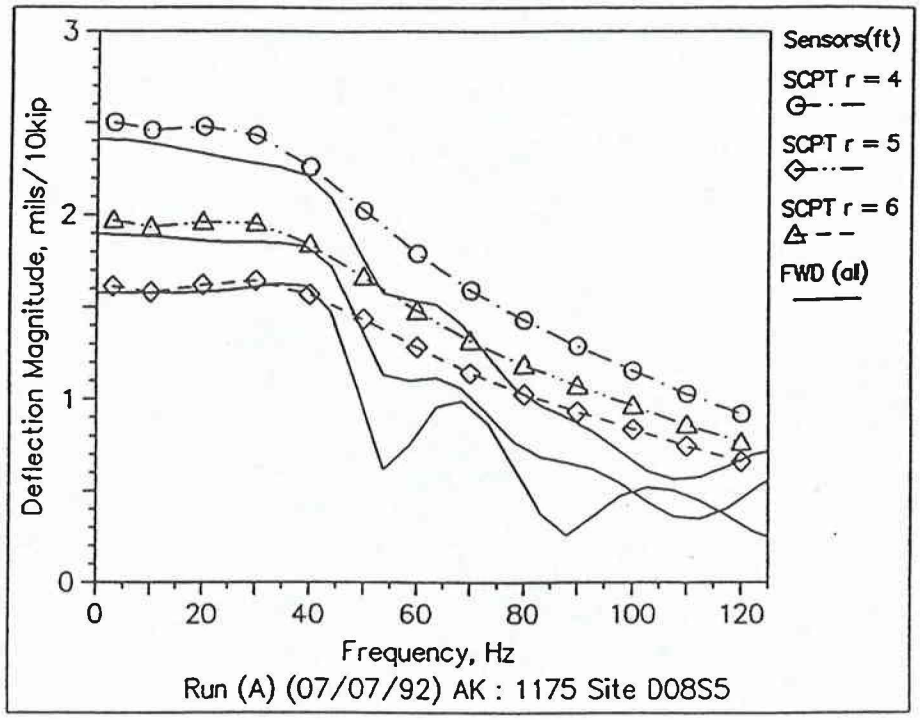

Figure 100. Section D08S5: Magnitude Plot for Outer Displacements (r=4.0, 5.0, and 6.0 ft.)

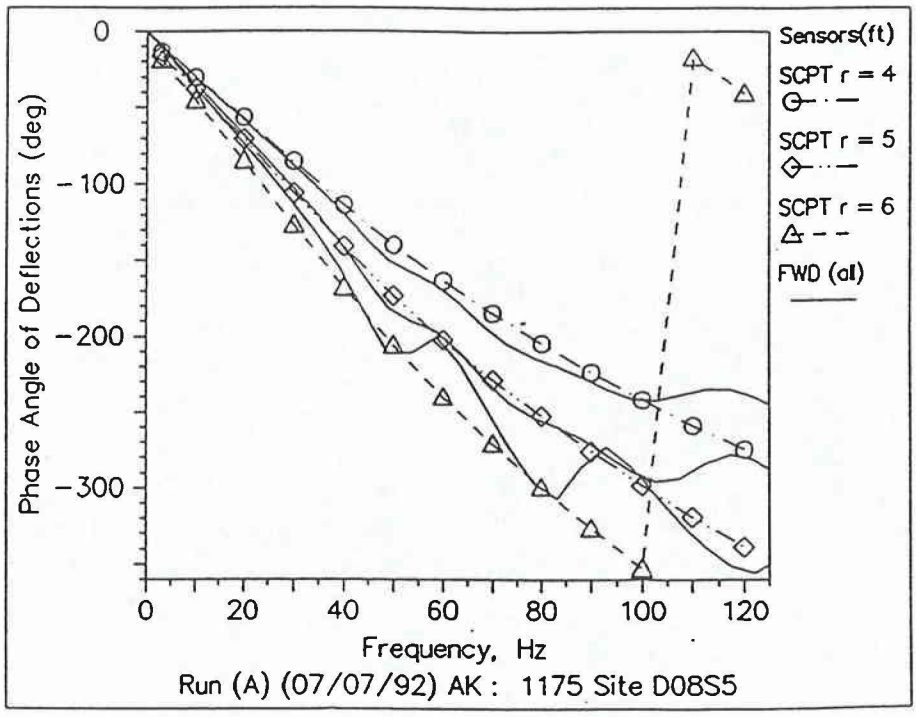

Figure 101. Section D08S5: Phase Angle Plot for Outer Displacements (r=4.0, 5.0, and 6.0 ft.)

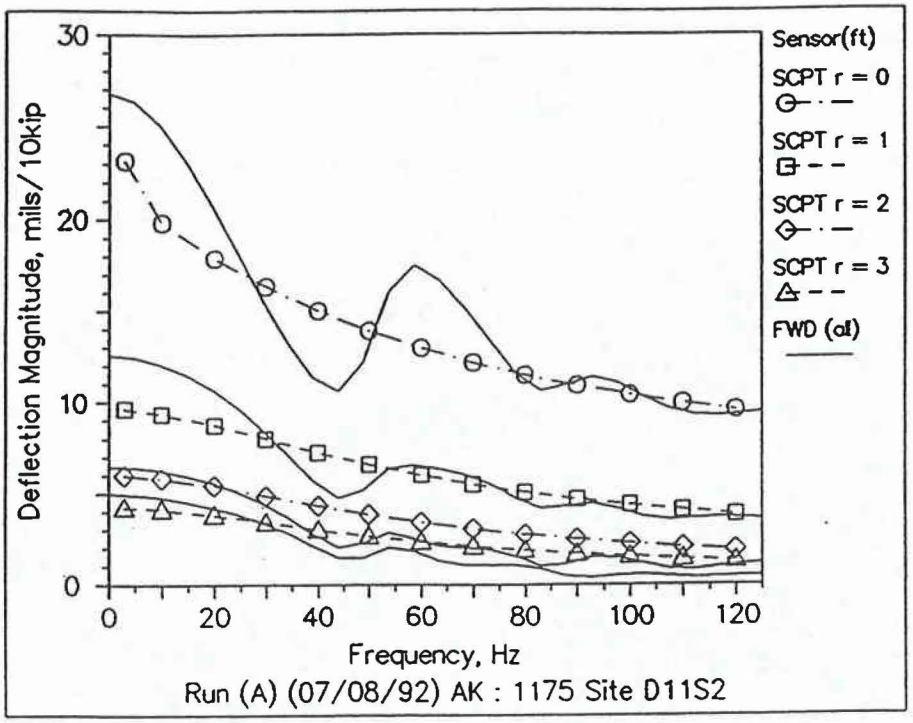

Figure 102. Section D11S2: Magnitude Plot for Inner Displacements (r=0, 1.0, 2.0, and 3.0 ft.)

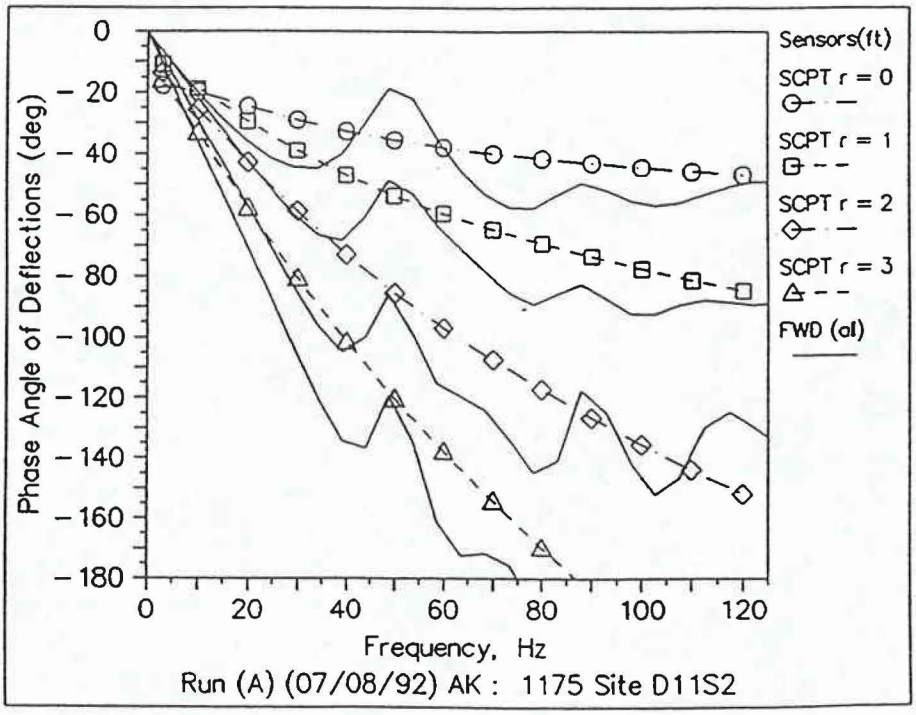

Figure 103. Section D11S2: Phase Angle Plot for Inner Displacements (r=0, 1.0, 2.0, and 3.0 ft.)

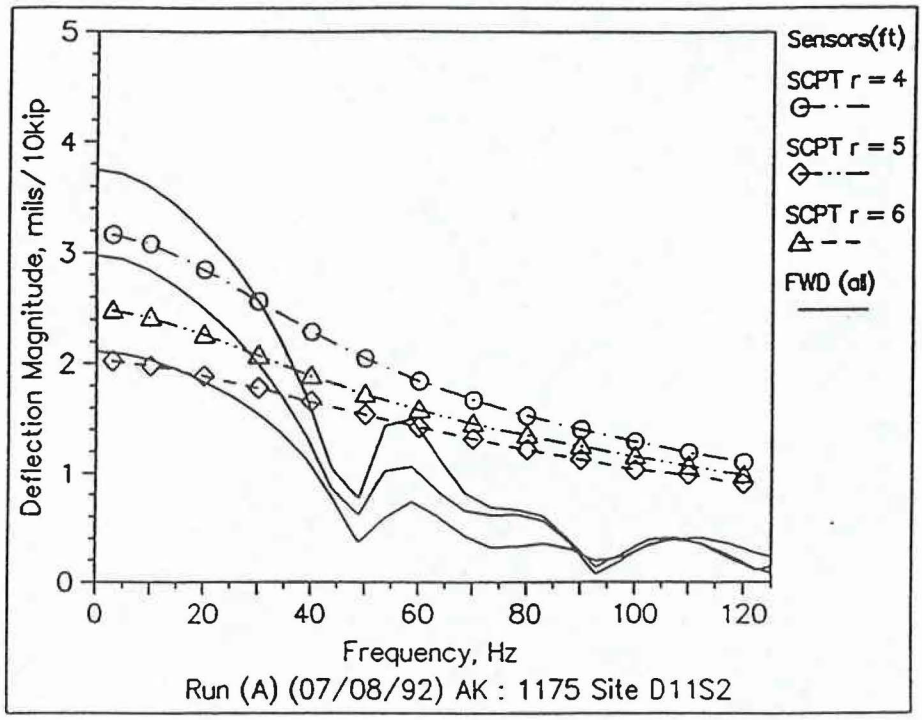

Figure 104. Section D11S2: Magnitude Plot for Outer Displacements (r=4.0, 5.0, and 6.0 ft.)

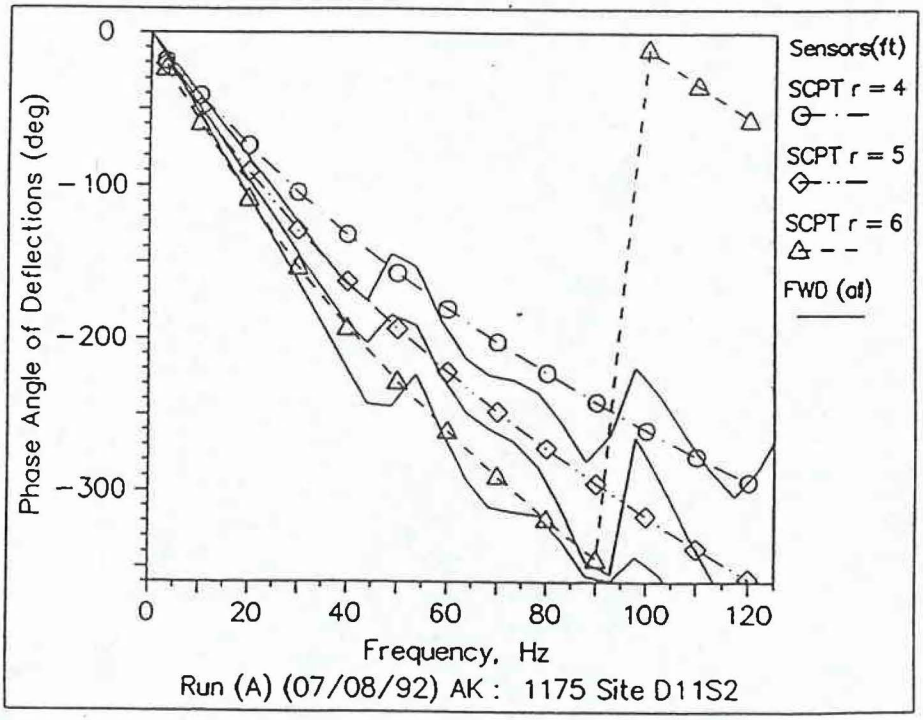

Figure 105. Section D11S2: Phase Angle Plot for Outer Displacements (r=4.0, 5.0, and 6.0 ft.)

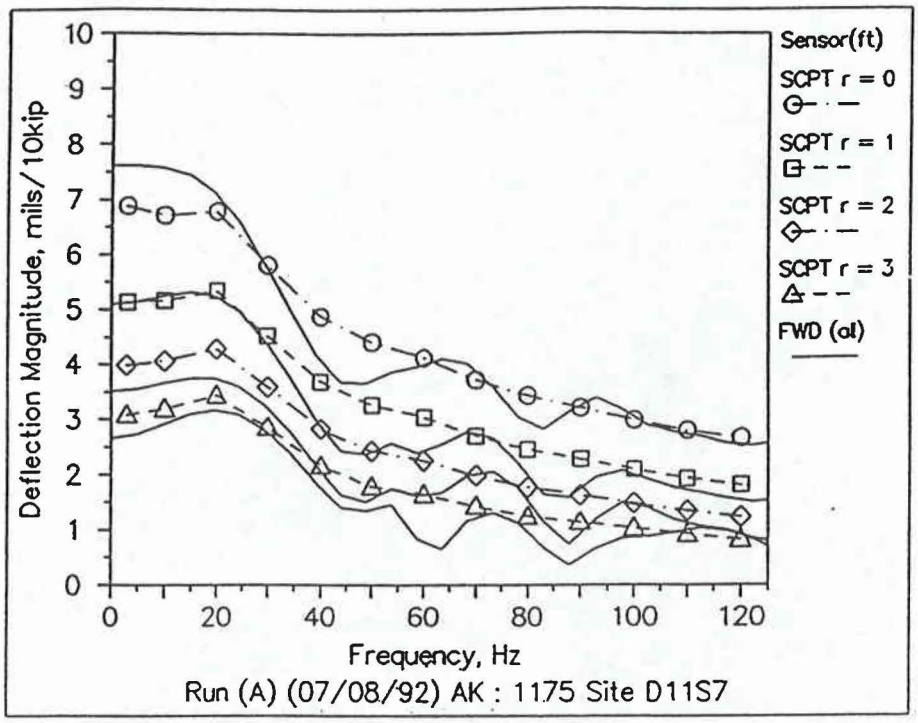

Figure 106. Section D11S7: Magnitude Plot for Inner Displacements (r=0, 1.0, 2.0, and 3.0 ft.)

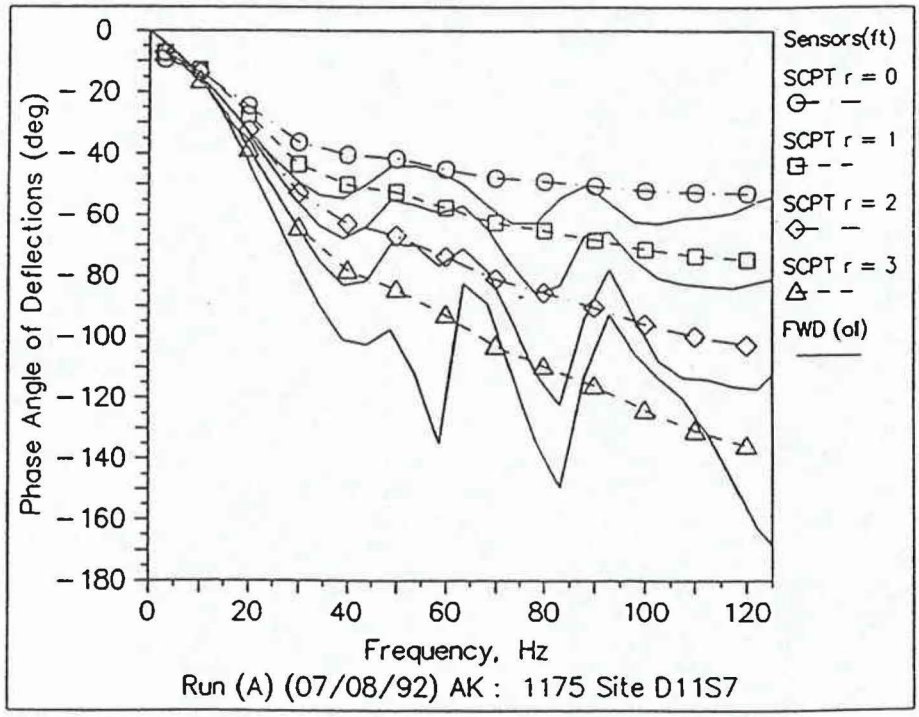

Figure 107. Section D11S7: Phase Angle Plot for Inner Displacements (r=0, 1.0, 2.0, and 3.0 ft.)

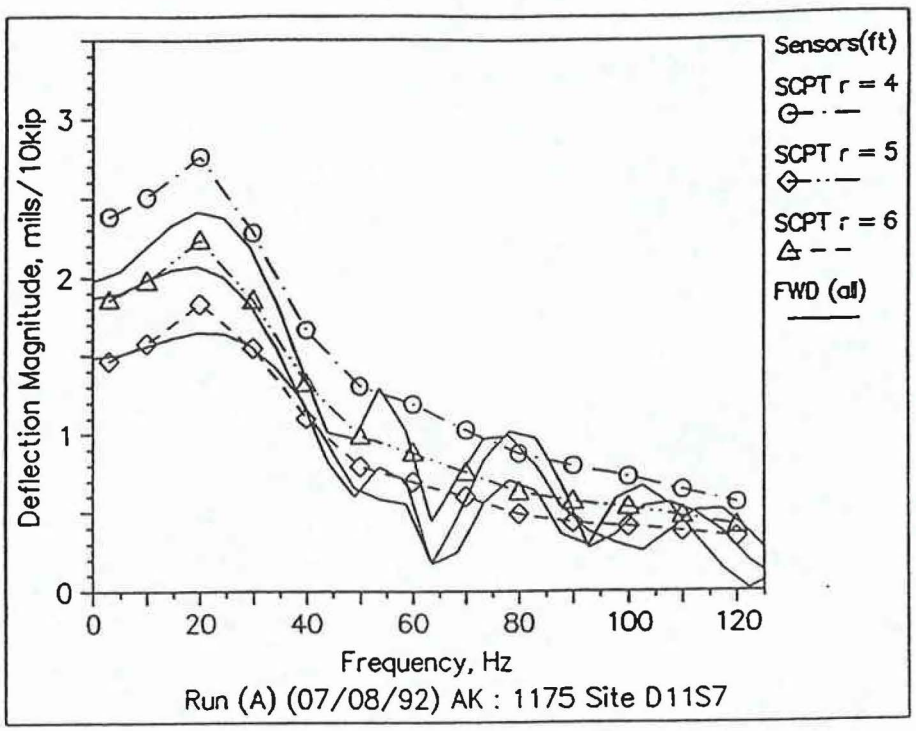

Figure 108. Section D11S7: Magnitude Plot for Outer Displacements (r=4.0, 5.0, and 6.0 ft.)

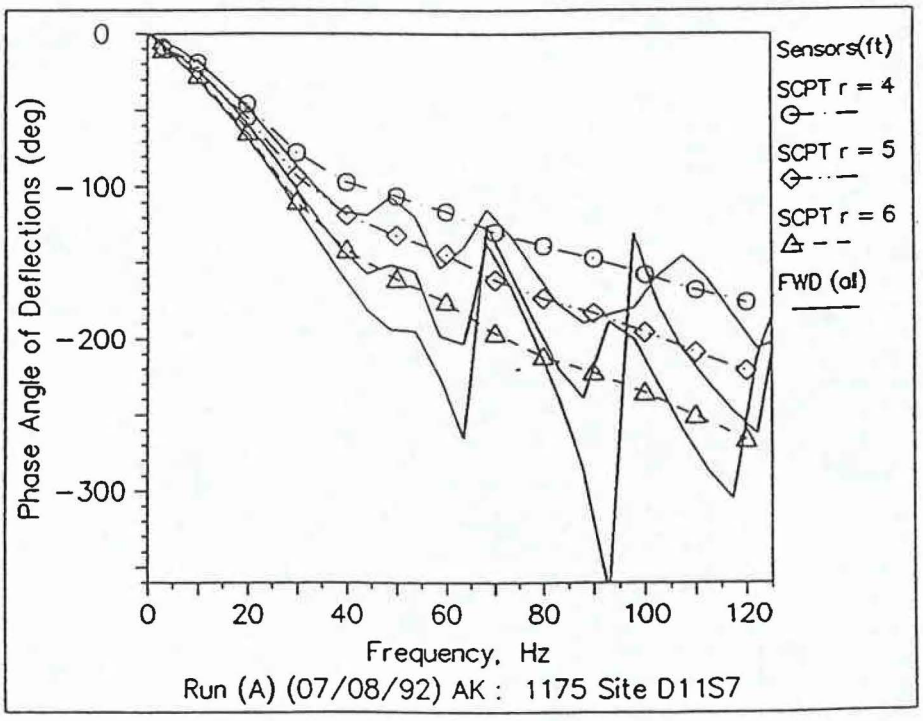

Figure 109. Section D11S7: Phase Angle Plot for Outer Displacements (r=4.0, 5.0, and 6.0 ft.)

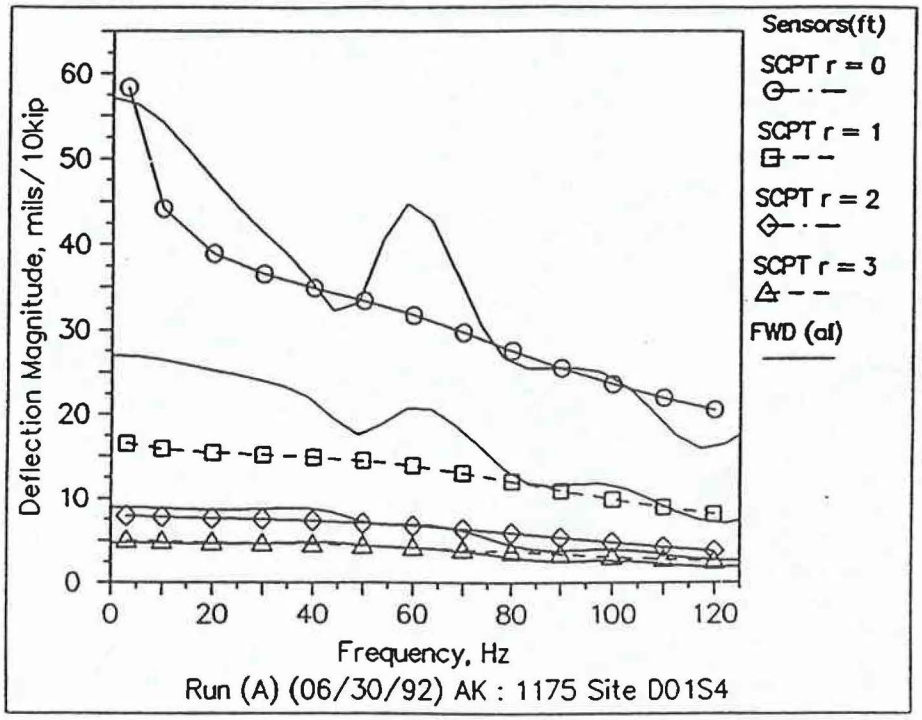

Figure 110. Section D01S4: Magnitude Plot for Inner Displacements (r=0, 1.0, 2.0, and 3.0 ft.)

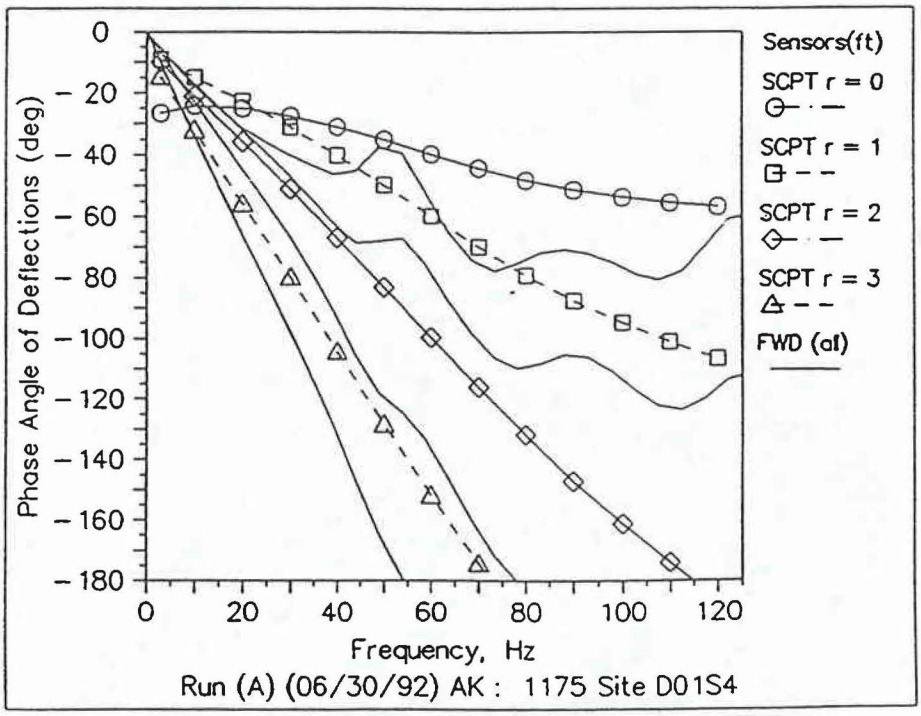

Figure 111. Section D01S4: Phase Angle Plot for Inner Displacements (r=0, 1.0, 2.0, and 3.0 ft.)

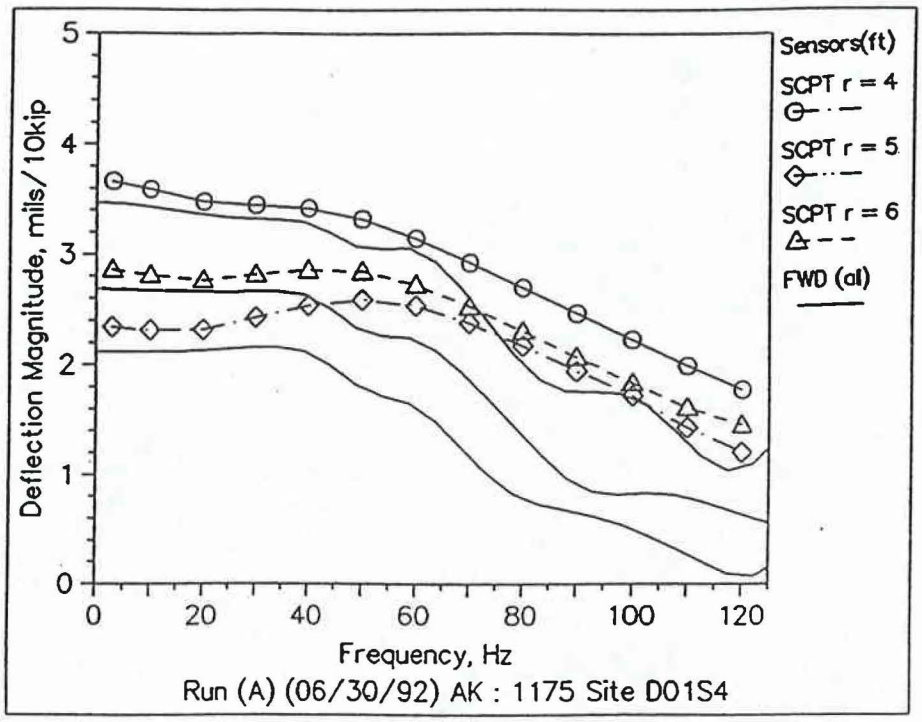

Figure 112. Section D01S4: Magnitude Plot for Outer Displacements (r=4.0, 5.0, and 6.0 ft.)

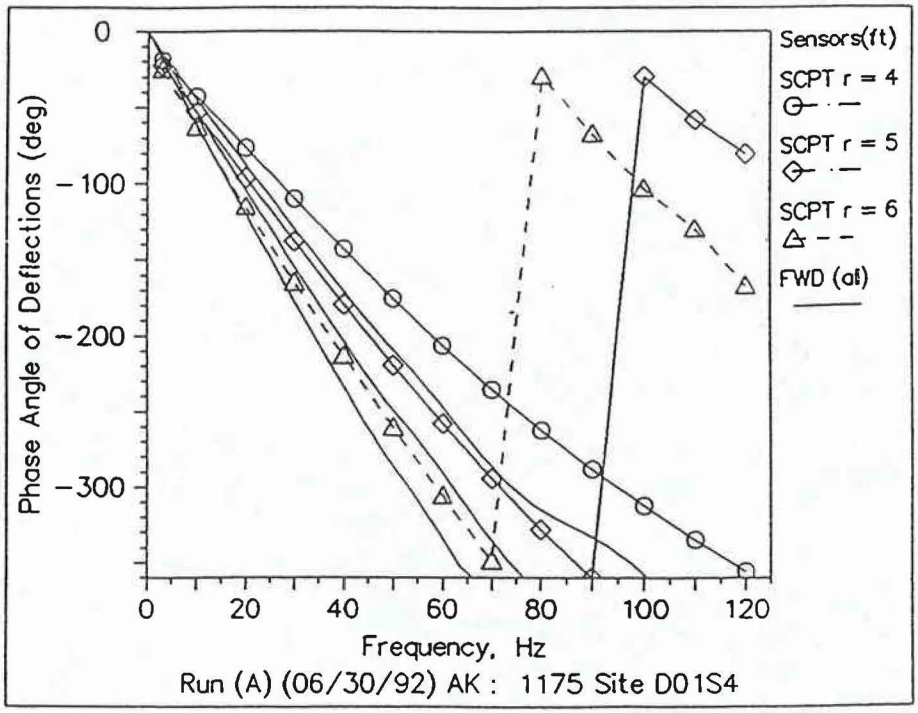

Figure 113. Section D01S4: Phase Angle Plot for Outer Displacements (r=4.0, 5.0, and 6.0 ft.)

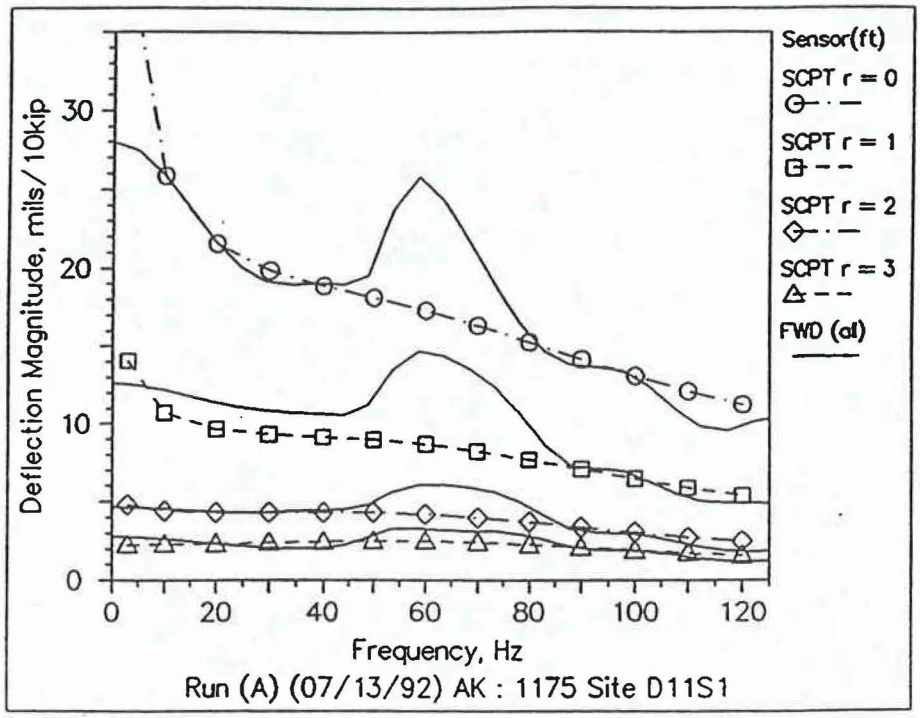

Figure 114. Section D11S1: Magnitude Plot for Inner Displacements (r=0, 1.0, 2.0, and 3.0 ft.)

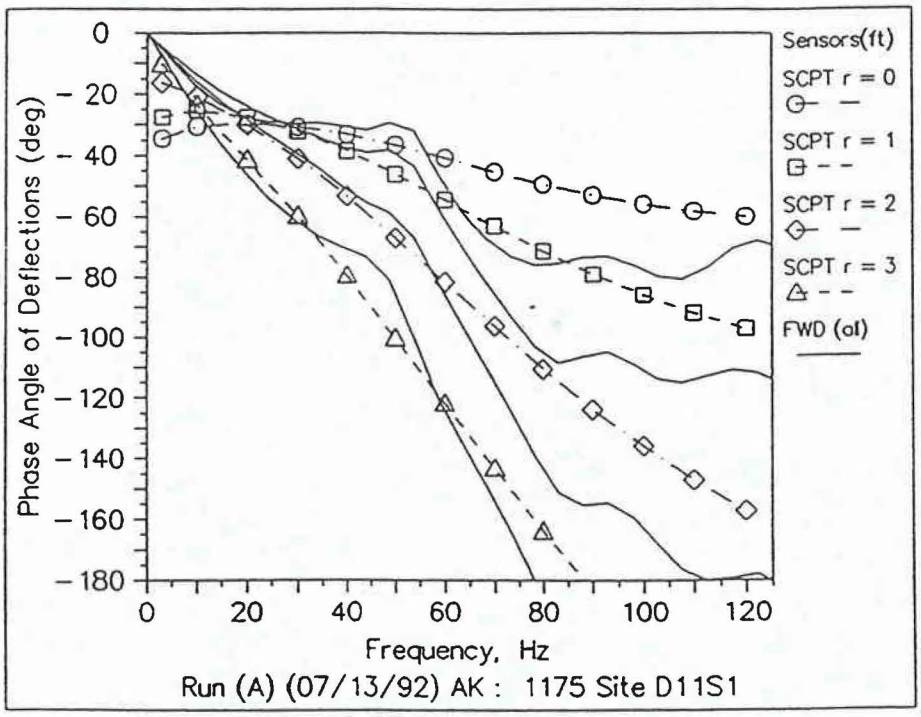

Figure 115. Section D11S1: Phase Angle Plot for Inner Displacements (r=0, 1.0, 2.0, and 3.0 ft.)

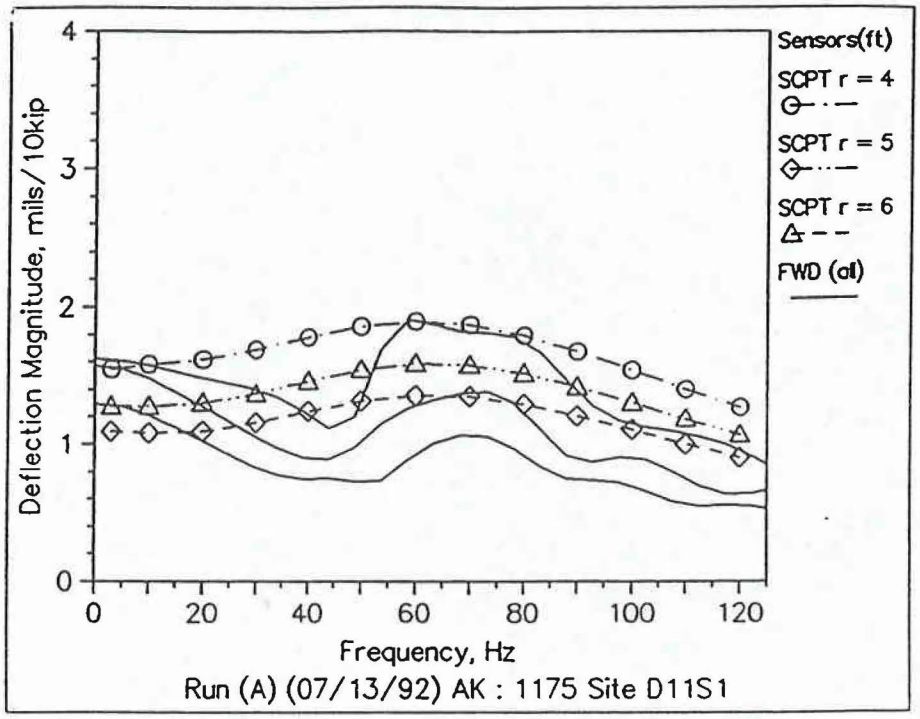

Figure 116. Section D11S1: Magnitude Plot for Outer Displacements (r=4.0, 5.0, and 6.0 ft.)

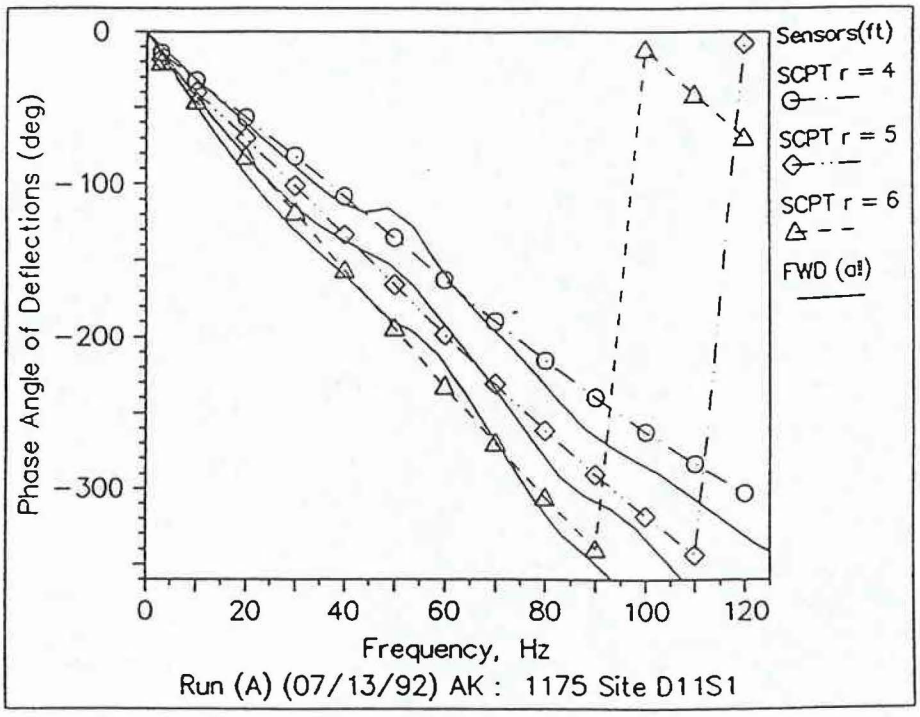

Figure 117. Section D11S1: Phase Angle Plot for Outer Displacements (r=4.0, 5.0, and 6.0 ft.)

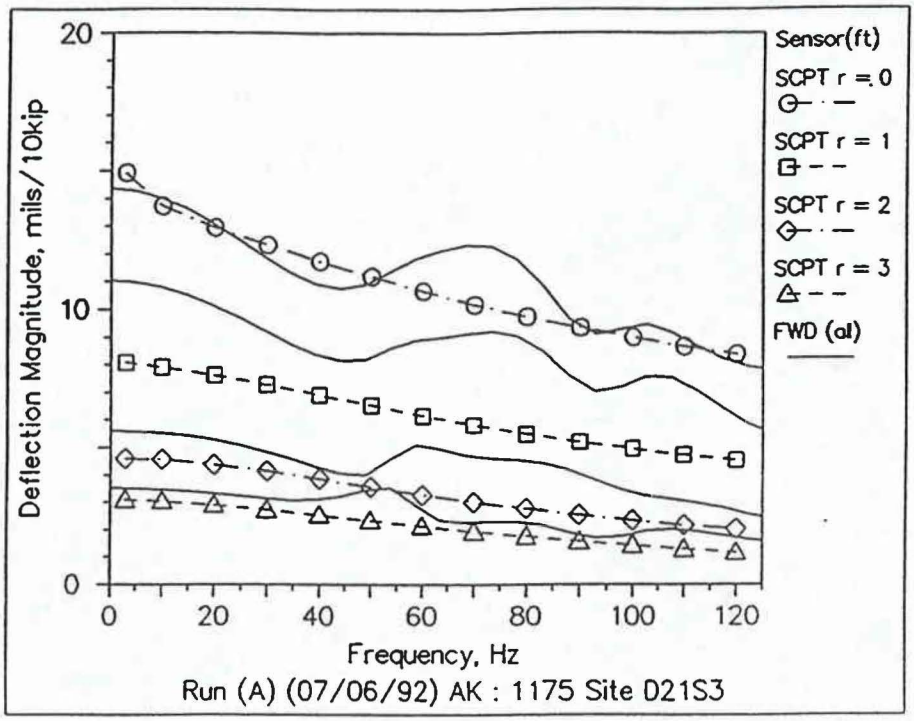

Figure 118. Section D21S3: Magnitude Plot for Inner Displacements (r=0, 1.0, 2.0, and 3.0 ft.)

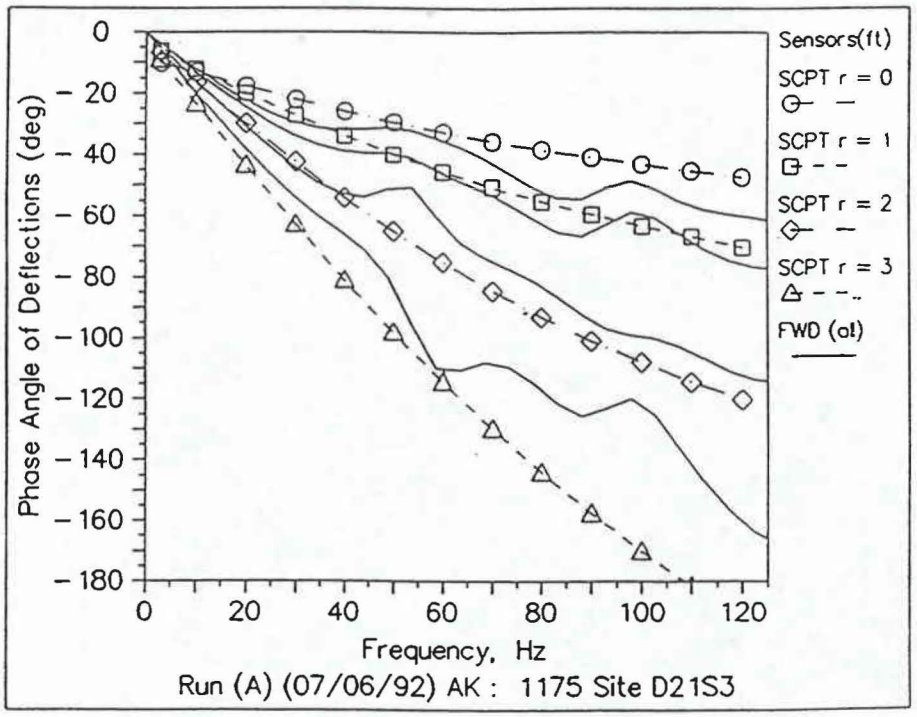

Figure 119. Section D21S3: Phase Angle Plot for Inner Displacements (r=0, 1.0, 2.0, and 3.0 ft.)

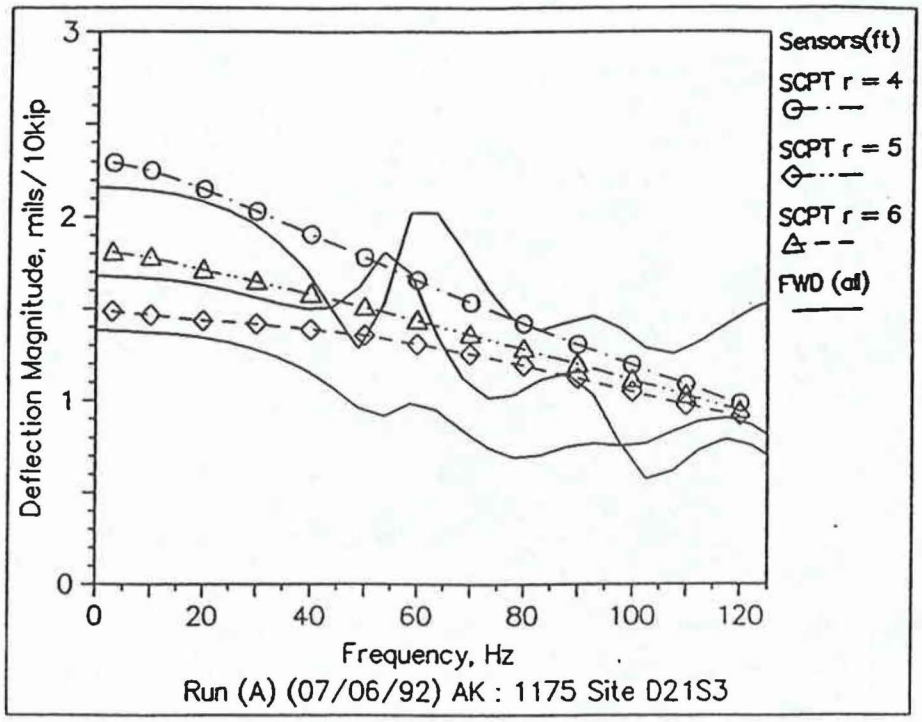

Figure 120. Section D21S3: Magnitude Plot for Outer Displacements (r=4.0, 5.0, and 6.0 ft.)

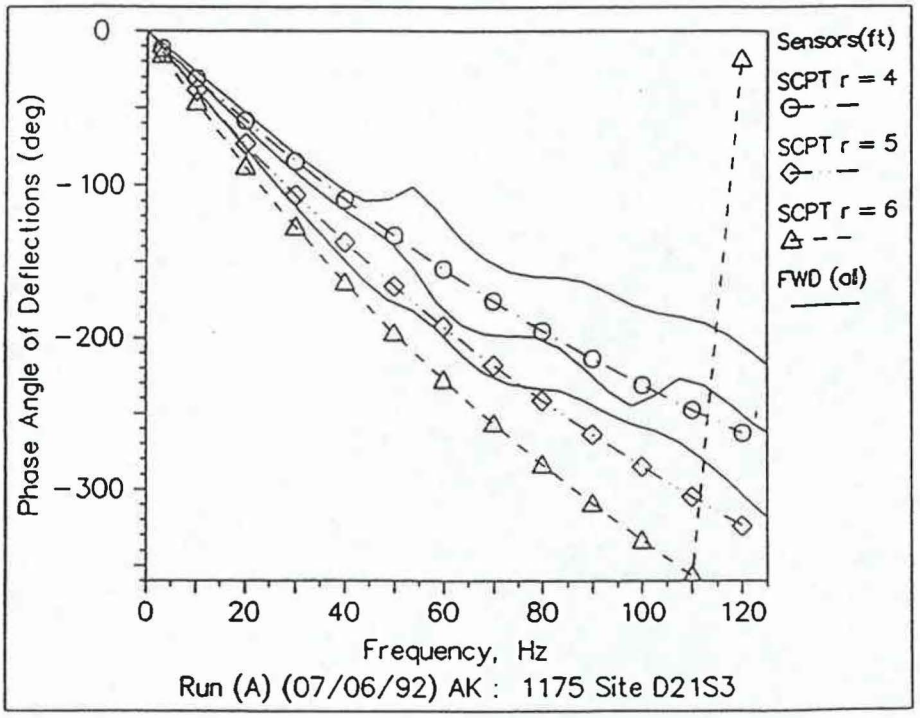

Figure 121. Section D21S3: Phase Angle Plot for Outer Displacements (r=4.0, 5.0, and 6.0 ft.)

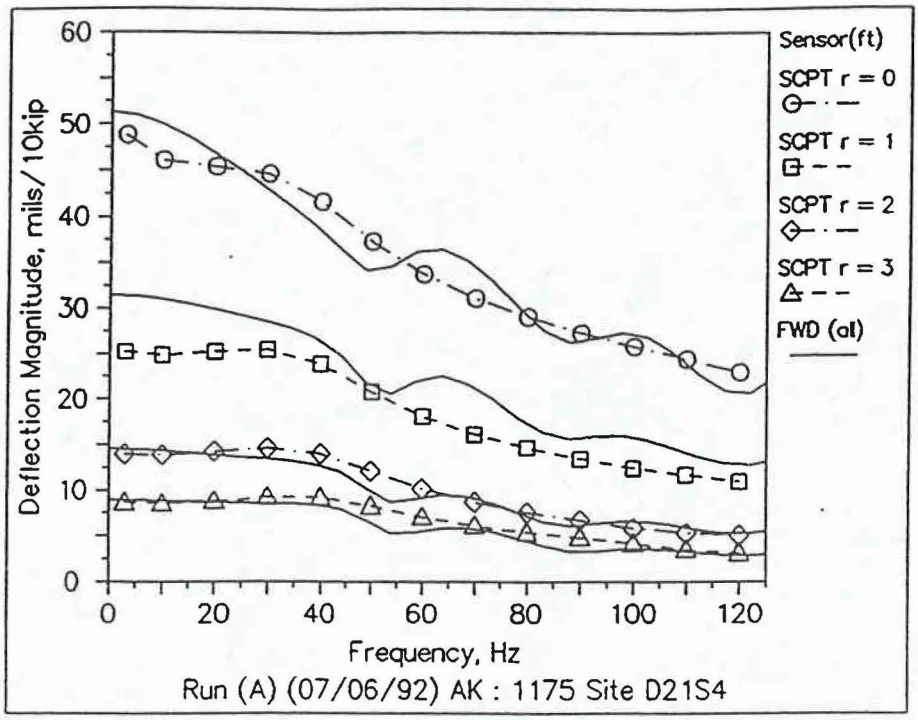

Figure 122. Section D21S4: Magnitude Plot for Inner Displacements (r=0, 1.0, 2.0, and 3.0 ft.)

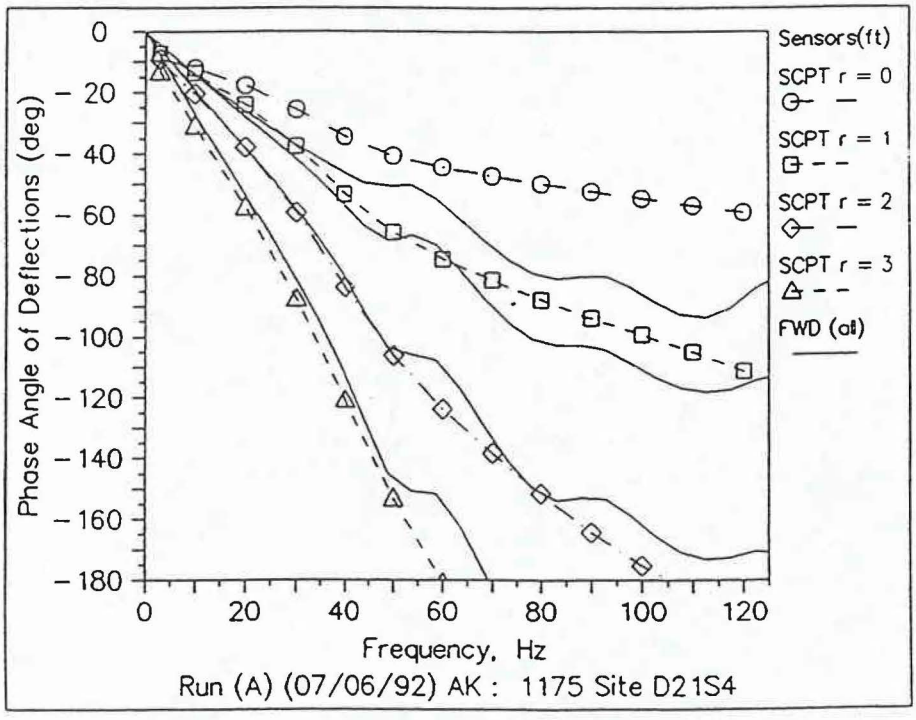

Figure 123. Section D21S4: Phase Angle Plot for Inner Displacements (r=0, 1.0, 2.0, and 3.0 ft.)

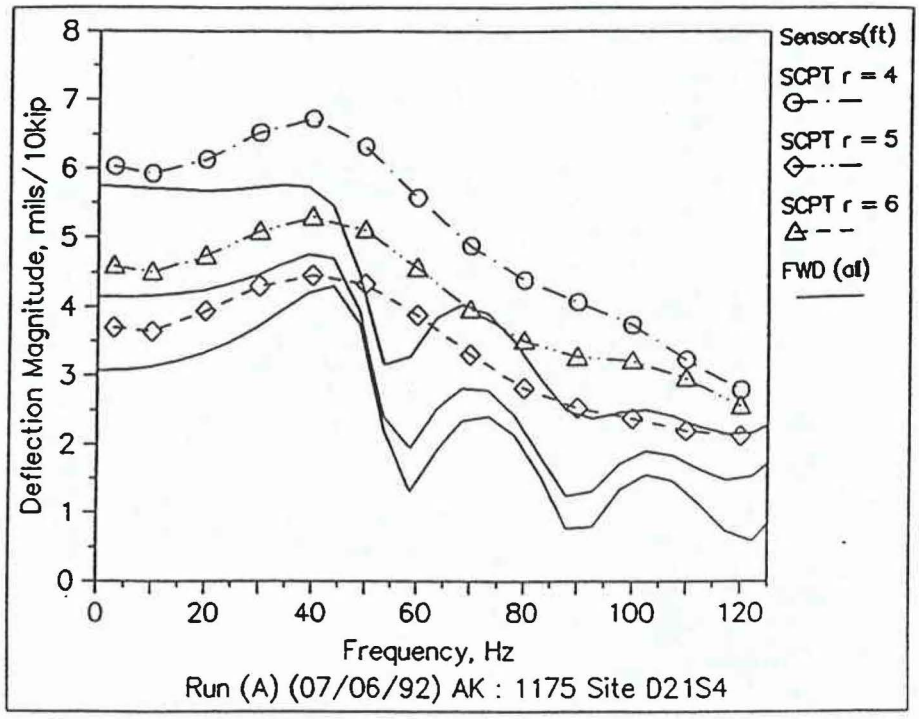

Figure 124. Section D21S4: Magnitude Plot for Outer Displacements (r=4.0, 5.0, and 6.0 ft.)

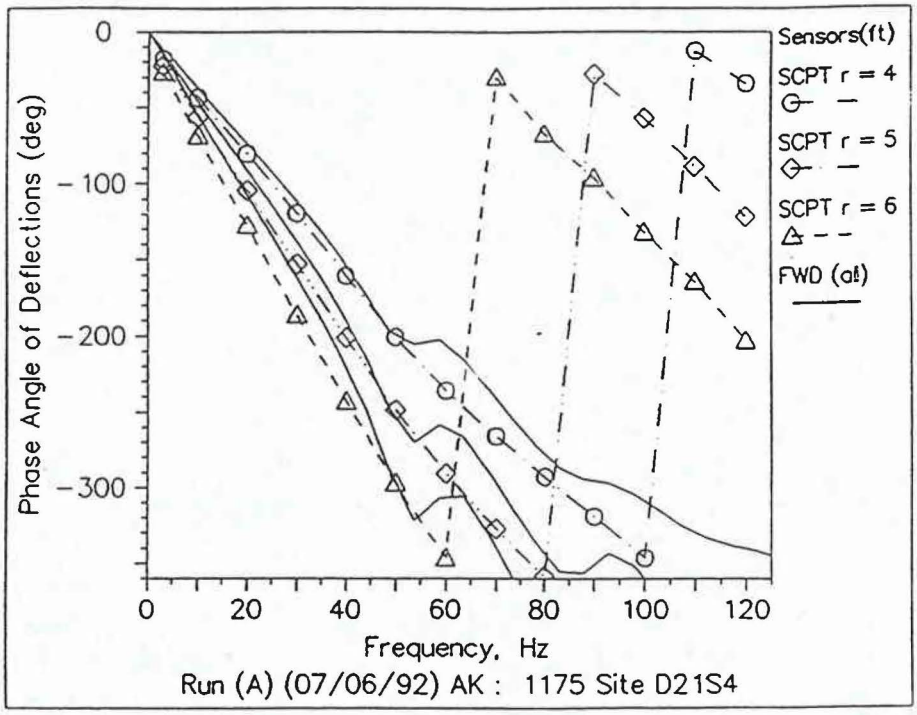

Figure 125. Section D21S4: Phase Angle Plot for Outer Displacements (r=4.0, 5.0, and 6.0 ft.)

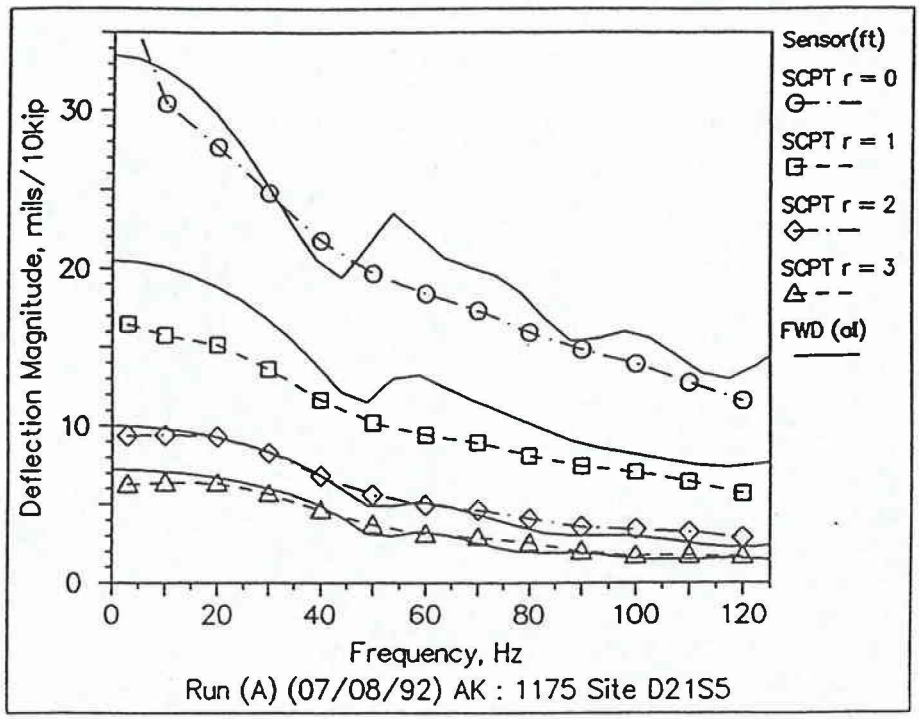

Figure 126. Section D21S5: Magnitude Plot for Inner Displacements (r=0, 1.0, 2.0, and 3.0 ft.)

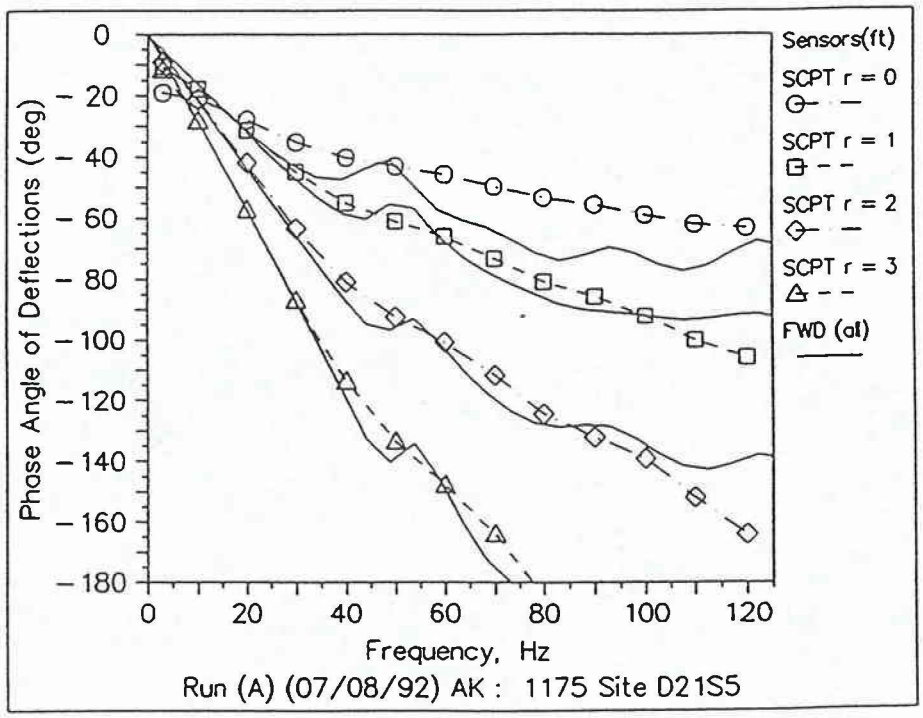

Figure 127. Section D21S5: Phase Angle Plot for Inner Displacements (r=0, 1.0, 2.0, and 3.0 ft.)

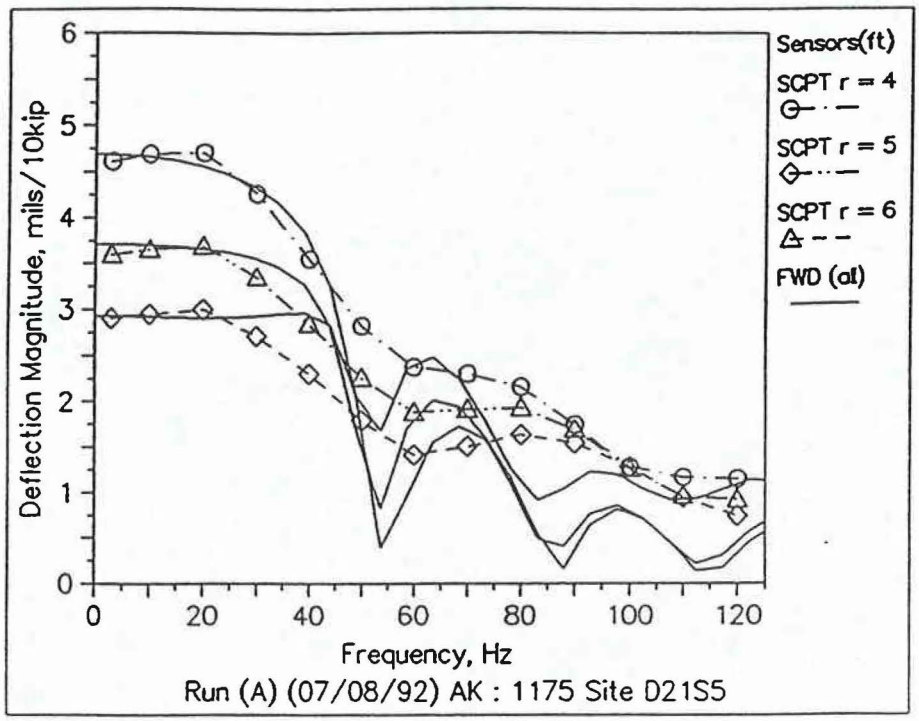

Figure 128. Section D21S5: Magnitude Plot for Outer Displacements (r=4.0, 5.0, and 6.0 ft.)

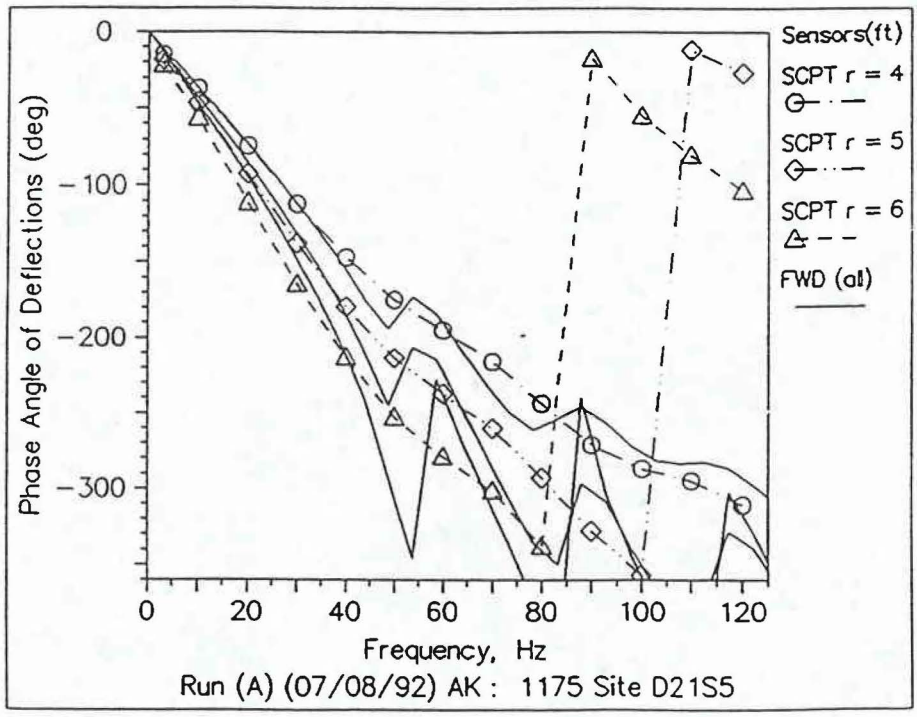

Figure 129. Section D21S5: Phase Angle Plot for Outer Displacements (r=4.0, 5.0, and 6.0 ft.)

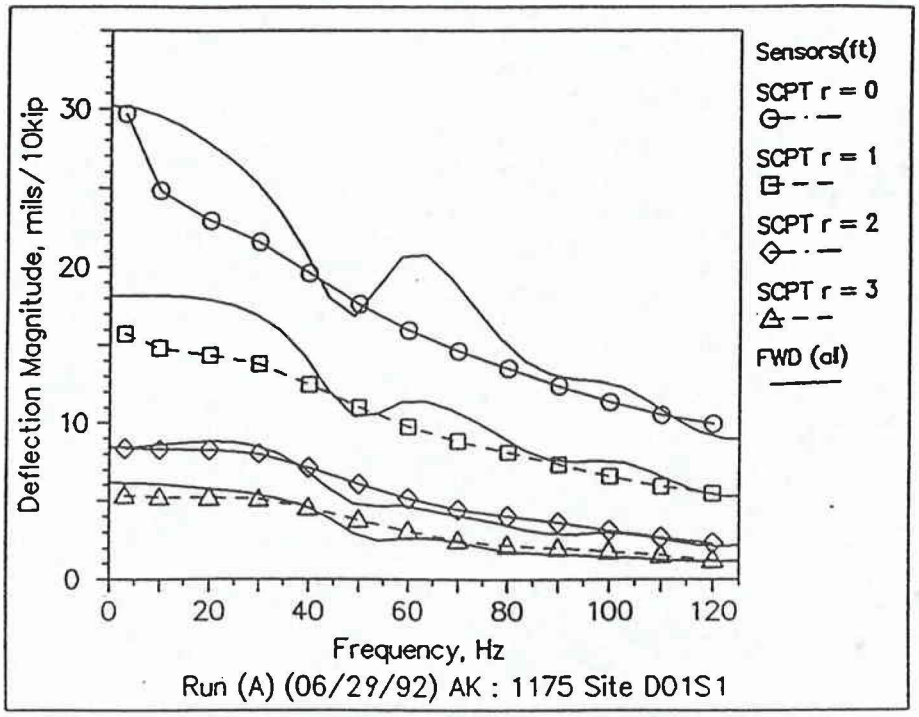

Figure 130. Section D01S1: Magnitude Plot for Inner Displacements (r=0, 1.0, 2.0, and 3.0 ft.)

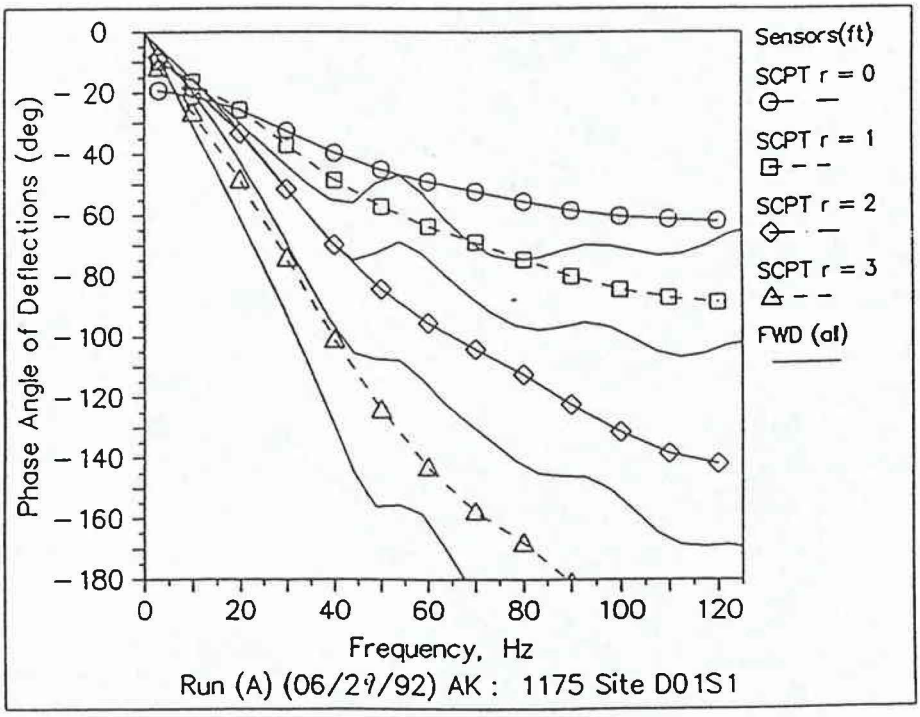

Figure 131. Section D01S1: Phase Angle Plot for Inner Displacements (r=0, 1.0, 2.0, and 3.0 ft.)

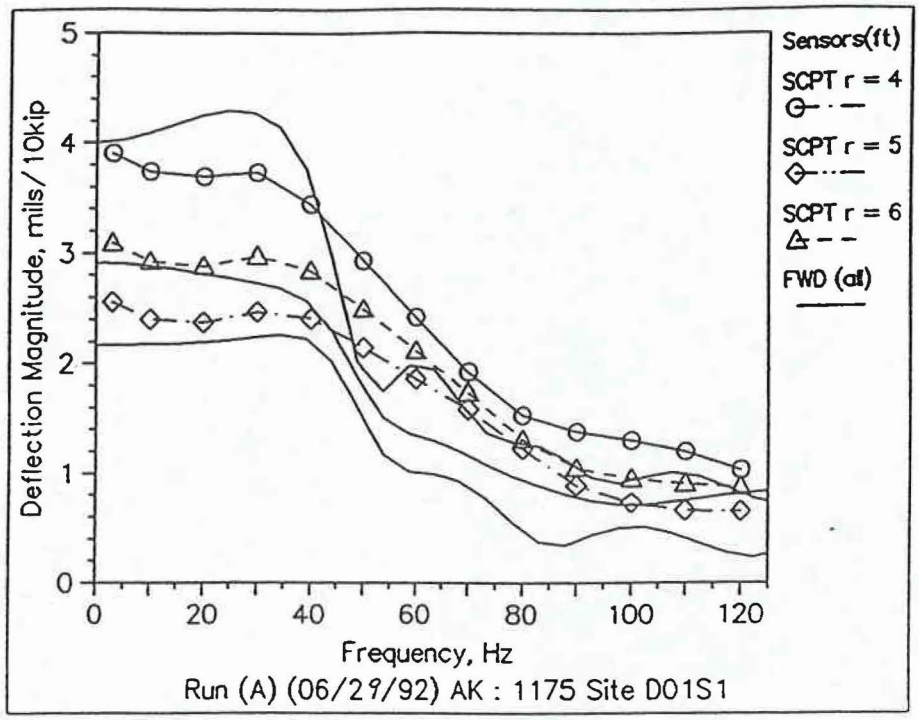

Figure 132. Section D01S1: Magnitude Plot for Outer Displacements (r=4.0, 5.0, and 6.0 ft.)

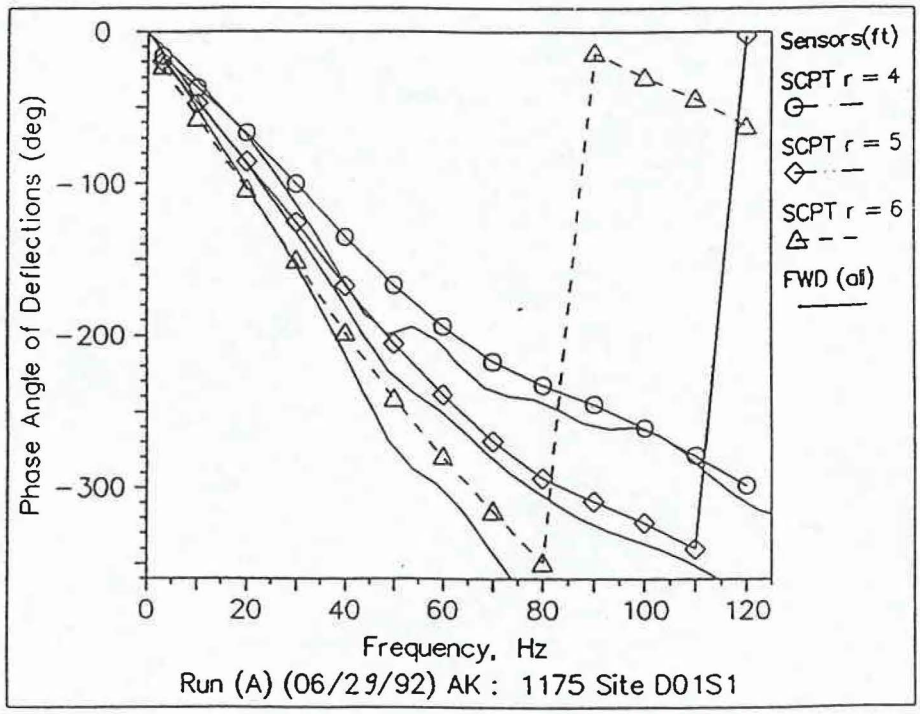

Figure 133. Section D01S1: Phase Angle Plot for Outer Displacements (r=4.0, 5.0, and 6.0 ft.)

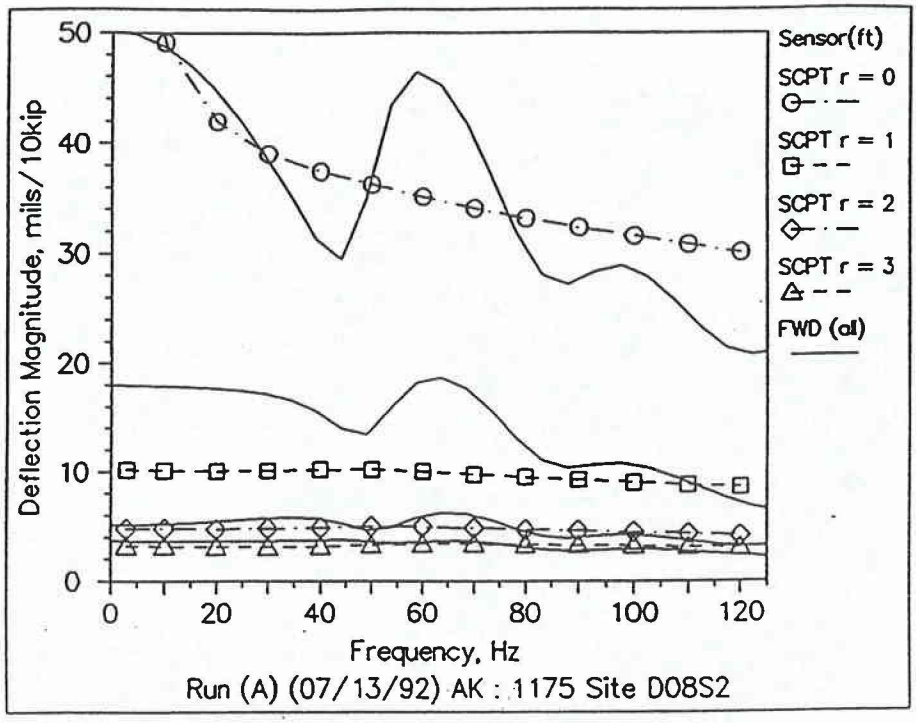

Figure 134. Section D08S2: Magnitude Plot for Inner Displacements (r=0, 1.0, 2.0, and 3.0 ft.)

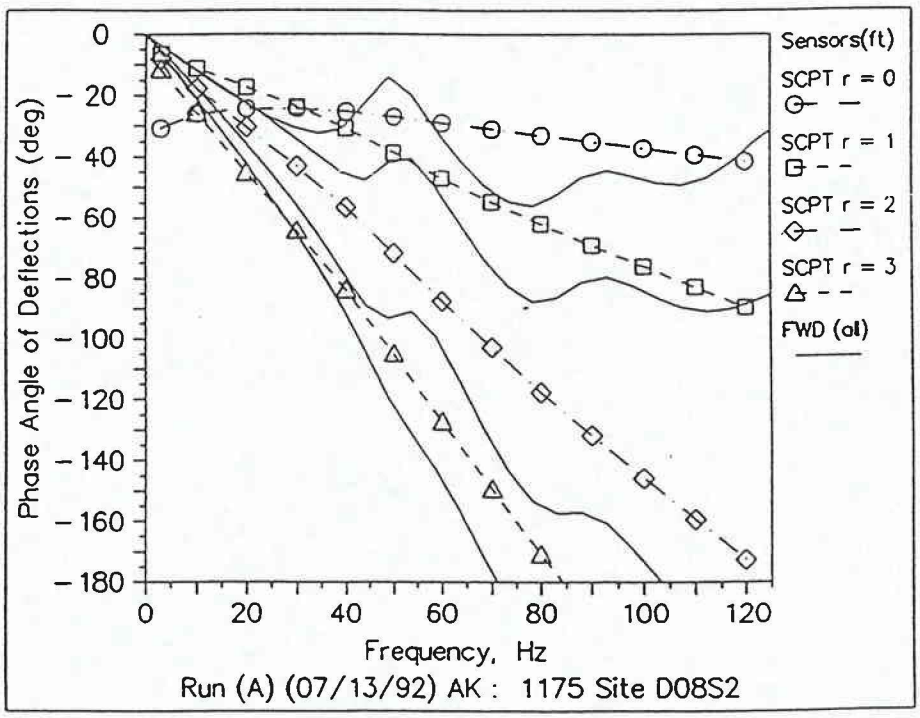

Figure 135. Section D08S2: Phase Angle Plot for Inner Displacements (r=0, 1.0, 2.0, and 3.0 ft.)

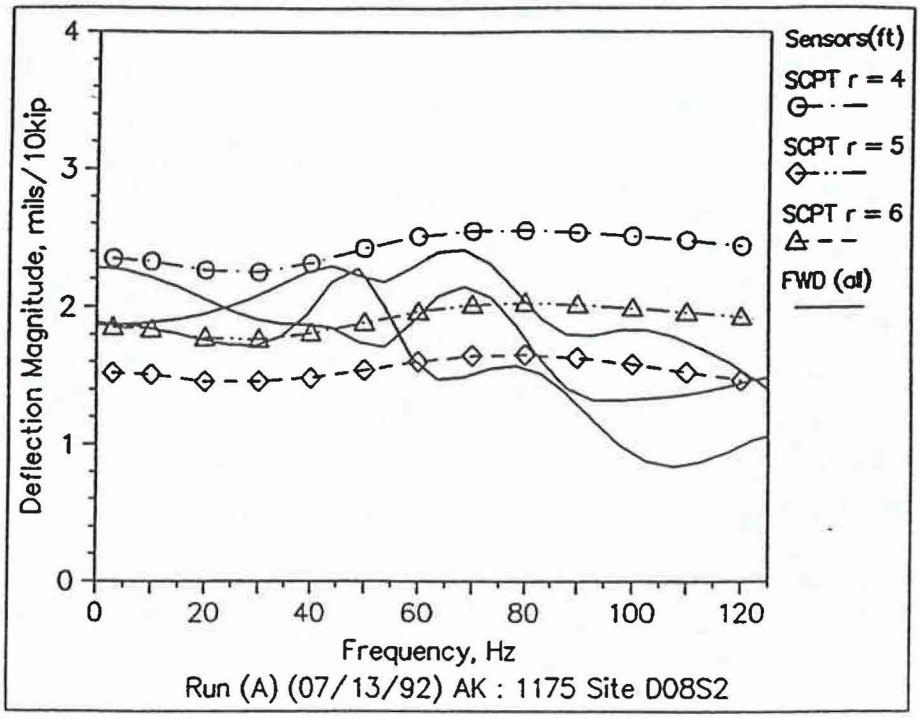

Figure 136. Section D08S2: Magnitude Plot for Outer Displacements (r=4.0, 5.0, and 6.0 ft.)

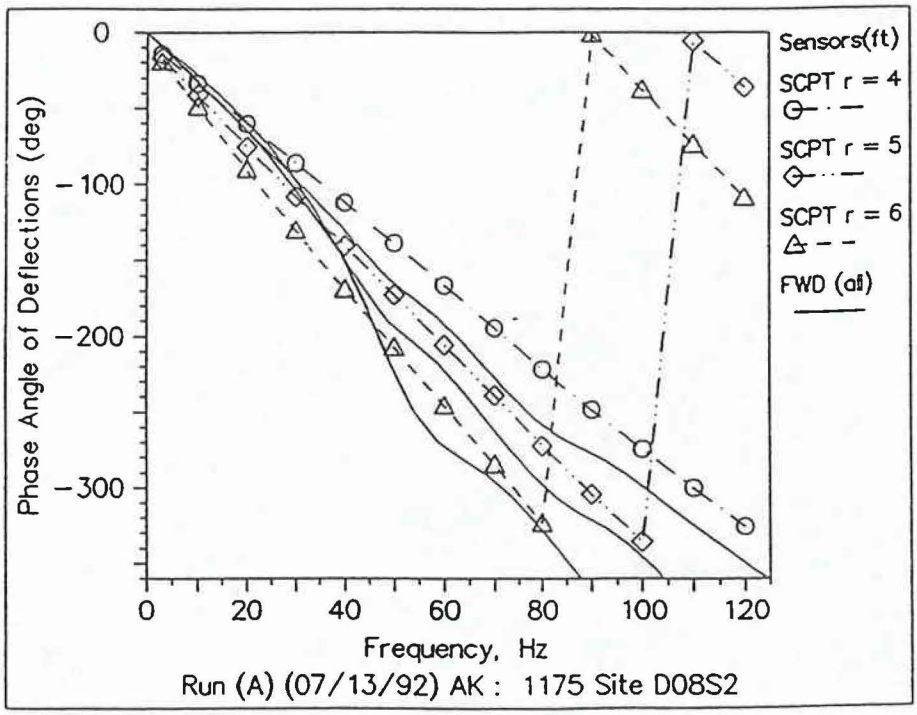

Figure 137. Section D08S2: Phase Angle Plot for Outer Displacements (r=4.0, 5.0, and 6.0 ft.)

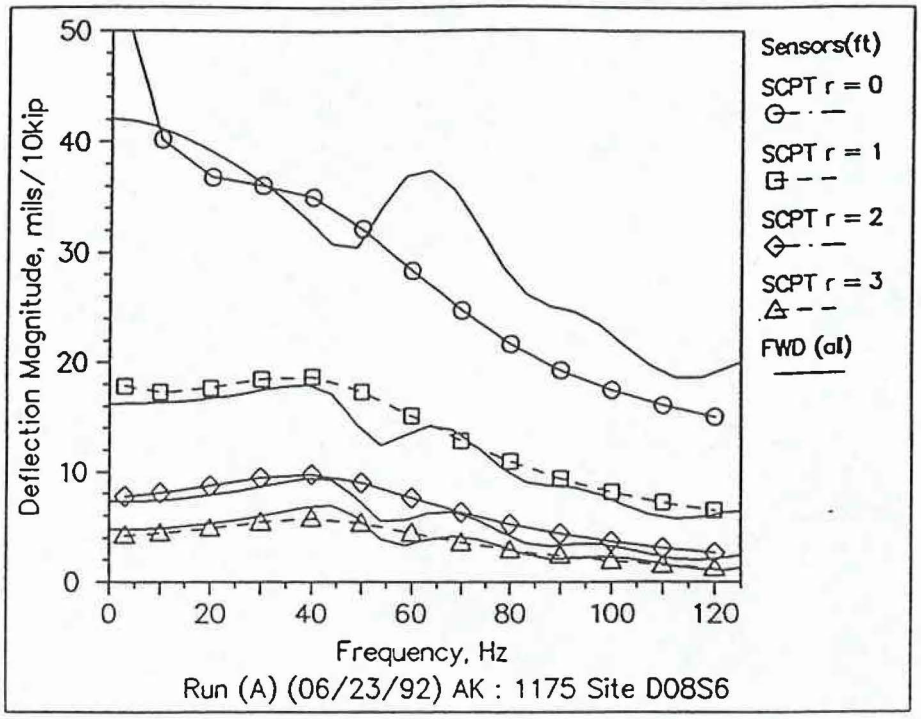

Figure 138. Section D08S6: Magnitude Plot for Inner Displacements (r=0, 1.0, 2.0, and 3.0 ft.)

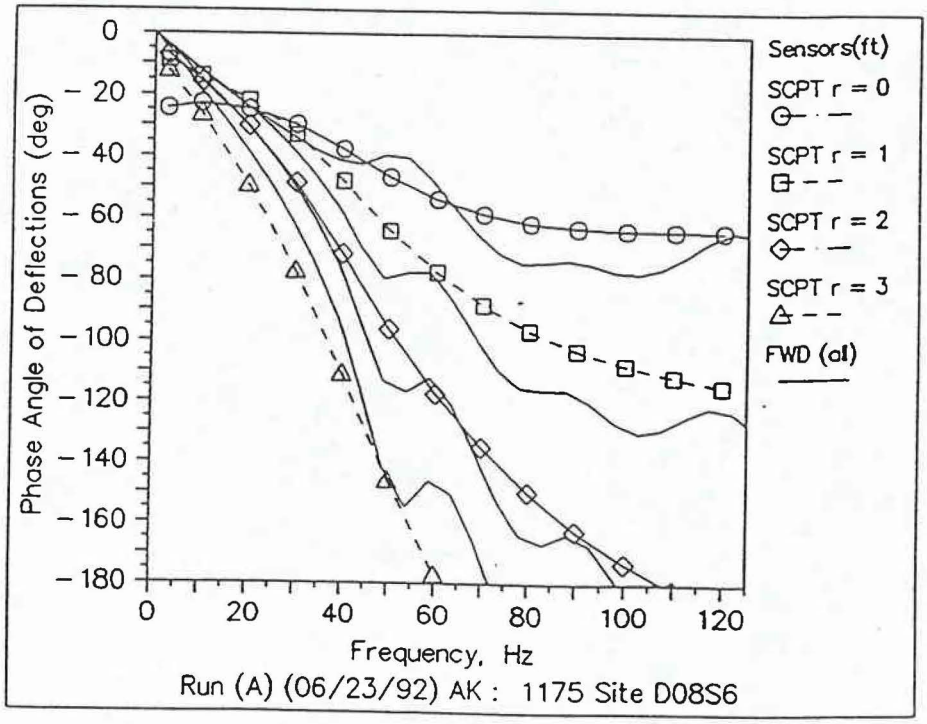

Figure 139. Section D08S6: Phase Angle Plot for Inner Displacements (r=0, 1.0, 2.0, and 3.0 ft.)

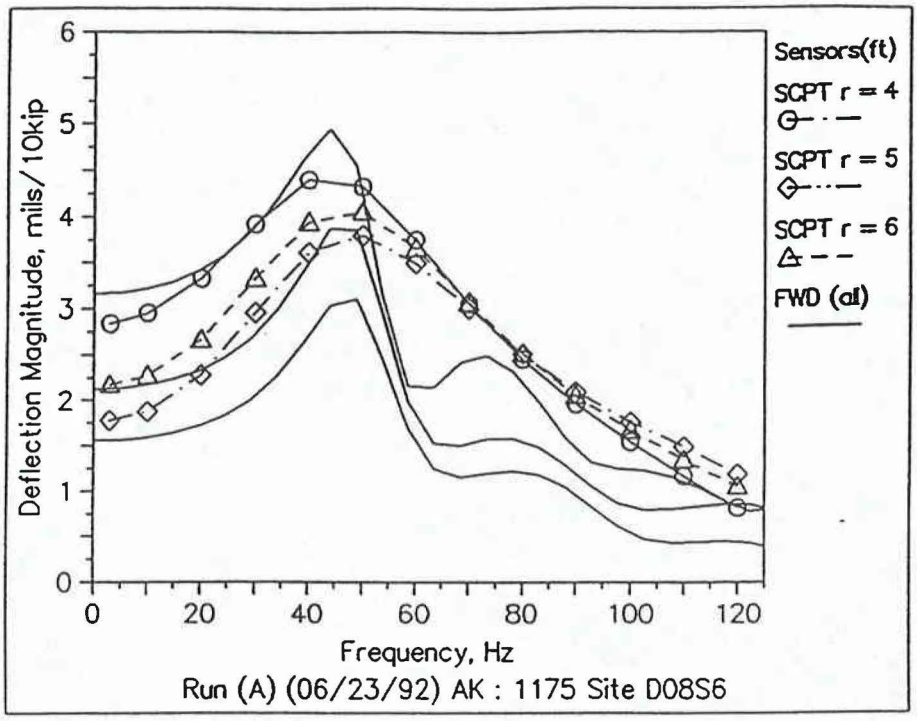

Figure 140. Section D08S6: Magnitude Plot for Outer Displacements (r=4.0, 5.0, and 6.0 ft.)

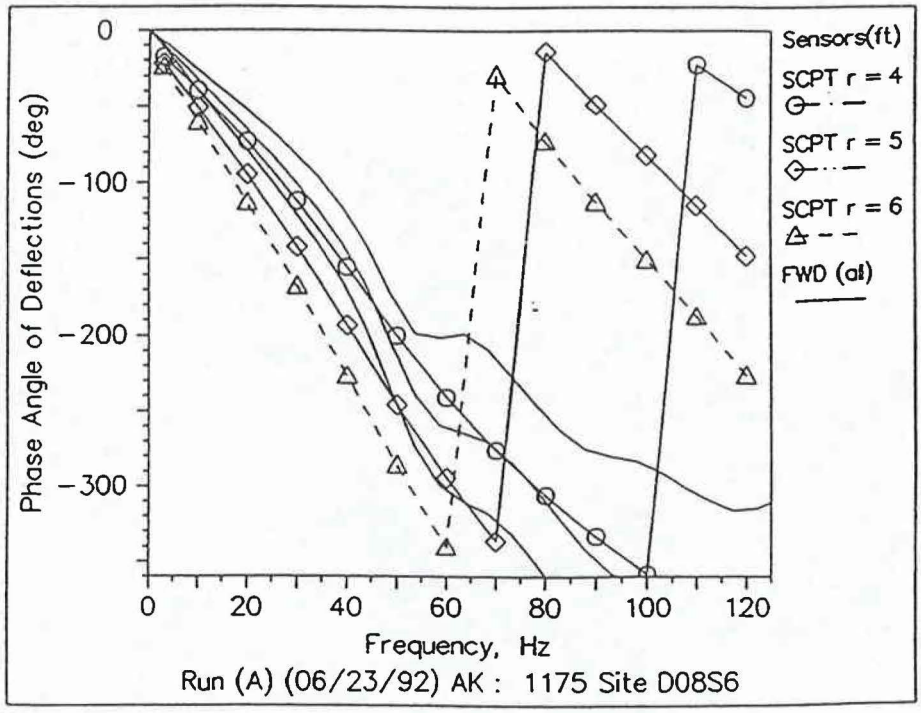

Figure 141. Section D08S6: Phase Angle Plot for Outer Displacements (r=4.0, 5.0, and 6.0 ft.)

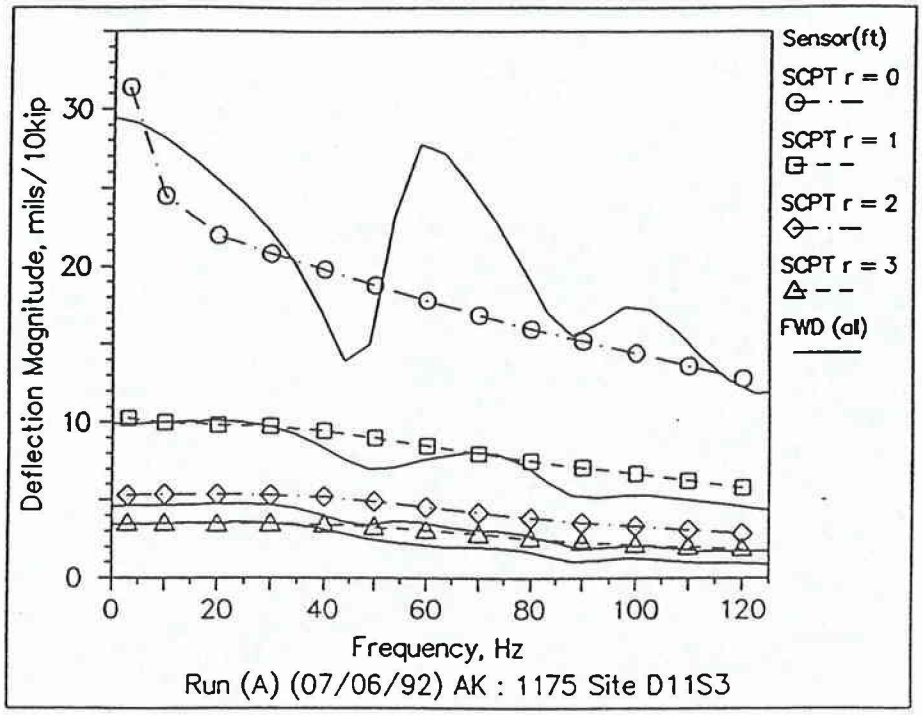

Figure 142. Section D11S3: Magnitude Plot for Inner Displacements (r=0, 1.0, 2.0, and 3.0 ft.)

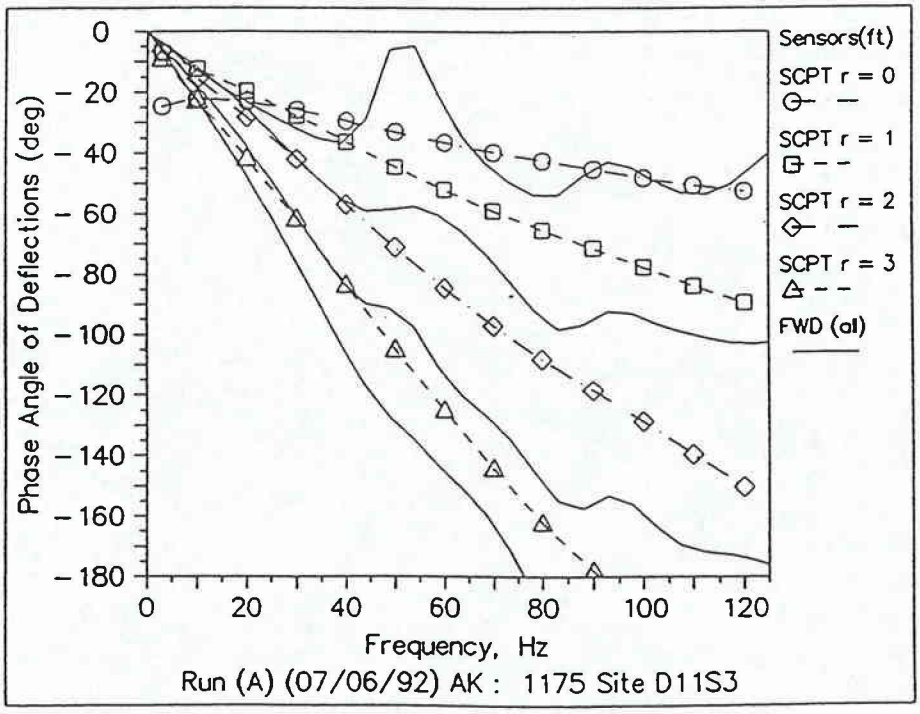

Figure 143. Section D11S3: Phase Angle Plot for Inner Displacements (r=0, 1.0, 2.0, and 3.0 ft.)

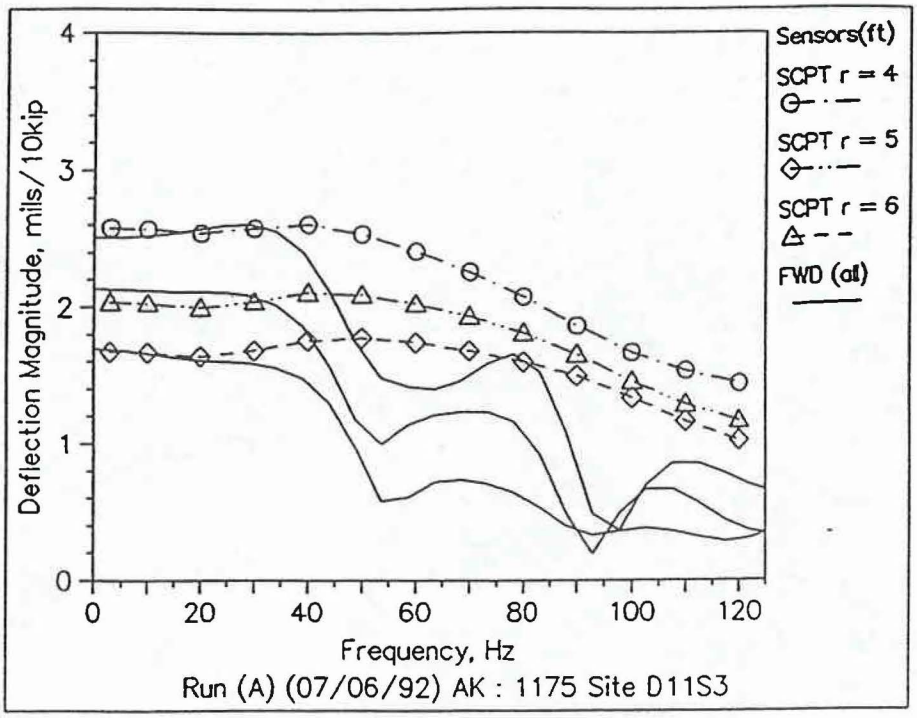

Figure 144. Section D11S3: Magnitude Plot for Outer Displacements (r=4.0, 5.0, and 6.0 ft.)

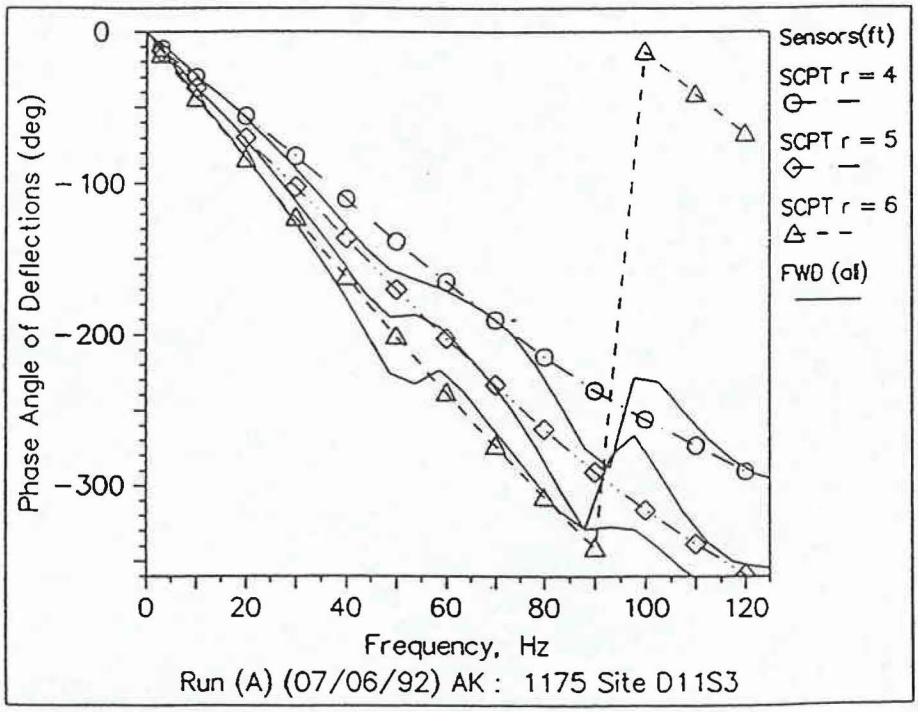

Figure 145. Section D11S3: Phase Angle Plot for Outer Displacements (r=4.0, 5.0, and 6.0 ft.)

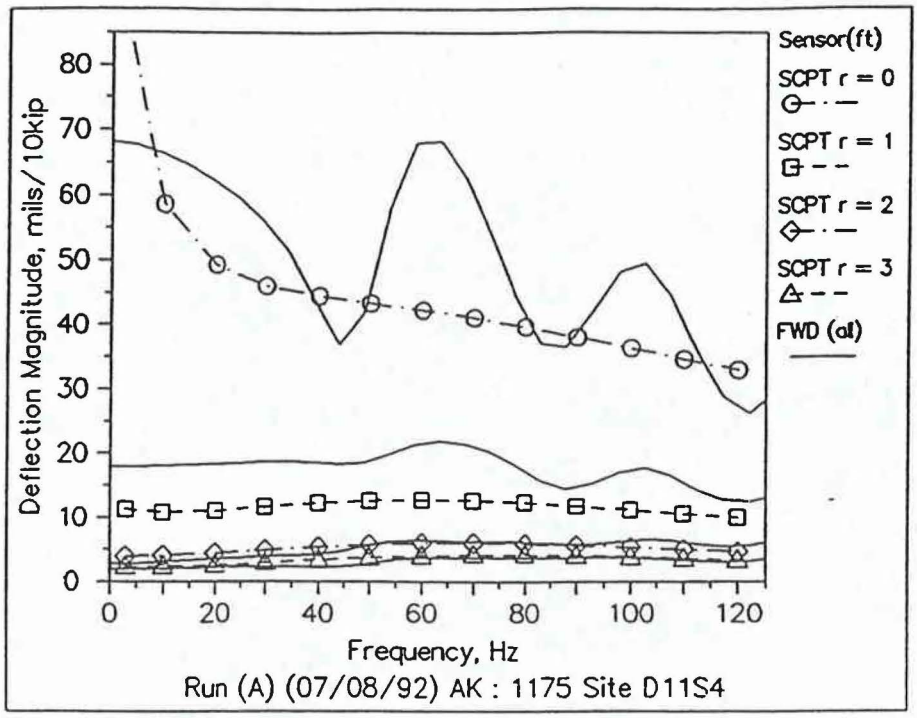

Figure 146. Section D11S4: Magnitude Plot for Inner Displacements (r=0, 1.0, 2.0, and 3.0 ft.)

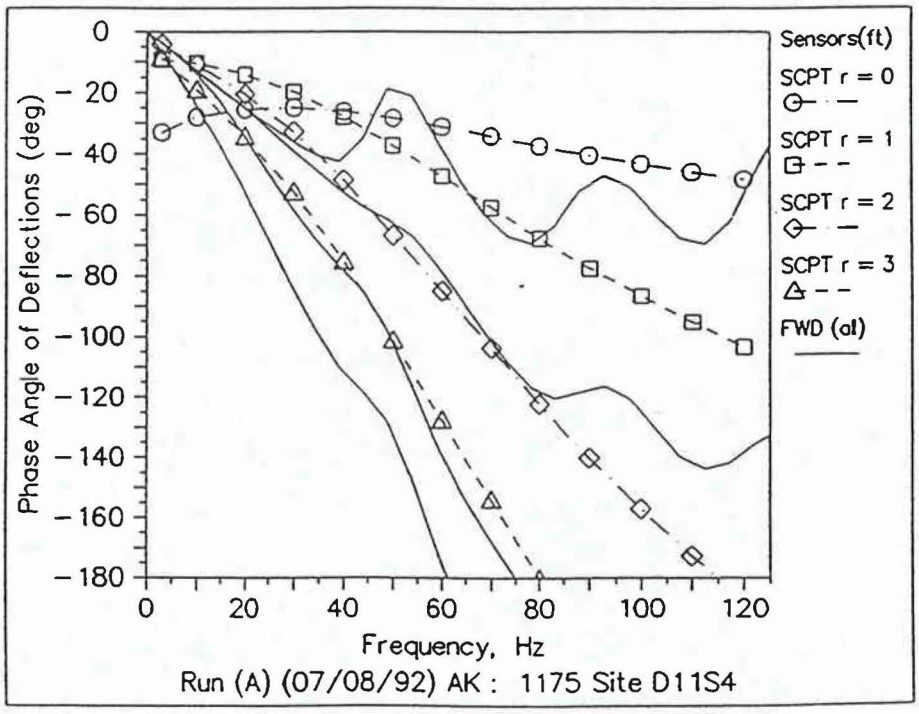

Figure 147. Section D11S4: Phase Angle Plot for Inner Displacements (r=0, 1.0, 2.0, and 3.0 ft.)

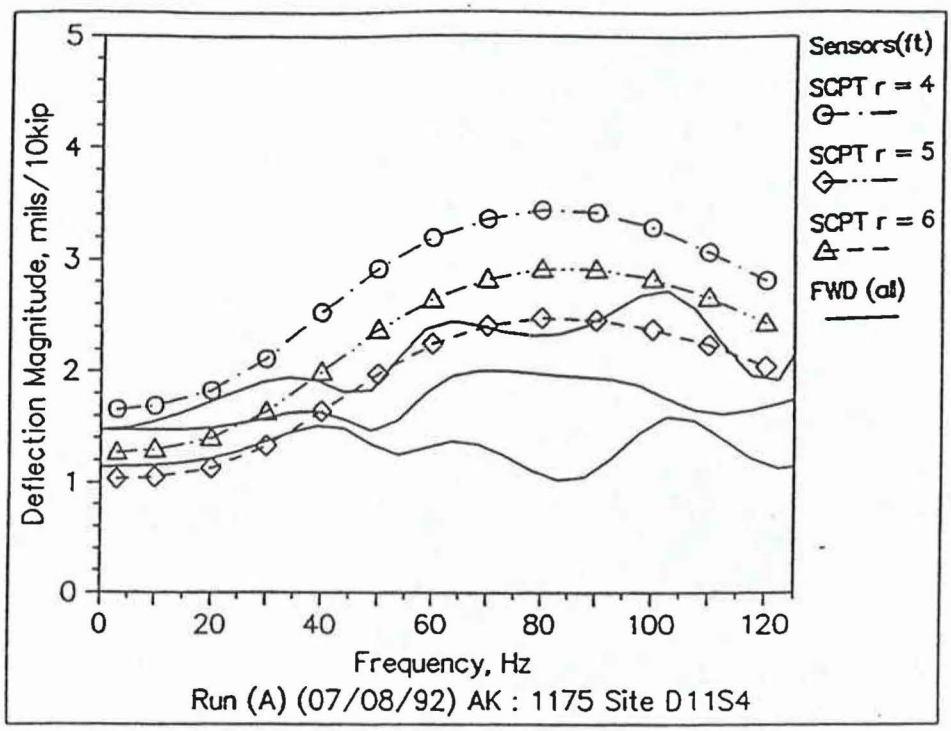

Figure 148. Section D11S4: Magnitude Plot for Outer Displacements (r=4.0, 5.0, and 6.0 ft.)

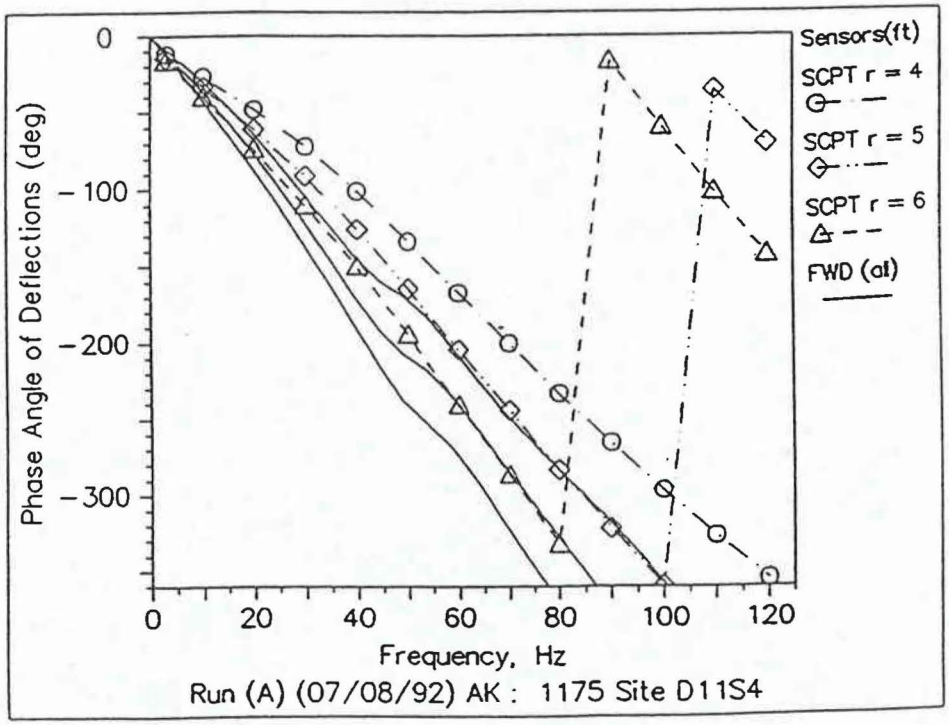

Figure 149. Section D11S4: Phase Angle Plot for Outer Displacements (r=4.0, 5.0, and 6.0 ft.)

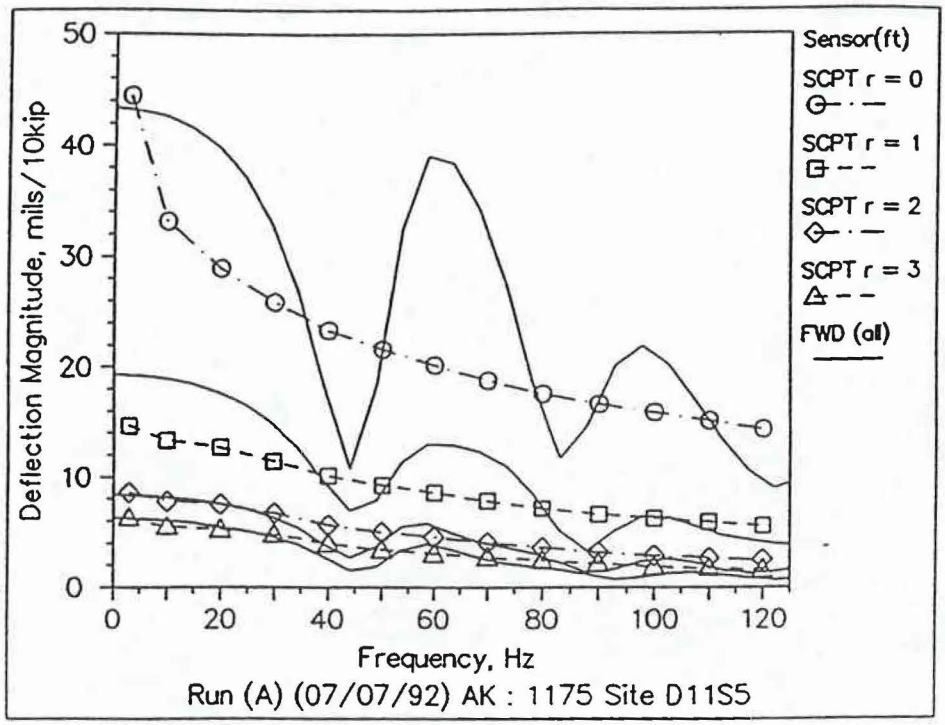

Figure 150. Section D11S5: Magnitude Plot for Inner Displacements (r=0, 1.0, 2.0, and 3.0 ft.)

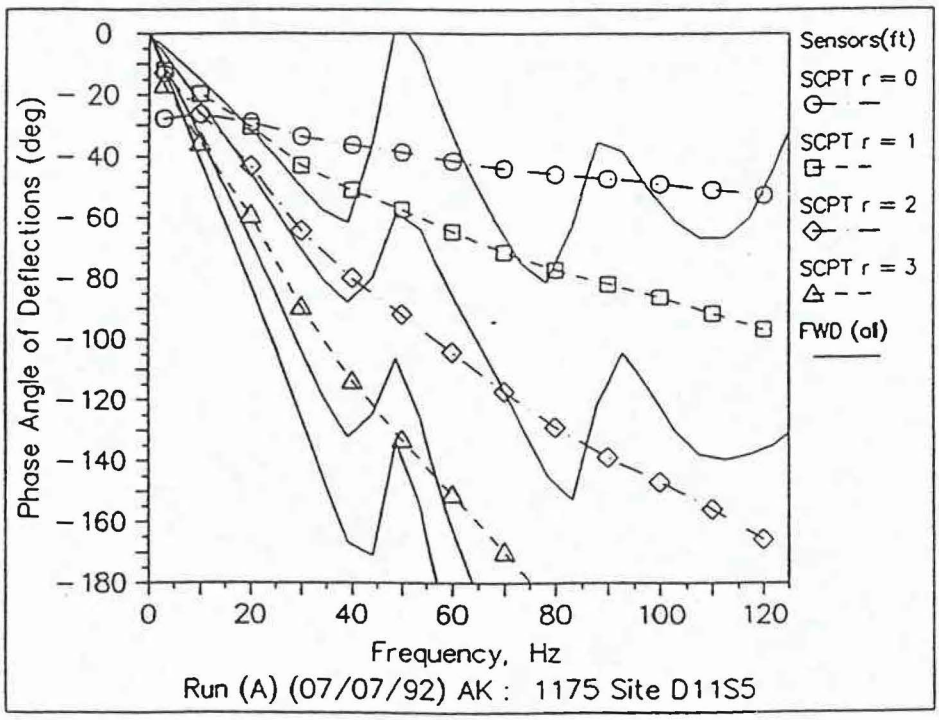

Figure 151. Section D11S5: Phase Angle Plot for Inner Displacements (r=0, 1.0, 2.0, and 3.0 ft.)

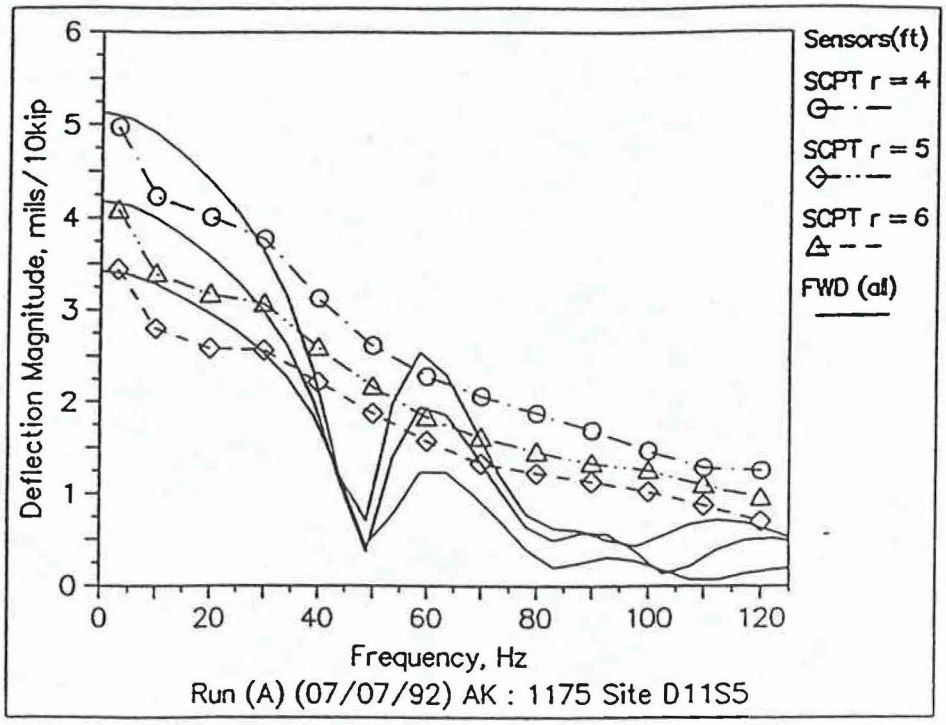

Figure 152. Section D11S5: Magnitude Plot for Outer Displacements (r=4.0, 5.0, and 6.0 ft.)

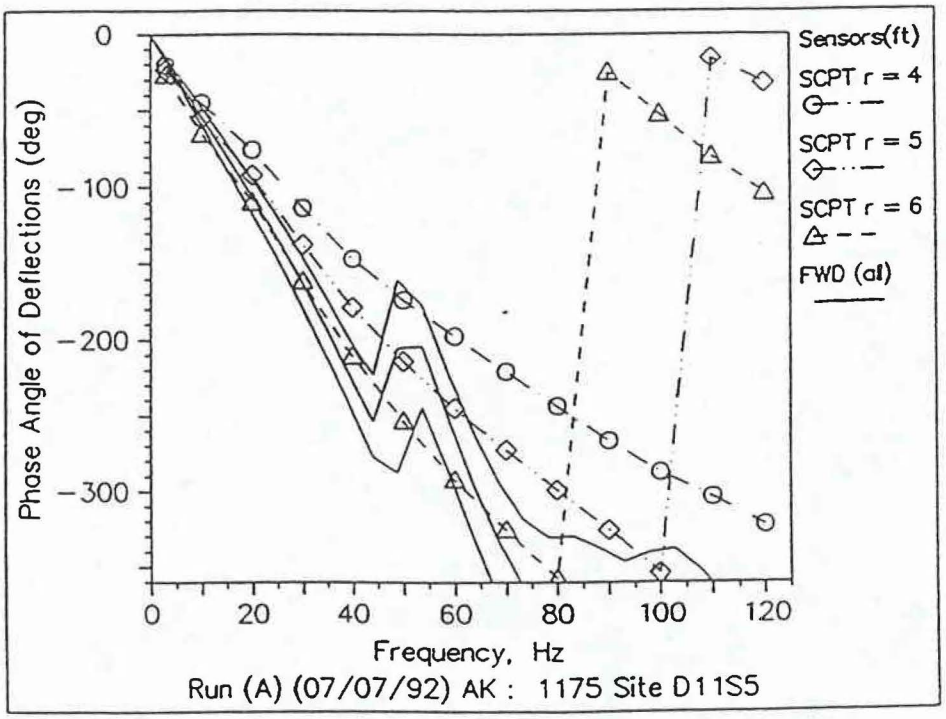

Figure 153. Section D11S5: Phase Angle Plot for Outer Displacements (r=4.0, 5.0, and 6.0 ft.)

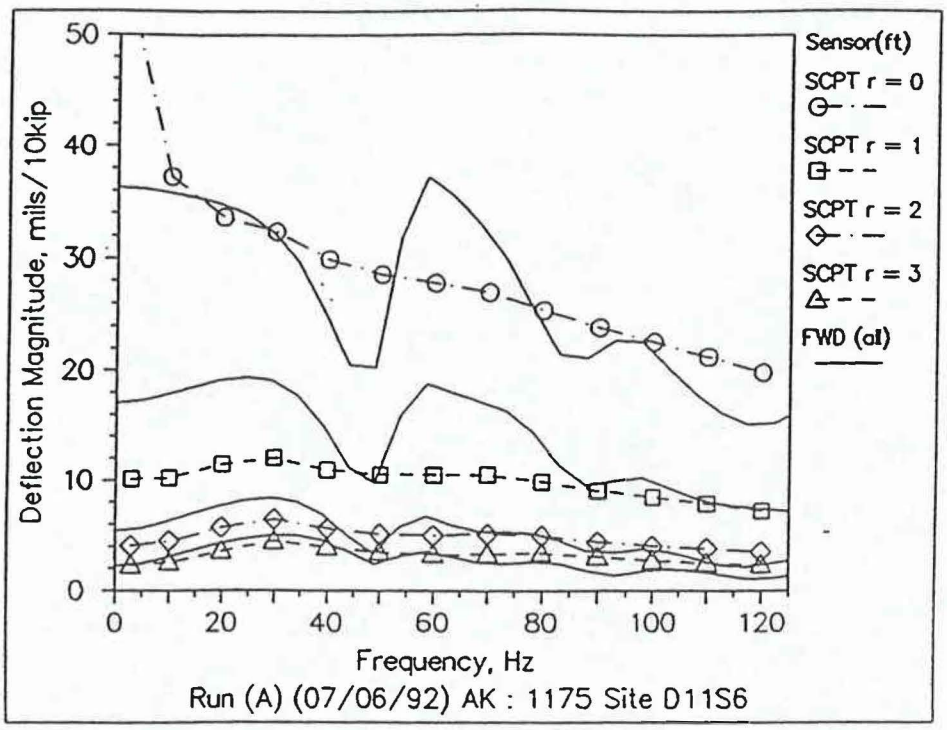

Figure 154. Section D11S6: Magnitude Plot for Inner Displacements (r=0, 1.0, 2.0, and 3.0 ft.)

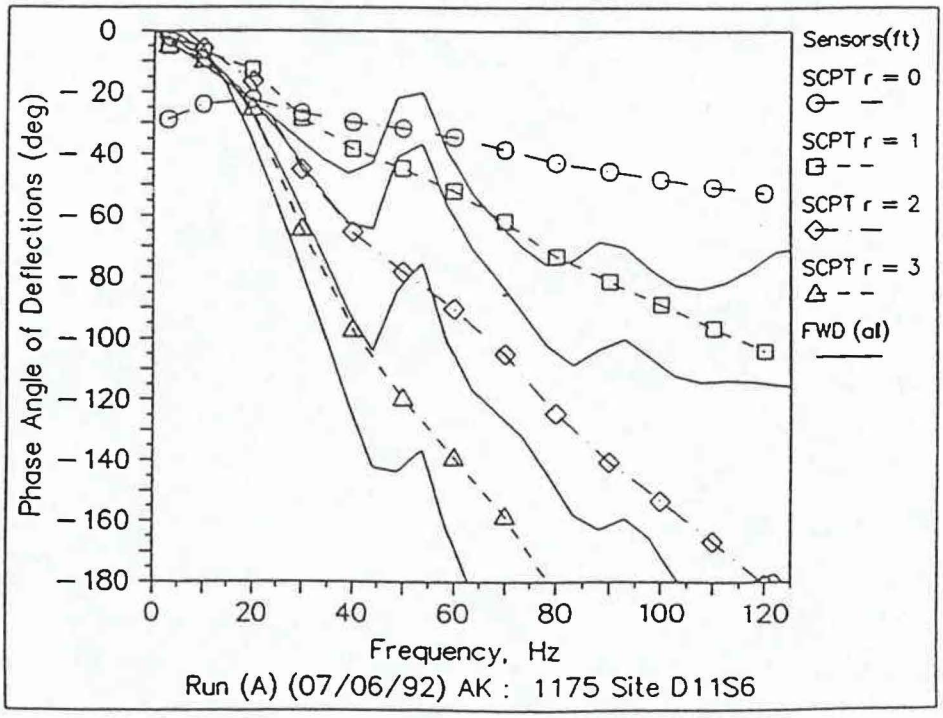

Figure 155. Section D11S6: Phase Angle Plot for Inner Displacements (r=0, 1.0, 2.0, and 3.0 ft.)

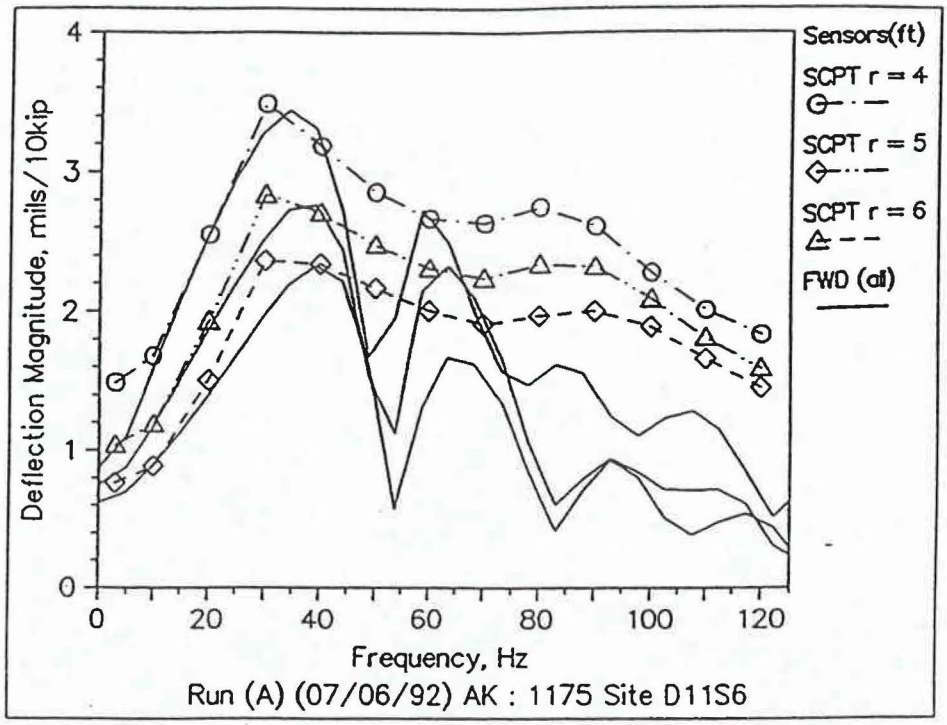

Figure 156. Section D11S6: Magnitude Plot for Outer Displacements (r=4.0, 5.0, and 6.0 ft.)

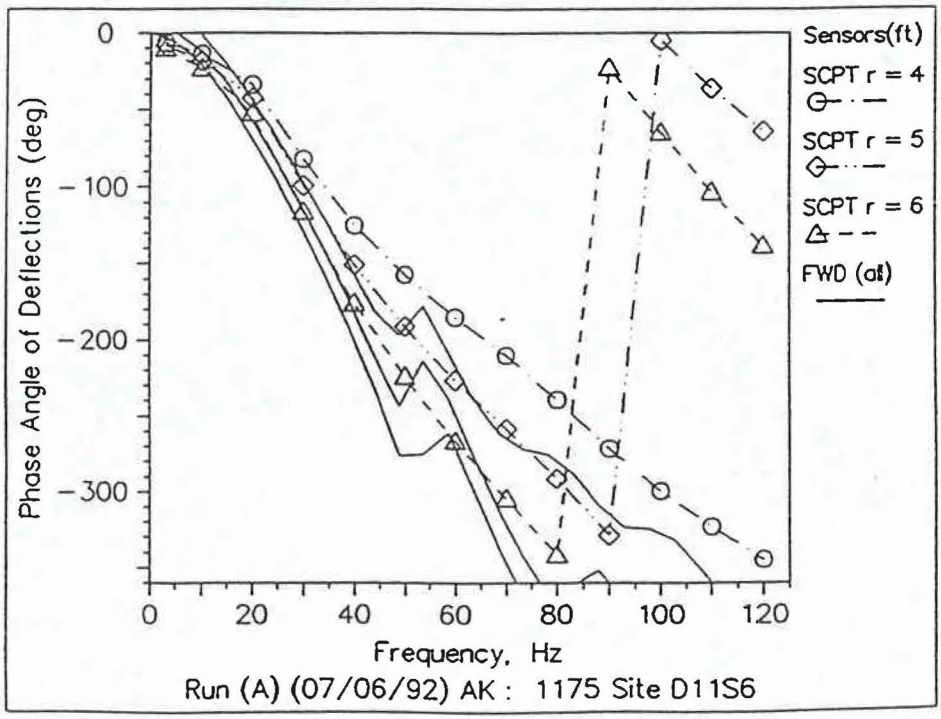

Figure 157. Section D11S6: Phase Angle Plot for Outer Displacements (r=4.0, 5.0, and 6.0 ft.)

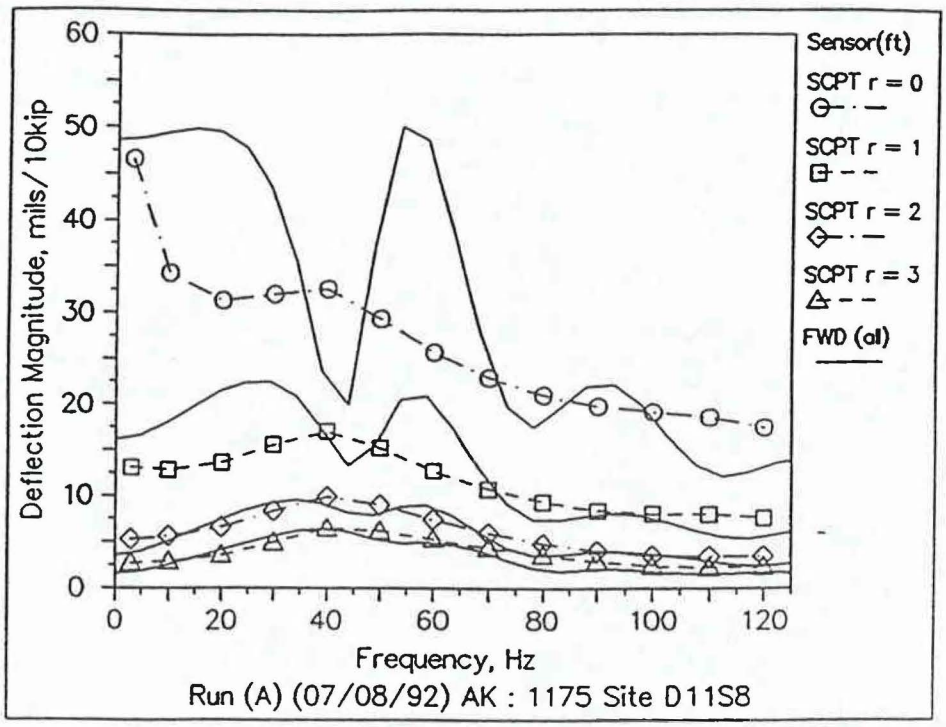

Figure 158. Section D11S8: Magnitude Plot for Inner Displacements (r=0, 1.0, 2.0, and 3.0 ft.)

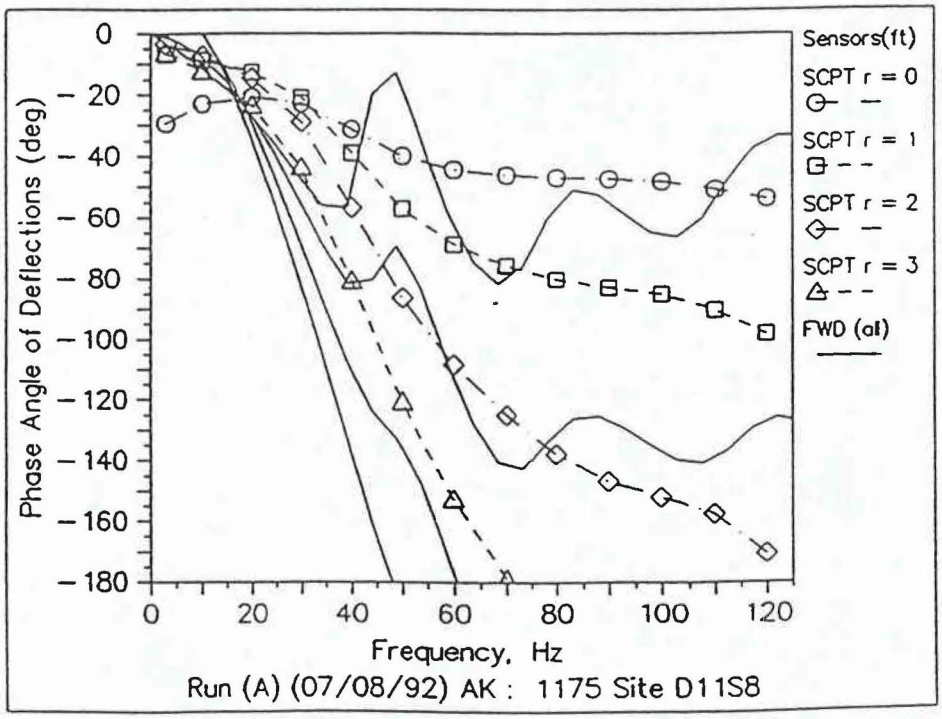

Figure 159. Section D11S8: Phase Angle Plot for Inner Displacements (r=0, 1.0, 2.0, and 3.0 ft.)

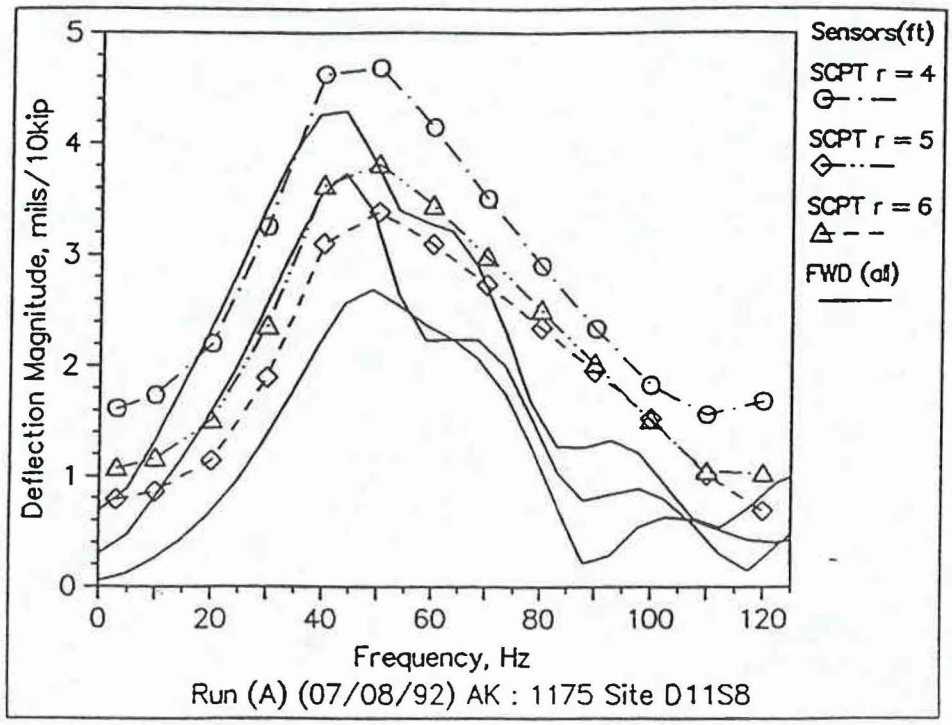

Figure 160. Section D11S8: Magnitude Plot for Outer Displacements (r=4.0, 5.0, and 6.0 ft.)

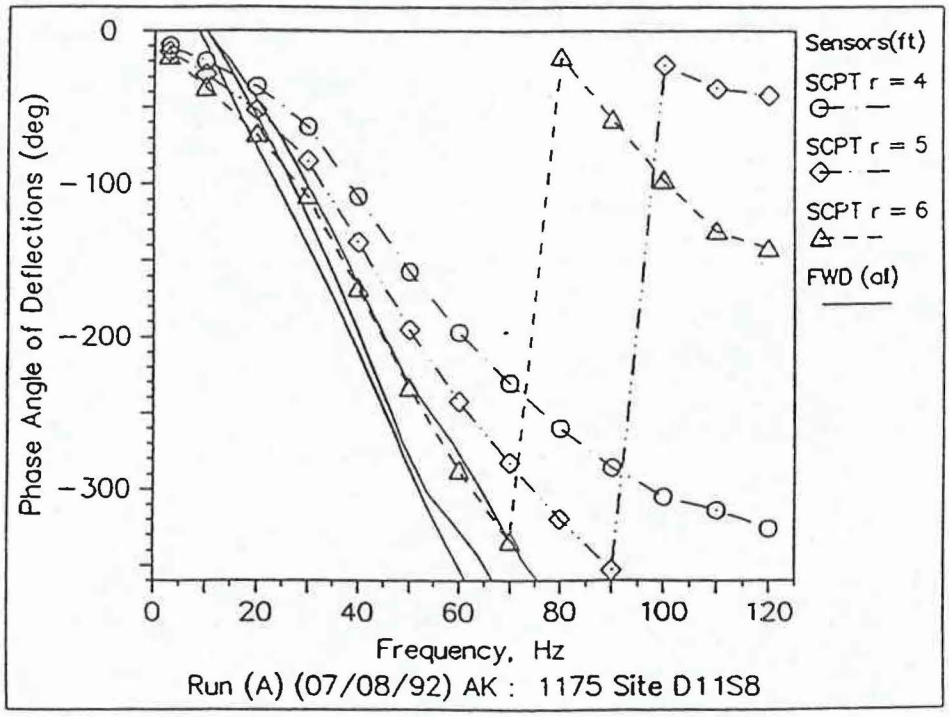

Figure 161. Section D11S8: Phase Angle Plot for Outer Displacements (r=4.0, 5.0, and 6.0 ft.)

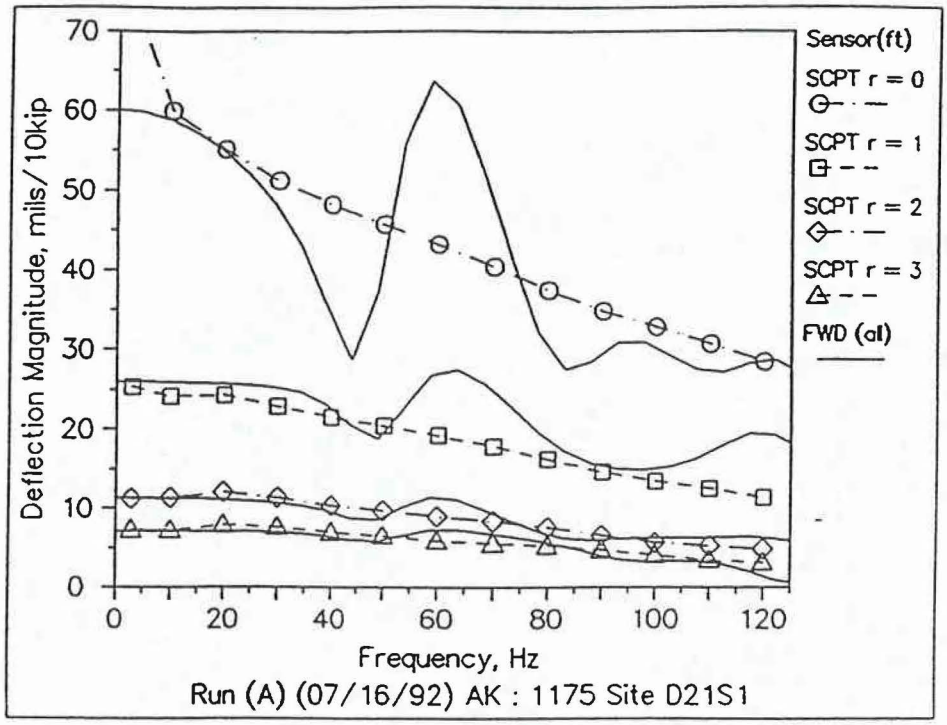

Figure 162. Section D21S1: Magnitude Plot for Inner Displacements (r=0, 1.0, 2.0, and 3.0 ft.)

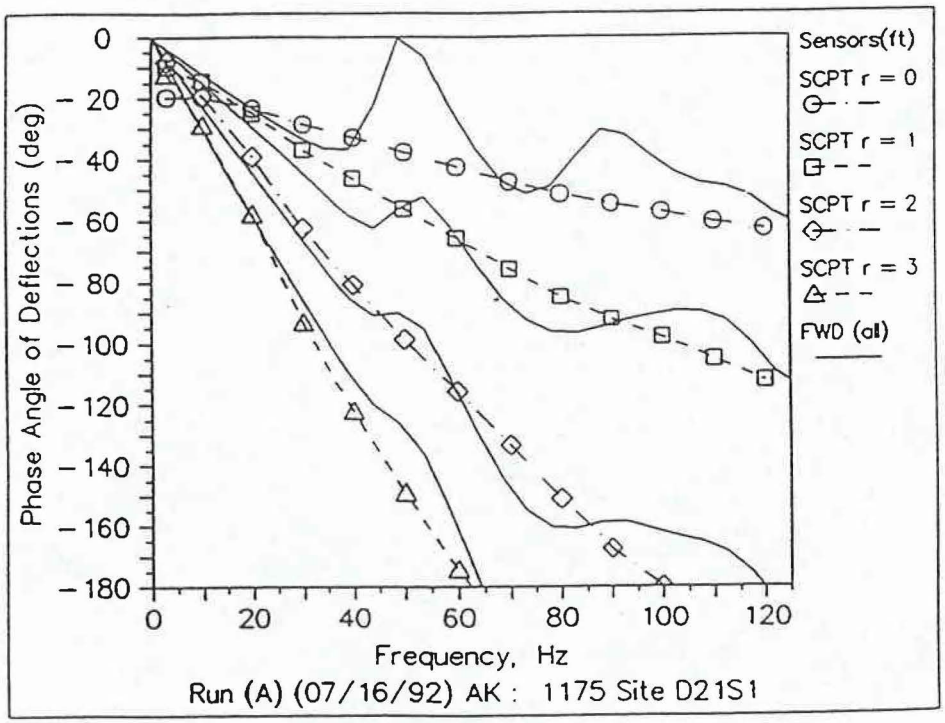

Figure 163. Section D21S1: Phase Angle Plot for Inner Displacements (r=0, 1.0, 2.0, and 3.0 ft.)

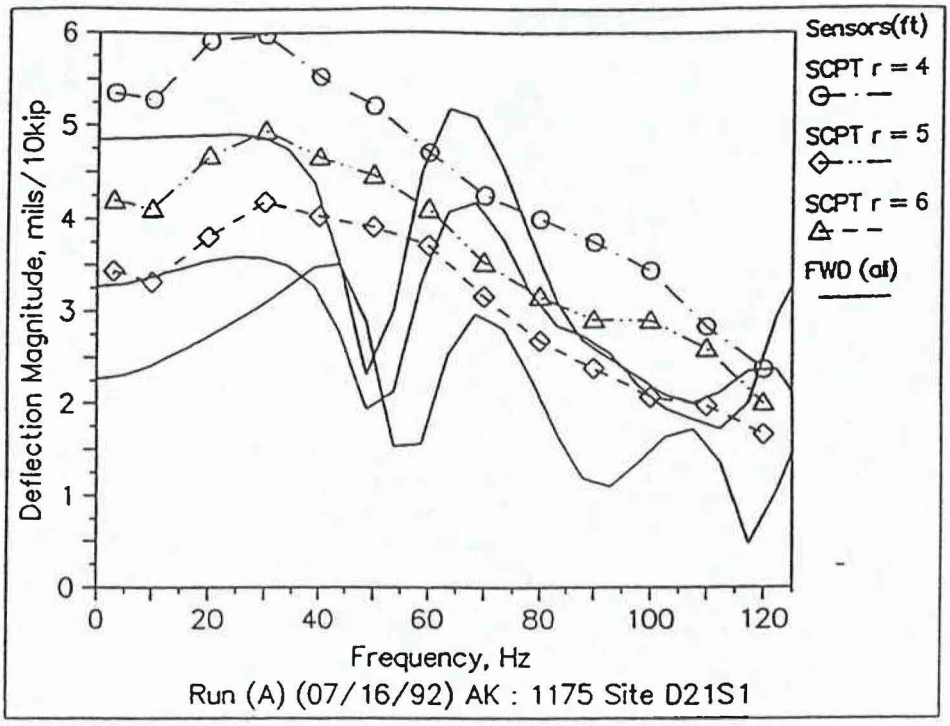

Figure 164. Section D21S1: Magnitude Plot for Outer Displacements (r=4.0, 5.0, and 6.0 ft.)

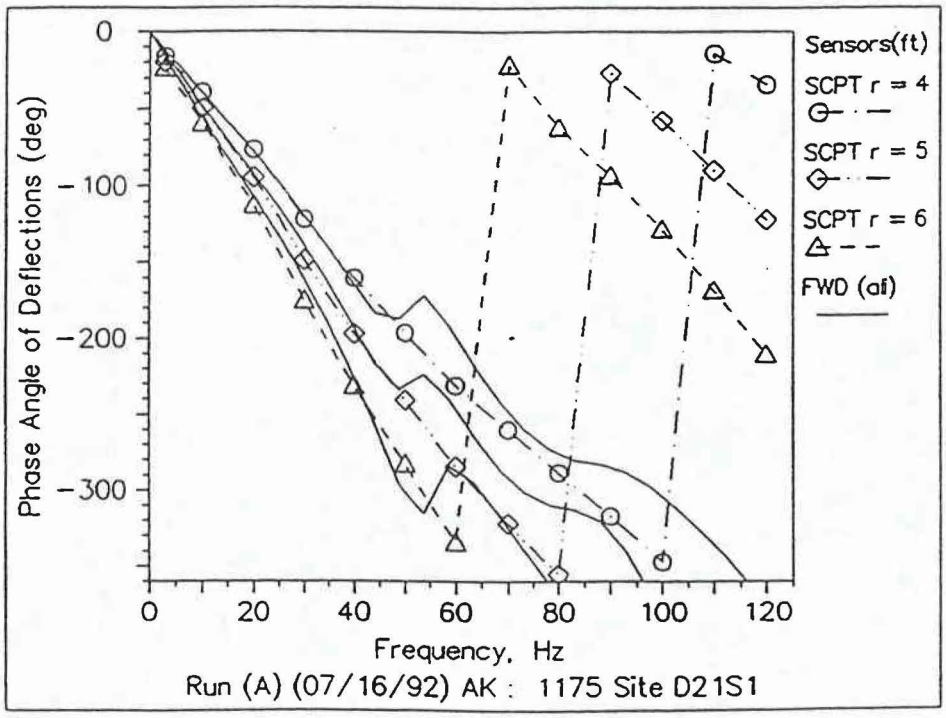

Figure 165. Section D21S1: Phase Angle Plot for Outer Displacements (r=4.0, 5.0, and 6.0 ft.)

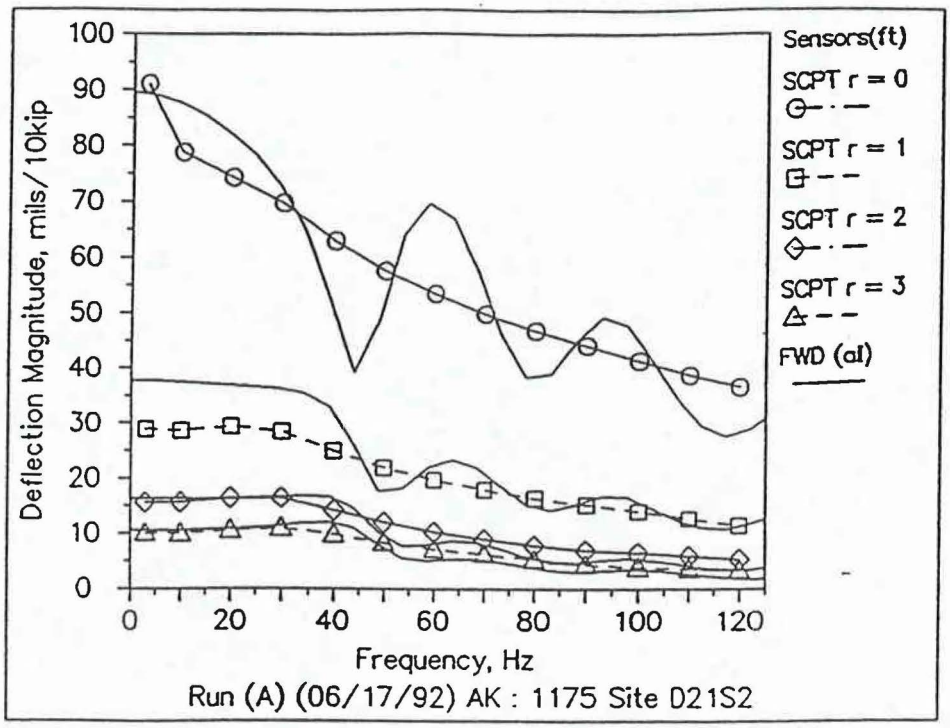

Figure 166. Section D21S2: Magnitude Plot for Inner Displacements (r=0, 1.0, 2.0, and 3.0 ft.)

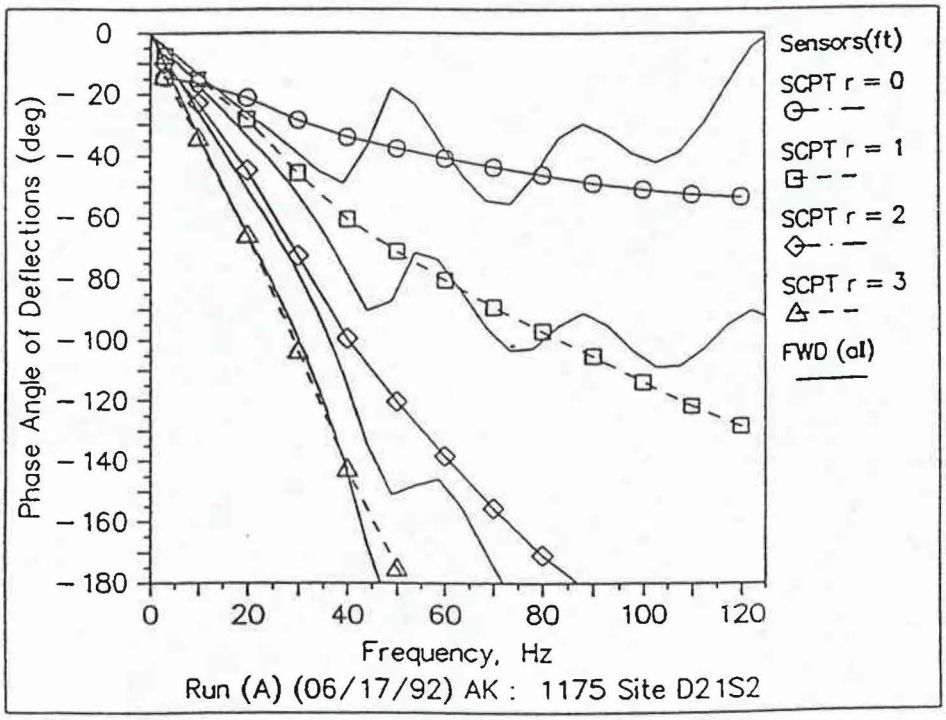

Figure 167. Section D21S2: Phase Angle Plot for Inner Displacements (r=0, 1.0, 2.0, and 3.0 ft.)

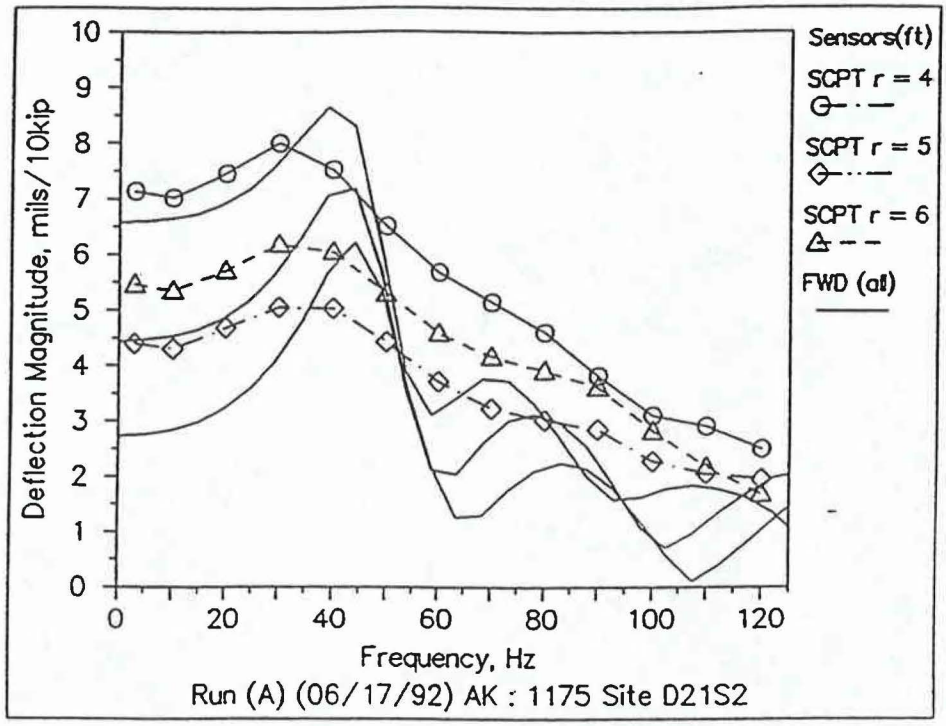

Figure 168. Section D21S2: Magnitude Plot for Outer Displacements (r=4.0, 5.0, and 6.0 ft.)

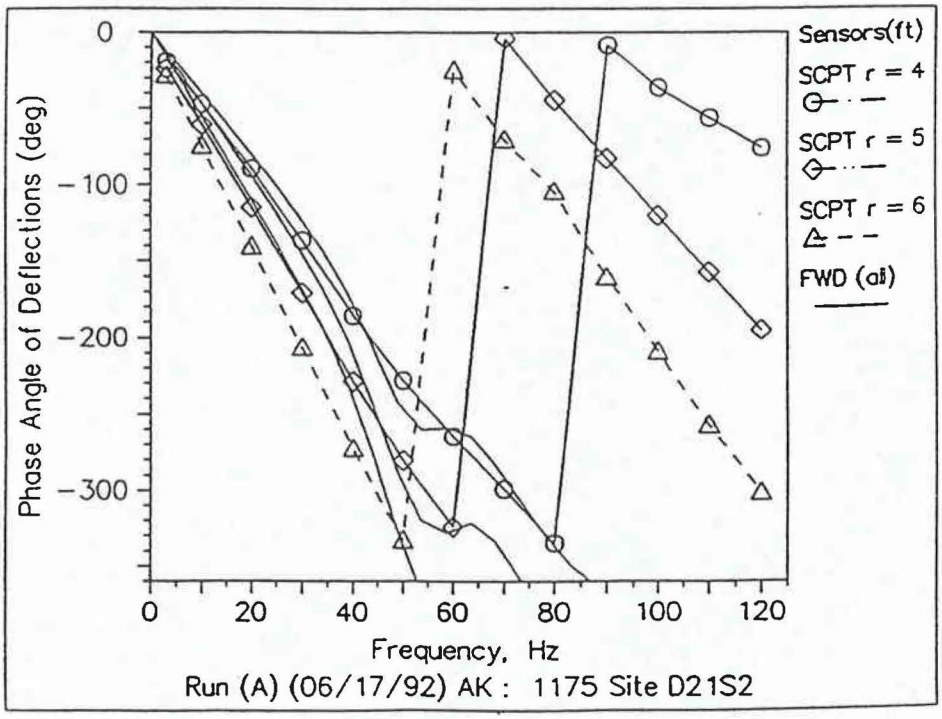

Figure 169. Section D21S2: Phase Angle Plot for Outer Displacements (r=4.0, 5.0, and 6.0 ft.)

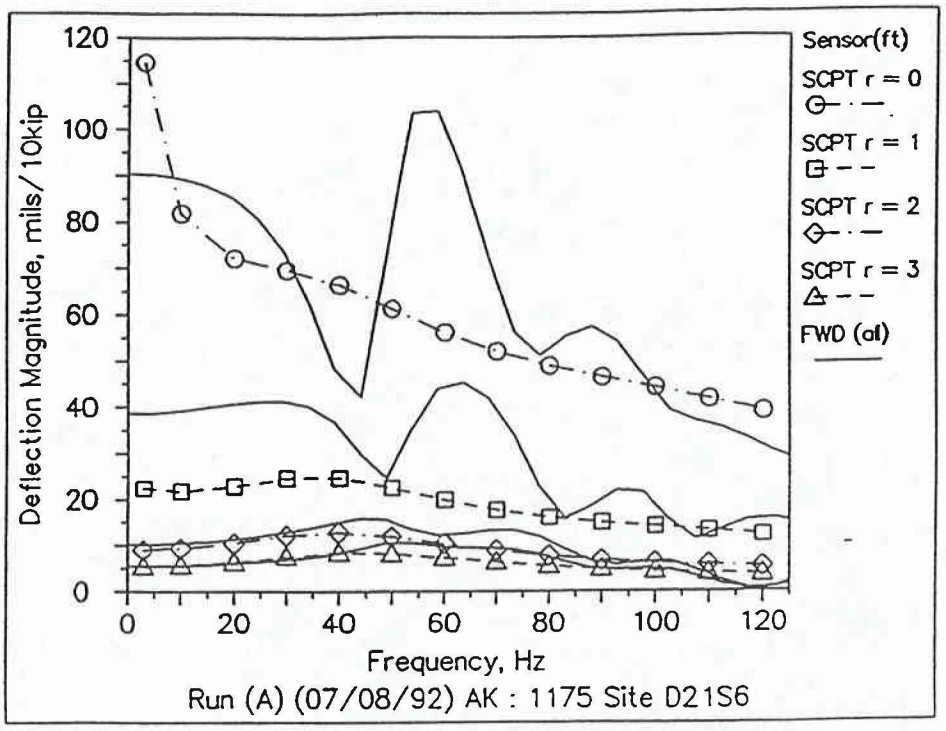

Figure 170. Section D21S6: Magnitude Plot for Inner Displacements (r=0, 1.0, 2.0, and 3.0 ft.)

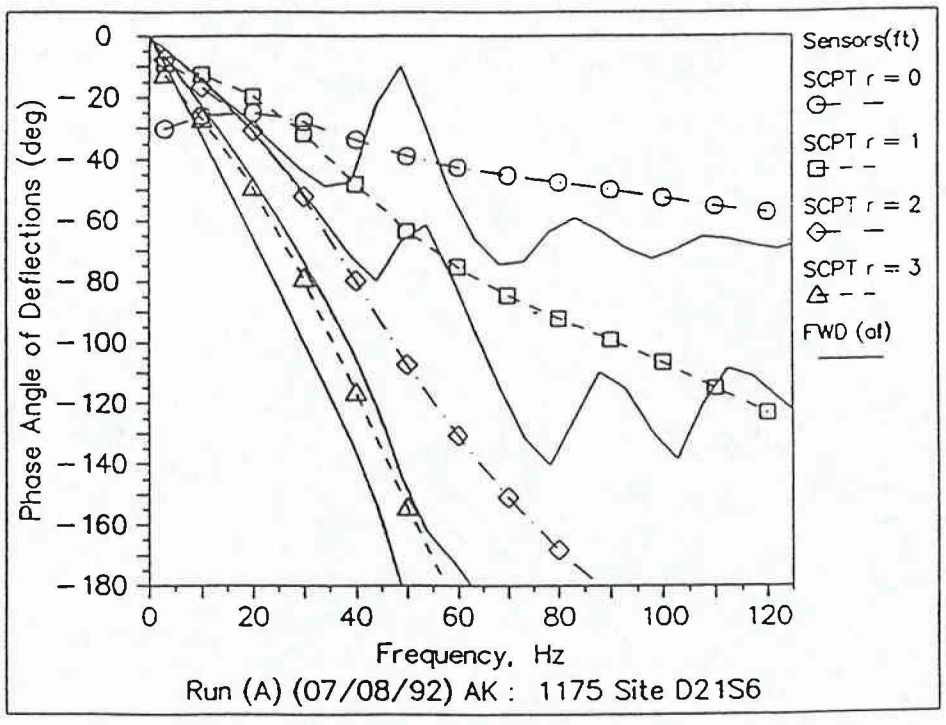

Figure 171. Section D21S6: Phase Angle Plot for Inner Displacements (r=0, 1.0, 2.0, and 3.0 ft.)

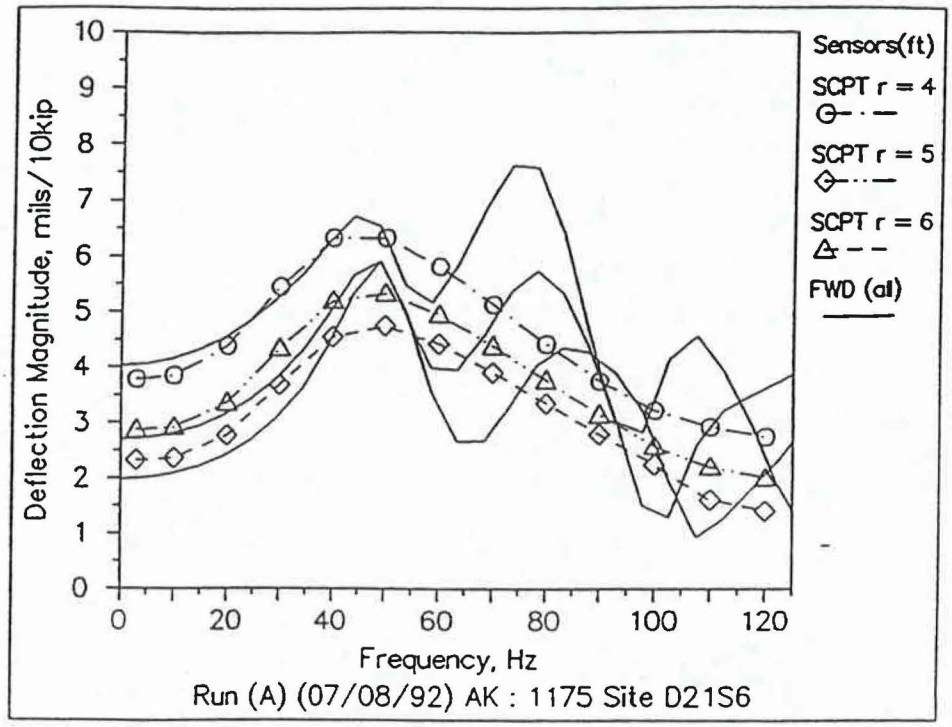

Figure 172. Section D21S6: Magnitude Plot for Outer Displacements (r=4.0, 5.0, and 6.0 ft.)

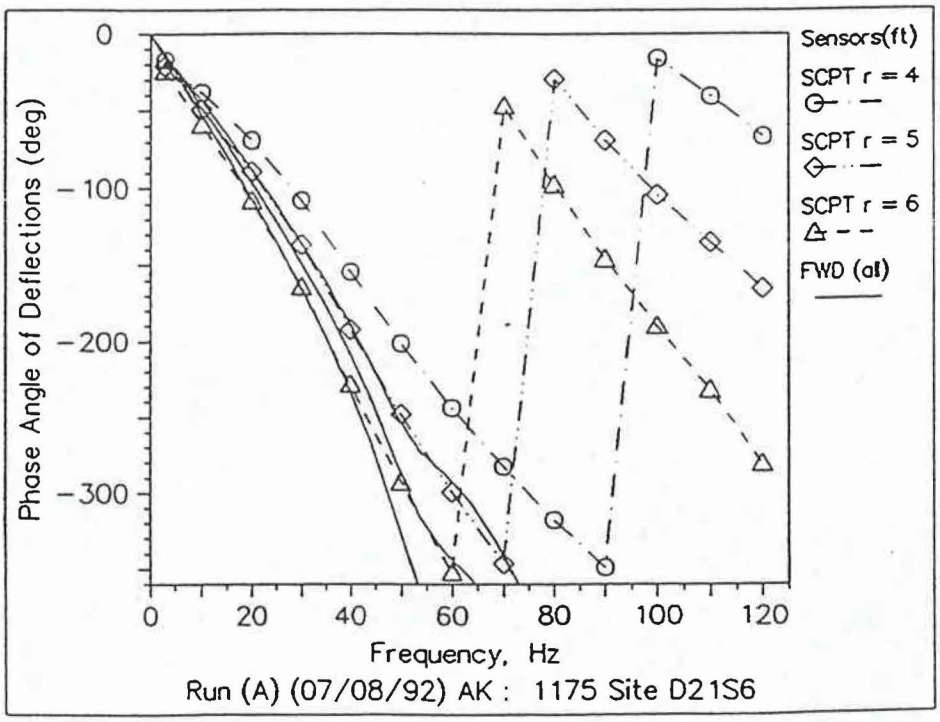

Figure 173. Section D21S6: Phase Angle Plot for Outer Displacements (r=4.0, 5.0, and 6.0 ft.)